IMPLICATIONS OF DYSREGULATED ANTIBODY HYPERMUTATION PATTERNS IN MULTIPLE SCLEROSIS PATIENTS

APPROVED BY SUPERVISORY COMMITTEE

Nancy L. Monson, Ph.D.

E. Sally Ward, Ph.D.

Ellen S. Vitetta, M.D., Ph.D.

Richard H. Scheuermann, Ph.D.

Betty A. Diamond, M.D.

DEDICATION

This work is dedicated to the patients who have consented to participate in research, in the hopes of helping their community receive better diagnostics and treatments. Elucidating the biological mechanisms of MS disease brings both researchers and clinicians closer to developing the optimal care for patients.

Thank you to my family, Jolanta, Jerzy, and Eva, for their continual support throughout my studies.

Thank you to my mentor, Dr. Monson, for allowing me to transition into molecular Immunology with a translational focus.

Thank you to my Thesis Committee (Dr. Ward, Dr, Vitetta, Dr. Scheuermann, and Dr. Diamond), who offered advice, insight, and novel directions.

IMPLICATIONS OF DYSREGULATED ANTIBODY HYPERMUTATION PATTERNS IN MULTIPLE SCLEROSIS PATIENTS

by

ANN JOLANTA LIGOCKI

DISSERTATION

Presented to the Faculty of the Graduate School of Biomedical Sciences

The University of Texas Southwestern Medical Center at Dallas

In Partial Fulfillment of the Requirements

For the Degree of

DOCTOR OF PHILOSOPHY

The University of Texas Southwestern Medical Center at Dallas

Dallas, Texas

May 2014

Copyright

by

ANN JOLANTA LIGOCKI, 2014

All Rights Reserved

IMPLICATIONS OF DYSREGULATED ANTIBODY HYPERMUTATION PATTERNS IN MULTIPLE SCLEROSIS PATIENTS

ANN JOLANTA LIGOCKI, Ph.D.

The University of Texas Southwestern Medical Center at Dallas, 2014

NANCY LEE MONSON, Ph.D.

The potential role of B cells in contributing to the pathology of the human autoimmune neurological disease multiple sclerosis (MS) has recently become of significant interest. MS is a complex disorder of the central nervous system (CNS) with various presentation types, symptoms, and damage that involves many different components of the immune system. Historically, the role of B cells was considered minimal and overshadowed by the impact of T cells. The main effector function of a B cell is mediated by the downstream production of antibodies, that bind to their cognate antigens.. Thus, detailed investigation of antibody genomics reveals important information regarding the response of a B cell to its environment. We previously discovered a pattern of somatic hypermutation in the antibody genes expressed isolated from cerebrospinal fluid (CSF) B cells of patients with MS and those at high risk for developing MS. The focus of this thesis project was to further characterize this pattern of mutation termed the antibody gene signature (AGS) and determine the biological significance of this shared AGS among patients. Secondly, I aimed to discover differences in B cell subtypes and antibody genomics in the two of the most common

initial presentations of clinically isolated syndrome (CIS) patients at high risk for converting to MS: optic neuritis (ON_{CIS}) and transverse myelitis (TM_{CIS}).

Through my work in analyzing antibody genomics, I demonstrated that the AGS is present at the site of MS disease, within the CNS tissue. This provides support for the study of CSF B cells since it recapitulates what is present within the parenchyma. I also determined that both ON_{CIS} and TM_{CIS} patients are enriched for AGS positive B cells within the CSF. This exemplifies that regardless of initial presentation, patients at high risk for converting to MS share this AGS. Further characterization of TM_{CIS} patients revealed that a subset harbor an expansion of plasmablasts in both the periphery and the CSF compared to ON_{CIS} patients. Furthermore, in depth analyses of the peripheral plasmablasts uncovered altered genomic selective pressures in the periphery. This differential expansion of plasmablasts may offer insight for future studies of the possible varied underlying biological processes between these two patient groups.

I aimed to determine the biological significance of this shared genomic pattern of the AGS by examining the CNS targeting potential. Immunohistochemical experiments revealed that AGS-enriched antibodies from ON_{CIS}, $TM_{CIS,}$ and MS patients target neurons and astrocytes within the gray matter. These novel findings provide future directions for elucidating the auto-antigen(s) responsible for eliciting the shared AGS. Furthermore, identifying the AGS-enriched antibody binding patterns could aid in identifying potential therapeutic targets to help reduce CNS damage in both CIS and MS patients.

TABLE OF CONTENTS

PUBLICATIONS

1. Ligocki A.J., Rounds W.H., Li M., Henson P.M., Rivas J.R, Guzman A.A., Graves D., Greenberg B.M., Frohman E.M., Diamond B., Ward E.S., Stowe A.M., Monson N.L. Gray matter neuron and astrocyte targeting of multiple sclerosis antibodies. In preparation, 2013

2. Ligocki A.J., Rounds W.H., Cameron E.M., Racke M.K., Frohman E.M., Greenberg B.M, Monson N.L, Vernino S. Immunophenotype of peripheral blood and cerebrospinal fluid lymphocytes in central and peripheral paraneoplastic neurological disorders. In preparation, 2013

3. Monson N.L., Ireland S.I., Ligocki A.J., Chen D., Rounds W.H., Li M., Huebinger R.M., Cullum C.M., Greenberg B.M., Stowe A.M., Zhang R. Elevated CNS inflammation in patients with preclinical Alzheimer's disease. Journal of Cerebral Blood Flow and Metabolism, 2013, in press.

4. Ligocki A.J., Rounds W.H., Cameron E.M., Harp C.T., Frohman E.M., Courtney A.M., Vernino S., Cowell L.G., Greenberg B., Monson N.L. Expansion of $CD27^{high}$ plasmablasts in transverse myelitis patients that utilize VH4 and JH6 genes and undergo extensive somatic hypermutation. Genes and Immunity, 2013, July; 14(5):291-301.

5. Ligocki A.J., Lovato L., Xiang D., Guidry P., Scheuermann R.H., Willis S.N., Almendinger S., Racke M.K., Frohman E.M., Hafler D.A., O'Connor K.C., Monson N.L. A unique antibody gene signature is prevalent in the central nervous system of patients with multiple sclerosis. Journal of NeuroImmunology, 2010; 2006(1-2):192-3.

LIST OF FIGURES

LIST OF TABLES

LIST OF ABBREVIATIONS

ADEM: acute disseminated encephalomyelitis

AGS: antibody gene signature

AID: activation-induced cytidine deaminase

APC: antigen presenting cell

ATP: adenosine triphosphate

AQP4: aquaporin 4

BAFF: B-cell activating factor

BBB: blood brain barrier

BCR: B cell receptor

BSA: bovine serum albumin

CD: cluster of differentiation

CDMS: clinically definite multiple sclerosis

cDNA: complementary DNA

CDR: complementarity determining region

CIS: clinically isolated syndrome

CNS: central nervous system

CNPase: 2-3-cyclic-nucleotide 3-phosphodiesterase

cPEP: cDNA primer extension preamplification

CSF: cerebrospinal fluid

CSR: class switch recombination

DAB: 3,3-Diaminobenzidine

DAPI: 4',6-diamidino-2-phenylindole

D_H: diversity segment

DMEM: Dulbecco's Modified Eagle Medium

dNTP: deoxyribonucleotide triphosphate

dsDNA: double stranded DNA

DTT: Dithiothreitol

EAE: experimental autoimmune encephalomyelitis

EDSS: Expanded Disability Status Scale

EDTA: Ethylenediaminetetraacetic acid

ELISA: enzyme-linked immunosorbent assay

FACS: fluorescence activated cell sorting

Fc: fragment crystallizable

FCS: fetal calf serum

FDC: follicular dendritic cell

FR: framework region

FSC: forward scatter

GA: glatiramer acetate

GC: germinal center

gDNA: genomic DNA

GFAP: glial fibrillary acidic protein

GM: gray matter

GWAS: Genome-Wide Association Studies

HC: healthy control

HEK 293T: Human Embryonic Kidney 293 cells

HEPES: hydroxyethyl piperazineethanesulfonic acid

HRP: horseradish peroxidase

IFC: immunofluorescence

IFN: interferon

Ig: immunoglobulin

IgG: immunoglobulin of the gamma isotype

IgK: immunoglobulin of the kappa isotype

IHC: immunohistochemistry

IRB: Institutional Review Board

ITS: insulin-transferrin selenium

J_H: junctional heavy segment

Jκ: junctional kappa segment

Jλ: junctional lambda segment

LB: Luria-Bertani broth

LCM: laser capture microdissection

MBP: myelin basic protein

MF: mutation frequency

MHC: major histocompatibility complex

MOG: myelin oligodendrocyte glycoprotein

MP4: myelin basic protein- proteolipid protein fusion protein

MRI: magnetic resonance imaging

mRNA: messenger RNA

MRS: magnetic resonance spectroscopy

MS: multiple sclerosis

MWCO: molecular weight cut off

NAA: N-acetyl aspartate

NAWM: normal appearing white matter

NeuN: neuronal nuclei

NF: neurofilament

NGS: next generation sequencing

NMDAR: N-methyl-D-aspartate receptor

NMO: neuromyelitis optica

OCB: oligoclonal band

O.C.T.: optimum cutting temperature compound

ON_{CIS}: clinically isolated syndrome optic neuritis

OND: other neurological disease

P: plaque

PB: peripheral blood

PBMC: peripheral blood mononuclear cells

PBS: phosphate buffered saline

PCR: polymerase chain reaction

PLP: proteolipid protein

PND: paraneoplastic neurological disorder

PNS: peripheral nervous system

PPMS: primary progressive multiple sclerosis

RA: rheumatoid arthritis

RAG1/2: recombination-activating genes

RF: replacement frequency

rhAb: full-length recombinant human antibody

RHP: random hexamer primer mix

RM: replacement mutation

rpm: revolutions per minute

RPMI: Roswell Park Memorial Institute medium

RRMS: relapsing remitting multiple sclerosis

R:S: replacement to silent mutation ratio

RSS: recombination signal sequence

RT: reverse transcription mix

s.e.m.: standard error of the mean

SHM: somatic hypermutation

SLE: systemic lupus erythematosus

SOB: super optimal broth

SOCS: super optimal culture solution

SPMS: secondary progressive multiple sclerosis

SSC: side scatter

TBE: Tris/Borate/EDTA

TCR: T cell receptor

TD: T cell dependent

TdT: terminal deoxynuclotidyl transferase

TI: T cell independent

TM_{CIS}: clinically isolated syndrome transverse myelitis

$TM_{CIS}A$: transverse myelitis- above

$TM_{CIS}B$: transverse myelitis- below

TMB: 3,3',5,5'-Tetramethylbenzidine

V_H: variable heavy segment

VHE: variable heavy external PCR

VHN: variable heavy nested PCR

Vκ: variable kappa segment

VKE: variable kappa external PCR

VKN: variable kappa nested PCR

Vλ: variable lambda segment

VLA-4: very late antigen-4 (alpha4beta1 integrin)

WM: white matter

CHAPTER ONE

INTRODUCTION

Multiple Sclerosis (MS)

MS overview and pathology

Multiple Sclerosis (MS) is an autoimmune inflammatory disease of the central nervous system (CNS) characterized by the demyelination of axons and the formation of lesions (1-5). In 1868, Charcot first characterized this disease by identifying hard sclerotic lesions in the post-mortem brain of afflicted patients. Approximately 0.1% of the population has MS, with a gender bias of 3 females to 1 male afflicted (6-8). MS is a heterogeneous disease, with both white matter (WM) and gray matter (GM) involvement and lesions characterized by different types of immune cells (6, 9-11). Genome-Wide Association Studies (GWAS) of MS patients have shown an increase in MS-risk associated the HLA-DR2 allele highlighting the importance of antigen presentation within the immune system in the disease process (12). Also, reduced signaling through the IL-7 receptor and polymorphisms in the IL-2 receptor, which may increase the soluble levels of the receptor, increases the risk of developing MS and are the first confirmed non-MHC associated genes among MS patients (12). Both IL-7 and IL-2 are important cytokines in the growth and proliferation of immune cells.

Perivascular demyelinated lesions are common since these areas are near lymphocyte accumulations consisting of B cells, T cells, and macrophages (2, 6, 7, 9). In addition to demyelination, axonal damage and transection occur early in MS in both lesions and normal appearing white matter (NAWM), and are associated with irreversible neurological deficits and cognitive decline (3, 4, 13, 14). Global diffuse injury to both the

WM and GM, beyond overt demyelination, is detected in MS CNS and contributes to pathology and symptoms (9, 15).

Myelin can be damaged through activated $CD4^+$ and $CD8^+$ T cells, macrophages, immunoglobulin (Ig), and microglia, which all induce an inflammatory assault against the previously immunoprivileged site. These inflammatory infiltrates are accompanied by a disturbance in the blood brain barrier (BBB) allowing for entry into the CNS (16-18). Magnetic resonance imaging (MRI) is used to detect and monitor progression of lesions and abnormalities *in vivo.* T1 weighted gadolinium images detect BBB breakdown and sites of active WM lesions (19) while T2 weighted images of lesion volume show changes over time that are used to monitor long-term disease activity (20). Increased T2 lesions are correlated with IgG index (a measure of IgG content in the CSF) whereas T1 lesions are correlated with $CD4^+$ T cell and total CSF cell numbers suggesting that different immunological mechanisms underlie the pathogenesis of different types of lesions (21). Immunological disturbances are also evident in the CSF during active MS with increased numbers of total CSF cells, activated $CD4^+$ T cells, and $CD19^+$ B cells (2, 21).

Exactly how MS disease is initiated is still debated, however one hypothesis is that the peripheral immune system becomes activated against previously immunoprivileged antigens that have drained from the CNS into cervical lymph nodes (22). Activated B and T cells can cross the BBB into the CNS. MS patients, as well as mice and marmosets induced to have a model of MS, have macrophages with engulfed myelin and neuronal antigens present in their cervical lymph nodes (23-25). This is not observed in healthy human individuals or mice (23-25). It is also likely that a break in

peripheral immune tolerance could occur and be perpetuated to mount an immune response against CNS components.

MS subtypes

Approximately 85% of patients are initially diagnosed with a relapsing remitting disease course (RRMS) characterized by acute relapse attacks of worsening clinical presentations and neurological dysfunction followed by a remission of symptoms to a quiescent state (8). About 10% of patients show a benign disease course with no accumulation of deficits and their expanded disability status scale (EDSS) score, a method of quantifying clinical disability in MS, remains below 3 (mild to moderate disability, though fully ambulatory) (26). These patients also have significantly fewer cortical lesions than patients with non-benign MS (27). A meta-analysis study reports that 66% of RRMS patients eventually develop secondary progressive MS (SPMS) characterized by progressive disability without remissions (28). The median time to developing SPMS is 15 years, and within 25 years after initial onset greater than 80% of patients progress to SPMS (28). 15% of patients present with primary progressive MS (PPMS) in which they do not experience an RRMS stage and instead have progressive accumulation of deficits from disease onset (8). PPMS patients do not respond to the same treatment approaches as RRMS and SPMS patients underscoring the different etiology of this disease form (29).

Contribution of damage to the white matter (WM) and gray matter (GM)

MS patients have damage and inflammation in both the WM and GM regions of the CNS. Historically, there has been greater focus on WM lesions, in part due to easier

detection via MRI and immunohistochemical techniques compared to GM lesions (30, 31). However, it has come to light that WM damage does not fully explain the progression and symptom characteristics of MS (32, 33) and instead a combination of changes in both WM and GM most effectively predicts clinical disease progression (34). Atrophy in the GM occurs at a higher rate than atrophy in the WM (35-38) and cortical demyelination is more extensive than in the WM (26.5% vs 6.5%) with the percentage of demyelination in the cortex increasing with disability and length of disease (31). Furthermore, GM atrophy and damage is associated with faster disease progression (27, 39-42). Cortical GM demyelination also occurs early in disease and is associated with inflammatory infiltrates (43). This is further supported by the finding that GM axon, neuronal, and synaptic proteins are already enriched in the CSF at the first clinical attack of MS (44). However, as disease progresses, cortical neurodegeneration continues without overt inflammatory infiltrates in SPMS patients (45).

Clinically isolated syndrome (CIS)

Patients that present with a first demyelinating attack are diagnosed with clinically isolated syndrome (CIS), which places them at high risk for developing clinically definite MS (CDMS). A CIS is the first clinical manifestation of a neurological event due to demyelination or inflammation in the CNS. The most common presentations of CIS are optic neuritis (ON_{CIS}) and transverse myelitis (TM_{CIS}) (46).

Optic Neuritis (ON_{CIS}) and Transverse Myelitis (TM_{CIS})

ON_{CIS} is characterized by visual impairments due to demyelination of the optic nerve (47-49). TM_{CIS} symptoms involve weakening of limbs or sensations of numbness

due to demyelination occurring across short segments of the spinal cord (50). Those at high risk for CDMS do not have any peripheral nervous system (PNS) involvement (51) but have lesions in the CNS (52, 53). While 30-48% of patients remain idiopathic, 44-60% go on to develop CDMS (52, 54). Acute complete TM_{CIS} patients with lesions longer than 2 segments typically are early neuromyelitis optica (NMO) patients whereas acute partial TM_{CIS} patients with short lesion segments are at risk for MS (53, 55, 56). Patients that present with either ON_{CIS} or TM_{CIS} have a high risk of converting to CDMS, but current risk stratification approaches depend on MRI findings in the brain. 82% of CIS patients with an abnormal baseline brain MRI convert to CDMS, compared to just 21% with a normal MRI (57). Furthermore, the presence of one lesion in the spinal cord of CIS patients is an independent risk factor for conversion to MS with a hazard ratio (HR) of 3.5 and those with 2 or more spinal cord lesions have a further increased HR of 5.9 (58). Within a year after the initial CIS, 58% of TM_{CIS} patients have converted to CDMS with a lower number of ON_{CIS} patients (37%) converted in the same time interval (59).

Additionally, ON_{CIS} patients have better long-term prognoses reaching an EDSS of 4 (ambulatory despite relatively severe disability) in about 13.5 years compared to other presentations including TM_{CIS} who reach that disability milestone in just 7 years (60). TM_{CIS} patients also have detectable levels protein 14-3-3, which is found in axons, in their CSF if they do not recover from an attack (61), a potential marker of permanent neurological disability with a shorter time to conversion to CDMS (3.7 vs 7 years) and a higher relapse rate (3.1 vs 1.8) (62). Differences in progression to CDMS, long-term prognosis, and location of initial lesions between ON_{CIS} and TM_{CIS} patients suggest differences in the underlying biology.

Importance of early diagnosis

Most CIS patients already have an abnormal MRI at the first clinical event indicating an ongoing destructive process (63). Further necessitating the importance of early and accurate diagnosis are the data suggesting that earlier treatment with disease modifying agents delays the progression of disease and accruement of disability (28, 57, 64-67). During early disease stages, irreversible CNS tissue loss is not typically detected by MRI, however it does develop 1-3 years post diagnosis in patients who convert to CDMS (39, 65) further highlighting the need to identify and treat patients early. The number of relapses within the first 2 years and rate of another clinical event in CIS correlates with future EDSS scores (28, 60, 68). Patients are also 3 times more likely to convert to SPMS if they experienced 5 or more attacks within the first years (28). Silent CNS damage accumulates at a proposed rate of 5-10 lesions for each clinical relapse (69), illustrating the progressive destructive course of the disease and need for early treatment.

The study of B cells in MS

While all immune cells play a role in the pathology of MS, more in-depth analysis of each cell type's contribution is needed to understand the global picture. B cells have been implicated in MS disease and research in this field has led to substantial findings in support of their pathological potential. Thus, the following sections detail B cell development.

B cell development

VDJ recombination

The development of a human B cell and its effector functions and fates are all determined by the immunoglobulin (Ig), or antibody, it expresses. Ig are rearranged using a set of germline encoding gene segments. The variable heavy chain (V_H) region is encoded by three types of gene segments, V (variable), D (diversity), and J (joining). There are 7 V_H families (V_H1-7) containing a total of 51 V_H gene segments, 27 D_H gene segments, and 6 J_H gene segments located on chromosome 14. V_H combinatorial diversity arises from the assortment of the three genes comprising the VDJ cassette. The variable light chain is encoded by two types of gene segments, V and J. There are two classes of light chains: variable kappa (Vκ) on chromosome 2 and variable lambda (Vλ) on chromosome 22. There are 6 Vκ families (Vκ1-6) containing a total of 40 Vκ gene segments and 5 Jκ gene segments. There are 11 Vλ families (Vλ1-11) containing a total of 29 Vλ gene segments and 4 Jλ gene segments. Combinatorial diversity is lower in the light chain VJ cassettes when compared to the heavy chain due to the absence of D segments.

Somatic V-region rearrangement (VDJ recombination) is carried out by the recombinase enzymes RAG-1 (recombination-activating gene-1) and RAG-2 (recombination-activating gene-2). V_H rearranges by creating a DJ cassette first which is then joined to a V gene. RAG1/2 bind as a complex to recombination signal sequence (RSS) regions and bring two gene segments together while cleaving the RSSs. The DNA that is looped out between the two gene segments is excised from the genome. Artemis:DNA-PK adds palindromic P-nucleotides to the open DNA hairpin. The open

ends are modified by terminal deoxynuclotidyl transferase (TdT) that randomly adds non-template-encoded N-nucleotides to the ends. Nucleotides are also deleted at the end of segments. This process of random addition and deletion of nucleotides, termed junctional diversity, adds to the variability of possible Igs produced. Not only does this exponentially increase the diversity, it also increases the chance for nonproductive rearrangements, which will be removed from the B cell progenitor pool during development.

B cell development in the bone marrow to the periphery

B cells develop from a common lymphoid progenitor within the bone marrow. The earliest B-lineage cell is the pro-B cell where antibody rearrangement begins. The early pro-B cell is identified by the rearrangement of the D-J cassette in the V_H gene followed by the late pro-B cell with the joining of the DJ cassette to a V gene. Once this VDJ has been rearranged, it is transiently joined to the μ chain region forming the pre-B cell receptor (BCR). The pre-BCR is comprised of a rearranged V_H and μ chain with a surrogate light chain and CD79a/CD79b (Ig-α and Ig-β), which is expressed on the surface of the cell. Signaling through the pre-B cell receptor allows the cell to pass an important checkpoint of successful V_H rearrangement and further rearrangement at this locus is halted. This large pre-B cell proliferates to form multiple clones of small pre-B cells. Light chain rearrangement of the V-J cassette begins in each of small pre-B cells first with the Vκ genes and only moves on to the Vλ genes once the first two Vκ chromosomes have failed at producing a successfully rearranged light chain. An intact monomeric IgM molecule with a productive heavy and light chain is expressed on the surface of an immature B cell.

The immature B cell is now tested within the bone marrow for tolerance to self-antigens. This process of negative selection, known as central tolerance, removes immature B cells that have a strong autoreactivity. There are four possible routes for a self-reactive immature B cell. One is death by apoptosis or clonal deletion due to strong binding to a cell-bound antigen creating an aggregation of BCR on the surface without a secondary signal in the absence of T cells (70). A second route is anergy, which makes the cell nonresponsive to stimuli. A B cell can also be immunologically ignorant due to the low level of self-antigen or unavailability of an antigen from an immunopriviledged site (71). While these B cells are not responding at the present time, they could become active if they encounter their antigen. This usually occurs only when antigen matriculates from the once immunopriviledged site. The fourth and final route is a process called receptor editing in which the BCR is altered by rearranging a new antibody or modifying the existing antibody in an attempt to abrogate self-recognition.

About 10% of B cells pass central tolerance and exit from the bone marrow. Immature B cells that pass selection in the bone marrow migrate into the periphery as mature B cells with IgM and IgD isotypes expressed on the cell surface. These immature B cells enter the transitional B cell stage prior to additional tolerance checks occur in the periphery. B cells that strongly cross-link antigens undergo clonal deletion or, to a lesser extent, receptor edit. If they do not encounter a strong signal, the transitional B cells migrate into the spleen and enter the red pulp where they become mature B cells. Once they migrate from the spleen, mature B cells circulate through the blood and lymphatic system until they encounters their cognate antigen. Antigens enter the lymph node through the afferent lymphatics and the immune cells enter through the high endothelial venules. T cells reside in paracortical areas and B cells are in follicles within the cortex of

the lymph node. B cells express CXCR5 and migrate towards CXCL13 produced by follicular dendritic cells (FDCs) residing in secondary lymphoid organ follicles. The B cells promote the follicle structure of the germinal center (GC) through the production of lymphotoxin-α, which is needed for FDC development. This GC reaction involving FDCs, $CD4^+$ T cells, and B cells is essential for creating effector B cells with increased affinity for their cognate antigen. The B cell has four fates after exiting the GC: it can become a memory cell which will circulate and respond quicker and more robustly to a second encounter with the antigen, a short lived mobile plasmablast which remains in the medulla of the node, or it can migrate to inflamed tissue, or will enter the bone marrow and become a long-lived plasma cell.

Somatic hypermutation (SHM) and affinity maturation

Signaling through the BCR directs the fate of the B cell. B cells can be activated through their BCR differently depending on the type of antigen that binds to the BCR. A T cell-independent (TI)-1 antigen is a B cell epitope linked to a polyclonal activator or mitogen. This leads to rapid differentiation into IgM plasmablasts with the BCR functioning as a dock for the mitogen to activate the cell. A TI-2 antigen is a polyvalent highly repetitive epitope, such as a carbohydrate, capable of cross-linking many BCRs to induce a signal. These B cells are $CD5^+$ B-1 cells that contain a restricted V region repertoire and secrete IgMs. Conventional B-2 cells respond to T-dependent (TD) antigens, which require cognate T cell help to mount a response.

Once a B cell interacts with an antigen and receives help from a $CD4^+$ T cell, it moves into the center of the germinal center (GC) and proliferates rapidly. This secondary follicle consists of proliferating B cells (centroblasts) in the center and smaller

non-proliferating B cells (centrocytes) at the edge interacting with FDCs and T cells. The dark zone of centroblasts is where affinity maturation occurs through the process of somatic hypermutation (SHM) and the light zone of centrocytes is where clonal selection and class switch recombination (CSR) occurs.

Within the expanded centroblast B pool, point mutations occur within the antibody predominately within the variable region's complementarity determining regions (CDRs) and less so in the framework regions (FRs). This process is termed somatic hypermutation (SHM) and creates a clonally related B cell pool with mutations in their BCRs. Activation-induced cytidine deaminase (AID) is the enzyme that promotes mutations along the gene by deaminating cytidine to uracil at preferential DNA motifs. This uracil is removed from the gene by strand breaks and low-fidelity DNA repair enzymes and polymerases. In competing for antigen bound to the surface of FDCs with the other expanded B cells, only those harboring beneficial mutations that increased their affinity for the antigen receive survival signals. This process is affinity maturation and clonal selection. In addition to SHM and clonal selection, B cells can also receive cytokine signals to class switch their antibody from IgM to a IgG, IgA, or IgE which have various effector functions. CSR also requires AID activity and occurs at the genome level to juxtapose the existing VDJ to a new constant region. IL-4 is the main cytokine signal involved in class switching to any isotype away from IgM. IL-21 is involved in switching human B cells to IgG_1 and IFNγ is a secretion factor for IgG_1. IL-4 is a switch factor for human B cells to IgE or IgG_4, and IL-5 or TGFβ to IgA. Alternative splicing of the mRNA leads to the formation of either surface bound or secreted Ig of the same specificity.

Receptor editing

Autoimmune B cells can escape to the periphery and the majority B cells emerging from the human bone marrow are auto-reactive (55-75%) (72). Self-reactive B cells in the bone marrow either undergo apoptosis or a process termed "receptor editing" in an attempt to survive selective pressure against self-reactivity (73-76). Receptor editing is a prominent feature in the bone marrow (77, 78). This process requires secondary rearrangement of antibody genes. Antibody heavy chain editing is complicated by the D_H gene, which is deleted during primary rearrangement in conjunction with the original 12 bp spacer RSS needed to combine with the 23 bp spacer RSS flanking the V_H or J_H genes. Despite this, editing at the heavy chain has been demonstrated to occur at cryptic RSS sites present in the 3' end of V_H genes which allows for V: VDJ replacement (79, 80). This cryptic RSS can be found in most V_H genes and allows for RAG binding to allow for the secondary rearrangement, though at a lower efficiency than during primary rearrangement (81). In the normal human B cell repertoire it is estimated that 5-10% of the BCRs are a product of V_H receptor editing (81). During replacement, a footprint of the previous V_H gene can sometimes be found within the newly formed CDR3 region (81) and can thus elongate the region. Despite using a different mechanism than light chain editing, it has been found that heavy chain rearrangement also utilizes downstream J_H genes, namely the final J_H6 segment (82). It is estimated that approximately 59% of mature B cells that leave the bone marrow can bind self-antigen (72). In the periphery, anergy, apoptosis, or gene replacement/editing must control these cells to prevent autoimmunity. Also, the lack of cognate T cell help can maintain peripheral tolerance since central tolerance is more robust in T cells compared to B cells.

B cell involvement in MS

Intrathecal Ig and oligoclonal banding (OCB)

The earliest evidence for a dysregulated B cell compartment in MS was the discovery of elevated intrathecal Ig levels and oligoclonal banding (OCB; clonal production of Igs) in the CSF (83-87). Reports suggest that 60% to over 90% of CIS and MS patients have OCBs in their CSF (88-91). Although other inflammatory neurological diseases can also present with OCB (88, 92), in these cases, once the infection or inflammatory insult has cleared, the OCB wanes. In MS, the OCB remains constant throughout the disease course pointing to a continual B cell response to self-antigens. Intrathecal IgG from MS patients recognizes similar peptides over time (93) reflecting a persistent response to self. CIS patients presenting with IgG OCB as compared to OCB negative patients have a higher risk (62% OCB+ convert vs 19% OCB-) and faster progression to CDMS (0.7-3 vs 9.9 years), and have a higher risk of greater EDSS accruement (risk ratios 1.65-2.03) once progressed to CDMS (91, 94, 95). Patients with the highest probability of converting to CDMS have both elevated IgG index and IgG OCB (96). Additionally, increased CSF IgG levels correlated more strongly with development of CDMS than an abnormal MRI in an ON_{CIS} cohort (after 8 years: 50% conversion with abnormal MRI, 100% conversion with increased CSF IgG) (89). OCB was also a better predictor than MRI of conversion to CDMS in a TM_{CIS} cohort after 2 years (81% conversion with abnormal MRI, 92% conversion with OCB) (97). Collectively, these findings suggest that elevated intrathecal B cell activity measured by antibody production is a metric of worse prognosis and that their Igs likely play a role in the pathogenesis of the disease.

Ig and complement in CNS lesions

MS is a heterogeneous disease with varied presentations and symptoms suggesting that there are diverse underlying immunopathologies among patients or within different regions of the CNS of patients. One seminal study that supports this hypothesis defined four patterns of demyelination based on immune cell representation and CNS targets (6). 53.5% of lesions follow pattern II demyelination with pronounced deposition of Ig and complement at the site of active demyelination. Pattern I (12.3%) lesions have B cells but no deposition of complement within lesions, pattern III (30.1%) lesions are dominated by T cells, and pattern IV (4.1%) lesions also have T cells but are characterized by oligodendrocyte abnormalities (6). Clinical studies of plasmapheresis treatment have shown significant symptom improvement in patients harboring pattern II lesions (98, 99), implicating the pathogenicity of antibodies in this patient group. Furthermore, the transfer of IgG from an MS patient responsive to immunoadsorption exacerbated the course of disease in experimental autoimmune encephalomyelitis (EAE), a mouse model of MS (100) demonstrating the pathogenic potential of these antibodies.

A number of immunopathology studies of MS CNS plaques suggest a role of Ig and complement in the lesion pathology. IgG and complement are present on disrupted myelin tracts in active demyelinating lesions and within the associated myelin laden macrophages (101-107). Deposits of IgG are also found along axons within MS CNS that are currently undergoing demyelination (108). Increased levels of complement components are detected in both CIS and MS CNS (106, 109) and CSF (110). Both increased intrathecal Ig synthesis (111, 112) and complement activation (113) are also associated with a more aggressive disease course. Accordingly these findings implicate a pathological role for antibodies in the pathoetiology of MS.

Elevated levels of B cells

B cells are rare in the CSF of normal humans, comprising only 0.5-1.0% of the total lymphocytes (114-116). In patients with MS, B cells represent 0.3-17% of the CSF lymphocytes (117, 118). Furthermore, these B cells in the CSF of MS patients are predominantly of the memory phenotype ($CD19^{+}CD27^{+}$) with the naïve to memory ratio being lower than 1 (118, 119). Memory B cells also more readily pass the BBB in comparison to their naïve counterparts through the upregulation of integrins (116). RRMS patients undergoing an attack have an expansion of B cells in the CSF (active RRMS: 1.6% vs stable RRMS: 0.8%), which are predominately of the memory phenotype (80-85%) (118, 119). Additionally, paired patient information revealed that those with the highest frequency of memory B cells in the CSF had the lowest frequency of memory B cells in the periphery (119) and that levels of $CD27^{+}$ B cells increased in the periphery of patients in remission as compared to relapse (120). This suggests that B cells are recruited to the CSF from the periphery in these patients, and recent repertoire data underscore this possibility with shared peripheral B cell progenitors and mutated clonally related daughter cells in the CSF (121). From a clinical view, elevated levels of B cells in the CSF correlate with lesion activity on MRI (5, 117). B cell expansion occurs early in both CIS and established RRMS patients, and correlates with brain inflammation in both types (122). These CSF B cells are hyperactive since *in vitro* culture of CSF derived B cells in the presence of IL-6 induces significant IgG secretion compared to CSF derived B cells from healthy controls (123). B cells (101, 124, 125) and plasma cells (6, 126, 127) have been detected in the CNS of MS patients.

Ectopic B cell lymphoid follicles

Ectopic B cell lymphoid follicles can be found in the meninges (128, 129), suggesting that B cell maturation and antigen driven selection can be sustained locally in the CNS. Patients who were positive for ectopic follicles have a more aggressive disease course with follicles found adjacent to cortical subpial lesions (128, 130) with a gradient of neuronal death outwards from these meningeal follicles (131). Elevated levels of CXCL13 and lymphotoxin alpha, chemokines necessary for GC follicle formation (132), are found in MS CNS (133, 134) and CSF (135, 136). The ability to find B cell subpopulations within the CSF representing the stages normally found within a GC (133) provides further evidence of locally derived B cell activation and differentiation. Tertiary follicles have also been found in the meninges and parenchyma of a B cell dependent myelin basic protein (MBP)-proteolipid protein (PLP) fusion protein (MP4) EAE model (137). Furthermore, there is evidence of T cell epitope spreading after follicle development (137). In the traditional MOG peptide-induced EAE, T cells interact with antigen presenting cells (APCs) within the spinal cord leptomeninges prior to entering the parenchyma (138) promoting a relevant role of ectopic follicles in diversification and progression of disease. Diseased-organ-associated ectopic B cell follicles are also found in other autoimmune diseases with chronic pathological B cell activation such as myasthenia gravis (139), rheumatoid arthritis (RA) (140, 141), Sjogren's syndrome (142, 143), Hashimoto's (144), and even during tuberculosis infection (145). The formation of ectopic GCs is considered a result of chronic inflammation and persistence of antigen(s).

Clinical evidence for a role of B cells in disease pathology

Disease modifying therapeutics administered to MS patients have effects on various immune cell populations. Clinical evidence of the known inhibitory effects on B cells in MS disease and is listed in Table 1-1.

Interferon (IFN) β-1a/β-1b (Avonex/Rebif/Betaseron)

Several clinical trials have demonstrated that treatment with any of the three preparations of IFN-β after the first clinical event delays the conversion to CDMS (146). IFN-β treatment of MS patients reduced the levels of $CD40L^+$ T cells to normal as compared to non-treated patients (8.3% vs 4%) (147). This could decrease the ability of T cells to interact and provide costimulation through CD40 on the B cell and reduce class switching. In fact, peripheral B cells from IFN-β treated RRMS patients had modest but significant reductions in class-switched memory B cells (17% vs 19%) and an increase in naïve B cells (66% vs 61%) (119). IFN-β treatment also lowered the expression of CD40 and CD80 on the B cells (CD40: 14.9% vs 11.9%, CD80: 5.5% vs 3.1%) (148) which is also necessary for B-T cell costimulatory interactions. Treatment can also cause reduced IL-12 and increased IL-10 levels from *in vitro* PBMC stimulation with bacterial components (149) which could reduce the activity of both B and T cells. However, it is puzzling that IFN-β treatment also increased serum B-cell activating factor (BAFF) levels (150), but this may account for elevated levels of neutralizing anti-IFN-β antibodies in some treated patients (151). In fact, neuromyelitis optica NMO patients (a neuroimmunological autoimmune disorder) respond poorly to IFN-β treatment and relapse with increased anti-aquaporin 4 (AQP4) titers (152-154) most likely due to BAFF supporting the development and survival of plasma cells in the periphery.

Glatiramer acetate (Copaxone)

Glatiramer acetate (GA) was initially developed as a synthetic MBP mimic to induce EAE but actually ameliorated disease (155) and has become a MS therapeutic. GA is a copolymer of a random assortment of alanine, lysine, glutamate, and tyrosine to roughly resemble MBP. Clinical trials demonstrated that GA treatment reduced the clinical attack rate and number of new lesions in RRMS patients (156, 157). Serum from GA treated patients have reduced TNFα and increased IL-10 levels (158) which could reduce the activity of both B and T cells. Monocytes from GA treated patients had an anti-inflammatory phenotype with an increase in IL-10 and decrease in IL-12 production (159). $CD8^+$ T cell proliferation could be reduced in the presence of B cells (as the APCs) and GA in an *in vitro* culture system in 83% (n=5/6) of MS patients (160). *In vitro* treatment of GA in B cell cultures does not alter B cell proliferation or cytokine secretion but the complex effects *in vivo* of these responses are being investigated (161).

Mitoxantrone (Novantrone)

Mitoxantrone is primarily an anti-cancer treatment and functions by disrupting DNA synthesis and repair and thus is a potent immunosuppressant. This drug is predominately perscribed for SPMS and not RRMS patients due to potential cardiac damage and risk of malignancy (162). A 2-year clinical trial of mitoxantrone treatment for patients with worsening RRMS or SPMS found a reduced progression of disability and exacerbations (163). In addition to being a immunosuppressant it has some modulatory activity in reducing levels of secreted antibodies (164) most likely due to the depletion of B cells proliferating into plasmablasts or plasma cells.

Fingolimod (Gilenya)

A more recent drug treatment applied to MS is fingolimod, an anti-sphingosine-1-receptor (S1P) antibody which blocks the egress of lymphocytes from secondary lymphoid tissue (165), leading to decreased global levels of circulating lymphocytes (166). These sequestered B and T cells still have the capacity to proliferate and make antibodies but physiologically are unable to leave the lymphoid tissues (167). In a 2-year phase 2/3 trial of fingolimod treatment in RRMS patients, patients had reduced annual relapse rate, disability progression, and new lesions on MRI (168). Fingolimod treatment of MS patients significantly reduced the levels of CSF lymphocytes but had no effect on intrathecal IgG levels and B cells were still present in the CSF (169) possibly due to a CNS compartmentalized regeneration of B cells in these patients.

Natalizumab (Tysabri)

Natalizumab is an anti-very-late-antigen-4 (VLA-4) antibody designed to block the entry of any immune cells into the CNS (170-173) leading to the increased retention of these cells in the periphery (174). In a 2-year phase 3 trial of natalizumab treatment, RRMS patients receiving the drug had reduced relapse rates and fewer new lesions as defined by MRI (175). Memory B cells express high levels of VLA-4 and utilize this to pass through the BBB into the CNS (116). Levels of B cells in the CSF are significantly decreased after treatment with natalizumab (169, 173) and remain low even 6 months after cessation of treatment (172). Circulating peripheral B cells increased 2.8 fold while other lymphocytes increased 1.5 fold 16 months after natalizumab therapy (176). Interestingly, a study of clinical response to the treatment showed that 44% (n=10/23) of the patients that remained relapse free had no difference in $CD4^+$ T cell levels but had

significantly lower intrathecal Ig synthesis levels and lower plasmablast levels (fell from 1.7%-0% in responding patients vs 2.3%-0.4% in non-responders) (177). One year after natalizumab treatment, levels of the neurodegeneration marker neurofilament (NF) light chains in the MS CSF were reduced to normal levels (178) indicating that this drug can help prevent axonal damage.

Rituximab (Rituxan)

Most interestingly, the clinical use of rituximab, a chimeric anti-CD20 B cell depleting antibody, has also provided evidence for the pathological role of B cells in MS. This was first used as a treatment for B-cell non-Hodgkin lymphomas and B cell malignancies expressing CD20. Rituximab treatment decreases brain inflammation in RRMS (179-181) and SPMS patients (182), with similar results seen with the humanized version ocrelizumab in RRMS patients (183). It also reduced the severity of recombinant human MOG-induced EAE in hCD20tg mice with reduced T cell responses and anti-MOG IgG levels (184). Reduced total IgG levels were not observed in patients who responded to rituximab therapy although they demonstrated a reduction in relapses and new lesion formation suggesting that B cells' main contribution to pathology is through APC functions and activation of T cells. However, in other autoimmune diseases treated with rituximab there are significant decreases in the disease-associated IgG but not the total levels of IgG.

Rituximab depletes both naïve and memory B cells. A high amount of antigen in an autoimmune setting promotes production of short-lived plasmablasts from memory precursors. This memory B cell pool is depleted after rituximab treatment, resulting in a decline of plasmablasts as well as autoantibody titers (185). In fact, levels of memory B

cells in NMO patients treated with rituximab mirror the levels of anti-aquaporin-4 (AQP4) antibodies with clinical relapses associated with peaks in both (186), suggesting that the plasmablast pool is replenished from the memory B cell pool. Vasculitis patients with somatically mutated and IgG class-switched antibodies against neutrophil serine protease protinase-3 (PR3) who responded favorably to rituximab treatment had concomitant reductions in anti-PR3 antibody levels without any significant differences in total IgG levels (187). Similarly, in systemic lupus erythematosus (SLE) patients, early relapse post rituximab treatment was associated with increase in autoantibody titers to dsDNA and Ro/SSA, with total IgG and responses to microbial antigens remaining unchanged in either patient group (188, 189). This trend of a specific reduction in autoantibodies and not total IgG is also seen in thrombotic thrombocytopenic purpura (190), RA (191, 192), pemphigus (193), anti-MAG neuropathy (194), and myasthenia gravis (195). Therefore, it is still too early to dismiss the therapeutic scope of rituximab on autoantibody levels in MS since the target auto-antigen(s) remains unknown.

Plasmablasts and autoimmunity

Plasmablasts are short-lived antibody producing cells and are identified by high levels of CD27 (196). CSF plasmablasts have been identified as the main effector B cell in active MS, levels correlate with disease activity as evidenced by MRI (117), and are clonally related (197). Treatment with natalizumab was effective in MS patients if they had lower levels of CSF plasmablasts before treatment and maintained low levels post-treatment (177). An abnormal expansion of $CD27^{high}$ plasmablasts has been documented in the afflicted compartments of several autoimmune diseases such as RA (198-200),

Sjogren's syndrome (142), SLE (200), pediatric SLE (201), NMO (202), ankylosing spondylitis (203), and pediatric ulcerative colitis (204).

Altered B cell repertoires in MS

The V_H chain has a larger number of contacts with the antigen and can impart a greater impact on antigen binding (205), though not always. Normally, the V_H repertoire has family usage that roughly mimics the germline prevalence of the available genes with V_H3 being the most commonly used family (46%) followed by V_H4 (21%), V_H1 (19%), V_H2 (6%), V_H5 (4%), V_H6 (2%), and V_H7 (2%) (206-210); this has been reconfirmed more recently using next generation sequencing (NGS) (208). A meta-analysis approach surveying V_H repertoires across various methodologies has found that the V_H gene usage is surprisingly constant between individuals (210). Analysis of Ig variable region repertoires offers additional evidence of a dysregulated B cell response in MS and CIS patients. Clonal expansion, accumulation of SHM, and class switched Igs are indicative of an antigen-driven B cell response. Dominant B-cell clones are found within CNS (211-213) and CSF (214-221). This also occurs at the early CIS stage of disease (216, 222, 223). Also, the MS CSF B cells accumulate high levels of somatic mutations and undergo the process of intraclonal diversification (214, 215, 218, 219). Conversely, class-switched marginal zone B cells isolated from mice, which do not participate in the GC reaction, have significantly lower levels of mutations than follicular B cells from the same mouse (224). Mice lacking AID have reduced severity of EAE disease accompanied by lower recall responses in $CD4^+$ T cells to myelin peptides (225) demonstrating the importance of SHM diversification of the B cell repertoire.

Previous work in our laboratory has demonstrated that MS CSF derived B cells undergo typical GC reactions (214, 220), as evidenced by mutational targeting to CDRs typical of GC selection (226, 227). 75% of MS patients (n=6/8) had CSF V_H repertoires with significantly higher mutation frequency (MF) accumulation compared to peripheral blood from healthy individuals (220). We have also reported clonal expansion of the V_H repertoire within the MS CSF (214, 220). Furthermore, intraclonal diversification and receptor editing of the Ig were evident (214). Our laboratory has also published a unique pattern of SHM in CSF V_H4^+ B cells from ON_{CIS} and MS patients indicative of similar auto-antigenic pressures (228).

Altered B cell repertoires have been isolated from the CNS tissue of MS patients. MS CNS Ig analysis by complementarity determing region 3 (CDR3) spectratyping revealed that V_H1 and V_H4 had the most OCBs (212). Further sequencing of these V_H4 and V_H1 samples showed clonal expansion in both (212). IgGs isolated from CNS tissue from both MS and measles infection of the CNS patients were analyzed to determine if the V_H gene usage would be similar in either case of neuroinflammation (229). In MS patients, V_H4 dominated (60%) while in measles CNS V_H1 dominated (43%) (229) illustrating that V_H4^+ B cells are characteristic of MS neuroinflammation. Additionally, these V_H4^+ IgG were all mutated and displayed GC-like targeting of an increased replacement to silent mutation ratio (R:S) in the CDR (229). Some of the V_H sequences found between two lesions within the same patient were shared but the majority were unique (229).

MS CSF, more readily accessible compared to CNS, also reveals altered B cell repertoires. CSF B cells from patients with either MS or viral meningitis patients were analyzed to determine whether clonal expansion would be similar in either case of

neuroinflammation (217). The viral meningitis patients (n=2) had a predominantly polyclonal response with equal amounts of IgG^+ and IgM^+ B cells while half (n=2/4) of the MS patients had a dominant IgG^+ B cell population, 1 had equal IgG^+ and IgM^+, and 1 had an IgM^+ populations (217). However, upon closer examination of the IgG repertoires, all MS patients had clonally expanded IgG sequences, with only one patient having an IgM clone (217). A similar study was done comparing the CSF repertoires of MS and other neurological disease (OND) patients including viral encephalitis and meningitis and also found an oligoclonal response in all the MS patients (n=10) and in 30% (n=3/10) of the OND, of which had CNS infections (218). The oligoclonal response in the MS patients had evidence of intraclonal diversification, which was absent in the OND patients (218). Another study also found a dominant V_H4 mutated and clonally expanded presence in the CSF of MS patients (215). V_H sequences isolated from both $CD19^+$ B cells and $CD138^+$ plasma cells from the CSF of MS patients also demonstrated mutated and clonally expanded repertoires in each of the populations (230). About 55% (B cell) and 70% (plasma cell) of the CSF repertoires were V_H4 family member genes, while in the PB of both MS and HC equal V_H4 usage was seen (32% and 23%) (230). This suggests that an abnormal expansion of V_H4 B cells may reflect responses to CNS antigens.

Comparisons of which B cells continue to develop into plasma cells was carried out by comparing the repertoire of $CD19^+$ B cells and $CD138^+$ plasma cells isolated from the CSF of 3 MS patients (221). Expanded and mutated clones were found in both populations with little sequence overlap between the $CD19^+$ B cells and $CD138^+$ plasma cells (221). This may be due to the relatively few number of sequences obtained, which may have missed some of the related V_H sequences. Alternatively, a small subset of B

cells may be responsible for the plasma cell population. A similar finding of infrequent overlap between the two B cell populations was also seen in CIS CSF (222). However, one study of 2 MS CSF repertoires reported shared V_H sequences between clonally related plasmablasts and plasma cells (197). V_H4 dominates the IgG (subclass unknown) plasma cells (67%) but not the IgM plasma cells (19%), and V_H1 genes are present in roughly 2% of the plasma cells (221). This demonstrates that the V_H4 expansion documented by others may be clinically relevant since they are present in the class switched complement-activating IgG class of antibodies.

Clonal expansion and a bias of V_H4 usage are already evident in CSF B cells isolated from ON_{CIS} patients but not in the periphery of the same patients (57% and 16%) (222). In the small study group, patients with either V_H4 or V_H2 repertoire bias progressed to CDMS within 2 years compared to those without this bias (222). Another similar study of B cells and plasma cells from ON_{CIS} patients demonstrated clonal expansion (17-75%) and evidence of intraclonal diversification within the members (223). In analyzing CDR3 regions, another group showed that 81% (n=13/16) of CIS patients have clonally expanded B cells in the CSF (compared to 9% ONDs, those positive had herpes or acute disseminated encephalomyelitis (ADEM) (216). Furthermore, 77% of the CIS patients that had clonally expanded B cells in the CSF converted to CDMS 1-6 years later (216), suggesting that this early expansion of B cells places the patient at a high risk to convert. Contrary to other reports, V_H3 dominated over V_H4 in the clonally expanded members but this could be due to a low number of clones analyzed (n=12) or to catching these patients at a very early stage where the V_H4 clones have not yet expanded fully (216). Overall, the repertoire had proper GC-like targeting to increased R:S within the

CDR vs FR (216) indicating an early antigen driven response is already occurring in these CIS patients.

A proteomic profile of CSF-derived Ig in MS and healthy controls undergoing anesthesia procedures was created to identify shared patterns of peptide sequences among the patient groups (231). Not surprisingly, they found an increase in V_H4 gene usage in MS patients compared to healthy individuals (231). Interestingly, 3 V_H peptides were shared between 3 or more of the 29 MS patients tested, which were all part of the CDR2, but they found no similar peptides among the proteome of the 30 healthy controls (231). This reinforces the hypothesis that similar auto-antigenic pressure drives mutation and gene selection of the Ig produced by activated MS B cells. A paired study of B cells from the CSF (proteome and transcriptomes) and CNS (transcriptomes) of the same MS patients found a strong overlap of V_H sequences (39-84%) between the compartments suggesting that the CSF reflects the CNS B cell compartment (232). They also found 3 dominant heavy chain genes used in the CSF B cells: 2 V_H4 genes and 1 V_H3 gene (232). The CSF proteome was compared to the transcriptome, to determine if the CSF B cells produce the Ig in the CSF, and it was found that they are closely related and predominately of the V_H4 family (233). Furthermore, 91-100% of the V_H sequenced belonged to the IgG_1 class and were somatically mutated, compared to only 17% IgG_1 found in healthy serum (233). Finding shared clonally expanded, mutated, and class switched B cells in both the CSF and CNS provides support for CSF repertoire analysis in reflecting what is present in the diseased CNS tissue.

Additional compartments have been simultaneously analyzed: V_H repertoires from MS meninges, plaques, NAWM, and CSF were examined to study the spread of B cell clones throughout the parenchyma (234). Clonal expansion in the meninges and

parenchyma was similar (24% and 28%) and both had dominant IgG representation (~90%) (234). There was some overlap between the two compartments, but when this was analyzed for only the clonally expanded and mutated sequences there was a range of 39-62% overlap in all patients tested (234). V_H4 usage was dominant in the plaques as expected, but also in the NAWM and meningeal repertoires (234).

However, comparing the V_H repertoire in paired CNS and PB MS patient samples revealed unique clones in each compartment suggesting a compartmentalization within the CNS (211). This was also found in a study of paired CSF and PB MS patient samples (218). Due to the emergence of next generation sequencing (NGS), the amount of sequences isolated from each patient has increased so that rare sequences are more easily detected. Using NGS, evidence of clonal exchange across the BBB with shared members in the peripheral blood (PB) and CSF of MS patients was detected albeit at low levels (~2%) (121).

Longitudinal studies of V_H repertoires isolated from MS CSF has identified related clonal members detected 4 years after initial sampling (219) with intraclonal diversity suggesting a continued antigen-driven response. A bias of V_H4 usage was also detected in the CSF plasma cells of a patient 3 years after initial sampling (230). Intraclonal diversification has been detected in the B cells from MS CSF (214, 218) and in one MS CSF patient, the same clones were detected 1 year later (218), again reinforcing the hypothesis of continual selective stimulation. Characterization of the altered B cell repertoires can offer insight into the antigens driving MS disease. This shared bias of V_H4 usage, clonal expansion, GC-like mutation targeting to CDR, class switched IgG, and increased mutation accumulation in the diseased CSF and CNS strongly suggests a shared set of auto-antigens driving activation of B cells.

Putative auto-antigen targets in MS

There are many possible auto-antigens (235-237), especially because MS is a heterogeneous disease with both WM and GM involvement. About 50 years ago, *in vitro* experiments of EAE sera demonstrated the ability of a humoral component to induce demyelination (238, 239). In the late 1980s, passive transfer of antibodies against myelin oligodendrocyte glycoprotein (MOG), a myelin component, induced demyelination in EAE models (240, 241) offering a clue that antibodies could mediate damage. Since then, research has been heavily focused on myelin components as immunological targets of MS disease. Novel non-myelin components have also been investigated as potential targets. Additionally, some posit that polyclonal activation of B cells by EBV infection can cause an exaggerated humoral response contributing to MS disease (242, 243) or that cross-reactivity between a pathogen and self can lead to autoimmunity (244, 245). Detection of candidate auto-antigens is predominately done by screening the reactivity of MS serum or CSF while other approaches include cloning of rearranged antibody gene segments isolated from MS patients and using these as molecular probes (235, 246). Both potential myelin and non-myelin targets are listed in Table 1-2.

Myelin components

Due to the fact that demyelination is a hallmark of MS disease, there has been substantial work focused on determining which myelin components are the target of the humoral response. These targets are also attractive candidates in a CNS-restricted disease since proteolipid protein (PLP) and myelin basic protein (MBP) account for over 50% and 30%, respectively, of the CNS myelin (247). In the peripheral nervous system (PNS),

PLP is minimal and MBP represents only 5% of the myelin (247). There is support for anti-myelin antigens being a target for part of the humoral response in CIS (248, 249), MS (250-255), and EAE (240, 256-258). There have been reports of a more severe disease course correlated with increased levels of anti-MOG antibodies (259, 260) although other reports do not see any relationship between anti-MOG titers and relapse, EDSS, or MRI measures (251, 261, 262).

However, there is debate in the field as to the specificity of anti-MBP and anti-MOG antibodies for MS as they can also be detected in healthy people (263), other neurological diseases (264), are of low affinity in MS patients (265), and do not recognize refolded MOG (266). This may be partly due to the fact that autoantibodies are enriched in the CNS tissue and thus not circulating in the PB or CSF (252), or that they are not major contributors to MS disease pathology. Two immunohistochemical studies of cloned antibodies from MS CSF did not show any staining to NAWM or the three major myelin proteins: MOG, MBP, or PLP (267, 268). Additionally, a flow based assay with whole human myelin from CNS tissue to preserve both conformation and post-translational modifications, found that half of the MS serum bound to this presentation of MOG while only 3% bound to traditionally purified MOG (251) illustrating complex recognition beyond singular protein candidates. This also suggests that these antibodies are recognizing conformational discontinuous epitopes. While serum from some MS patients had the ability to demyelinate and damage axons *in vitro*, commercial anti-MBP or anti-PLP antibodies were unable to elicit the same damage (269) either due to being raised to altered epitopes or not recognizing the cellular presentation of the epitopes. This further illustrates the complexity of potential demyelinating targets from MS antibodies beyond that of the traditional myelin components.

Oligodendrocytes

Oligodendrocytes are the specialized CNS cells that make the myelin sheath around axons. If these are targeted by the immune system, the remyelinating capacity of the CNS is reduced. In fact, as disease progresses it becomes less likely that a lesion will be repaired and remyelination becomes more sparse (270). Incubating CSF from active MS, and not quiescent disease, with a myelinating culture *in vitro* lysed oligodendrocyte progenitor cells in the presence of added complement (271), but it is unknown if this damage is due only to complement mediated lysis or to other damaging factors in the CSF from the patient. Increased levels of intrathecal anti-nogo-A (transmembrane protein on oligodendroctyes) antibody were seen in MS (272). 2-3-cyclic-nucleotide 3-phosphodiesterase (CNPase), another oligodendrocyte membrane protein, was identified as a target using proteomics approaches (273) and also isolated from immune complexes deposited in the CNS (274). One group found reactivity to oligodendrocyte specific protein in MS using denatured protein on a western blot to detect CSF antibodies (275). However, this may be an epiphenomenon of post damage clean up as this finding was later refuted using a cell-based methodology to preserve the native conformation of oligodendrocyte specific protein (276). Transaldolase in oligodendrocytes, needed for producing large amounts of lipids, is diminished along with MBP within lesions and anti-transaldolase, but not anti-MBP, antibodies were found in MS CSF (277, 278). Oligodendrocytes may be potential targets present in some MS patient's B cell pool, which could contribute to demyelination.

Neurons and axons

Neurons and axons can be the primary targets for the humoral response rather than the traditional myelinating cells and the sheaths themselves. Incubation of CSF from aggressive RRMS with neurons *in vitro* induced cell damage, transected axons (279), and correlated with poor recovery post relapse (280). Antibodies isolated from clonally expanded B cells within MS lesions and CSF bind to axons (281, 282). Additionally, rats immunized with rMOG develop disease with axonal transection and apoptotic retinal ganglion neurons (283). A loss of neuronal precursors can reduce the ability of oligodendrocytes to remyelinate lesions (284) and have been identified as a putative cellular target in a flow cytometric assay using MS serum (285).

The most commonly studied neuronal auto-antigen is the neurofilament (NF) comprising the cytoskeleton. Increased level of heavy NF in the CSF, presumably released after neuronal damage, is associated with increased disability and MS relapses (286-288). Additionally, antibodies to both the heavy and light NF are detected in CSF and are associated with more aggressive disease from both MS (289-291) and CIS (288) patients indicating that axonal damage occurs at the earliest disease step. Immunization of mice with light NF induced an EAE disease with axonal degeneration in both the WM and GM of the spinal cord with an "inside-out" demyelinating process with axonal death preceding subsequent myelin sheath degradation (292, 293). Elevated CSF antibodies to tubulin, another neuronal cytoskeletal protein, are also detected in MS CSF (294, 295). Neurofascin at the axo-glial junction was identified as another axonal auto-antigen targeted in MS (296, 297), which could potentially block remyelination (298). Contactin-2 is another component in the axo-glial junction that was identified as a MS immune target through both autoantibody production and T cell proliferation, and also induces an

EAE disease with dominant GM damage (299). Neuron-specific enolase autoantibodies and auto-reactive T cells are detected in MS patients (300) and levels of neuron-specific enolase are increased in early EAE disease (301). Neuronal targeting is evident in tandem with myelin targeting during MS disease and may explain the prevalence and significance of GM damage in the disease.

Astrocytes and BBB

Astrocytes in the CNS are necessary to maintain the BBB as well as homeostatic support to surrounding cells in the CNS. Astrocyte damage occurs early in the inflammatory MS lesions (302). Astrocytes have been shown to be critical in promoting the remyelinating ability of oligodendrocytes (303, 304) and increase the ability for the BBB to heal after an assault (305). Antibodies against the astrocyte protein, GFAP, are present in the early pre-clinical stages of guinea pig EAE (306) and axonal/myelin damage at the same stage is detected in the same areas as astrocyte damage (307). AQP4 on astrocytes is a well-described target auto antigen on astrocytes in the related autoimmune disease NMO. Antibodies to AQP4 are diagnostic for NMO patients, pathogenic, and produce NMO-like lesions in mice (308-310) even in the absence of antigen-specific T cells (311-313). In MS serum, a recent study has identified the astrocyte protein KIR4.1 as a potential humoral target and this serum disrupted astrocyte morphology after injection into mice (314).

Another route in disrupting the BBB is with immune responses directed to the BBB itself. Both active and, to a lesser extent, inactive MS lesions have vessels disrupted in the BBB (16). Serum from active MS patients, but not inactive patients, stained brain microvascular endothelial cells and this staining correlated with increased number of

lesions by MRI (315) reflecting a breach of the BBB. Antibody binding to human umbilical vein endothelial cells was seen using serum from both MS and NMO patients, and correlated with increased spinal cord lesions and relapses in the MS cohort (316). Serum from SPMS patients induced both neuronal damage *in vitro* and a reduction in BBB proteins in an endothelial culture (317). Interestingly, *in vitro* cultures simulating the BBB have the highest functionality and resistance to permeability when both astrocytes and neurons are present to synergistically induce the endothelial cells to form a BBB (317, 318). Therefore, there may be complex physiological effects resulting from immune mediated targeting and damage of any of the major CNS cellular components.

Summary

Evidence of clonally expanded and mutated B cells in MS and their proximal location to diseased tissue suggests that B cells are responding to CNS auto-antigen(s). This in conjunction with the wide array of putative auto-antigens proposed in the field and the heterogeneity of disease presentations and symptoms suggests that the targets are most likely complex and numerous. The aim of my work was to expand on the initial finding in the laboratory of a shared set of SHM rearranged immunoglobulin genes (the antibody gene signature (AGS)) in the CSF B cell repertoires of MS and high-risk ON_{CIS} patients. We sought to determine whether this signature could also be detected at the site of disease within the CNS tissues. Also, we recruited TM_{CIS} patients to determine the prevalence of the AGS in the other major CIS presentation. Furthermore, a more detailed analysis of both B cell subpopulations and BCR genomics was conducted to identify possible differential B cell representations and genomic pressures in TM_{CIS} patients compared to ON_{CIS} patients. After further characterizing B cell subpopulations and mutation patterns, the underlying goal was to determine the biological impact of a shared

mutation pattern on antibody targeting. A series of immunohistochemical techniques were employed to elucidate the biological relevance of the AGS in the targeting of antibody molecules to CNS tissue. Genomic and targeting studies of MS and CIS B cells could provide for a better understanding of the underlying pathological mechanisms of disease in order to offer future directives in the clinical care of these patients.

TABLES FOR CHAPTER ONE: INTRODUCTION

Table 1-1: Immunomodulatory therapeutics in MS and their B cell inhibitory effects		
Drug	***Inhibitory effects on B cells in MS patients***	***References***
IFN-β	Reduces the levels of $CD40L^+$ T cells, reduces costimulation	(147)
	Reduces expression of CD40 and CD80 on B cells	(148)
	Reduces class-switched memory B cells and increased naïve B cells in periphery	(119)
	Reduces IL-12 and increased IL-10 levels in serum, inhibitory	(149)
Glatiramer acetate	Reduces TNFα, IL-12 and increased IL-10 levels in serum and from monocytes, inhibitory	(158, 159)
	Reduces *in vitro* $CD8^+$ T cell proliferation cultured with B cells and GA	(160)
Mitoxantrone	Immunosuppressant and reduces antibody secretion	(164)
Fingolimod	Blocks egress of lymphocytes from secondary lymphoid tissue	(165, 167)
Natalizumab	Blocks entry of immune cells into the CNS	(170-173)
	Significantly reduces B cells in CSF	(169, 172, 173)
	Patients who respond well have lower intrathecal Ig synthesis and CSF plasmablasts	(177)
Rituximab	Depletes B cells, which reduces brain inflammation and relapses, no difference in intrathecal Ig synthesis	(179-182)
Ocrelizumab	Depletes B cells, which reduces brain inflammation and relapses, no difference in intrathecal Ig synthesis	(183)

Table 1-2: Highlighted putative auto-antigen targets in MS		
Target	**Evidence**	**References**
Myelin components		
MOG	Anti-MOG in patient serum/CSF	(248-250, 253, 254, 259)
	Antibodies purified from CNS bind to MOG	(252)
	Serum from high-titered of anti-MOG patients stain WM tracts	(250)
	Transfer of anti-MOG antibodies exacerbates EAE	(240, 241, 319)
MBP	Anti-MBP in patient serum/CSF	(248, 249, 259, 320)
	Cloned antibodies from CSF bind to MBP	(255)
PLP	Fusion MBP-PLP protein induces antibody mediated EAE	(257)
	Anti-PLP in patient CSF	(321)
	Antibodies from PLP induced EAE bind to myelin and neurons	(322)
Whole myelin	Anti-myelin binding IgG in CSF	(249, 251)
	Patient serum/CSF tested on arrays reacts to multiple myelin components	(236, 323-325)
	In vitro demyelination from incubation with serum from MS and EAE	(238, 239, 269)
Oligodendrocytes		
OPCs	*In vitro* OPC death from incubation with patient CSF	(271, 326)
	Anti-OPC in patient serum	(285)
Nogo-A	Anti-NogoA in patient serum/CSF	(272)
CNPase	Cloned antibodies from CSF bind to CNPase	(255)
	Anti-CNPase in patient serum/CSF	(273, 274)
OSP		
Transaldolase	Anti-transaldolase in patient serum/CSF	(277)
Neurons and axons		
Axons	*In vitro* axonal damage from incubation with patient CSF	(279)
	Bound antibodies to axons in CNS lesions	(282)
	Cloned antibodies from CSF bind to axons	(281)
NPC/neurons	*In vitro* neuron damage from incubation with patient serum	(317)
	Anti-NPC and neuron in patient serum/CSF	(285, 327)
	MOG induced EAE had apoptotic retinal neurons	(283)
NF	Anti-NF heavy in patient CSF	(288)
	Anti-NF light in patient CSF	(289, 290)
	NF light induced EAE had GM and myelin lesions	(292, 293)
Tubulin	Anti-tubulin in patient CSF	(294)
Neurofascin	Anti-neurofascin in patient serum	(296)
	Anti-neurofascin transfer exacerbated EAE	(296)
Contactin-2	Anti-contactin-2 in patient serum	(299)
	Contactin-2 induced EAE had GM lesions	(299)
Astrocytes and BBB		
GFAP	Anti-GFAP in early EAE serum	(306)
KIR4.1	Anti-KIR4.1 in patient serum and transfer into mice disrupted astrocytes	(314)
Endothelial cells	Anti-endothelial cell in patient serum	(315, 316)
	In vitro BBB damage from incubation with patient serum	(317)

CHAPTER TWO

METHODOLOGY

Overview of patient sample acquisition

Cerebrospinal fluid (CSF) was obtained by lumbar puncture and peripheral blood (PB) by venipuncture on the same day from patients recruited to be in a study at UT Southwestern Medical Center (UTSWMC) in accordance with the UTSWMC Institutional Review Board (IRB). None of the patients had received immunomodulatory agents for at least one month prior to lumbar puncture. The PB cells were centrifuged after being underlaid with a polysaccharide Ficoll gradient that collects the peripheral blood mononuclear cells (PBMCs) in a separate layer. The cells were then washed, counted, stained with fluorescently labeled antibodies, and sorted for bulk populations of $CD19^+$ B cells, $CD4^+$ T cells, $CD8^+$ T cells, and $CD138^+$ plasma cells through a $CD45^+$ lymphocyte gate. CSF cells were collected as a pellet after centrifugation, washed, counted, stained with fluorescently labeled antibodies, and sorted for single $CD19^+$ B cells through a $CD45^+$ lymphocyte gate. A second blood sample was obtained from four TM_{CIS} patients and these were sorted for single cells through a $CD45^+$ lymphocyte gate to separate the $CD19^+CD27^+$ memory B cell and the $CD19^+CD27^{high}$ plasmablast populations.

The plasma, CSF supernatant, unused PB lymphocytes, sorted PB populations, and sorted CSF populations were all aliquoted and archived in freezers. Single sorted plates were stored at -80°C until processed for cDNA primer extension preamplification (cPEP). During all sorts, flow cytometry data were collected for immunophenotype analyses on both the PB and CSF. Available clinical information from CSF diagnostic

tests (CSF Ig synthesis rate and CSF Ig index), as well as patient age and disease duration at time of lumbar puncture sampling were obtained in accordance with the UTSWMC IRB.

A total of 46 samples were collected, 42 were paired PB and CSF samples and the remaining 4 were a second PB draw from 4 previously sampled TM_{CIS} patients. The diagnosis at the time of sampling for the 42 paired samples are: 3 CDMS, 20 TM_{CIS}, 7 ON_{CIS}, 7 undefined CIS, 2 PND, and 2 NMO patients. 6 patients were male (14%) and the remaining 36 were female (86%). The median age was 40 and the average was 43. 8 additional postmortem B cell V_H repertoires from MS CNS tissue were generated by collaborators.

Peripheral blood (PB) processing for flow cytometry

PB was acquired by venipuncture into an EDTA tube, with a median of 5.5 mL per patient sample. The blood was diluted with an equal amount of 1x PBS and was underlaid with a matching volume of Ficoll to the original blood. Alternatively, the blood and PBS mixture was overlaid onto the Ficoll layer. A Ficoll gradient was created by centrifuging at 1900 rpm for 25 minutes at room temperature without a brake, to not disturb the gradient layers formed. The top layer of plasma was removed, aliquoted, and archived at -80°C for downstream ELISA assays. The peripheral blood mononuclear cells (PBMCs) were pipetted from the buffy coat layer between the plasma and the high-density erythrocytes and granulocytes at the bottom. These PBMCs were diluted to a final volume of 10 mL with PBS and passed through a mesh cell strainer into a 50 mL conical tube. 40 mL of PBS was passed through the mesh cell strainer to wash the cells. A 10 μL

sample was removed and diluted with 90 μL of trypan blue (1:10 dilution) for counting cells in a hemacytometer. The cell count and initial sample volume were recorded. The PBMCs were washed to remove the excess Ficoll by centrifuging the diluted 50 mL mixture at 1500 rpm for 5 minutes at 4°C. The pelleted cells were resuspended in FACS Buffer (filtered 4% heat inactivated FCS in PBS) to achieve a cell concentration of $2x10^6$ cells per mL. A total of $5.5x10^6$ cells were reserved for fluorescent staining for FACS analysis and the remaining were resuspended in freezing media and placed in cryotubes for archiving at -120°C.

Cerebrospinal fluid (CSF) processing for flow cytometry

CSF was acquired by lumbar puncture, with a median of 11 mL per patient sample. The CSF was centrifuged at 1000 rpm for 12 minutes at 4°C. The CSF supernatant was removed, aliquoted, and archived at -80°C for downstream ELISA assays. The pelleted cells were resupended in 1 mL of FACS Buffer. A 10 μL sample was removed and diluted with 10 μL of trypan blue (1:1 dilution) for counting cells in a hemacytometer. The cell count and initial sample volume were recorded. All the cells were utilized for fluorescent staining for FACS analysis.

Usage of HMv3 Cocktail

In cases were the patient sample was received and a FACS sorting appointment could not be immediately made, the HMv3 cocktail was used to maintain the cells overnight or up to 2 days. After centrifuging the CSF to obtain the cells, the pellet was resuspended in 300-400 μL HMv3 cocktail (a proprietary mixture). After washing and

obtaining the PBMCs, the pellet was resuspended in 700 μL HMv3. Both samples were stored on ice overnight at 4°C. After further experience, the PBMCs were no longer stored with HMv3 and were instead kept overnight in the EDTA tube on a slow speed rocker to avoid coagulation.

Fluorescent labeled antibody staining for flow cytometry

All analyses were conducted using a 6-color fluorochrome flow cytometry panel. Cells were pipetted into round bottom polypropylene tubes: $5x10^5$ PBMCs (250 μL) per compensation stain, $2x10^6$ PBMCs (1 mL) for PB full color stain, and all CSF cells (1 mL) for full color stain. FACS Buffer was added to each tube for a final volume of 2 mL and centrifuged at 1500 rpm for 5 minutes at 4°C. After the centrifugation, the supernatant was removed using a vacuum aspirator. The resuspended cells were incubated with 20 μL blocking buffer (780 μL FACS buffer with 20 μL mouse sera) for 10 minutes on ice. Fluorescently labeled antibodies (Table 2-1) were added to the appropriate tubes: 1 compensation tube with no antibodies, 6 compensation tubes with an individual fluoresencently labeled antibody, and 2 full 6-color panel tubes (PB and CSF). The volumes of each antibody added were according to manufacturer's recommendations (Table 2-1). The single-color compensation tubes used the same antibody as was utilized for the full 6-color panel except for PE. CD138-PE was switched to CD8-PE for compensation due to the normally very low abundance of $CD138^+$ cells in the samples. The cells were incubated for at least 30 minutes on ice and protected from light exposure. After the incubation, the excess antibodies were washed with 1 mL of FACS buffer and centrifuged at 1500 rpm for 5 minutes at 4°C. The supernatant was removed using a

vacuum aspirator. The cell pellets were resuspended in 150 μL Flow sugar mix (120 mL colorless RPMI, 4.8 mL FCS, 120 μL 100X insulin-transferin-selenium, 1.23 mL L-glutamine). The cells were kept on ice and protected from light exposure during flow cytometry transport.

Single-cell and Bulk-cell sorting

Flow data were collected and sorts were performed on either the FACS Aria flow cytometer (Becton Dickinson, San Jose, CA) or the MoFlo High-Performance Cell Sorter (Cytomation, Ft. Collins, CO). Flow cytometry data were collected in conjunction with cell sorting for analysis of lymphocyte subpopulations. Events were collected and analyzed post-sort with Flowjo Software (Treestar). Cells were gated on live and single cells based on forward scatter (FSC) and side scatter (SSC) characteristics. Within this gate, a $CD45^+$ lymphocyte gate was created and all cell population analyses were conducted within this gate. The gating was created and compared in parallel using the CSF and PB data from the same patient. Sample gating strategy is shown in Figure 2-1. The patient information and cell population percentages for each sample are shown in Table 2-2 for the CSF compartment and Table 2-3 for the PB compartment.

Dot-plot scatter view was used for sorting all populations into appropriate gates. The gating strategy was a single cell live gate (FSCxSSC) followed by a lymphocyte gate ($CD45^+$). Bulk-cell sorts were conducted on the PBMCs and collected in FACS tubes containing 250 μL of Flow sugar mix. Four populations were collected: $CD4^+$ T cells, $CD8^+$ T cells, $CD19^+$ B cells, and $CD138^+$ plasma cells. The number of events sorted into each of the populations was recorded and purity was tested using the $CD4^+$ population.

Upon returning to the laboratory the sorted cells were transferred to 1.7 mL snap-cap tubes and centrifuged at 1500 rpm for 5 minutes at 4°C. The supernatant was removed using a vacuum aspirator and the tubes were snap-frozen using liquid nitrogen. Cells were archived at -80°C and their location was logged.

Single-cell sorts were conducted on CSF cells into 96-well PCR plates containing 4 μL of cDNA primer extension preamplification (cPEP) sort mix in each well, described in further detail within section "*cDNA primer extension preamplification (cPEP)"*. One $CD19^+$ B cell was sorted into each well and the number of wells sorted was recorded. If there was a sufficient amount of cells, the last well contained 100 sorted cells. This bulk well served as a PCR positive control and was used for downstream analysis for next-generation sequencing (NGS) in comparison to the single-cell sequencing. Many patients did not have enough cells sorted in order to generate a B cell repertoire, but all had sufficient cells for immunophenotype characterization. Four TM_{CIS} patients had blood re-sampled and single-cell sorts were done in the same manner as the CSF sorts. Instead of total $CD19^+$ B cells, 2 plates of $CD19^+CD27^+$ memory B cells and 2 plates of $CD19^+CD27^{high}$ plasmablast cells were sorted per patient. All plates were sealed and frozen immediately on dry ice post sort to help preserve the mRNA for efficient cDNA creation downstream. Upon returning to the laboratory, the plates were stored at -80°C until cPEP was conducted.

Designation of TM_{CIS}A and TM_{CIS}B patient subgroups

The patients were divided into two groups by the initial clinical presentation of disease. The ON_{CIS} group (n=11) presented with optic neuritis (ON) and the TM_{CIS} group

(n=22) presented with transverse myelitis (TM). The TM group was further divided into TM_{CIS}A(Above) and TM_{CIS}B(Below) based on the percentage of $CD19^{+}CD27^{high}$ plasmablast cells determined by flow cytometry. The threshold for the TM_{CIS}A group was determined by calculating the mean percentage of $CD19^{+}CD27^{high}$ plasmablasts in the ON_{CIS} patients and adding two s.e.m. Patients whose percentage fell below this threshold were designated TM_{CIS}B, and those whose percentage fell above this threshold were designated TM_{CIS}A. This grouping was done separately for both the PB and CSF compartments.

cDNA primer extension preamplification (cPEP)

The original mRNA from each single well was reverse transcribed into cDNA using modifications to a previously described procedure (328). The 96-well plates were stored at -80°C post sort with cells frozen in 4 μL cPEP sort mix (10% 0.1M Dithiothreitol (DTT), 9% recombinant RNAsin (Promega) in 0.5x PBS). The cDNA was made within the same plate, in a sterile RNA and DNA free environment including the storage space, working space, reusable and disposable components, equipment, and a dead-air hood. The plate was kept either on a bed of dry ice or on a metal plate holder previously stored at -20°C. 3.5 μL of the random hexamer primer (RHP) mix was added quickly to each well with a multi channel pipette to prevent the mix from freezing in the pipette tip. This step also included a surfactant (10% Igepal CO-630) to break open the cell membrane without disrupting the nuclear membrane, resulting in clean access to mRNA. The plate was sealed and placed in a PCR cycler (Eppendorf Mastercyclers) and incubated for 1 minute at 68°C. After the incubation, the plate was removed and cooled

on an ice block. The plate was then transferred to a new ice block and returned to the sterile RNA and DNA free environment. 7 μL of the reverse transcription (RT) mix was added to each well with a multi channel pipette and mixed by pipetting 6-8 times. Each of the wells was then topped with 20 μL of mineral oil to protect and seal the reaction. The plate was sealed with a film and pulse-spun in a balanced mini-plate centrifuge or an eppendorf centrifuge with plate adaptors. The cDNA reaction was run in the PCR cycler with a 42°C initial hot-start for 5 minutes followed by 25°C for 10 minutes, the annealing and extension cycle was at 50°C for 120 minutes and the reaction was completed and inactivated at 94°C for 5 minutes. Once completed, the plate with cDNA was stored at -20°C as template for downstream PCR amplifications. See Table 2-4 for the formulations and component specifics for the cPEP sort, RHP, and RT mixes.

Amplification of variable heavy (V_H) immunoglobulin regions

The cDNA created at the cPEP step was the template DNA for the multiplexed variable heavy external reaction (VHE) designed to amplify all V_H family members from the complex cDNA mixture. 1.5 μL of the cPEP was added to 48.5 μL of VHE master in a new 96 well PCR plate. The master mix contained 0.5 μM of each primer (VH1E, VH2E, VH3E, VH4E, and JHE), which was heated at 95°C for 5 minutes before adding the remaining components. The remaining was composed of 1x PCR Buffer, 1.5 mM $MgCl_2$, 0.2 mM dNTPs, and 1 unit/reaction of Go-Taq polymerase (Promega). Each of the wells was then topped with 20 μL mineral oil to protect and seal the reaction. The plate was sealed with a film and pulse-spun in a balanced mini-plate centrifuge or an

Eppendorf centrifuge with plate adaptors. The VHE reaction was run in the PCR cycler. Both the formulations and program details are listed in Table 2-4.

Four family specific nested PCR reactions (VH1N, VH2N, VH3N, and VH4N) were each run with their respective primer set using 5 μL of the VHE reaction as the template. The primer, $MgCl_2$, dNTP, buffer, and Go-Taq polymerase concentrations remained the same as the VHE reaction with a final volume of 50 μL. Each of the wells was then topped with 20 μL mineral oil to protect and seal the reaction. The plate was sealed and pulse-spun in a balanced mini-plate centrifuge or an eppendorf centrifuge with plate adaptors. The VHN reactions were run in the PCR cycler. The program details are listed in Table 2-4. See Table 2-5 for primer sequences and Table 2-6 for master mix components for each reaction.

Amplification of variable kappa (Vκ) immunoglobulin regions

Only wells that had amplified productive V_H sequenced products were selected for Vκ amplifications. The cDNA created at the cPEP step was the template DNA for 3 different multiplexed external reactions (VK12E, VK3E, and VK45E) designed to amplify the Vκ family members from the complex cDNA mixture. 1.5 μL of the cPEP was added to 48.5 μL master mix for each of the VKE reaction plates in new 96-well PCR plates per external reaction. The master mix contained 0.5 μM of each primer for the respective external reactions, which was heated at 95°C for 5 minutes before adding the remaining components. The remaining was composed of 1X PCR Buffer, 0.2 mM dNTPs, and 1 unit/reaction of Go-Taq polymerase (Promega). The optimized $MgCl_2$ concentrations varied among the VKE reactions: 3.5 mM for VK12E, 2.5 mM for VK3E,

and 2 mM for VK45E. Each of the wells was then topped with 20 μL mineral oil to protect and seal the reaction. The plate was sealed with a film and pulse-spun in a balanced mini-plate centrifuge or an Eppendorf centrifuge with plate adaptors. The VKE reactions were run in the PCR cycler. Both the formulations and program details are listed in Table 2-4.

Five family specific nested PCR reactions (VK1N, VK2N, VK3N, VK4N, and VK5N) were each run with their respective primer set using 5 μL of the corresponding VKE reaction as the template. The primer, $MgCl_2$, dNTP, buffer, and Go-Taq polymerase concentrations remained the same as for the VKE reactions with a final volume of 50 μL. Each of the wells was then topped with 20 μL mineral oil to protect and seal the reaction. The plate was sealed with a film and pulse-spun in a balanced mini-plate centrifuge or an Eppendorf centrifuge with plate adaptors. The VKN reactions were run in the PCR cycler. Both the formulations and program details are listed in Table 2-4. See Table 2-5 for primer sequences and Table 2-6 for template, primer list, $MgCl_2$ concentration, and PCR reaction cycles for each of reactions.

PCR product visualization and purification

The PCR buffer used in the nested reactions contained a dye for running in an agarose gel. The entire 50 μL nested reaction was visualized on a 2% agarose gel in 0.5x TBE (5.4 g Tris-Base, 2.75 g Boric Acid, and 2 mL 0.5 M EDTA per liter Millipore water) with 20 μL ethidium bromide in a 400 mL gel volume. 5-10 μL of 100 bp DNA ladder (NEB) was included in each gel lane for estimation of PCR product base pair length. The gel was run at 145 volts for 45 minutes. The ethidium bromide in the gel

allowed for visualization using the AlphaImager to see and document the resulting product bands for each of the nested reactions. Bands at the correct height for a V_H or Vκ product (~250bp; to distinguish from high primer dimer bands) were excised from the gel using a razor and placed into a 1.7 mL snap-cap tube labeled with the patient code, V family primer amplified, and well ID (column and row) to ensure proper matching of V_H and Vκ products for downstream cloning.

The excised gel product was purified using the Wizard SV Gel and PCR cleanup kit (Promega). The membrane binding solution was added to the tube with the excised gel piece at a ratio of 10 μL solution to 10 mg of agarose gel. On average, 250 μL of solution was added to the gel piece to fully immerse the gel. The tube was incubated at 65°C for 10 minutes and flick mixed to ensure it was completely melted. Vortexing was avoided in order to not shear the DNA. A SV minicolumn was placed in a labeled collection tube for each product. The dissolved gel mixture was transferred to each respective minicolumn and incubated at room temperature for 1 minute. This incubation was followed by a centrifugation in the table-top microcentrifuge at 14000 rpm for 1 minute and the flow through discarded. The minicolumn was washed by adding 700 μL membrane wash solution and centrifuged at 14000 rpm for 1 minute, and the flow through discarded. This wash was repeated with 500 μL membrane wash solution. The minicolumns were centrifuged again with out any fluid at 14000 rpm to allow for the evaporation of residual alcohol. The minicolumn was transferred to a clean 1.7 mL snap-cap tube labeled with the patient code, V family primer amplified, and well ID (column and row), and date to ensure proper matching of V_H and Vκ products for downstream cloning. 30-50 μL, depending on the intensity of the band when visualized in the gel, of nuclease-free water

was added directly to the center of the column to completely wet the filter and incubated at room temperature for 1 minute. The purified PCR product was eluted by centrifuging at 14000 rpm for 1 minute and archived at -20°C.

PCR product sequencing and processing

A 2 μL sample from the purified PCR product eluate was used for measuring DNA concentration using the Epoch Nano (Biotek). The concentration and purity, based on the 260/280 ratio, were recorded. 12 ng of each product was added to a tube with 6 μL of 1 mM of the corresponding forward primer matching the amplification primer used in the PCR reaction. The volume was adjusted to 12 μL with nuclease-free water. These products were sent to the McDermott Center for DNA sequencing core facility at UTSWMC. Samples were amplified using Applied Biosystems Inc. (ABI) Big Dye Terminator 3.1 chemistry, and were analyzed on ABI capillary instruments. The sequences were returned as .txt files and .abi electropherogram files for analysis.

FinchTV was used to visualize the electropherogram for each sequence. Sequences were visually examined to identify any early sequence miss-reads or missed bases and fixed manually. The sequences were also verified to be complete to the end of the Jκ or J_H genes to ensure the entire variable region read was intact from the start of CDR1 through the start of FR4.

Germline rearrangements were inferred using the IMGT/V-QUEST immunoglobulin sequence analysis tool (http://imgt.cines.fr) (329). The FASTA formatted names were normalized to ensure proper long-term identification and for column values once parsed by the Perl-based extraction program: “>patient code-

primer_well" (i.e. >CIS348-VH4_A3). BLAST was run to produce a text format output with all selections marked in the detailed view. Only sequences that were productive were included for analysis and saved in the PCR product log. Sequences were considered productive provided that codon 104, the beginning of FR4, remained in frame and no stop codons were inserted throughout the length of the V gene from codons 31-104. The resulting BLAST output was saved as a .txt file using the TextWrangler program and saved with the file name matching the PCR log number. The PCR log number is a unique identifier for all productive sequences and is never repeated within the laboratory, it is also then labeled on the top of the PCR product archived in the -20°C freezer and entered into the master PCR product log. This enables the long-term efficient retrieval of both sequence information in electropherogram, text file of the IMGT/V-QUEST BLAST output, physical location of product, and detailed sequence information parsed by the Perl-based extraction program.

CNS extracted V_H sequences

Two sources of V_H repertoires from B cells isolated from MS CNS tissues were obtained from collaborators. All human subject research was approved from the local human research IRBs. One set included 4 repertoires generated using cDNA amplification from extracted tissues from Dr. David Hafler and Dr. Kevin O'Connor, Yale University. This set included autopsy material from 4 subjects with CDMS. Specimens were immediately snap-frozen then stored at -80°C. Variable region libraries were assembled from tissue sections prepared on a cryostat and tissue was excised using laser capture microdissection (LCM). RNA was extracted from 14-μm thick tissue

sections using the RNAeasy Mini Kit (Qiagen) according to the manufacturer's instructions. From the total RNA, cDNA was synthesized and human Ig variable region genes were amplified as described previously (330).

The second set included 4 repertoires generated using genomic DNA template of total B cells extracted from 4 CDMS patients generated by Dr. Scott Boyd and Dr. Andrew Fire. High-throughput next-generation DNA sequencing (NGS) was performed using the 454 platform with Titanium chemistry, as previously described (331). Only V_H sequences amplified with the BIOMED-2 consortium framework 1 (FR1) primers and J segment primer were used, as these provide longer amplicons for study than the framework 2 (FR2) primers (332).

Bulk PB $CD19^+$ B cell NGS sequencing

9 CIS, 1 MS, and 4 HC bulk sorted PB $CD19^+$ B cell pellets were sent to Dr. Scott Boyd and Dr. Andrew Fire for NGS sequencing. The 10 CIS/MS samples chosen had single-cell PCR repertoires generated from CSF $CD19^+$ B cells. Total gDNA was extracted using the QIAamp DNA blood mini kit (Qiagen). 20 μL of QIAGEN protease (a proteinase K) was pipetted into a 1.7 mL snap-cap tube. The thawed $CD19^+$ B cell pellets were each adjusted to a final volume of 200 μL using PBS and added to the protease tube. 200 μL of Buffer AL was added to each tube and mixed by pipetting to avoid shearing of DNA. This mixture was incubated at 56°C for 10 minutes. After the cell lysis was complete, 230 μL of 100% EtOH was added to the sample and mixed by pipetting. This mixture was added to a QIAamp Mini spin column in a 2 mL collection tube and centrifuged in a table-top microcentrifuge at 14000 rpm for 1 minute. The

column was then placed in a new 2 mL collection tube and 500 μL of Buffer AW1 was added followed by centrifugation at 14000 rpm for 1 minute. The column was then placed in a new 2 mL collection tube and 500 μL Buffer AW2 was added followed by centrifugation at 14000 rpm for 3 minutes. The flow through was discarded and the column was centrifuged again at 14000 rpm for 1 minute to remove any residual liquids. The column was placed in a labeled 1.7 mL snap-cap tube and 50 μL of Buffer AE was added to the center of the filter and incubated for 5 minutes at room temperature. The extracted gDNA was eluted by centrifuging at 14000 rpm for 1 minute. The tubes were placed in a speedvac to remove extraneous liquid and resuspended in 15 μL of Buffer AE in order to generate yield and concentration reads using picogreen.

The resulting gDNA was then amplified using the REPLI-g Mini kit (Qiagen). 5 μL of template gDNA was added to a PCR tube. 5 μL of Buffer D1 was added and mixed by pipetting followed by a 3 minute incubation at room temperature. 10 μL of Buffer N1 was added and mixed by pipetting. A master mix containing 29 μL of REPLI-g Mini reaction buffer and 1 μL of REPLI-g Mini DNA polymerase was added to each reaction tube containing denatured DNA. The tubes were sealed with 20 μL of mineral oil and then capped. They were placed in the PCR cycler and incubated at 30°C for 16 hours, inactivated at 70°C for 3 minutes, and stored at -20°C once completed. 2 μL of the 50 μL reaction was removed for quantification of dsDNA produced via picogreen.

1000 ng of REPLI-g material from each of the 14 samples were sent to Dr. Scott Boyd and Dr. Andrew Fire. High-throughput NGS was performed using the 454 platform with Titanium chemistry, as previously described (331). V_H sequences were only

amplified with the BIOMED-2 consortium framework 1 (FR1) primers and J segment primers.

Database generation

Sequences were analyzed and compiled into databases containing V_H gene, J_H gene, CDR3 amino acid sequence, and mutation information using a Perl-based program developed at UTSWMC by William H. Rounds which utilizes the IMGT/V-QUEST tool as a basis for extracting the sequence information from the saved text files (333). The most recent version of the Perl program is "AligntoEnd5.pl" and all databases were modified using Excel-based scripts to match the output from this program. All outputs were also further processed to create summary tables for a given group of sequences using Excel-based scripts and handling. Sample output for a sequence and summary table for a patient's repertoire are shown in Figure 2-2. V_H gene distributions, average mutation frequency (MF), complementarity determining region (CDR) replacement mutations (R): silent mutations (S), and framework (FR) R:S are shown per patient for all single-cell sorted CSF B cell cPEP derived productive V_H sequences in Table 2-7. The same information is shown for the single-cell sorted PB B cell cPEP derived productive V_H sequences from $TM_{CIS}A$ memory and plasmablast sorts in Table 2-8. A limit was set within the lab to dismiss sequences with less than 85% homology to their V_H germline gene segment. This was chosen to avoid introducing potential V_H gene miscalls into the databases.

Of the productive sequences, those which contained 2 or more nucleotide mutations were designated as antigen experienced and included for further study when comparing to healthy control databases. This was done to ensure that comparisons could

be made to the healthy controls, which do not exhibit enrichment for memory cells similar to diseased repertoires. The healthy control peripheral blood (HCPB) database was obtained from previous publications using similar single cell sequencing methodologies and consists of 217 antibody rearrangements (207, 209).

Utilizing this criterion for memory-like cells, the MS CSF database consists of 327 $CD19^+$ B cell antibody rearrangements from 1 PPMS and 10 RRMS patients. The MS PB database consists of 58 PB $CD19^+$ B cells from 4 of the previous MS patients. The CIS CSF database consists of 518 $CD19^+$ B cells antibody rearrangements from 6 ON_{CIS} and 11 TM_{CIS} patients. This was divided into CIS subgroups, ON_{CIS} (6 patients, 148 sequences), $TM_{CIS}A$ (6 patients, 285 sequences), and $TM_{CIS}B$ (5 patients, 85 sequences). The peripheral $TM_{CIS}A$ databases consist of 169 $CD19^+CD27^+$ memory B cells and 223 $CD19^+CD27^{high}$ plasmablasts from 4 $TM_{CIS}A$ patients. The MS CNS database contains 918 V_H sequences compiled from the 4 CNS tissues from Dr. David Hafler and Dr. Kevin O'Connor. The MS CNS database using the 454 platform contains 555 V_H sequences from 4 CNS tissues from Dr. Scott Boyd and Dr. Andrew Fire. The PB databases compiled from the bulk sorted PB $CD19^+$ B cells from 1 MS, 10 CIS patients, and 4 HC donors contains 96072 V_H sequences produced by Dr. Scott Boyd and Dr. Andrew Fire using the 454 platform.

V_H rearrangement read length and mutation frequency determination

The Kabat codon numbering system was used (334), and the IMGT/V-QUEST definitions present in the BLAST outputs were converted to Kabat numbering by the aforementioned Perl-based program. V_H read length was defined as the number of

nucleotides from codon 31 to 92 (CDR1, FR2, CDR2, and FR3). The 3' end of the V_H gene segment was defined as codon 92 and the CDR3 read contained codons 93-102.

Mutation frequency (MF) was determined by dividing the number of mutations in a given V_H rearrangement between codons 31 and 92, by the number of nucleotides in that region. For example, a sequence of 206 nucleotides with 1 mutation would have a MF of 1/206 or 0.48%, which can be translated into 99.52% identical to the germline variable gene. FR1 codons were not included in any of the analyses.

CDR3 length and charge determination

The CDR3 region begins at codon 93 within the V gene, extends through the D segment and ends at codon 102 of the J_H segment, as defined by Kabat (334). CDR3 charge was calculated by translating the CDR3 nucleotide sequence into the corresponding amino acids and summing the charges, counting each arginine (R) and lysine (K) as a positive one charge, and each aspartic acid (D) and glutamic acid (E) as a negative one charge. Histidine was not included because it holds relatively no charge at physiologic pH (335). This calculation was done using the Perl-based program developed at UTSWMC.

Antibody gene signature (AGS) calculation

All productive V_H4 sequences in a subject's repertoire with at least one replacement mutation (RM) were included for the calculation of the subject's AGS score. An AGS codon is defined as having a significantly higher replacement frequency (RF) in MS CSF V_H4 repertoire than HCPB repertoire. This was previously discovered in the lab

and published by Dr. Elizabeth Cameron (228). An AGS score was calculated using the RF values at the following 6 codons within the V_H4 gene: 31B, 40, 56, 57, 81, and 89. A Z-score was calculated for each codon (RF at codon – avg RF in HCPB (1.6)/ stdev of avg RF in HCPB (0.9)), and the 6 scores were added together to arrive at the AGS for the subject's repertoire. This was modified in the current studies to include RMs occurring only between codons 31-92 to standardize RF calculations across sequences of varying read lengths.

Statistical analyses

Cell population frequencies, V_H and J_H gene usages, MF, and J_H4:J_H6 ratio were compared using Chi-square analysis. CDR3 lengths and charge, and AGS scores were compared using the Student's t-test. Pearson's correlation was used to compare the plasmablast numbers and percentages to patient clinical measures. P-values equal to or less than 0.05 were considered significant.

PCR modification of original patient products for cloning full-length recombinant human IgG_1 antibodies (rhAbs)

Sequences from CDMS, ON_{CIS}, and TM_{CIS} patients were chosen as candidates for cloning into full-length expression vectors based on their V_H genomics. The criteria were: expressing a V_H4 gene and have 2 or more of the 6 AGS codons mutated. 60% were also clonally expanded by identifying another V_H sequence within the same patient with identical CDR3 amino acids. The corresponding Vκ sequence was amplified from the same well as the V_H sequence to identify the antibody binding region of the single CSF B cell. Sequence and patient details for the 32 rhAbs selected for cloning and production

are shown in Table 2-9.

Additional rounds of PCR were performed to add restriction enzyme sites to both the 5' and 3' ends of the original PCR products. This was done to facilitate insertion of the variable regions into the expression vectors using modifications of previously published primers (336). The primers used are listed in Table 2-10. V_H4, Vκ3-20, and Vκ3-15 sequences all required a two-step PCR procedure (shuttle and Ig PCR) to build up the missing regions from the original patient PCR products. The remaining Vκ sequences required one PCR procedure (Ig PCR). All reactions were run in a final volume of 25 μL containing 0.5 μM each of forward and reverse primer, 1x Phusion reaction buffer (NEB), 0.2 μM dNTPs (Promega), 0.5 units Phusion DNA polymerase (NEB), and 5 ng of purified nested PCR product as the template.

The VH4 shuttle PCR was first tested at: 98°C, 1min; {98°C, 10sec; 64°C, 15sec; 72°C, 6sec} x25 cycles; 72°C, 10min; 4°C, ∞. Depending on the resulting bands, no bands, or indiscriminate hazes on the gel, the shuttle program was modified to include a 2-step annealing process: 98°C, 1min; {98°C, 10sec; 52°C, 15sec; 72°C, 6sec} x5 cycles; {98°C, 10sec; 66°C, 15sec; 72°C, 6sec} x5 cycles; 72°C, 10min; 4°C, ∞. The VHIg PCR from a purified VH4 shuttle product was first run with the same settings as the first VH4 shuttle PCR with the annealing temperature changed to 68°C. The VK shuttle PCR was first tested at: 98°C, 1min; {98°C, 10sec; 70°C, 15sec; 72°C, 6sec} x25 cycles; 72°C, 10min; 4°C, ∞. The VKIg PCR was run from either a purified VK shuttle product or VKN product with the annealing temperature changed to 64°C. The PCR annealing temperature, times, and 1 or 2-step processes were modified as needed to accommodate each template and primer pairing and to optimize results after visualization on a gel.

Dr. Betty Diamond provided two control full-length recombinant human antibodies (rhAbs) cloned from systemic lupus erythematosus (SLE) patient derived B cells using the same expression vector system. B1 has been shown to not bind to mouse brain and G11 has been shown to bind to NMDARs in the mouse brain as well as dsDNA (337). These two antibodies have been studied and published and were used as controls for the full-length IgG_1 rhAb construct in all the immunohistochemistry and immunofluorescence experiments.

Gel purification of PCR inserts and cut IgG and IgK backbone vectors

The first and final PCR steps were all visualized on a 1% agarose gel run at 120 volts for 1 hour and the desired bands were excised using a razor blade. The double restriction enzyme digested IgG and IgK backbone vectors were visualized on a 0.7% gel run at 100 volts for 1.5 hours. Products were purified using the QIAquick gel extraction kit (Qiagen). 3 volumes of Buffer QG were added to 1 volume of gel (i.e. 300 μL Buffer to each 100 mg gel) with a maximum of 400 mg of gel per purification column. The tubes were incubated at 50°C for 10 minutes until the gel was completely dissolved and flick mixed. Vortexing was avoided to prevent shearing of the DNA. After the gel was dissolved, 1 gel volume equivalent of isopropanol was added to the sample and mixed by inversion. This increased the yield of DNA fragments smaller than 500 bp and larger than 4 kb. This was transferred to a labeled QIAquick column (maximum 800 μL per pass) and centrifuged in a table-top microcentrifuge at 13000 rpm for 1 minute. The flow through was discarded and 500 μL of Buffer QG was added to the column to clear traces of agarose and centrifuged at 13000 rpm for 1 minute and the flow through discarded. For

salt-sensitive applications such as cloning, the salts were cleared by adding 750 μL Buffer PE to the column and incubating for 2-5 minutes followed by centrifugation at 13000 rpm for 1 minute. The flow through was discarded and the column was centrifuged at 13000 rpm for an additional minute to remove residual alcohol. The column was transferred to a pre-labeled 1.7 mL snap-cap tube and 30-50 μL of nuclease-free water was added to the filter and incubated for 1-2 minutes. The volumes of water were varied depending on the intensity of the band when visualized in the gel. The DNA was eluted by centrifuging at 13000 rpm for 1 minute and the product was stored at either 4°C for short term or archived at -20°C for long term storage. A 2 μL sample from the purified product eluate was used for measuring DNA concentration using the Epoch Nano. The concentration and purity based on the 260/280 ratio were recorded.

Double restriction enzyme digests of IgG and IgK backbone vectors

Dr. Michel Nussenzweig (The Rockefeller University) provided the backbone expression vectors for both the IgG and IgK chains for the production of rhAbs. These vectors and the procedure have been extensively described for the production of monoclonal human IgG_1 (328). The protocol for the restriction enzyme digestion is shown in Table 2-6. The vectors were first linearized with a single restriction enzyme that had the lowest efficiency of cutting, the 3' enzyme for both backbones. 2 fold excess of the 3' restriction enzyme was added to 4 μg of plasmid backbone. The IgG vector was incubated with 5 μL SalI HF (2000 u/mL; 50x, NEB) and 5 μL of NEB buffer #4 in a final volume of 50 μL adjusted with nuclease-free water at 37°C for 20 minutes. After 20 minutes, and additional 5 μL SalI HF was added and incubated at 37°C for 20 minutes.

Denaturing the enzyme at 65°C for 20 minutes halted the reaction. The IgK vector was incubated with 2 μL BsiWI (1000 u/mL; 10x, NEB) and 5 μL of NEB buffer #1 in a final volume of 50 μL adjusted with nuclease-free water at 55°C for 20 minutes. After 20 minutes, and additional 2 μL BsiWI was added and incubated at 55°C for 20 minutes. Denaturing the enzyme at 80°C for 20 minutes halted the reaction. Both of these single-cut backbones were run out on a 0.7% agarose gel at 100V for 1.5 hours and the linearized vector was excised and gel purified. This ensured that only the backbone plasmids that were effectively cut were then included in the next reaction.

Then a second restriction enzyme digest was performed to make the final cut at the 5' site at 1 fold excess. Both vectors were incubated with 2.5 μL AgeI HF (2000 u/mL; 50x, NEB), 5 μL of NEB buffer #4, and 0.5 μL of 10x BSA in a final volume of 50 μL adjusted with nuclease-free water at 37°C for 20 minutes. Denaturing the enzymes at 65°C for 20 minutes halted the reaction. Due to the small change in base pairs and the high efficiency of the enzyme these were not run out on a gel and were column purified by skipping the initial agarose gel dissolving steps. This resulted in double-cut vector backbones. A 2 μL sample from the purified product eluate was used for measuring DNA concentration using the Epoch Nano. The concentration and purity, based on the 260/280 ratio, were recorded.

The purity of each batch was evaluated by following the T4 DNA-ligase procedure, without adding insert, and the result was transformed into DH5α cells.This was plated on LB agarose plates with ampicillin and incubated at 37°C overnight. If there were a high number of colonies the next day, this indicated that the restriction enzyme digestions were not efficient, making it unusable for cloning in a PCR insert.

Double restriction enzyme digests of PCR inserts

Both the 5' and 3' restriction enzyme digestions were conducted simultaneously as opposed to the procedure followed for vector backbones. There were two potential sources of Vκ and V_H inserts, one from PCR used to add restriction sites to the original patient PCR product, and the other purchased as an insert inside of a plasmid from Integrated DNA Technologies (IDT, IA, USA). The protocol for both is shown in Table 2-11. The maximum amount of input DNA into the reaction was 2 μg from an IDT vector and 200 ng from a PCR product. The V_H inserts were incubated with 1.25 μL AgeI HF (2000 u/mL; 50x, NEB), 2.5 μL SalI HF (2000 u/mL; 50x, NEB), 5 μL of NEB buffer #4, and 0.5 μL of 10x BSA in a final volume of 50 μL adjusted with nuclease-free water at 37°C for 20 minutes. Denaturing the enzymes at 65°C for 20 minutes halted the reaction. The Vκ inserts were incubated with 1.25 μL AgeI HF (2000 u/mL; 50x, NEB), 2 μL BsiWI (1000 u/mL; 10x, NEB), 5 μL of NEB buffer #1, and 0.5 μL of 10x BSA in a final volume of 50 μL adjusted with nuclease-free water at 37°C for 20 minutes. Denaturing the enzymes at 80°C for 20 minutes halted the reaction. Due to the small change in base pairs these were not run out on a gel and were column purified by skipping the initial agarose gel dissolving steps. This resulted in double-cut variable region segments for insertion into their respective backbones. A 2 μL sample from the purified product eluate was used for measuring DNA concentration using the Epoch Nano. The concentration and purity, based on the 260/280 ratio, were recorded.

Ligation of double-cut vector and insert

Ligation of purified double-cut vector and the corresponding double-cut insert

was conducted using the T4 DNA ligase (NEB). After initial purchase, the 10x ligase buffer was vigorously vortexed and aliquoted into PCR tubes at 10 μL each and stored at -20°C to avoid repeated freeze/thaws and degradation of the ATP. The cut vector and insert was added in a 1 vector : 3 insert ratio (i.e. 50 ng vector: 15 ng insert). 2 μL of ligase buffer was added and the volume was adusted to 19 μL with nuclease-free water. 1 μL of T4 DNA ligase was added and flick mixed to avoid DNA shearing and incubated at room temperature for 10 minutes. The reaction was then stored at -20°C until ready for bacterial transformation or chilled on ice and used immediately.

Chemically competent DH5α cells

The creation of chemically competent DH5α E.coli cells for transformation was modified from a protocol in the literature (338). 10-50 μL of DH5α cells were plated on a LB agar plate without any antibiotics overnight in a 37°C oven. The next morning, 10-12 large colonies were plucked and added to 250 mL SOB media (0.5% yeast extract, 2% tryptone, 10 mM NaCl, 2.5 mM KCl, 10 mM $MgCl_2$, and 10 mM $MgSO_4$ dissolved in Millipore water and autoclaved) in a 1 L flask. This was incubated at 19°C with vigorous shaking to an OD600+0.5, which took approximately 24-36 hours. The 1 L of cell growth was divided into Sorvall bottles and incubated on ice for 10 minutes. Care was taken to minimize temperature fluctuations and to keep the cells on ice at all times when not in the centrifuge. The cells were pelleted by centrifuging at 4000 rpm in the Sorvall floor centrifuge for 10 minutes at 4°C. Cells were gently resuspended in 80 mL ice-cold TB solution (55 mM $MnCl_2*4H_2O$, 15 mM $CaCl_2*2H_2O$, 250 mM KCl, and 10 mM PIPES solution in Millipore water and sterilized by filtration) in order to not break open the cells

and incubated on ice for 10 minutes. The cells were pelleted by centrifuging at 4000 rpm in the Sorvall floor centrifuge for 10 minutes at 4°C. Cells were gently resuspended in 20 mL ice-cold TB solution and 1.4 mL DMSO. This cell slurry was aliquoted into tubes at 50-250 μL per tube. The batch of DH5α cells were tested for chemical competency by transforming with a known control plasmid and plating on selective antibiotics to test for positive transforments. The cells were kept at -80°C and would be discarded if they reached temperatures above ice.

Bacterial transformation of ligations

Chemically competent DH5α were created and stored at -80°C in small aliquots. These were always kept on ice; once they were warmed above ice temperature they were no longer competent. A 1.7 mL snap-cap tube was chilled on ice and then 50 μL slurry of competent DH5α was added to the tube. 7 μL of the ligation reaction was added to the bacteria and mixed by gently swirling the pipette tip. The bacteria were heat shocked to disrupt the membrane and allow for uptake of the plasmid DNA at 42°C for 30 seconds. The tube was chilled on ice for 30 minutes, allowing for the bacteria to recover. LB agar plates were prepared by adding the selective antibiotic: 40 μL of ampicillin stock (at 100 mg/mL) diluted in 110 μL water and this 150 μL antibiotic mix was spread on to the agar with an alcohol and flame sterilized metal spreader. These were placed right-side up in the 37°C oven for absorption during the 30 minute bacterial recovery step. After the 30 minute ice incubation, 400 μL of SOCS media (96 mL SOB, 4 mL 0.5 M filtered glucose) was added to the tube, flick mixed, and incubated at 37°C in a shaker incubator set at ~100 rpm for 45 minutes. The tubes were mixed by inversion halfway through the

incubation to avoid excessive sedimentation. The entire 457 μL transformed bacterial mixture was added to the prepared LB agar + ampicillin plates and spread with an alcohol and flame sterilized metal spreader. These were inverted and placed in a 37°C oven overnight for colony growth.

Miniprep amplification of colony DNA

Individual colonies from the transformed plates were grown for miniprep amplification of the colony for a maximal yield of 20 μg of plasmid DNA (Qiagen, CA, USA). Only the center of colonies were chosen to ensure that only a single clone was being selected and reduced satellite colony contamination. The center of a colony was plucked with a pipette tip and added to 8 mLs of LB broth with selective antibiotic (10 μL of ampicillin stock) in a 14 mL culture tube. The cultures were grown in a shaker incubator overnight at 37°C. The following morning, 1 mL of growth was reserved at 4°C for re-growth. The remaining cells were harvested by centrifuging 7 mL of the growth at 8000 rpm in the Sorvall floor centrifuge for 4 minutes. The supernatant was discarded and the pellet was resuspended in 250 μL Buffer P1 (with added RNase A and LyseBlue reagent, stored at 4°C) which was equilibrated to room temperature. This bacterial slurry was transferred to a labeled 1.7 mL snap-cap tube. 250 μL Buffer P2 was added to the tube and mixed thoroughly by inverting the tube 4-6 times avoiding vortexing to not shear the DNA. If properly lysed, the cell suspension turned blue. The reaction was not to exceed 5 minutes and was halted by adding 350 μL Buffer N3 and mixed immediately and thoroughly by inverting the tube 4-6 times. All traces of blue would be gone and a homogenous colorless suspension devoid of localized precipitate

was the desired goal. The tube was centrifuged in a table-top microcentrifuge at 13000 rpm for 10 minutes to form a compact white pellet. The supernatants containing the plasmid DNA were carefully pipetted to avoid the white precipitate and added to a QIAprep spin column. The column with the supernatant was centrifuged at 13000 rpm for 1 minute and the flow through discarded. 750 μL Buffer PE was added to the column to wash and was centrifuged at 13000 rpm for 1 minute and the flow through discarded. The column was centrifuged without any liquid for an additional 1 minute to remove the residual alcohol and wash buffer. The QIAprep column was transferred to a labeled 1.7 mL snap-cap tube and 50 μL nuclease-free water was added to the filter. It was incubated for 1 minute and the DNA was eluted by centrifuging at 13000 rpm for 1 minute. A 2 μL sample from the purified product eluate was used for measuring DNA concentration using the Epoch Nano. The concentration and purity, based on the 260/280 ratio, were recorded. The purified plasmid DNA was stored at -20°C for short term and archived at -80°C for long-term storage.

Plasmid sequencing and verification

800 ng of miniprep plasmid DNA was mixed with 6 μL of 1 μM 5' Absence primer in final volume of 12 μL with nuclease-free water. These products were sent to the McDermott Center for DNA sequencing core facility at UTSWMC. Samples were amplified using Applied Biosystems Inc. (ABI) Big Dye Terminator 3.1 chemistry, and were analyzed on ABI capillary instruments. The sequences were returned as .txt files and .abi electropherogram files for analysis.

FinchTV was used to visualize the electropherogram for each sequence. Sequences were visually examined to identify any early sequence miss-reads or missed bases and fixed manually. The inserts were verified to match the original patient nested PCR sequence from Kabat codon 31 (start of CDR1) through codon 104 (start of FR4). Any insertions or deletions invalidate the sequence regardless of their location. The FR1 region had to exactly match the region covered by the primer but other point mutations were valid because they were unable to be read from the original patient nested PCR sequence read. Mutations induced/imposed by the cloning JH primer were dismissed. The restriction enzyme sites were verified to be in the correct locations. Up to 30 base pairs before and after the restriction sites were verified to match the backbone sequences to insure that the plasmids remained in frame after insertion of the variable regions. If the sequence matched these criteria, it was logged and archived at -80°C.

Glycerol stock creation and verification

A 14 mL culture tube with 10 mL LB media and ampicillin was inoculated with 30 μL of the corresponding miniprep culture that was verified to contain the correct cloned in frame and patient matching insert IgG or IgK vector. This was grown overnight in a shaker incubator at 37°C. The next morning a cryovial, labeled with the Ig clone code, patient # and well ID, with 500 μL of 60% sterile filtered glycerol had 1 mL of overnight culture added. The tube was inverted to mix and placed in a Mr. Frosty overnight in the -80°C and then archived the next day and logged. The overnight growth was verified to still match the previous sequence by repeating the Qiagen miniprep on 3 mL of bacterial growth.

Midiprep amplification of DNA for transfection

Miniprep DNA yields were insufficient for transfections. The IgG and IgK of each rhAb was expanded using midiprep growth for a maximal yield of 100 μg plasmid DNA (Qiagen). Three 14 mL culture tubes with 10 mL of LB media with ampicillin were inoculated with glycerol stock scrapings from a still frozen tube. The cultures were grown in a shaker incubator overnight at 37°C. The cells were harvested the following morning by centrifuging 30 mL of the growth at 8000 rpm in the Sorvall floor centrifuge for 15 minutes. The supernatant was discarded and the pellet was resuspended in 4 mL Buffer P1 that was equilibrated to room temperature. This bacterial slurry was transferred to a labeled 15 mL conical tube. 4 mL of Buffer P2 was added to the tube and mixed thoroughly be inverting the tube 4-6 times avoiding vortexing to not shear the DNA. If properly lysed, the cell suspension turned blue. The reaction was not to exceed 5 minutes and was halted by adding 4 mL of chilled Buffer P3 and mixed immediately and thoroughly by inverting the tube 4-6 times and incubated on ice for 15 minutes. All traces of blue would be gone and a homogenous colorless suspension devoid of localized precipitate was the desired goal. The tube was centrifuged in the Sorvall floor centrifuge at 8000 rpm for 30 minutes at 4°C to form a compact white pellet. The supernatants containing the plasmid DNA were carefully pipetted to avoid the white precipitate and added to a new 15 mL conical tube. The supernatant was centrifuged again in the Sorvall at 8000 rpm for 15 minutes at 4°C and the supernatant was removed immediately into a new 15 mL conical tube. QIAGEN-tip 100 columns were equilibrated by adding 4 mL

Buffer QBT and allowed to empty by gravity flow. The supernatant from the 15 mL conical was added to the equilibrated column and allowed to pass through the resin by gravity flow. The column was washed twice with 10 mL of Buffer QC each time. The waste conicals were discarded and a new 15 mL conical was added below the columns. The DNA was eluted using 5 mL Buffer QC and allowing it to pass through by gravity flow. 3.5 mL of isopropanol was added to the eluted DNA to aid in precipitation and incubated at -20°C overnight.

The following day, the tubes were removed and mixed by inversion to visualize the precipitate. The tubes were centrifuged in the Sorvall at 8000 rpm for 1 hour at 4°C. The supernantant was carefully decanted with a serological pipette as the DNA pellet was glassy and loose. The DNA pellet was washed with 1 mL 70% EtOh and transferred to a 1.7 mL snap-cap tube. These were centrifuged using a table-top microcentrifuge at 13000 rpm for 10 minutes at 4°C. This wash was performed twice and the supernatant carefully removed with a pipette. The DNA pellet was air-dried for 5-15 minutes and then dissolved in 200-400 μL nuclease-free water depending on the concentration needs for downstream applications. A 2 μL sample from the purified product eluate was used for measuring DNA concentration using the Epoch Nano. The concentration and purity, based on the 260/280 ratio, were recorded. The purified plasmid DNA was stored at -20°C for short term and archived at -80°C for long-term storage. A sample was sent for re-sequencing to verify that the patient insert and plasmid still matched and was in frame.

Production of monoclonal rhAbs

Human embryonic kidney fibroblast (HEK) 293T cells were archived in $5x10^5$ cell aliquots at -120°C. A frozen stock was removed and quickly thawed in a 37°C water bath with constant swirling until a small floating ice crystal was left. This was added to 10 mL cold RegMed (500 mL DMEM, 50 mL heat-inactivated FCS, 5 mL HEPES, and 5 mL L-Glutamine mixed and filtered) to avoid heat-shock. The conical tube was mixed by inversion and cells were pelleted by centrifuging at 1500 rpm for 3 minutes. The cell pellet was gently resuspended in 10 mL RegMed and plated in a T25 flask and placed in a 5% CO_2 water-jacketed incubator (Nuaire) at 37°C. These were grown for ~3 days to reach 80-90% confluency. Cells were lifted with 1 mL trypsin for 5-10 minutes at room temperature, neutralized with 5 mL RegMed, and centrifuged at 1500 rpm for 5 minutes. The pellet was resuspended in 30 mL RegMed and passaged into a T75 flask. These were grown for 1.5-2 days to reach 80-90% confluency for a maximum yield of ~$20x10^6$ cells per flask.

10 cm coated tissue culture dishes were prepared for transfection by plating $2.1x10^6$ cells in 10 mL RegMed 24 hours prior to transfection. These plates were grown to 50-80% confluency, as any higher density would lead to failed transfection. One hour prior to transfection (23 hours post plating) the media was removed and replaced with 5 mL UltraLow Media (same as RegMed expect that the FCS was replaced with ultra-low IgG FCS). The dishes were placed back in the incubator while preparing the transfection solution. JetPEI solution (Polyplus transfection) was used with optimized modifications to manufacturer's recommendations. Paired IgG and IgK DNA that composed a rhAb were mixed in a 1.7 mL snap-cap tube. 6.25 μg of each plasmid (12.5 μg total DNA) was

added to the tube and the volume adjusted to 250 μL with the provided 150 mM NaCl solution. In a separate 1.7 mL snap-cap tube, 25 μL JetPEI was diluted with 225 μL 150 mM NaCl solution for a final volume of 250 μL. Both tubes were flick mixed; vortexing was avoided to not shear the DNA. The JetPEI solution was added to the DNA solution tube and flick mixed. The mixture was incubated at room temperature for 20-30 minutes. The 10 cm dishes were removed from the incubator and placed in the laminar flow hood. The DNA-JetPEI precipitate solution was evenly added dropwise to the media and then the plate was tapped gently on each of the 4 sides to homogenize the mixture before replacing it in the incubator. Two hours after transfection, an additional 15 mL UltraLow media was added slowly to not disrupt the cell layer and the plates were returned to the incubator.

Supernatants were collected on days 3, 5, 7, and 10 (day 1 was the day after transfection). 20 mL supernatants were collected in 50 mL conical tubes and centrifuged at 1500 rpm for 5 minutes to pellet any cell debris. The supernatant was transferred to a new conical tube and stored at -20°C until further downstream processing. Prior to freezing, a 20 μL aliquot was taken and frozen in a 0.6 mL snap-cap tube for ELISA measurements of growth yield and concentration of all the collection days.

Quantification of rhAb production and concentration

ELISAs were used to determine the yield and the concentration of the rhAbs produced in culture. This was also repeated downstream to obtain an accurate measurement post-concentrating or column purifying of the rhAbs. Goat anti-human IgG Fc antibody (Santa Cruz) was diluted to 10 μg/mL in coating solution (0.1 M anhydrous

$NaHCO_3$ dissolved in water) and added at 100 μL per well of an ELISA plate (2HB Immulon) as the primary catch antibody. The plate was sealed and incubated overnight at 4°C. The following morning, the wells were washed with PBS/Tween (0.2% Tween in PBS) by adding 200 μL solution to each well and allowing the plate to sit for 1 minute and then inverted to remove liquid and pounded out on a paper towel to remove residual wash solution. This was repeated twice. Blocking buffer (1% BSA in PBS) was added at 200 μL per well and incubated at room temperature for 30 minutes. The wells were washed twice with PBS/Tween as before.

2.5 μL of human reference serum (stock at 4.4 mg/mL) was diluted in 11 mL blocking buffer. This was serially diluted using 500 μL of the previous reference serum solution with 500 μL blocking buffer. 10 standards were created: 500, 250, 125, 62.5, 31.3, 15.6, 7.8, 3.9, 1.95, and 0 ng/mL. The standards were added in duplicate at 100 μL per well in the ELISA plate. The samples were diluted 100x using blocking buffer. Each supernatant collection day for a rhAb was tested: days 3, 5, 7, and 10. These 4 sample dilutions were added in duplicate at 100 μL per well in the ELISA plate. The plate was sealed and the samples and standards were incubated at room temperature for 2 hours. The wells were washed five times with PBS/Tween as before.

Goat anti-human IgG Fc HRP-conjugated antibody (SantaCruz) was diluted to 100 ng/mL in blocking buffer and added at 100 μL per well of the ELISA plate as the secondary detection antibody. The plate was sealed and incubated at room temperature for 1 hour. The wells were washed with PBS/Tween as before with the additional 30 second pause between each wash. This was repeated 5 times. Tetramethylbenzidine (TMB) substrate solution (Ebioscience) was added at 100 μL per well. This was

incubated for ~1-10 minutes in the dark and development was regularly checked and stopped when the samples developed a blue color in the middle range of the standard curve. The reaction was stopped by added 50 μL of 1 M HCl turning the solution in the wells from blue to yellow. The plate was read at 450 nm using the Greiner 96 round bottom plate setting in the Epoch Nano software. Standard curves and rhAb concentrations were interpolated using GraphPad Prism 6.

Concentrating rhAb supernatant

Successful growth of rhAbs was determined using the aforementioned ELISA. Collection days with sufficient production were thawed overnight at 4°C. Supernatants were concentrated using the 10kDa MWCO Amcion Ultra centrifugal filter units (Millipore) following manufacturer's recommendations. The minimal concentration was 18 ng/μL for downstream applications and the maximum was set at ~120 ng/μL. ELISA results were used to obtain a close estimate to the yield and concentration of the supernatants. This was used to estimate the target volume needed to concentrate the rhAbs. Supernatant was added to the Amicon Ultra centrifugal filter unit and centrifuged at 4000 rpm for 20 minutes at 4°C. This was repeated until the desired volume endpoint was achieved. Aliquots of the concentrated rhAb supernatant were created and stored at -80°C. A second ELISA was performed on the concentrated stocks of rhAbs to determine an accurate final concentration. Additionally, a non-transfected cell culture supernatant was confirmed to not contain any IgG above ELISA detection. These concentrated rhAbs were used as primary antibodies for all mouse brain immunohistochemistry (IHC) and immunofluorescence (IFC) experiments.

Column purification of rhAbs

A set of 10 AGS-enriched rhAbs and 2 control rhAbs were purified by passing supernatant through a 5 mL column with a bed of protein G sepharose beads (Pierce). The column was set up by filling the column and funnel extender with DPBS with the bottom portion plugged. A frit was pushed down to the bottom and bubbles were tapped out. DPBS was then allowed to flow through and refilled after which the bottom was plugged. 1 mL of protein G sepharose bead slurry was pipetted into the DPBS and equilibrated for 30 minutes. The column was then un-plugged and allowed to drain. 2.5 mL of freshly made elution buffer (0.751 g glycine, 0.877 g NaCl, in 100 mL Millipore water, pH 2.5-2.8 adjusted with HCl) was added to the column followed by a 10 mL DPBS rinse. A glass bottle was then placed below the column to collect the rhAb supernatant flowthrough. Supernatants were passed through the column and drained by gravity flow. After all the rhAb supernatant was passed through, 40 mL of DPBS was used to rinse the column. The flow through was stored at 4°C until the column purification was verified to be successful.

The rhAbs were eluted in three fractions: 3.5 mL elution + 583 μL neutralization (2 M TrisHCl, pH 8), 2.5 mL elution + 417 μL neutralization, and 5 mL elution + 833 μL neutralization. The column was preserved by rinsing with 10 mL DPBS followed by an additional 10 mL DPBS with 50 μL of 10% NaN_3, sealed, and stored at 4°C. 20 μL of each elution was sampled for coomassie gel to visualize which elutions contained the rhAb. The samples were run on a 4-15% SDS-page gel and the resulting bands were visualized by staining in coomassie stain for 1 hour followed by a 30 minute rinse in water. Typically, the rhAb was present mostly in elution 1, with a lesser amount in

elution 2, and none in elution 3.

Elutions that contained rhAb were dialyzed in Spectra/Por Dialysis Membrane (6000-8000 MWCO) tubing in 2 L of PBS with a stir bar added to agitate the PBS overnight at 4°C. The next morning, the tubings were added to a fresh 2 L of PBS. Approximately 8-10 hours later, they were transferred to 2 L DPBS. Samples were removed the next day and stored in 15 mL conical tubes at 4°C. 10 μL of sample was removed for concentration and yield determination via ELISA. Once the concentration was determined, if the rhAb needed to be further concentrated for downstream applications this was done using the10kDa MWCO Amcion Ultra centrifugal filter units (Millipore, MA, USA) followed by filtering. 10% NaN_3 was added to the purified rhAbs for a final concentration of 0.01% NaN_3 as a preservative and then stored at 4°C.

Biotinylation of column purified rhAbs

A set of 10 AGS-enriched rhAbs and 2 control rhAbs were biotinylated using 106 μg of column-purified product following manufacturer's instructions for the Thermo Scientific EZ-Link Micro NHS-PEG4-Biotinylation kit (Thermo Scientific, MA, USA). 106 μg accounted for the ~95% recovery post de-salt for a final yield of ~100 μg of biotinylated rhAb. Minimum concentration of column purified rhAbs was 151.42 ng/μL to account for the maximum 700 μL reaction volume. 106 μg of column-purified rhAb was added to a 1.7 mL snap-cap tube and the volume was adjusted to 700 μL with PBS. One microtube of NHS-PEG4-Biotin was cut from the strip stored in a desiccated pouch at 4°C. A 20 mM biotin solution was created by piercing the foil with a pipette tip and adding 170 μL of PBS and mixed by pipetting. 1.77 μL of the 20 mM biotin solution was

added to the tube with 106 μg of rhAb and flick mixed. This was incubated for 2 hours on ice. Excess unbound biotin and salts were removed using the provided Zeba Spin Desalting Column (7000 MWCO). A column was cleared by removing the bottom plug and centrifuging in a 15 mL conical waste tube at 1000 xg for 2 minutes at 4°C. The column was then equilibrated by adding 1 mL of PBS to the top of the resin bed and centrifuging at 1000 xg for 2 minutes at 4°C and the flow through was discarded. This was repeated three times. The column was placed into a new 15 mL conical tube for collection. The biotin-rhAb solution was added directly onto the center of the resin bed and allowed to be fully absorbed into the resin (~2-5 minutes). The biotinylated rhAb was recovered by centrifuging at 1000 xg for 2 minutes at 4°C. The flow-through was the purified biotinylated-rhAb and was collected and transferred to a labeled 1.7 mL snap-cap tube. The volume recovered was documented so the concentration could be determined. 10% NaN_3 was added to achieve a final concentration of 0.05% NaN_3 as a preservative and then stored at 4°C. These biotinylated rhAbs were used as primary antibodies for all human brain IHC and IFC experiments.

Processing of mouse brain tissue for freezing

Mice were sacrificed 2-3 days post stroke induction as previously described (339) and were provided by Dr. Ann Stowe (UTSWMC). A perfusion pump was set up with heparinized saline (1000 units/mL of PBS) in a syringe fitted with a butterfly syringe. A mouse was placed in an isoflurane chamber and once it stopped breathing its four legs were pinned to a styrofoam board with its back flush against the board. An incision was made across the abdomen and through the ribs and diaphragm to expose the heart. The

butterfly needle attached to the perfusion pump was pierced through the left ventricle and the right atrium was cut to release the blood. Each mouse was perfused with 50 mL of heparinized saline at a rate of 5 mL/minute to flush the entire body of blood. The saline was then replaced with 40 mL of 4% paraformaldehyde and perfused at the same rate to achieve full-body rigidity.

Extraction of the brain began by severing the head and carefully cutting through the eye sockets and skull. The skull was pried free from the brain avoiding any surface damage to the cortex. The brain was pulled out keeping the cerebellum intact and immersed in a vial of 4% paraformaldehyde for 48 hours at 4°C to preserve it. The brains were then cryoprotected by sequential incubations at 4°C in 15% sucrose for at least 24 hours (or longer if needed, until the brain sank) followed by 30% sucrose for at least 48 hours.

Processing of frozen human brain tissue

Post-mortem human brain samples were provided by the Human Brain and Spinal Fluid Resource Center (UCLA, Los Angeles, CA). Three samples were used for the studies: white matter (WM) from a healthy control without neurological complications (HC), white matter plaque from a patient with clinically definite MS (MS-P), normal appearing WM from the same MS patient (MS-WM), and normal appearing gray matter (MS-GM) on the same sample as the MS-WM. Mean time to sampling from time of death was 16 hours. A test using a mouse brain snap-frozen with liquid nitrogen and then placed in -80°C for a week to simulate post-mortem human tissue conditions was conducted to confirm that the human samples could be processed in the same manner as

the mouse samples. Upon removing human brain samples from -80°C, they were preserved similarly to mouse brains with 4% paraformaldehyde for 48 hours at 4°C followed by cryoprotection in sequential 15% and 30% sucrose solutions.

Processing and cryostat sectioning of frozen tissue

All tissues were embedded in O.C.T freezing compound and stored at -20°C until cryosectioned. The brain tissues were drained and wiped down to remove excess sucrose. A layer of O.C.T. freezing compound was added to the bottom of a mold and the brain tissue was placed in an upright position. The mold was filled with O.C.T. and then placed in an isopropanol bath on top of dry ice. Once the O.C.T. froze to an opaque white color, it was placed at -20°C for at least 24 hours before further processing.

Tissue sections (12-16μm) were cut and attached to charged glass slides using a cryostat (Thermo Scientific MICROM) and frozen at -20°C. Mouse brain tissue was cut to produce 3 coronal sections per slide. Human brain tissues did not have a planar orientation and were cut to produce 3 sections per slide.

Cresyl violet staining

Tissues were stained with cresyl violet to validate the integrity and the preservation of the tissue. Cresyl violet binds to nissl substance in neurons and cell nuclei and is visualized as purple under a light microscope. Slides were removed from -20°C and air-dried for 1-3 minutes. They were then immersed in cresyl violet stain (188 mL of 0.6% acetic acid, 12 mL of stock base (1.3 g NaOAc in 100 mL water) and 25 mL of stock dye (1.2 g cresyl violet in 900 mL water)) for 20 minutes. The slides were then

rinsed in deionized water and immersed in 70% EtOH for 3 minutes followed by 95% EtOH for 3 minutes, 100% EtOH for 3 minutes, and xylenes for 5 minutes. The slides were mounted with ~120-150 µL permount:xylene (3:1 ratio) mixture and a coverslip was placed on top. Slides were imaged using a 40x brightfield lens on the NanoZoomer (Hammatsu, Japan). Images were visualized using NDP.view software (Hammatsu, Japan) and 20x images were exported for visualization and adjustments to brightness and contrast were done with ImageJ software (NIH, USA).

Diaminobenzidine (DAB)-immunohistochemistry (IHC) staining of mouse brain tissue

All 32 AGS-enriched rhAbs and the 2 control rhAbs (B1 and G11) were assayed for binding to brain using DAB on mouse brain tissue. Binding to brain was visualized by brown precipitates formed by the DAB reaction and could be seen using a light microscope. Slides were removed from -20°C and air dried for 1-3 minutes until most of the condensation was removed. The slides were placed in PBS until the unmasking solution was ready. Care was taken at all steps to protect the tissue from drying out which would lead to non-specific signals due to damaged tissue. Tissues were subjected to antigen retrieval by boiling for 2 minutes in low pH citric acid based antigen unmasking solution (Vector Laboratories) prepared by diluting 15 mL of solution in 1.6 L deionized water. Post boiling, the slides were immediately transferred to a deionized water bath to cool for 2 minutes. Once the slides were cool, they were transferred to PBS for 2-5 minutes in order to rehydrate. Each slide was removed one at a time and carefully dried around the tissue and a circular waxy barrier was drawn around each of the 3 samples using a pap pen. PBS was added to the brains in a drop-wise fashion to cover them in

liquid and they were placed in a humidifying chamber (a slide box lined with water soaked paper towels).

Removal of any liquid on the tissues was done by vacuum aspiration using care to not touch the brain with the pipette tip. Most of the liquid was removed with a small film remaining to prevent tissue desiccation and damage. PBS was removed and the brains were incubated with 100 µL of 3% H_2O_2 for 5 minutes to block endogenous peroxidases. The tissues were washed with PBS for 5 minutes followed by a 10 minute blocking incubation with 100 µL of 3% normal goat serum in PBS. The tissues were washed with PBS for 5 minutes. 1 µg of primary rhAb antibody (10ng/µL diluted in blocking buffer) was added to each brain slice and incubated overnight at 4°C.

The next morning, the tissues were washed twice with PBS for 5 minutes to maximize the removal of all unbound rhAb. Tissues were probed with 100 µL of biotinylated goat anti-human secondary antibody (Vectastin Elite ABC Kit for human: 5 mL PBS, 3 drops normal goat serum, 1 drop biotinylated secondary antibody) for 1 hour at room temperature. In the interim, the ABC reagent was prepared (5 mL PBS, 2 drops reagent A, 2 drops reagent B) and allowed to sit in a dark drawer for at least 30 minutes prior to use. Once the secondary incubation was complete, the tissues were washed with PBS for 5 minutes. 100 µL of ABC reagent was added to each brain slice and incubated for 30 minutes at room temperature. The tissues were washed with PBS for 5 minutes; all the liquid was removed at this step to limit the amount of free conjugates that would increase the background staining. The tissues were developed using 100 µL of DAB substrate solution (2.5 mL DI water, 2 drops buffer stock, 2 drops DAB, 1 drop H_2O_2; Vector Laboratories) and incubated for 1-4 minutes depending on the rate of development.

The reaction was stopped by removing the DAB solution and adding PBS to the tissues. The slides were dehydrated and cleared in a dipping rack in the fume hood in the following order: 70% EtOH for 5 minutes, 95% EtOH for 5 minutes, 100% EtOH for 5 minutes (repeated twice), xylenes for 5 minutes (repeated twice). The slides were mounted with ~120-150 µL permount:xylene (3:1 ratio) mixture and a coverslip was placed on top. They were air dried for 1 hour prior to imaging the slides and stored long term at 4°C. All three brain slices on each slide were imaged using a 40x brightfield lens on the NanoZoomer (Hammatsu, Japan). Images were visualized using NDP.view software (Hammatsu, Japan) and 20x images were exported for visualization and adjustments to brightness and contrast were done with ImageJ software (NIH, USA).

DAB-IHC staining of human brain tissue

Initial processing of the human brain tissue sections remained the same as the mouse tissue. After blocking with 3% normal goat serum in PBS for 10 min at room temperature, an additional blocking step was performed with BloxAll for 10 min at room temperature (Vector Laboratories). Due to the presence of IgG deposits even in healthy brain and as an artifact of post-mortem tissue preparation (106), the set of 10 rhAbs and the 2 control rhAbs used in the mouse brain IFC were biotinylated to eliminate the need for a species specific secondary antibody. Therefore, the tissues were instead incubated overnight at 4°C with 1 µg biotinylated-rhAb (diluted to 10 ng/µL in blocking buffer) per brain slice. The next day, these biotinylated-rhAbs were detected without a secondary antibody and instead with ABC reagent alone (Vector Laboratories). Dehydration, clearing, mounting, and visualization of the human tissue followed the same procedure as

the mouse tissue

Immunofluorescence (IFC) staining of mouse brain tissue

Ten AGS rhAbs and 2 control rhAbs from the DAB panel were selected for further experiments using IFC. Tissue sections were subjected to antigen retrieval in the same manner as was done for DAB-IHC. The sections were blocked with 1% normal goat serum and 1% Tween-20/PBS for 1 hour at room temperature. The tissues were washed three times with PBS for 5 minutes. Most of the rhAbs were diluted in blocking solution. Pierce Immunostain Enhancer (Thermo Scientific) was used as the diluent for the primary rhAb incubation as well as the secondary Alexa Fluor488 for the following two rhAbs: AJL03, AJL15. Slides were washed three times with PBS for 5 minutes, and then incubated overnight at 4°C with 1 µg rhAb (10 ng/µL) per brain slice.

The following morning, the sections were washed three times with PBS for five minutes. They were then incubated for 1 hour at room temperature with 100 µL of the secondary antibody Alexa Fluor 488 goat anti-human IgG Fc (1:400; Life Technologies) and care was taken to minimize light exposure. The tissues were washed three times with PBS for 5 minutes. Then 100 µL of a colocalization marker, either GFAP (Abcam) or NeuN (Chemicon) were used at 1:1000 and 1:100 dilutions respectively, was incubated for 1 hour at room temperature. The tissues were washed three times with PBS for 5 minutes. The colocalization markers were then probed with 100 µL of the appropriate secondary antibody Alexa Fluor 594 anti-rabbit IgG Fc for GFAP or Alexa Fluor 594 anti-mouse IgG Fc for NeuN detection (1:400; Life Technologies) for 1 hour at room temperature. The tissues were washed three times with PBS for 5 minutes. Next, the

stained tissue sections were incubated for three minutes with DAPI (1:1000) as a counterstain for nuclei (Life Technologies). The sections were washed twice with PBS for 5 minutes and once with DI water for 5 minutes. They were dried of excess buffer and water and then wet mounted with 2-3 drops of Fluoro-Gel (Electron Microscopy Diatome). Slides were viewed with a fluorescent Leica TCS SP5 confocal microscope (Leica microsystems) in the UTSWMC Live Cell Imaging Core with three channel spectral detection. The original .lif files generated were viewed, adjusted in brightness and contrast, and overlaid images were created using ImageJ software (NIH, USA). See Table 2-12 for specifics on the antibodies utilized for IFC.

IFC staining of human brain tissue

Initial processing of the human brain tissue sections for IFC remained the same as the mouse tissue. Again, biotinylated rhAbs were used to eliminate the need for a species-specific secondary antibody. After the initial blocking, endogenous biotin was blocked per manufacturers instructions using the streptavidin-biotin blocking kit (Vector Laboratories). The tissues were incubate with streptavidin solution for 15 minutes, washed twice with PBS for 5 minutes, incubated with biotin solution for 15 minutes, and then washed three times with PBS for 5 minutes. Pierce Immunostain Enhancer (Thermo Scientific) was used as the diluent for the primary rhAb incubation as well as the secondary Alexa Fluor 488 for all human tissue IFC. Slides were incubated overnight at 4°C with 2 µg rhAb (20 ng/µL) per brain slice.

The following morning, the sections were washed with 0.05%Tween/PBS three times for 5 minutes. They were then incubated for 1.5 hours at room temperature with

100 µL of the secondary antibody Alexa Fluor 488 goat anti-streptavidin (1:400; Life Technologies) and care was taken to minimize light exposure. The tissues were then washed with 0.05% Tween/PBS three times for 5 minutes. The colocalization with either GFAP or NeuN, DAPI counterstain, mounting and visualization followed the same procedure as the mouse brain tissue.

IFC staining with Lamin A on mouse brain tissue

Additional IFC using lamin A as a colocalizing marker for the nuclear membrane was performed on a subset of 7 rhAbs that colocalized with NeuN. IFC was done on mouse brains obtained from EAE immunized with full-length recombinant human MOG. Initial processing of frozen mouse brain tissue was performed as for the previous IFC experiments. Slides were incubated overnight at 4°C with 1 µg rhAb (10 ng/µL) simultaneously with lamin A antibody (1:400) diluted in 100µL of Pierce Immunostain Enhancer per brain slice.

The following morning, the sections were washed with 0.05%Tween/PBS 3 times for 5 minutes. They were then incubated for 2 hours on a rotating shaker at 4°C with 100 µL of the secondary antibody Alexa Fluor 488 goat anti-human IgG Fc simultaneously with Alexa Fluor 594 anti-rabbit IgG Fc (both 1:400; Life Technologies). The tissues were then washed with 0.05% Tween/PBS three times for 5 minutes. The DAPI counterstain, mounting and visualization followed the same procedure as the previous IFC on mouse brain tissue experiments.

FIGURE LEGENDS FOR CHAPTER TWO: METHODOLOGY

Figure 2-1. ***Gating strategy for analysis of lymphocyte subpopulations.*** A representative CIS patient's flow cytometry data is shown with arrows indicating the direction of gate analyses. The initial gate was a single/live cell gate followed by a $CD45^+$ lymphocyte gate. From the lymphocyte gate, $CD4^+$, $CD8^+$, $CD138^+$ and $CD19^+$ gates were formed. Naïve ($CD27^-$), memory ($CD27^+$), and plasmablast ($CD27^{high)}$ B cell gates were created within the $CD19^+$ gate. This immunophenotyping was done for each compartment once per patient.

Figure 2-2. ***Sample work-flow of sequence processing and database generation.*** A representative initial individual V_H sequence and resulting paitent total V_H reperotoire summary table are shown with arrows indicating the direction of work-flow. Post purification of PCR product and sending for sequencing, the initial electropherogram is visualized and edited manually for missing nucleotides. This sequence is blasted using IMGT/V-QUEST detailed analysis and the resulting alignment information is imported into TextWrangler and saved as a text file. All the text files comprising a patient's V_H repertoire are run using the perl-based script (AligntoEnd5.pl) generating vgene and mutation information excel databases. These output databases are used to generate summary tables utilizing excel-based scripts.

Figure 2-1

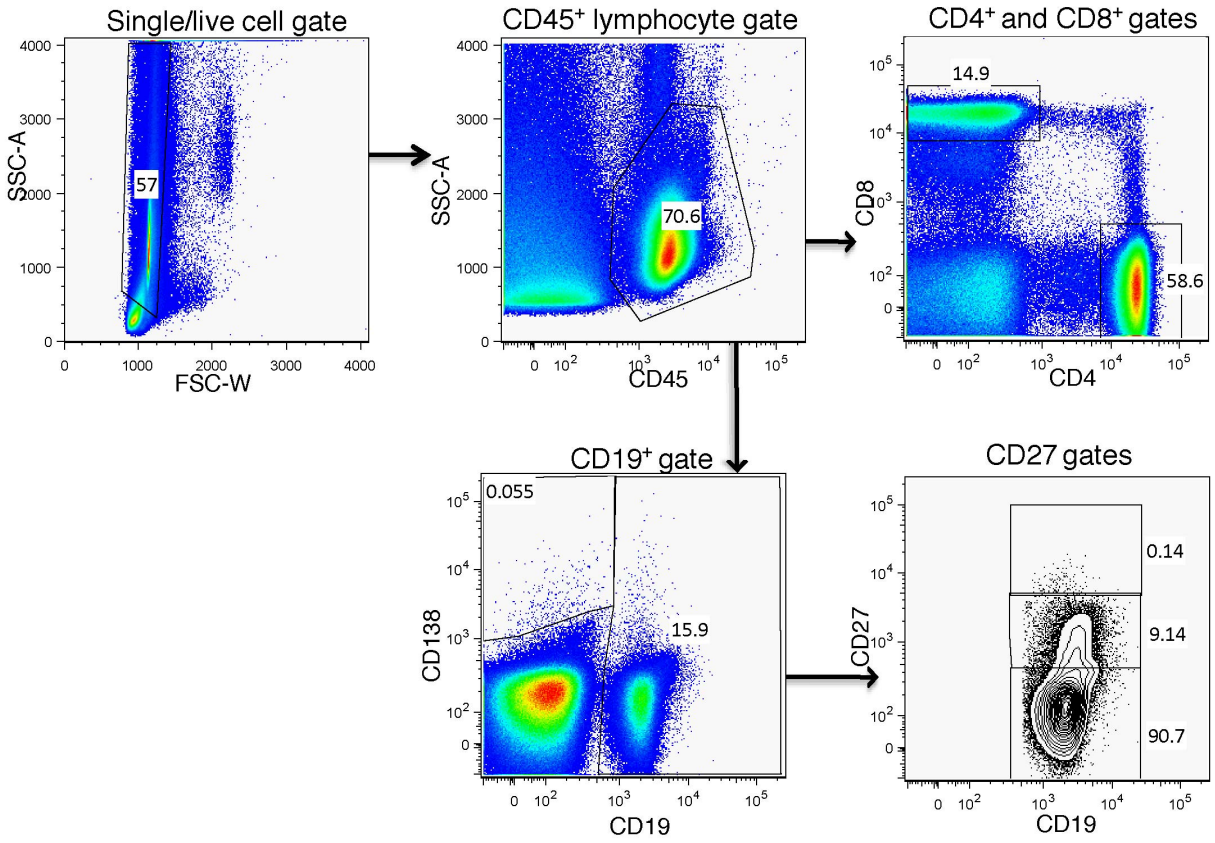
Single/live cell gate
SSC-A
FSC-W
57
CD45⁺ lymphocyte gate
SSC-A
CD45
70.6
CD4⁺ and CD8⁺ gates
CD8
CD4
14.9
58.6
CD19⁺ gate
CD138
CD19
0.055
15.9
CD27 gates
CD27
CD19
0.14
9.14
90.7

Figure 2-2

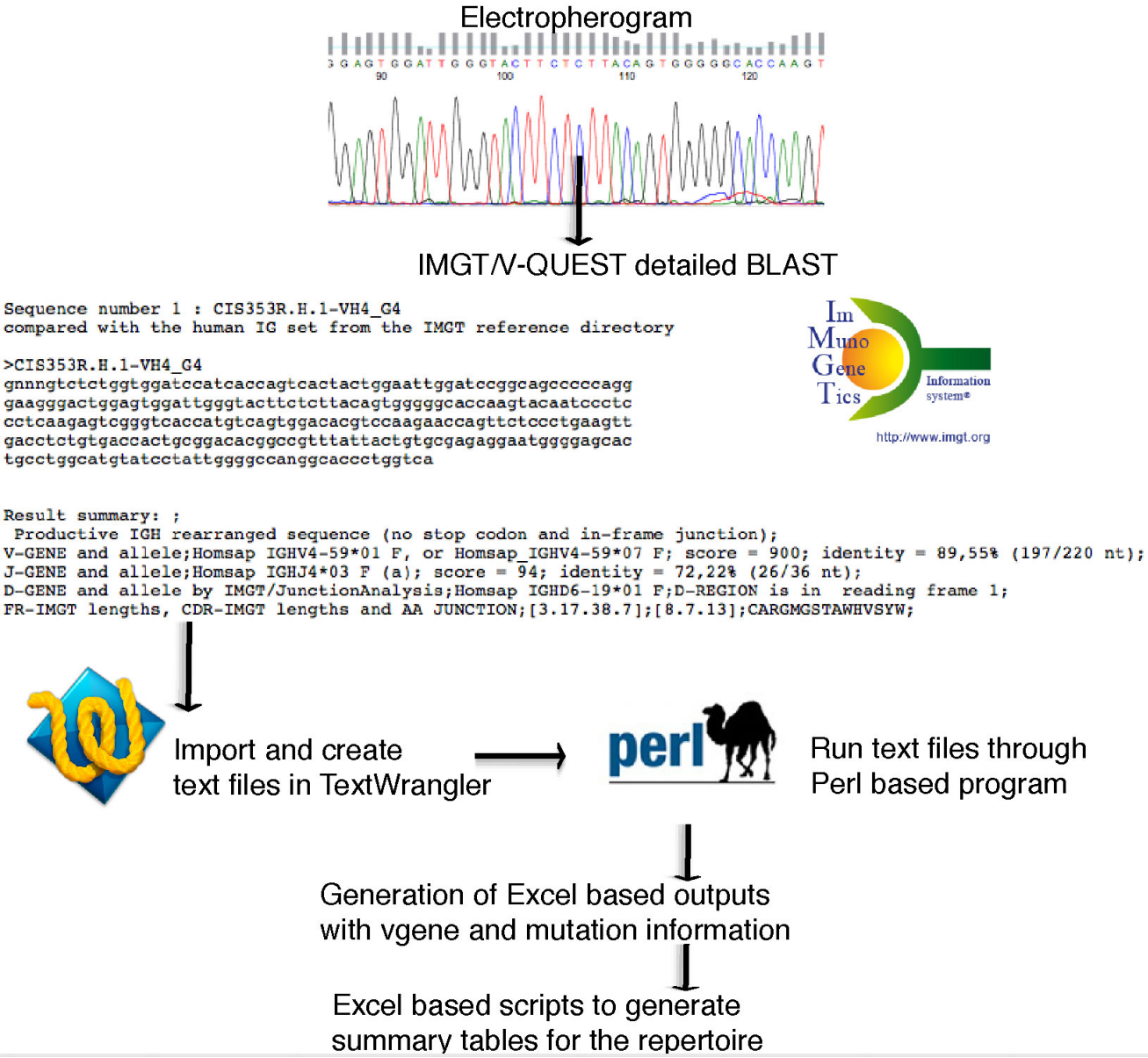
Electropherogram
IMGT/V-QUEST detailed BLAST
Sequence number 1 : CIS353R.H.1-VH4_G4
compared with the human IG set from the IMGT reference directory
>CIS353R.H.1-VH4_G4
gnnngtctctggtggatccatcaccagtcactactggaattggatccggcagcccccagg
gaagggactggagtggattgggtacttctcttacagtgggggcaccaagtacaatccctc
cctcaagagtcgggtcaccatgtcagtggacacgtccaagaaccagttctccctgaagtt
gacctctgtgaccactgcggacacggccgtttattactgtgcgagaggaatggggagcac
tgcctggcatgtatcctattggggccanggcaccctggtca
Im Muno Gene Tics Information system®
http://www.imgt.org
Result summary: ;
Productive IGH rearranged sequence (no stop codon and in-frame junction);
V-GENE and allele;Homsap IGHV4-59*01 F, or Homsap_IGHV4-59*07 F; score = 900; identity = 89,55% (197/220 nt);
J-GENE and allele;Homsap IGHJ4*03 F (a); score = 94; identity = 72,22% (26/36 nt);
D-GENE and allele by IMGT/JunctionAnalysis;Homsap IGHD6-19*01 F;D-REGION is in reading frame 1;
FR-IMGT lengths, CDR-IMGT lengths and AA JUNCTION;[3.17.38.7];[8.7.13];CARGMGSTAWHVSYW;
Import and create text files in TextWrangler
perl
Run text files through Perl based program
Generation of Excel based outputs with vgene and mutation information
Excel based scripts to generate summary tables for the repertoire

Figure 2-2 (continued)

	VH1	VH2	VH3	VH4	VH5	VH6	VH7	Totals	
N	2	1	32	14	2	0	0	51	Total VH
% of total re	3.92%	1.96%	62.75%	27.45%	3.92%	0.00%	0.00%	51	Total J
JH1 N	0	0	3	2	0	0	0	5	JH1 N
JH2 N	0	0	2	1	0	0	0	3	JH2 N
JH3 N	1	0	5	2	1	0	0	9	JH3 N
JH4 N	0	1	16	5	0	0	0	22	JH4 N
JH5 N	0	0	3	2	1	0	0	6	JH5 N
JH6 N	1	0	3	2	0	0	0	6	JH6 N
JH1 %	0.00%	0.00%	9.38%	14.29%	0.00%			9.80%	JH1 %
JH2 %	0.00%	0.00%	6.25%	7.14%	0.00%			5.88%	JH2 %
JH3 %	50.00%	0.00%	15.63%	14.29%	50.00%			17.65%	JH3 %
JH4 %	0.00%	100.00%	50.00%	35.71%	0.00%			43.14%	JH4 %
JH5 %	0.00%	0.00%	9.38%	14.29%	50.00%			11.76%	JH5 %
JH6 %	50.00%	0.00%	9.38%	14.29%	0.00%			11.76%	JH6 %
JH4:JH6	0.00		5.33	2.50				3.67	JH4:JH6
CDR-Mut%	9.85%	7.25%	8.61%	6.59%	1.52%			7.80%	CDR-Mut%
FR-Mut%	2.65%	6.06%	3.27%	4.06%	0.76%			3.42%	FR-Mut%
Total-Mut%	5.05%	6.47%	5.05%	4.90%	1.01%			4.88%	Total=Mut%
%M in CDR	32.50%	38.46%	49.27%	31.98%	25.00%			42.71%	%M in CDR
(targeting)									(targeting)
Total R/S	0.80	1.40	2.16	2.10	3.00			2.03	Total R/S
CDR-R/S	1.75	1.50	4.00	4.89	#DIV/0!			3.91	CDR-R/S
FR-R/S	0.17	1.33	1.21	1.27	1.00			1.16	FR-R/S
CDR3 length	17.50	12.00	15.09	15.07	20.50			15.33	CDR3 length
CDR3 charge	-0.50	1.00	-0.41	0.07	0.50			-0.22	CDR3 charge
% acidic (-)	50.00%	0.00%	46.88%	50.00%	0.00%			45.10%	% acidic (-)
% basic (+)	50.00%	100.00%	21.88%	35.71%	50.00%			29.41%	% basic (+)
% neutral (0	0.00%	0.00%	31.25%	14.29%	50.00%			25.49%	% neutral (0)
max charge	1	1	1	4	1	0	0	4	max charge
min charge	-2	0	-3	-3	0	0	0	-3	min charge
RF (Rcodons	6.06%	10.45%	8.96%	8.87%	2.27%			8.59%	RF (Rcodons/codor
CDR RF	15.91%	13.04%	16.91%	14.25%	4.55%			15.58%	CDR RF
FR RF	1.14%	9.09%	4.97%	6.17%	1.14%			5.08%	FR RF

TABLES FOR CHAPTER TWO: METHODOLOGY

Table 2-1. Fluorescently-labeled antibodies used for FACS

Cell marker	Fluorochrome	BD #	Clone	master mix[1]	compensation[2]
CD45	APC-Cy7	557833	2D1	8 μL	3 μL
CD4	PE-Cy7	557852	SK3	8 μL	3 μL
CD8	APC	555369	RPA-T8	16 μL	5 μL
CD8	PE	555367	RPA-T8	N/A	10 μL
CD19	PerCP-Cy5.5	561295	HIB19	8 μL	3 μL
CD27	FITC	555440	M-T271	32 μL	10 μL
CD138	PE	550805	DL-101	32 μL	N/A

Abbreviations: FACS: fluorescence activated cell sorting, CD: cluster of differentiation, BD: BD Biosciences; N/A: not applicable

[1]Volumes added of each antibody to the master mix of which 34μL was added to CSF cells and 68μL was added to PB cells.

[2]Volumes added of each antibody to the individual respective compensation tubes.

Table 2-2: Patient information and CSF flow cytometry determined cell population percentages															
Patient ID	**Patient Type**	**Age/ Gender**	**CSF mL**	**Cells/mL[1]**	**Single/ Live%**	**CD45$^+$ %[2]**	**CD4$^+$ %**	**CD8$^+$ %**	**4:8 ratio[3]**	**CD138$^+$ %**	**CD19$^+$ %**	**CD27$^-$ %**	**CD27$^+$ %**	**CD27^{high} %**	**N:M ratio[4]**
M357	RRMS	19/F	17.0	10176	74.0	77.8	57.6	19.5	2.95	0.15	5.03	1.16	3.33	0.53	0.30
M423	RRMS	53/F	14.5	n.d.[5]	92.3	75.4	55.7	17.0	3.28	0.41	2.56	0.24	2.26	0.05	0.11
M562	RRMS	n.d./F	10.5	3810	84.5	52.7	55.0	7.2	7.60	1.08	4.34	0.42	3.88	0.05	0.11
NMO316	NMO	43/F	10.0	1580	78.8	16.9	35.0	6.0	5.83	0.55	1.53	0.37	1.04	0.12	0.32
NMO296	NMO	53/F	14.0	14100	92.1	44.4	66.0	26.6	2.48	0.06	2.41	0.29	1.41	0.70	0.14
OND516	PND	74/F	15.0	1700	85.7	55.6	40.9	3.2	12.66	0.35	1.73	0.04	1.69	0	0.03
OND955	PND	63/F	12.5	400	89.5	27.4	57.0	17.8	3.20	0.34	2.01	0.52	1.38	0.10	0.35
CIS166	CIS	31/F	9.5	1579	95.5	7.8	51.6	19.4	2.66	1.87	6.05	0.14	5.35	0.56	0.02
CIS248	CIS	29/F	7.0	2857	84.8	59.1	46.0	11.0	4.18	0.17	1.43	0.49	0.61	0.33	0.52
CIS319	CIS	43/F	10.0	1500	84.3	29.1	59.5	19.6	3.04	0.83	0.16	0	0.10	0.06	0
CIS424	CIS	58/F	11.5	325000	99.9	4.0	69.8	8.0	8.68	0.03	2.26	0.48	1.78	0	0.27
CIS457	CIS	48/F	7.0	30000	84.5	5.6	26.0	27.2	0.96	0.46	7.03	1.85	3.52	1.67	0.36
CIS825	CIS	31/F	14.0	7500	87.7	37.7	54.0	19.4	2.78	0.09	1.94	0.75	1.10	0.09	0.63
CIS968	CIS	65/F	12.5	800	72.4	13.7	27.1	n.d.[5]	n.d.[5]	0.48	4.41	0.31	4.11	0	0.07
CIS212	ON_{CIS}	30/F	20.0	750	97.0	63.0	37.8	18.2	2.08	1.39	12.00	0.51	11.11	0.38	0.04
CIS348	ON_{CIS}	34/F	20.0	8400	96.3	66.7	60.6	19.5	3.11	0.13	6.90	0.60	5.98	0.32	0.10
CIS426	ON_{CIS}	30/M	20.0	n.d.[5]	84.4	59.5	54.3	15.4	3.53	0.11	3.01	0.21	2.60	0.20	0.08
CIS563	ON_{CIS}	40/F	13.5	2593	95.7	46.1	75.0	13.0	5.77	1.02	2.00	0.18	1.28	0.54	0.10
CIS826	ON_{CIS}	35/M	11.0	3409	43.0	16.8	48.0	13.3	3.61	0.56	1.86	0.21	1.51	0.13	0.13
CIS831	ON_{CIS}	40/F	15.0	1000	98.5	59.3	68.9	16.4	4.20	0.74	6.11	1.12	3.21	1.78	0.22
CIS919	ON_{CIS}	21/F	15.0	9000	97.2	86.5	76.3	10.3	7.41	0.02	3.43	1.07	2.04	0.32	0.45
CIS964	ON_{CIS}	54/F	22.0	63181	99.1	1.7	56.9	17.1	3.33	0.67	1.79	0.23	1.13	0.43	0.15
CIS111	TM_{CIS}	62/F	10.0	1500	71.4	88.5	49.4	37.4	1.32	0.15	0.67	0.08	0.23	0.36	0.14
CIS251	TM_{CIS}	54/F	10.0	37500	57.1	3.8	51.4	15.8	3.25	0.37	1.90	0.17	1.69	0.05	0.10
CIS287	TM_{CIS}	46/F	15.0	5600	92.5	32.3	45.6	15.6	2.92	0.4	6.35	1.06	2.69	2.60	0.20
CIS328	TM_{CIS}	33/M	12.0	5000	98.9	86.1	27.9	12.4	2.25	0.13	1.53	0.30	1.20	0.03	0.24
CIS335	TM_{CIS}	34/F	13.0	3846	89.0	81.1	44.2	23.6	1.87	0.95	14.90	1.04	5.72	8.14	0.08
CIS353	TM_{CIS}	58/F	10.5	1905	54.1	8.0	62.4	8.3	7.53	2.46	3.14	0.23	1.47	1.40	0.08
CIS371	TM_{CIS}	56/F	10.0	1000	89.5	6.1	61.0	10.1	6.04	2.82	2.36	0.34	1.77	0.25	0.17

Table 2-2 CONTINUED: Patient information and CSF flow cytometry determined cell population percentages															
Patient ID	**Patient Type**	**Age/ Gender**	**CSF mL**	**Cells/mL[1]**	**Single/ Live%**	**CD45$^+$ %[2]**	**CD4$^+$ %**	**CD8$^+$ %**	**4:8 ratio[3]**	**CD138$^+$ %**	**CD19$^+$ %**	**CD27$^-$ %**	**CD27$^+$ %**	**CD27^{high} %**	**N:M ratio[4]**
CIS431	TM_{CIS}	28/F	14.5	1793	94.0	55.9	40.4	5.7	7.10	0.44	4.78	1.11	2.02	1.65	0.30
CIS527	TM_{CIS}	43/F	16.0	3000	80.8	12.1	77.7	7.8	9.99	0.59	2.59	0.66	1.81	0.12	0.34
CIS663	TM_{CIS}	32/F	10.5	1905	34.4	4.6	55.8	14.3	3.90	1.98	1.98	0	0.74	1.24	0
CIS683	TM_{CIS}	40/F	20.0	1000	90.8	89.3	71.8	15.9	4.52	0.16	0.97	0.06	0.61	0.29	0.07
CIS699	TM_{CIS}	37/F	10.0	1400	78.9	21.1	58.1	17.8	3.26	0.65	2.78	0.28	2.43	0.08	0.11
CIS787	TM_{CIS}	33/M	10.0	1650	62.3	30.7	67.4	20.0	3.37	0.37	2.39	0.83	1.08	0.47	0.53
CIS793	TM_{CIS}	69/M	9.5	1579	64.9	13.8	47.4	13.2	3.59	0.46	4.47	1.21	3.26	0	0.37
CIS799	TM_{CIS}	29/F	10.0	5500	98.0	88.9	68.0	10.5	6.48	0.19	9.53	0.80	5.88	2.84	0.09
CIS834	TM_{CIS}	57/F	9.0	83333	50.7	81.5	61.9	18.5	3.35	0.18	12.70	0.62	11.37	0.71	0.05
CIS873	TM_{CIS}	20/F	11.0	21818	86.8	7.8	48.1	13.8	3.49	0.28	9.14	2.22	5.01	1.91	0.32
CIS924	TM_{CIS}	69/M	21.5	3256	96.5	5.1	14.7	14.7	1.00	0.95	1.59	0.04	1.10	0.45	0.02
CIS942	TM_{CIS}	53/F	9.5	2105	65.4	7.0	65.4	16.7	3.92	0.51	1.41	0.14	1.21	0.06	0.11
CIS991	TM_{CIS}	34/F	10.0	1000	78.5	60.2	63.4	6.1	10.41	0.43	1.59	0.31	1.13	0.15	0.24

[1] Cells/mL was determined using cell counts with a hemacytometer
[2] All immune cell population percentages are determined from the $CD45^+$ lymphocyte gate
[3] 4:8 ratio is determined by dividing the $CD4^+$% by the $CD8^+$ %
[4] naïve (N): memory (M) ratio is determined by dividing the $CD19^+CD27^-$ % by the sum of the $CD19^+CD27^+$ and $CD19^+CD27^{high}$ %'s
[5] not determined (n.d.) due to unavailable information

Table 2-3: Patient information and PB flow cytometry determined cell population percentages															
Patient ID	**Patient Type**	**Age/ Gender**	**PB mL**	**Cells/mL[1]**	**Single/ Live%**	**CD45$^+$ %[2]**	**CD4$^+$ %**	**CD8$^+$ %**	**4:8 ratio[3]**	**CD138$^+$ %**	**CD19$^+$ %**	**CD27$^-$ %**	**CD27$^+$ %**	**CD27^{high} %**	**N:M ratio[4]**
M357	RRMS	19/F	5.0	$1.86x10^6$	17.2	57	43.4	24.5	1.77	0.04	10.7	7.99	2.51	0.21	2.94
M423	RRMS	53/F	5.0	n.d.[5]	81.6	36.3	36.4	17.1	2.13	0.10	13.5	6.59	6.86	0.11	0.95
M562	RRMS	n.d./F	5.0	$5.75x10^6$	70.8	73.9	34.8	13.8	2.52	0.05	9.48	4.45	4.97	0.06	0.88
NMO316	NMO	43/F	10.0	$1.39x10^6$	44.8	57.9	44.9	9.56	4.70	0	6.08	4.77	1.27	0.05	3.60
NMO296	NMO	53/F	5.0	$1.50x10^6$	72.5	68.1	57.4	22.8	2.52	0	3.70	2.80	0.85	0.03	3.19
OND516	PND	74/F	4.5	$1.16x10^7$	75.5	79.6	17.6	6.8	2.63	0.18	16.7	15.73	0.95	0.02	16.28
OND955	PND	63/F	3.0	$1.25x10^6$	70.1	90.6	27.6	12.1	2.28	0	5.96	3.77	2.04	0.14	1.73
CIS166	CIS	31/F	5.0	$1.45x10^6$	98.4	47.0	44.5	19.1	2.33	0.04	16.90	13.11	3.45	0.27	3.53
CIS248	CIS	29/F	10.0	$1.45x10^6$	93.6	27.8	38.7	14.8	2.61	0.04	15.20	13.07	1.81	0.31	6.17
CIS319	CIS	43/F	8.0	$1.38x10^6$	96.6	23.3	37.2	24.4	1.52	0.04	11.20	9.05	1.98	0.09	4.37
CIS424	CIS	58/F	10.0	$3.25x10^6$	98.0	58.7	50.7	10.2	4.97	0.01	12.10	11.40	0.68	0.02	16.19
CIS457	CIS	48/F	5.5	$1.82x10^6$	97.3	22.6	51.8	11.2	4.63	0.02	18.50	14.04	3.87	0.71	3.07
CIS825	CIS	31/F	7.5	$2.67x10^6$	97.4	29.3	58.3	15.3	3.81	0.01	10.60	7.50	2.96	0.19	2.38
CIS968	CIS	65/F	5.0	$2.00x10^6$	75.2	41	44.3	n.d.[5]	n.d.[5]	0.03	17.40	11.61	5.79	0	2.00
CIS212	ON_{CIS}	30/F	12.5	$1.74x10^6$	98.1	73.9	52.4	11.4	4.60	0.01	14.10	9.52	4.39	0.17	2.09
CIS348	ON_{CIS}	34/F	10.0	$1.30x10^6$	96	43.8	32.2	29.7	1.08	0.01	14.40	5.04	9.23	0.03	0.54
CIS426	ON_{CIS}	30/M	15.0	$1.58x10^6$	97.6	49.2	51.0	14.9	3.42	0.05	6.29	3.81	2.48	0	1.53
CIS563	ON_{CIS}	40/F	10.0	$2.15x10^6$	96.5	42.3	65.3	16.9	3.86	0.03	11.20	4.58	6.56	0.06	0.69
CIS826	ON_{CIS}	35/M	5.5	$4.77x10^6$	31.5	53.8	42.4	11.4	3.72	0.04	10.00	6.11	3.82	0.05	1.58
CIS831	ON_{CIS}	40/F	1.0	$1.25x10^6$	98.4	23.2	43.2	18.1	2.39	0.11	12.70	6.85	5.80	0.14	1.15
CIS919	ON_{CIS}	21/F	4.0	$9.38x10^5$	85.4	80.8	46.6	18.3	2.55	0	9.60	6.09	3.44	0.09	1.73
CIS964	ON_{CIS}	54/F	14.0	$1.06x10^6$	97.8	48.0	46.6	14.9	3.11	0.07	7.85	4.18	3.56	0.11	1.14
CIS111	TM_{CIS}	62/F	5.5	$2.05x10^6$	54.5	79.9	39.3	37.5	1.05	0.22	5.43	2.63	1.59	1.21	0.94
CIS251	TM_{CIS}	54/F	5.0	$4.50x10^6$	20.9	20.8	47.5	19.1	2.49	0.17	12.50	7.74	4.66	0.13	1.61
CIS287	TM_{CIS}	46/F	5.0	$1.00x10^6$	98.8	60.9	27.7	24.9	1.11	0.05	6.28	3.51	2.41	0.36	1.27
CIS328	TM_{CIS}	33/M	5.0	$3.00x10^6$	99.2	71.2	24.9	16.6	1.50	0.05	16.90	12.98	3.92	0.01	3.30
CIS335	TM_{CIS}	34/F	6.0	$3.86x10^6$	75.7	30.7	46.8	16.6	2.82	0.08	8.24	3.87	4.05	0.35	0.88
CIS353	TM_{CIS}	58/F	5.0	$3.00x10^6$	14.7	68.3	53.2	15.3	3.48	2.22	5.06	1.52	2.89	0.65	0.43
CIS371	TM_{CIS}	56/F	2.25	$4.17x10^6$	27.9	40.7	47.7	24.6	1.94	0.38	2.36	0.34	1.77	0.25	0.17

Table 2-3 CONTINUED: Patient information and PB flow cytometry determined cell population percentages															
Patient ID	**Patient Type**	**Age/ Gender**	**PB mL**	**Cells/mL[1]**	**Single/ Live%**	**$CD45^+$ %[2]**	**$CD4^+$ %**	**$CD8^+$ %**	**4:8 ratio[3]**	**$CD138^+$ %**	**$CD19^+$ %**	**$CD27^-$ %**	**$CD27^+$ %**	**$CD27^{high}$ %**	**N:M ratio[4]**
CIS431	TM_{CIS}	28/F	10.0	$3.31x10^6$	97	49.8	42.1	12.1	3.48	0.02	14.10	11.22	2.62	0.26	3.90
CIS527	TM_{CIS}	43/F	5.0	$1.50x10^6$	97.6	7.41	43.4	15.1	2.87	0.05	23.50	8.81	14.50	0.81	0.60
CIS663	TM_{CIS}	32/F	5.0	$2.75x10^6$	113	54.7	54.3	22.4	2.42	1.84	9.25	1.40	5.42	2.16	0.18
CIS683	TM_{CIS}	40/F	15.0	$3.75x10^6$	98.8	45.6	65.2	10.3	6.33	0.05	7.00	4.63	2.33	0.04	1.95
CIS699	TM_{CIS}	37/F	4.5	$4.22x10^5$	93.4	11.4	36.1	22.1	1.63	0.06	22.40	11.56	10.44	0.20	1.09
CIS787	TM_{CIS}	33/M	5.5	$1.82x10^6$	62.9	64.1	58.6	14.8	3.96	0.07	16.00	14.51	1.46	0.02	9.77
CIS793	TM_{CIS}	69/M	5.5	$4.55x10^6$	80.7	41.1	30.2	6.5	4.65	0.18	52.00	33.38	18.62	0.01	1.79
CIS799	TM_{CIS}	29/F	10.0	$3.13x10^6$	98.3	39.9	61.3	10.9	5.62	0.07	13.70	6.00	7.38	0.32	0.78
CIS834	TM_{CIS}	57/F	5.5	$6.59x10^6$	54.2	23.1	15.6	6.5	2.40	1.03	26.30	7.84	18.30	0.15	0.42
CIS873	TM_{CIS}	20/F	5.0	$9.12x10^5$	95.7	21.1	33.0	18.9	1.75	0.09	26.30	17.86	7.84	0.61	2.11
CIS924	TM_{CIS}	69/M	5.0	$1.55x10^6$	97.6	72.2	36.2	15.1	2.40	0.01	9.73	3.87	5.35	0.52	0.66
CIS942	TM_{CIS}	53/F	5.0	$3.25x10^6$	39	36.1	47.7	10.5	4.54	0.25	13.70	8.33	5.29	0.08	1.55
CIS991	TM_{CIS}	34/F	4.0	$1.88x10^6$	56.3	50.0	59.1	10.1	5.85	0.03	10.50	6.84	3.42	0.25	1.86
CIS111R	TM_{CIS}		72.0	$1.18x10^6$	82.3	39.7	40.4	34.2	1.18	0.86	9.76	6.08	3.53	0.15	1.65
CIS431R	TM_{CIS}		67.0	$4.25x10^6$	73.3	64.1	44.5	24.1	1.85	0.85	16.8	12.18	4.50	0.10	2.64
CIS353R	TM_{CIS}		73.0	$7.7x10^5$	44.2	85.8	42.5	29.8	1.43	1.23	7.7	5.15	2.53	0.03	2.02
CIS683R	TM_{CIS}		72.0	$1.28x10^6$	73.2	41.7	69.8	9.81	7.12	1.77	3.17	2.70	0.43	0.03	5.82

[1] Cells/mL was determined using cell counts with a hemacytometer

[2] All immune cell population percentages are determined from the $CD45^+$ lymphocyte gate

[3] 4:8 ratio is determined by dividing the $CD4^+$% by the $CD8^+$ %

[4] naïve (N): memory (M) ratio is determined by dividing the $CD19^+CD27^-$ % by the sum of the $CD19^+CD27^+$ and $CD19^+CD27^{high}$ %'s

[5] not determined (n.d.) due to unavailable information

Table 2-4. Formulations for mixes used for one cPEP plate[1]			
cPEP sort mix			
Component	*Vendor*	*Volume*	
0.1 M DTT (from SSRT III kit)[2]	Invitrogen/ Life-Technologies	53.7 μL	
Recombinant RNAsin	Promega	48.3 μL	
0.5x PBS	Cellgro	454 μL	
		536.3 μL	***Final volume***[3]
		4 μL	***volume per well***
Random Hexamer Primer (RHP) mix			
Component	*Vendor*	*Volume*	
Random Hexamer primers (3 μg/μL)	Invitrogen/ Life-Technologies	7.67 μL	
10% Igepal CO-630	Sigma	76.7 μL	
Recombinant RNAsin	Promega	23.33 μL	
Nuclease-free water	Biotex	392 μL	
		499.7 μL	***Final volume***[3]
		3.5 μL	***volume per well***
Reverse Transcription (RT) mix			
Component	*Vendor*	*Volume*	
5x First strand buffer (from SSRT III kit)[2]	Invitrogen/ Life-Technologies	396 μL	
10 mM dNTP	Promega	261.6 μL	
Recombinant RNAsin	Promega	26.4 μL	
Nuclease-free water	Biotex	8.4 μL	
Superscript RT III	Invitrogen/ Life-Technologies	33 μL	
		857.4 μL	***Final volume***[3]
		7 μL	***volume per well***

[1] One cPEP plate (96 wells) contained both the sorted cells and the cPEP reaction was performed in the same sorted plate.
[2] These reagents were provided as part of the kit with the Superscript RT III (SS RT III) enzyme.
[3] Final volume of the mix accounted for volume loss due to pipetting and transferring to reagent reservoirs.

Table 2-5. Primer sequences for V_H and Vκ amplifications	
Primers for V_H amplifications	
Primer name	Sequence (all in direction for ordering: complement)
VH1E	CAGCTKGTRCAGTCTGG
VH2E	CAGRTCACCTTGAAGGA
VH3E	GTGCAGCTGKTGGAG
VH4E	CAGSAGTSGGGCBCAG
JHE	CTGARGAGACRGTGAC
VH1N	GTCTGGRSCTGAGGTGAAGAAG
VH2N	GAGTCTGGTCCTRYGCTGGTG
VH3N1	GGAGTCTGGGGGAGGYBTGGT
VH3N2	GAGKCKTGGTMCAGCCTGGG
VH3N3	GGAGGCTTRRTYCAGCCTGGG
VH4N	GGCBCAGGACTGKTGAAGCCTT
JH1245N	GTGACCRTKGTCCCTTGGCCC
JH36N	TGACCAGGGTKCCMYGGCCC
Primers for Vκ amplifications	
VK12E	GCTCAGCTCCTGGGGCT
VK3E	GGAARCCCCAGCDCAGC
VK45E	CTSTTSCTYTGGATCTCTG
JK2E	ACGTTTGATCTCCAGCTTG
JK5E	CTTACGTTTAATCTCCAGTC
VK1N	CATCCAGWTGACCCAGTCTCC
VK2N	TCCAGTGGGGATATTGTGATGAC
VK3N	GTCTKTGTCTCCAGGGGAAAGAG
VK4N	GACATCGTGATGACCCAGTCTC
VK5N	GGGCAGAAACGACACTCACGCA
JK2N	CAGCTTGGTCCCCTGGCCAAA
JK5N	CCAGTCGTGTCCCTTGGCCG
IUPAC nucleotide codes for mixed bases: R (A or G), Y (C or T), S (G or C), W (A or T), K (G or T), M (A or C), B (C, G, or T), D (A, G, or T), H (A, C, or T), V (A, C, or G), N (any base)	

Table 2-6. Template, primers, $MgCl_2$ concentration, and PCR reaction cycles for V_H and Vκ amplifications[1]				
V_H amplifications				
Reaction name	Template	Primers[2]	$MgCl_2$	PCR cycles
VHE	1.5 μL cPEP	VH1E, VH2E, VH3E, VH4E, JHE	1.5 mM	95°C, 7min; {94°C, 1min; 52°C, 30sec; 72°C, 1.5min} x45 cycles; 72°C, 10min; 4°C, ∞
VH1N	5 μL VHE	VH1N; JH1245N; JH36N	1.5 mM	95°C, 5min; {94°C, 1min; 67°C, 30sec; 72°C, 1.5min} x50 cycles; 72°C, 10min; 4°C, ∞
VH2N	5 μL VHE	VH2N; JH1245N; JH36N	1.5 mM	*Same as VH1N*
VH3N	5 μL VHE	VH3N1; VH3N2; VH3N3; JH1245N; JH36N	1.5 mM	*Same as VH1N*
VH4N	5 μL VHE	VH4N; JH1245N; JH36N	1.5 mM	*Same as VH1N*
Vκ amplifications				
Reaction name	Template	Primers	$MgCl_2$	PCR cycles
VK12E	1.5 μL cPEP	VK12E; JK2E; JK5E	3.5 mM	95°C, 5min; {94°C, 1min; 56°C, 30sec; 72°C, 1.5min} x40 cycles; 72°C, 5min; 4°C, ∞
VK3E	1.5 μL cPEP	VK3E; JK2E; JK5E	2.5 mM	*Same as VK12E*
VK45E	1.5 μL cPEP	VK45E; JK2E; JK5E	2 mM	*Same as VK12E*
VK1N	5 μL VK12E	VK1N; JK2N; JH5N	3.5 mM	95°C, 7min; {94°C, 1min; 65°C, 1min; 72°C, 1.5min} x50 cycles; 72°C, 5min; 4°C, ∞
VK2N	5 μL VK12E	VK2N; JK2N; JH5N	3.5 mM	*Same as VK1N*
VK3N	5 μL VK3E	VK3N; JK2N; JH5N	2.5 mM	*Same as VK1N*
VK4N	5 μL VK45E	VK4N; JK2N; JH5N	2 mM	*Same as VK1N*
VK5N	5 μL VK45E	VK5N; JK2N; JH5N	2 mM	*Same as VK1N*

[1] All reactions were in a final volume of 50 μL adjusted with nuclease free water. The final concentrations of dNTPs (0.2mM), 5x PCR buffer (1x), and Go-Taq DNA polymerase (1 unit/reaction) did not vary between the different PCR reactions.
[2] All primers were used at a final concentration of 0.5 μM and heated at 95°C for 5 minutes prior to adding to the master mix. The sequences for each primer are listed in table 2-5.

Table 2-7: V_H gene usage and mutation overview of single cell PCR amplified from CSF $CD19^+$ B cells

Patient ID	Patient Type	# V_H	% V_H1	% V_H2	% V_H3	% V_H4	% V_H5	% V_H6	% V_H7	Average MF[1]	CDR R:S[2]	FR R:S[2]
M357	RRMS	82	14.63	3.66	25.61	56.10	0	0	0	4.48	4.96	1.42
CIS212	ON_{CIS}	4	0	0	50.0	50.0	0	0	0	3.76	4.67	2.00
CIS348	ON_{CIS}	79	8.86	3.80	30.38	51.90	5.06	0	0	5.96	4.99	1.44
CIS426	ON_{CIS}	8	0	0	37.5	62.5	0	0	0	5.47	2.15	1.35
CIS563	ON_{CIS}	24	0	4.17	16.67	79.17	0	0	0	8.04	3.62	1.83
CIS831	ON_{CIS}	120	10.00	4.17	30.00	50.83	4.17	0	0.8	4.68	2.87	1.70
CIS964	ON_{CIS}	5	0	0	40.0	60.0	0	0	0	3.14	5.00	2.4
CIS251	TM_{CIS}	13	23.08	0	53.85	23.08	0	0	0	4.93	3.58	1.55
CIS287	TM_{CIS}	12	0	0	41.70	58.30	0	0	0	5.42	5.11	1.11
CIS328	TM_{CIS}	31	64.52	0	19.35	16.31	0	0	0	4.16	3.82	0.75
CIS335	TM_{CIS}	95	8.42	3.16	26.32	61.05	1.05	0	0	6.75	2.93	1.86
CIS353	TM_{CIS}	36	25.00	0	38.89	19.44	16.67	0	0	3.72	2.53	1.77
CIS371	TM_{CIS}	31	0	3.23	29.03	64.52	0	3.23	0	3.96	2.47	1.04
CIS431	TM_{CIS}	51	21.57	0	39.22	27.45	1.96	7.84	1.96	5.42	4.16	0.96
CIS527	TM_{CIS}	22	13.64	4.55	40.91	40.91	0	0	0	2.71	5.22	0.93
CIS683	TM_{CIS}	5	0	0	0	100	0	0	0	8.56	4.17	2.00
CIS787	TM_{CIS}	69	18.84	4.35	44.93	26.09	5.80	0	0	2.83	4.38	1.61
CIS834	TM_{CIS}	89	26.97	5.62	30.34	30.34	3.37	0	3.37	3.70	4.21	1.47
CIS873	TM_{CIS}	40	2.50	2.50	32.50	62.50	0	0	0	5.00	4.46	1.12

[1] Average mutation frequency (MF) represents the number of nucleotide mutations across the sequence read length
[2] Replacement : Silent (R:S) mutation ratios represents the number of R mutations divided by the number of S mutations within the given regions

PCR amplifications done on all available $CD19^+$ sorted cells within the patient's 96 well plate. All amplified, productive, V_H segments are reported here.

Table 2-8: V_H gene usage and mutation overview of single cell PCR amplified from PB $CD19^+$ B cell subsets

Patient ID	Patient Type	# V_H	% V_H1	% V_H2	% V_H3	% V_H4	% V_H5	% V_H6	% V_H7	Average MF	CDR R:S	FR R:S
PB $CD19^+CD27^+$ memory B cells												
CIS111R	TM_{CIS}	14	7.14	0	42.86	42.86	7.14	0	0	6.73	2.14	1.26
CIS431R	TM_{CIS}	71	14.08	0	49.30	29.58	4.23	0	2.82	5.00	3.05	1.61
CIS353R	TM_{CIS}	54	7.41	5.56	51.85	33.33	1.85	0	0	4.83	2.95	1.63
CIS683R	TM_{CIS}	61	9.84	3.28	57.38	22.95	6.56	0	0	3.96	5.44	1.53
PB $CD19^+CD27^{high}$ plasmablasts												
CIS111R	TM_{CIS}	58	22.41	3.45	37.93	32.76	3.45	0	0	7.01	3.41	1.35
CIS431R	TM_{CIS}	81	12.35	0	67.90	18.52	1.23	0	0	6.75	4.62	1.41
CIS353R	TM_{CIS}	51	3.92	1.96	62.75	27.45	3.92	0	0	4.88	3.91	1.16
CIS683R	TM_{CIS}	63	7.94	3.17	58.73	22.22	6.35	1.59	0	6.06	3.96	1.60

[1] Average mutation frequency (MF) represents the number of nucleotide mutations across the sequence read length
[2] Replacement : Silent (R:S) mutation ratios represents the number of R mutations divided by the number of S mutations within the given regions

PCR amplifications done on all available $CD19^+CD27^+$ or $CD19^+CD27^{high}$ sorted cells within the patient's 96 well plate. All amplified, productive, V_H segments are reported here.

Table 2-9. Patient, gene, and AGS overview of the 32 cloned rhAbs						
Patient #; code	Diagnosis	rhAb	Clone	# AGS[1]	V_H; J_H[2]	Vκ; Jκ[3]
1; M357	CDMS	AJL02	No	2	4-31; 4	1-39; 2
		AJL03	No	2	4-39; 1	1-33; 2
2; CIS563	ON_{CIS}	AJL10	No	4	4-4; 6	2-28; 5
		AJL11	No	3	4-39; 5	3-20; 2
		WR12[4]	Yes	2	4-30; 4	2-28; 4
		WR13[4]	Yes	2	4-30; 4	2-28; 2
3; CIS831	ON_{CIS}	AJL06	No	3	4-30; 4	1-33; 2
		AJL07[5]	Yes	3	4-59; 4	1-13; 2
		AJL08	Yes	3	4b; 4	1-5; 2
		AJL09	Yes	2	4-59; 5	1-13; 5
		AJL13[5]	Yes	3	4-59; 4	2-30; 5
4; CIS431	TM_{CIS}	AJL01	Yes	3	4-34; 3	3-20; 5
		WR10[6]	Yes	2	4-4; 6	3-20; 5
		WR11[6]	Yes	2	4-4; 6	3-11; 4
5; CIS873	TM_{CIS}	AJL14	No	3	4-61; 6	4-1; 2
		AJL15	Yes	4	4-39; 5	2D-29; 2
		AJL16	Yes	3	4-39; 5	1-33; 5
6; CIS787	TM_{CIS}	AJL18	Yes	5	4-31; 5	1-39; 1
		AJL19	Yes	3	4-34; 3	3-20; 2
		AJL20	No	3	4-39; 4	1-27; 4
7; M125	CDMS	WR01[7]	Yes	2	4-59; 6	3-20; 2
		WR02[7]	Yes	2	4-30; 6	3-20; 2
8; M584	CDMS	WR03	No	3	4-4; 3	3-20; 1
		WR04	No	3	4-39; 4	3-15; 2
		WR05	No	4	4-61; 1	1-5; 4
		WR06	No	3	4-39; 3	1-5; 3
9; M522	CDMS	WR07	No	4	4-39; 4	3-20; 1
10; CIS348	ON_{CIS}	AJL04	Yes	3	4-59; 5	1-16; 5
		AJL05	Yes	4	4-39; 4	1-16; 5
		AJL12	No	3	4-39; 5	3-20; 1
		WR08[8]	Yes	2	4-31; 4	2-30; 5
		WR09[8]	Yes	2	4-31; 4	3-20; 2

Abbreviations: CDMS: clinically definite multiple sclerosis, ON_{VIS}: clinically isolated syndrome-optic neuritis, TM_{CIS}: clinically isolated syndrome- transverse myelitis, rhAb: recombinant human antibody, AGS: antibody gene signature; V_H: variable heavy, J_H: junctional heavy, Vκ: variable kappa, Jκ: junctional kappa, N/A: not applicable

[1] Number of mutated AGS codons (6 total possible) in the VH gene of the rhAb.

[2] V_H and J_H genes utilized in the heavy chain of the rhAb.

[3] Vκ and Jκ genes utilized in the light chain of the rhAb.

Clonally related sequences: [4] WR12 and WR13; [5] AJL07 and AJL13; [6] WR10 and WR11; [7] WR01 and WR02; [8] WR08 and WR09

Table 2-10. Primer sequences for rhAb cloning PCR		
Primers for V_H4 rhAb constructs		
Primer name	V_H4/J_H genes	Sequence (all in direction for ordering: complement)
VH4shuttle	All except 4-34	TGCAGGAGTCGGGCCCAGG
VH4-34shuttle	4-34	TACAGCAGTGGGGCGCAGG
VH4Ig	All except 4-34, 4-39	CTGCA**ACCGGT**GTACATTCCCAGGTGCAGCTGCAGGAG
VH4-34Ig	4-34	CTGCA**ACCGGT**GTACATTCCCAGGTGCAGCTACAGCAGTGGG
VH4-39Ig	4-39	CTGCA**ACCGGT**GTACATTCCCAGCTGCAGCTGCAGGAG
JH12Ig	J_H1, J_H2	TGCGAA**GTCGAC**GCTGAGGAGACGGTGACCAG
JH3Ig	J_H3	TGCGAA**GTCGAC**GCTGAAGAGACGGTGACCATTG
JH45Ig	J_H4, J_H5	TGCGAA**GTCGAC**GCTGAGGAGACGGTGACCAG
JH6Ig	J_H6	TGCGAA**GTCGAC**GCTGAGGAGACGGTGACCGTG
Primers for Vκ rhAb constructs		
Primer name	Vκ/Jκ genes	Sequence (all in direction for ordering: complement)
VK3-20shuttle	3-20	AGTCTCCAGGCACCCTGTCTTTGTCT
VK3-15shuttle	3-15	AGTCTCCAGCCACCCTGTCTGTGTCT
VK1-5Ig	1-39,1D-39,1-33,1D-33,1-27,1-17,1D-16, 1-12,1D-12,1-5	CTGCA**ACCGGT**GTACATTCTGACATCCAGATGACCCAGTC
VK1-9Ig	1-9	TTGTGCTGCA**ACCGGT**GTACATTCAGACATCCAGTTGACCCAGTCT
VK1-13Ig	1-13,1D-13	TTGTGCTGCA**ACCGGT**GTACATTCAGCCATCCAGTTGACCCAGTCT
VK1D-43Ig	1D-43,1-8, 1-6	CTGCA**ACCGGT**GTACATTGTGCCATCCGGATGACCCAGTC
VK2-24Ig	2-40, 2D-40, 2-29, 2-24	CTGCA**ACCGGT**GTACATGGGGATATTGTGATGACCCAGAC
VK2-28Ig	2-28, 2D-28	CTGCA**ACCGGT**GTACATGGGGATATTGTGATGACTCAGTC
VK2-30Ig	2-30, 2D-30	CTGCA**ACCGGT**GTACATGGGGATGTTGTGATGACTCAGTC
VK3-15Ig	3-15, 3D-15, 3D-7	CTGCA**ACCGGT**GTACATTCAGAAATAGTGATGACGCAGTC
VK3-20Ig	3-20, 3D-20, 3-11, 3D-11	TGTGCTGCA**ACCGGT**GTACATTCAGAAATTGTGTTGACGCAGTCT
VK4-1Ig	4-1	CTGCA**ACCGGT**GTACATTCGGACATCGTGATGACCCAGTC
JK1Ig	Jκ1	GCCAC**CGTACG**TTTGATYTCCACCTTGGTC
JK2Ig	Jκ2	GCCAC**CGTACG**TTTGATYTCCAGCTTGGTC
JK3Ig	Jκ3	GCCAC**CGTACG**TTTGATATCCACTTTGGTCCCAGGGC
JK4Ig	Jκ4	GCCAC**CGTACG**TTTGATCTCCACCTTGGTCCCTCCGC
JK5Ig	Jκ5	GCCAC**CGTACG**TTTAATCTCCAGTCGTGTC

Table 2-11. Procedure for double restriction enzyme digestion of vector backbone and variable region inserts		
Procedure for Vector Backbone cuts (max DNA/reaction = 4µg)		
Component (NEB)	IgG vector	IgK vector
SalI HF (20000 u/mL; 50x)	5 µL (2 fold)	-
BsiWI (10000 u/mL; 10x)	-	2 µL (2 fold)
Buffer (stock at 10x)	5 µL of #4	5 µL of #1
Add H_2O up to 50 µL		
20 minute incubation at:	37°C	55°C
After 20 minutes add same amount of enzyme again; another 20 minute incubation		
20 minute denaturation at:	65°C	80°C
Run reaction on 0.7% gel at 100V for 1.5 hours. Gel purify linearized band.		
AgeIHF (20000 u/mL; 50x)	2.5 µL (1 fold)	2.5 µL (1 fold)
Buffer (stock at 10x)	5 µL of #4	5 µL of #4
BSA	0.5 µL	0.5 µL
Add H_2O up to 50 µL		
20 minute incubation at:	37°C	37°C
20 minute denaturation at:	65°C	65°C
Column purify doubly-cut vector backbones		
Procedure for Variable region insert cuts (max DNA/reaction = 2 µg from vector, 200 ng from PCR reaction)		
Component (NEB)	IgG insert	IgK insert
AgeHF (20000 u/mL; 50x)	1.25 µL (1 fold)	1.25 µL (1 fold)
SalI HF (20000 u/mL; 50x)	2.5 µL (2 fold)	-
BsiWI (10000 u/mL; 10x)	-	2 µL (2 fold)
Buffer (stock at 10x)	5 µL of #4	5 µL of #1
BSA	0.5 µL	0.5 µL
Add H_2O up to 50 µL		
20 minute incubation at:	37°C	37°C
20 minute denaturation at:	65°C	80°C
Column purify doubly-cut variable region inserts		

Table 2-12. Antibodies used for IFC experiments					
Antibody	**Species**	**Fluorochrome**	**Vendor**	**Vendor #**	**Working dilution**
rhAb	Human	N/A	N/A	N/A	10 ng/μL[1]
NeuN[2]	Mouse	N/A	Chemicon (Millipore)	MAB377	1:100
GFAP	Rabbit	N/A	Abcam	ab7260	1:1000
Lamin-A	Rabbit	N/A	Abcam	ab26300	1:400
Human IgG Fc	Goat	Alexa Fluor 488	Life Technologies	A-11013	1:400
Rabbit IgG Fc	Goat	Alexa Fluor 594	Life Technologies	A-11012	1:400
Mouse IgG Fc	Goat	Alexa Fluor 594	Life Technologies	A-11005	1:400
Streptavidin	N/A	Alexa Fluor 488	Life Technologies	S-11223	1:400

[1] 10 ng/μL was used for all mouse IHC, IFC and human IHC. The concentration was changed to 20 ng/μL for human IFC.
[2] NeuN was clone A60. All other antibodies were polyclonal

CHAPTER THREE

RESULTS

AIM I: AGS POSITIVE B CELLS ARE ENRICHED IN MS DISEASE

Overview and rationale

The laboratory has previously published AGS scores and enrichment in CSF B cells from MS and ON_{CIS} patients at high risk to convert (228). An AGS score over 6.8 in an ON_{CIS} patient's repertoire was predictive of conversion to CDMS. This is unique to the MS diseased compartment since the average AGS score from 3 OND patients was 4.5, and from 3 MSPB patient samples was 2.0. Since publication, the AGS scores have been recalculated for all patients' repertoires past and present to re-anchor the replacement mutation (RM) counts to only include codons 31-92. This was done to better accommodate and standardize across different sources of repertoires, but has not changed the overall conclusions derived from the initial findings.

It was unknown if the same AGS enrichment could also be detected in CNS B cells from MS patients. Finding the same genomic marker in diseased tissue would provide support for further study of CSF B cells as they are reflective of the CNS B cell repertoire. In collaboration with Drs. Hafler and O'Connor, we received V_H repertoires from 4 postmortem MS CNS specimens using laser capture microdissection (LCM) to isolate B cells and PCR their V_H regions. The resulting AGS scores have been published (340). Post publication, in collaboration with Drs. Fire and Boyd we received V_H repertoires from 4 postmortem MS CNS specimens using NGS to obtain the antibody

sequences. AGS enrichment was found in both sets of MS CNS B cell repertoires isolated from NAWM as well as plaques.

CSF B cell V_H repertoires were previously provided by Drs. Owens and Bennett (University of Colorado Denver) in order to determine the ability for the AGS score to predict conversion of an ON_{CIS} patient to CDMS (228). It was unknown whether patients with the other major initial presentation, TM_{CIS}, also displayed enrichment of the AGS in their CSF B cell repertoires. Since the anatomical location of the lesions and general prognosis differs between ON_{CIS} and $TM_{CIS,}$ it was possible that the influences shaping the B cell repertoire may be different, resulting in a different genomic pattern. We found that regardless of the patient's initial presentation, those at high risk to convert to CDMS harbor an enrichment of the AGS in their CSF B cell repertoires.

AGS ENRICHMENT IS PREVALENT IN THE CNS OF MS PATIENTS

The following study has been published in the journal, *Journal of Neuroimmunology.* Ligocki A.J, Lovato L., Guidry P., Scheuermann R.H., Willis S.N., Almendinger S., Racke M.K., Frohman E.M., Hafler D.A., O'Connor K.C., Monson N.L., *A unique antibody gene signature is prevalent in the central nervous system of patients with multiple sclerosis*, 2010, volume 226, issue 1-2, pages 192-193, and is reproduced here with the permission of Elsevier under the issued license number 3275541014401

Introduction

The involvement of B cells in the pathogenesis of multiple sclerosis (MS) has been reviewed elsewhere (341-344) and is supported by the therapeutic efficacy of the B cell depleting anti-CD20 drug rituximab in patients with MS (179, 345). This finding supports the concept that the B cell pool in MS patients harbors a subset that contributes to disease pathology. We hypothesized that if the cellular pool in MS patients is dysregulated, one would expect that antibody genes utilized by B cells circulating within the cerebrospinal fluid (CSF) would display a pattern of somatic hypermutation not found in healthy donors or patients with other neurological diseases. Indeed, our laboratory has recently identified a novel pattern of somatic hypermutation that is unique to MS CSF B cells and not found in control derived sequences (228). We investigated the utility of this antibody gene signature (AGS) as a molecular genomic tool to identify CIS patients at risk of developing definite MS. Application of the AGS tool demonstrated the ability to predict conversion to definite MS with an accuracy of 91% (228). The goal of this current

study was to determine whether this MS-specific AGS identified in the CSF is also present in the CNS tissue of patients with MS.

Results and Discussion

The calculated AGS scores derived from the four subjects are listed in Table 3-1. We had previously established (228) that the AGS scores of CSF B cells from patients with MS had an average AGS score of 14.87. The AGS scores for the LCM-CNS tissue antibody repertoires ranged from 12.05-17.86 (average combined AGS score of 14.80) (Table 3-1). These data demonstrate that the AGS is not unique to the CSF but is also present in CNS tissue of MS patients. Of note, the average AGS score of $CD19^+$ CSF B cells from three patients with other neurological diseases was 4.5 and the average AGS score of $CD19^+$ peripheral blood B cells from 3 MS patients was 2.0.

The presence of a strong AGS score in this CNS tissue antibody gene repertoire database provides important corroboration of our principal hypothesis that AGS enriched B cells are present at the site of the disease process in MS, as well as in the circulating CSF. Our observations are in keeping with the current conceptualization of MS pathogenesis, which includes the matriculation of brain-reactive B cells from the periphery into brain tissue via the circulating CSF (9, 10, 125, 129, 346-348). Thus, if high AGS scores are a common feature of CSF B cells from MS patients, it should also represent a common characteristic of B cells localized to CNS tissue, as we have demonstrated here. A limitation in this current study is the low number of patient samples evaluated, however it provides a preliminary look into the localization of the AGS and justifies further research into the area. Ultimately, the AGS prevalence of B cells in CSF and CNS tissue of MS patients supports the hypothesis that a restricted population of B

cells are involved in the biological underpinning of the disease process in MS. Further characterization of these AGS enriched B cells in MS is currently under active investigation.

Acknowledgments

The authors thank the patients and their families who consented to donating post-mortem samples for this study.

TABLES FOR CHAPTER THREE: RESULTS

Table 3-1. CNS specimen details and AGS scores for LCM-CNS[1] samples

Subject	Age/gender	Disease duration (years)	MS course	Anatomical location	AGS score	#V_H4 sequences with RM
MS-1	38/F	n.a.	RRMS	Plaque	12.05	20
MS-2	65/M	n.a.	CPMS	Plaque	17.86	12
MS-3	43/F	20	CPMS	Plaque	14.97	9
MS-4	39/F	13	CPMS	NAWM	14.31	30

Abbreviations: LCM-CNS: laser capture microdissection CNS, RM: replacement mutation, n.a.: not available, RRMS: relapsing remitting MS, CPMS: chronic progressive MS, NAWM: normal appearing white matter

[1] LCM-CNS V_H sequences provided by Drs. Hafler and O'Connor

CHAPTER FOUR

RESULTS

AIM II: MUTATION CHARACTERISTICS AND B CELL SUBPOPULATIONS DIFFER BETWEEN CIS PATIENTS PRESENTING WITH ON_{CIS} vs TM_{CIS}

Overview and rationale

Patients at high risk of converting to MS present with lesions at two different anatomical locations: the optic nerve and the spinal cord. Patients afflicted with TM_{CIS} (lesions in the spinal cord) tend to have worse clinical prognosis than ON_{CIS} (lesions in the optic nerve) if they convert to CDMS (47, 349). CIS patients have higher CSF cell counts than patients with established MS (350), which may indicate that lymphocytes circulate more readily in the CNS during the highly inflammatory state of the early acute disease. In fact, while B cells are rare in the CSF of normal donors (114, 115), MS patients undergoing an attack have an expansion of memory B cells in the CSF (118), and a contraction of memory B cells in the periphery (119), suggesting possible recruitment to the CSF from the periphery or entry of memory B cells into lymphoid or peripheral tissues.

One of the goals of this published study was to determine if there are any irregularities in the B cell subpopulations of TM_{CIS} patients compared to ON_{CIS} patients (333). We found that a subset of TM_{CIS} patients, stratified as the TM_{CIS}A patient subgroup, had a unique expansion of $CD27^{high}$ plasmablasts in the CSF. The majority of these TM_{CIS}A patients also demonstrated an expansion of plasmablasts in the periphery.

Expansion of plasmablasts was not observed in any of the ON_{CIS} patients in either compartment. The frequency of $CD27^{high}$ plasmablasts is also elevated in several autoimmune diseases and occurs in the diseased tissues where the putative auto-antigens are present (142, 198, 203, 204).

These plasmablasts from the periphery of $TM_{CIS}A$ patients exhibit evidence of heavy chain receptor editing through positive selective pressure of $V_H4^+J_H6^+$ B cells. Additionally, this plasmablast expansion amplifies in the periphery proportionally with time to clinical visit, suggesting that chronic untreated neuroinflammation can expand the V_H4^+ plasmablasts in these patients. Receptor editing may be a driving force contributing to J_H6 selection in the periphery, but is a mechanism absent in the CSF compartment where disease pathology is localized and autoreactive B cells continue to expand. Perhaps this expansion of abnormally selected plasmablasts at the early stage of TM_{CIS} affects the course of neuroinflammation in these patients.

EXPANSION OF $CD27^{HIGH}$ PLASMABLASTS IN TM_{CIS} PATIENTS THAT HARBOR $V_H4^+J_H6^+$ B CELLS WITH EXTENSIVE SHM

The following study has been published in the journal, *Genes and Immunity.* Ligocki A.J, Rounds W.H., Cameron E.M., Harp C.T., Frohman E.M., Courtney A.M., Vernino S., Cowell L.G., Greenberg B., Monson N.L., *Expansion of CD27^{high} plasmablasts in transverse myelitis patients that utilize VH4 and JH6 genes and undergo extensive somatic hypermutation*, 2013, volume 14, issue 3, pages 291-301, and is reproduced here with the permission of Nature Publishing Group for use in a printed thesis more than 6 months after initial publication with the original manuscript located at: doi:10.1038/gene.2013.18

Introduction

Patients that present with a first demyelinating attack are diagnosed with clinically isolated syndrome (CIS), which places them at high risk to develop Multiple Sclerosis (MS), an autoimmune inflammatory disease of the central nervous system characterized by the demyelination of axons and the formation of lesions (1-5). The most common presentations are optic neuritis (ON_{CIS}) and transverse myelitis (TM_{CIS}) (46). ON_{CIS} is characterized by visual impairments due to demyelination of the optic nerve (47). TM_{CIS} symptoms involve weakening of limbs or sensations of numbness due to demyelination occurring across short segments of the spinal cord (50). Patients that present with either ON_{CIS} or TM_{CIS} have a high risk of converting to MS, but current risk stratification approaches depend on brain MRI findings. Compounding the importance of

early and accurate diagnosis are the data suggesting that earlier treatment delays the progression of disease and accruement of disability (64, 65). The presence of lesions in the brain of TM_{CIS} patients also increases the risk of conversion to MS (58) and these patients typically have a faster occurrence of a second attack than ON_{CIS} patients (46, 349). Additionally, ON_{CIS} patients have better long-term prognosis than other presentations including TM_{CIS} (47, 349, 351). Differences in progression to clinically definite MS and location of initial lesions between ON_{CIS} and TM_{CIS} patients may suggest different underlying biology. One possible difference could be variations in the composition of lymphocytes involved in the autoimmune pathology associated with these disease presentations.

B cells have been implicated in the pathogenesis of MS (5, 6, 83-85, 101, 102, 105, 108, 118, 126, 133, 352), highlighted by the finding that rituximab, a B cell depleting agent, can decrease brain inflammation in MS patients (179-181). Of particular interest are plasmablasts, a B cell subset that is indentified by high CD27 expression (196). An abnormal expansion of $CD27^{high}$ plasmablasts has been documented in the afflicted compartments of several autoimmune diseases such as rheumatoid arthritis (RA) (198), Sjogren's (142), systemic lupus erythematosus (SLE) (200), neuromyelitis optica (NMO) (202), ankylosing spondylitis (AS) (203), and pediatric ulcerative colitis (204). In addition, patients with active systemic lupus erythematosus (SLE) have greater counts of $CD27^{high}$ plasmablasts in the periphery than healthy controls or patients with inactive disease (199-201, 353, 354), suggesting these expanding plasmablasts may be contributing to damage associated with these autoimmune diseases.

Since patients presenting with TM_{CIS} have a worse prognosis than patients presenting with ON_{CIS} (46), (47, 351), we hypothesized that the plasmablast subset would

be expanded in TM patients and subsequently, that the antibody genomics of TM patients would demonstrate irregularities. To test this hypothesis, we characterized subpopulations and antibody genomics of B cells in the cerebrospinal fluid (CSF) and peripheral blood of patients experiencing their first TM_{CIS} event. Interestingly, the TM_{CIS} patients could be segregated into two groups based on the percentage of $CD19^{+}CD27^{high}$ B cells in either the blood or CSF, which was not seen in the ON_{CIS} patients. This increase in $CD27^{high}$ plasmablasts in the TM_{CIS} patients who have the worst clinical prognosis parallels what is seen in other autoimmune disorders. In addition, we found abnormal antibody gene distributions and mutation patterns in the $CD27^{high}$ plasmablasts isolated from the periphery of TM_{CIS} patients that are absent from the $CD27^{+}$ memory B cells from the same patients.

Results

A subset of TM patients have an expanded plasmablast compartment

Initial characterization of lymphocyte ($CD45^{+}$), $CD4^{+}$ T cell, $CD8^{+}$ T cell, $CD19^{+}$ B cell, and $CD138^{+}$ plasma cell percentages and absolute numbers were similar in ON_{CIS} and TM_{CIS} patients in both the CSF and peripheral blood compartments (Table 4-1). The percentages and absolute numbers of $CD27^{-}$ naïve B cells and $CD27^{+}$ memory B cells were also similar between the ON_{CIS} and TM_{CIS} patients, regardless of compartment (Table 4-1). Additionally, the ratios of CD4:CD8 T cells and naïve:memory B cells were also similar between ON_{CIS} and TM_{CIS} patients in both the CSF and peripheral PB compartments (Table 4-1).

In contrast, a subset of TM_{CIS} patients demonstrated an expansion of the plasmablast B cell pool identified by high expression of CD27 (Figure 4-1) in both the CSF (Figure 4-1A, C) and PB (Figure 4-1B, D) compared to the ON_{CIS} patients. Therefore we stratified the TM_{CIS} patients into the TM_{CIS}A (Above) and TM_{CIS}B (Below) patient subsets. This analysis demonstrated that 41% (9/22) of TM_{CIS} patients had an expansion of plasmablasts in the CSF and 45% (10/22) of TM_{CIS} patients had an expansion of plasmablasts in the periphery (Table 4-2). Of the 9 TM_{CIS}A patients with plasmablast expansion in their CSF, 7 of them also had plasmablast expansion in the periphery (Table 4-2). This suggests that abnormal plasmablast expansion can be detected in the periphery of some TM patients.

We also analyzed the percent of $CD27^{high}$ plasmablasts present in nine patients with paraneoplastic disease (PND), another neuroinflammatory disease group. PND patients also have characteristic high levels of various autoantibodies and expansion of CSF B cells (355-357), and thus could potentially have elevated levels of plasma cells or plasmablasts. Eight of the PND patients had a mean of 0.050% $CD27^{high}$ plasmablasts within the blood that falls below the TM_{CIS}A threshold (Table 4-3). One of the patients had a significant elevation of plasmablasts in the blood that may be due to the patient having a possible lymphoma. None of nine PND patients had elevated $CD27^{high}$ plasmablast levels within the CSF compartment with the mean being 0.051% (Table 4-2). In both the blood and CSF compartments, there is no evidence of elevated plasmablast levels in PND patients.

Due to the increase in plasmablasts in the TM_{CIS}A patients, we reasoned that the CSF immunoglobulin (Ig) synthesis rate (mg/24hr) and the CSF Ig index (measure of Ig in the CSF) could be affected. Despite the increased plasmablast frequency in the CSF,

there was no correlation between these two clinical markers and plasmablast expansion (Table 4-4). There were also no correlations with age at the time of sampling for any of the patient groups (Table 4-5). However, there was a positive correlation between peripheral plasmablast expansion and the length of time the $TM_{CIS}A$ patients remained untreated for their disease (R=0.67, p=0.034) (Table 4-5). The ON_{CIS} and $TM_{CIS}B$ patients did not show this correlation.

Increased V_H4 usage and mutation accumulation in CSF repertoires

Since the $TM_{CIS}A$ patients had elevated plasmablasts in the CSF, we reasoned that the B cell antibody repertoires of this subgroup would display skewing. Previous data from our group and others demonstrates that CSF-isolated B cells from MS and ON_{CIS} patients often display enrichment of V_H4 antibody genes that is not observed in peripheral memory B cell populations of healthy control donors (214, 220, 222, 228-230, 358). Indeed, the $TM_{CIS}A$ and $TM_{CIS}B$ patient subgroups were enriched for V_H4^+ B cells in the CSF as observed in established MS patients (MS: 38.84%, $TM_{CIS}A$: 43.86%, $TM_{CIS}B$: 30.59%) (Figure 4-2A). The ON_{CIS} patients displayed a further expansion of V_H4 usage compared to the MS patients (ON_{CIS}: 49.32%, p=0.032) (Figure 4-2A). V_H3 usage by MS and all CIS patient subgroups was similar to that observed in the periphery of HC subjects (data not shown).

Accumulation of somatic hypermutations (SHM) in antibody genes is a second indication that particular B cells are being selected in a repertoire through an antigen-driven process. To determine whether B cells expressing V_H4 genes were being selected at this level in the ON_{CIS}, $TM_{CIS}A$ and $TM_{CIS}B$ patients, we calculated mutation frequencies (MF) of V_H3^+ B cells and compared them to MFs of V_H4^+ B cells (Figure 2B).

As expected, we found that the V_H4^+ B cells from the CSF of MS patients accumulate more mutations when compared to V_H3^+ B cells from the same patients (Figure 4-2B). V_H4^+ B cells from the CSF of CIS patients also accumulate more mutations when compared to V_H3^+ B cells from the same patients (Figure 4-2B). This positive selection of V_H4^+ B cells was also evident independently in each CIS patient subtype: ON_{CIS}, $TM_{CIS}A$, and $TM_{CIS}B$ (Figure 4-2B). Preferential accumulation of mutations in V_H4^+ B cells in the CSF compartment is a shared characteristic across all disease groups.

Positive selection of CSF $V_H4^+J_H4^+$ B cells is not maintained in $TM_{CIS}A$

A characteristic of typical selection is the preferential usage of J_H4 segments over J_H6 segments in the memory B cell antibody repertoire (208). All patient groups had a 1.5-3 fold increased usage of J_H4 segments compared to J_H6 in the V_H4^+ B cell pool (Figure 4-2C). In addition, V_H4^+ B cells from the MS, CIS, ON_{CIS}, and $TM_{CIS}B$ patients utilizing J_H4 segments had higher MFs than V_H4^+ B cells utilizing J_H6 segments (Figure 4-2D). However, V_H4^+ B cells from $TM_{CIS}A$ patients using J_H4 segments had equal MFs compared to those using J_H6 segments (Figure 2D). $TM_{CIS}A$ patients had more $V_H4^+J_H4^+$ B cells (Figure 4-2C), but they are not selected relative to the $V_H4^+J_H6^+$ B cells (Figure 4-2D).

CSF V_H4^+ B cells have similar CDR3 charge and length

Self-reactive B cells from healthy donors emerge from the bone marrow with an enrichment of positively charged CDR3 residues in their V_H genes (72) and V_H receptor editing favors the addition of positively charged arginines in the CDR3 (359). Following peripheral selection, enrichment of positively charged CDR3 residues is diminished. To

address whether V_H4^+ B cells from these groups displayed selection at this level, we calculated the overall charge of the CDR3 segments of V_H4^+ B cells from the MS patients and compared them to the CIS, ON_{CIS}, $TM_{CIS}A$ and $TM_{CIS}B$ patient subgroups. As expected, none of the patient groups were enriched for positively charged residues in the V_H4^+ B cell pool (Figure 4-2E). The V_H4^+ B cell pool from MS patients trended towards accumulating more negative charges in the CDR3, but this did not reach statistical significance.

We reasoned that if V_H4^+ B cells from the patient subgroups were undergoing selection typical of what occurs in the germinal center, bias for productive sequences with short CDR3 lengths (206, 360) would also be intact, as they are in MS and CIS patients. CDR3 length analysis was also important because receptor editing can elongate the V_H CDR3 region (359). To address this, we calculated the CDR3 length of V_H4^+ B cells from the CSF of MS patients and compared it to the CDR3 length of V_H4^+ B cells from the CIS, ON_{CIS}, $TM_{CIS}A$, and $TM_{CIS}B$ patients. In all cases, the CIS as a whole and the CIS patient subgroups had similar CDR3 lengths in comparison to V_H4^+ B cells from established MS patients (Figure 4-2F).

Decreased V_H1 usage and mutation accumulation in $TM_{CIS}A$ and ON_{CIS}

The CIS patients and the ON_{CIS}, $TM_{CIS}A$, and $TM_{CIS}B$ patient subgroups had enrichment of V_H4^+ B cells similar to the MS patients, as described above. The V_H1 family also displayed variation in usage across the patient repertoires. The ON_{CIS} and $TM_{CIS}A$ patient subgroups displayed a decrease in V_H1^+ B cells as compared to the MS patients (MS: 23.85%, ON_{CIS}: 4.73% $p<0.0001$, $TM_{CIS}A$: 16.84% $p=0.032$) (Figure 4-

3A). The $TM_{CIS}B$ patients had a similar V_H1^+ B cell frequency compared to the MS patients ($TM_{CIS}B$: 29.41%) (Figure 4-3A).

The MS patients had an increase of SHM accumulation in the V_H1^+ B cells when compared to the V_H3^+ B cells (Figure 4-3B) indicating that in addition to selection of V_H4^+ B cells, V_H1^+ B cells were also selected over V_H3^+ B cells. The $TM_{CIS}B$ patients did not differ from MS patients in V_H1 gene usage (Figure 4-3A), but displayed positive selection of V_H1^+ B cells over V_H3^+ B cells as measured by SHM accumulation (Figure 4-3B). The ON_{CIS} and $TM_{CIS}A$ patients had the lowest V_H1 usage (Figure 4-3A), and similar SHM accumulation in the V_H3^+ and V_H1^+ B cells (Figure 4-3B), indicating a lack of positive selection for V_H1^+ B cells in these patient groups.

Positive selection of CSF $V_H1^+J_H6^+$ B cells in $TM_{CIS}A$

J_H4 usage was similar to MS patients in the V_H1^+ B cells of the CIS, ON_{CIS}, $TM_{CIS}A$, and $TM_{CIS}B$ patient subtypes (Figure 4-3C). SHM accumulation in V_H1^+ B cells from the MS, CIS, ON_{CIS} and $TM_{CIS}B$ patients using J_H4 segments was either greater or equal to SHM accumulation in V_H1^+ B cells using J_H6 segments (Figure 4-3D), similar to what was found in the V_H4^+ B cell pool. In contrast, SHM accumulation in V_H1^+ B cells from the $TM_{CIS}A$ patients using J_H6 segments was higher than V_H1^+ B cells using J_H4 segments ($p=0.001$) (Figure 4-3D).

CSF V_H1^+ B cells have similar CDR3 charge and length except $TM_{CIS}B$

The V_H1^+ B cell pools were not enriched for positively charged residues in MS and CIS patients (Figure 4-3E), as was observed in the V_H4^+ B cell pool (Figure 4-2E). However, there was a significant accumulation of negative charges in the CDR3s of the

V_H1^+ B cells in the $TM_{CIS}B$ patients when compared to the MS patients (Figure 4-3E). As with the V_H4^+ B cells, there were no statistically significant differences in CDR3 lengths for V_H1^+ B cells in the $TM_{CIS}A$ and ON_{CIS} patient groups (Figure 4-3F).

Increased V_H4 mutation accumulation in peripheral B cell repertoires of $TM_{CIS}A$

Since 41% of the TM patients had an enrichment of peripheral $CD27^{high}$ plasmablast B cells, we next focused on determining whether the antibody repertoires from peripheral plasmablast B cells of these patients also demonstrated skewing of their antibody gene repertoire characteristics. To do this, we sorted memory ($TM_{CIS}A$-$CD27^+$) and plasmablast ($TM_{CIS}A$-$CD27^{high}$) B cells from the PB of four $TM_{CIS}A$ patients. A MS PB database was used to determine antibody repertoire differences in established disease compared to the initial clinical stage. As expected, V_H4^+ $CD27^+$ memory B cells were expanded in the periphery of MS patients compared to the HC (HC: 19.35%; MS: 36.21%, p=0.007) (Figure 4-4A). The frequency of peripheral V_H4^+ plasmablasts in the $TM_{CIS}A$ patients (23.77%) was also similar to HC subjects (19.35%) (Figure 4-4A), but the frequency of PB memory B cells in the $TM_{CIS}A$ patients demonstrated an increased frequency of V_H4^+ B cells (28.99%, p=0.027) but not to the extent observed in MS patients.

Next, we assessed the selection of V_H4^+ B cells by measuring the accumulation of SHM. As expected, there was no SHM accumulation in V_H4^+ B cells from HCs, as their MF was similar to the MF of V_H3^+ B cells (Figure 4-4B). Positive selection for V_H4^+ B cells was observed in the MSPB (Figure 4-4B) similar to V_H4^+ B cells in the CSF of the MS patients. Interestingly, the non-expanded V_H4^+ plasmablasts from the same patients (Figure 4-4A) had an increased MF compared to V_H3^+ plasmablasts from the same

patients (Figure 4-4B). The expanded peripheral V_H4^+ memory B cells (Figure 4-4A) also had increased MF compared to V_H3^+ memory B cells from the same patients (Figure 4-4B). The PB memory B cells and $CD27^{high}$ plasmablasts from early TM disease shared the V_H4^+ dysregulation observed in CSF memory B cells from established MS patients.

Positive selection of peripheral $V_H4^+J_H6^+$ B cells only in plasmablasts

V_H4^+ B cells from HC subjects use J_H4 segments more frequently than J_H6 segments, and $V_H4^+J_H6^+$ B cells from HCs displayed higher SHM than $V_H4^+J_H6^+$ B cells from HCs (Figure 4-4C,D). In contrast, V_H4^+ B cells from the MS patients used J_H6 segments approximately 2-fold more frequently than J_H4 segments (Figure 4-4C), but did not display higher SHM than V_H4^+ B cells using J_H4 segments (Figure 4-4D). The V_H1^+ B cells from MS patients also utilized J_H6 segments more and these were positively selected over J_H4 segments in addition to accumulating significant positive charge (Figure 4-5D). Similar to the CSF V_H4^+ B cell patient groups, the peripheral blood V_H4^+ repertoires did not have any difference in CDR3 charge (Figure 4-4E) or length (Figure 4-4F). Contrary to the trend towards more J_H4 usage in the $TM_{CIS}A$ memory B cell pools, the plasmablast B cell pools from the $TM_{CIS}A$ patients using V_H4 genes had an increased trend towards J_H6 usage, but this did not reach significance. Nevertheless, the $V_H4^+J_H6^+$ plasmablast B cell pool preferentially accumulated SHM compared to the $V_H4^+J_H4^+$ plasmablast B cell pool from the same $TM_{CIS}A$ patients ($V_H4^+J_H4^+$:6.27% vs $V_H4^+J_H6^+$:9.40%, p=0.001) (Figure 4-4D). Peripheral V_H4^+ memory B cells from the $TM_{CIS}A$ patients did not demonstrate this level of selection ($V_H4^+J_H4^+$:6.22% vs $V_H4^+J_H6^+$:6.57%, p=0.611) (Figure 4-4D). This depth of selection in the $TM_{CIS}A$ patients

was unique to V_H4^+ peripheral $CD27^{high}$ plasmablasts since no selection was observed for V_H1^+ peripheral $CD27^{high}$ plasmablasts from the $TM_{CIS}A$ patients (Figure 4-5D).

Discussion

Patients with high risk to convert to MS present with lesions at two different anatomical locations: the optic nerve and the spinal cord. Patients afflicted with TM_{CIS} (lesions in the spinal cord) tend to have worse clinical prognosis than ON_{CIS} (lesions in the optic nerve) if they convert to MS (47, 349). CIS patients have higher CSF cell counts than patients with established MS (350), which may indicate that lymphocytes circulate more readily in the central nervous system during the highly inflammatory state of the early acute disease. In fact, while B cells are rare in the CSF of normal donors (114, 115), MS patients undergoing an attack have an expansion of memory B cells in the CSF (118) and a contraction of memory B cells in the periphery (119). This suggests that B cells are recruited to the CSF from the periphery in these patients, and recent data underscore this possibility (121).

One of the goals of this study was to determine if there are any irregularities in the B cell subpopulations of TM_{CIS} patients compared to ON_{CIS} patients. We found that a subset of TM_{CIS} patients, termed the $TM_{CIS}A$ patient subgroup, had a unique expansion of $CD27^{high}$ plasmablasts in the CSF. The majority of these $TM_{CIS}A$ patients also demonstrated an expansion of plasmablasts in the periphery. Expansion of plasmablasts was not observed in any of the ON_{CIS} patients in either compartment. The frequency of $CD27^{high}$ plasmablasts is elevated in several autoimmune diseases (142, 198, 203, 204) and occurs in the diseased tissues where the putative autoantigens are present.

Clinical evidence of plasmablast activity has been found in patients with NMO (186), RA (198, 361), and SLE (192, 353, 354, 362) who receive the B cell depleting agent Rituximab and are more likely to relapse early if their memory B cells, and more importantly their $CD27^{high}$ plasmablasts return earlier. In addition, mRNA from RA patients who are non-responsive to rituximab treatment demonstrate increases in mRNA markers of plasmablasts (361). NMO patients who are positive for anti-aquaporin-4 antibodies have increased plasmablasts in the periphery, which are further increased during a relapse (202). Indeed, one of the $TM_{CIS}A$ patients in this present study was diagnosed with NMO and had a high frequency of plasmablasts in both the CSF and periphery. The remaining $TM_{CIS}A$ patients all tested negative for the NMO diagnostic anti-aquaporin-4 IgG reactivity and are at high risk to convert to MS. All these data suggest that the re-emergence of symptoms in autoimmune diseases may be marked or potentially caused by an abnormal increase in $CD27^{high}$ plasmablasts. Future studies may find this expansion in additional autoimmune diseases in which humoral immunity is a component of the pathology.

Furthermore, plasmablasts are correlated with neuroinflammatory disease activity as evidenced by MRI of MS patients (117). Treatment with Natalizumab, which blocks the entry of cells into the CNS, was effective in MS patients if they had lower levels of CSF plasmablasts before treatment and maintained low levels post-treatment (177). Other studies have found that during a MS relapse, memory B cells are readily recruited to the CSF (119, 120), possibly through a VLA-4 dependent mechanism, since memory B cells (116) and plasmablasts (116, 174) express high levels of VLA-4. Trafficking of B cells may be an early disease step, as CIS patients have higher levels of VLA-4 on their transitional B cells than is observed in MS patients (363). Such an initial step would

enable B cells to enter the CNS, encounter their autoantigen and undergo germinal center-like reactions as evidenced by SHM accumulation and altered selection of V_H genes.

We were surprised to find that the $CD27^{high}$ plasmablast expansion could also be detected in the periphery of many $TM_{CIS}A$ patients, since the pathology of the disease is confined to the CNS. The detection of these plasmablasts in the periphery at this early stage of disease may be due to the activation of B cells in the periphery prior to migration into the CNS where they participate in formation of ectopic germinal centers (129, 134). Alternatively, this activation could occur in the CSF compartment, leading to cell migration into the periphery. Unlike plasma cells, plasmablasts are quite motile (364), but their travel direction in the TM_{CIS} patients is unknown from this current study. The occurrence of peripheral expansion of plasmablasts found in the TM_{CIS} patients is unique to this particular CIS presentation of an early stage of the MS disease course.

We also found that the percentage of $CD27^{high}$ plasmablasts in the periphery of the $TM_{CIS}A$ group increased the longer the patient had been untreated. This may reflect an accumulation of over-activated B cells, which develop into plasmablasts in a state of extended neuroinflammation. Presumably, lack of treatment can prolong the immune response time to the triggering antigen(s), and the resulting potent inflammatory milieu may promote aberrant cell activation. This correlation was not seen in the CSF compartment, possibly due to plasmablasts entering niches in the inflamed tissue (364) or exiting back into the periphery over time after expanding in the CSF.

Next we analyzed the patient B cell repertoires for distinctions in antibody genomics. V_H4^+ B cells were expanded in the CSF of all patients experiencing both acute (CIS) and chronic (MS) neuroinflammation, which corroborates previous findings.(220,

222, 230) Interestingly, CSF B cells from the ON_{CIS} patients had the greatest enrichment of V_H4 gene usage and the greatest contraction of V_H1 gene usage among the examined patient groups. In addition to the expansion of V_H4 genes in the CSF of MS and CIS patients, there was evidence of positive selection of these V_H4^+ B cells in the CSF of MS and CIS patients. This aberrant selection of V_H4^+ B cells in the CSF was also observed at the early stages of disease represented by the ON_{CIS}, $TM_{CIS}A$ and $TM_{CIS}B$ patient subgroups.

In contrast, V_H4^+ gene usage was not increased in peripheral $CD27^{high}$ plasmablasts from the $TM_{CIS}A$ patients. However, SHM accumulation in peripheral V_H4^+ plasmablasts was extensive in comparison to V_H3^+ plasmablasts in the $TM_{CIS}A$ patients. Furthermore, the V_H4^+ plasmablasts using J_H6 segments accounted for this depth of SHM accumulation. V_H1^+ plasmablasts from the same $TM_{CIS}A$ patients did not demonstrate this level of selection. Taken together, these data suggest that within the peripheral $CD27^{high}$ plasmablast pool of $TM_{CIS}A$ patients, there is a subgroup of V_H4^+ plasmablasts enriched for J_H6 segment use that are undergoing affinity maturation at a faster rate than their V_H4^+ counterparts that utilize J_H4 segments.

High J_H6 usage is an indicator of V_H receptor editing, which is a process that is estimated to occur in 5-10% of healthy B cell pools (81, 359). Autoreactive B cells often demonstrate skewing to J_H6 segment use, but do not typically accumulate mutations at a high rate as their selection has been arrested due to self-reactivity (365). Yet the V_H4^+ plasmablasts in the periphery of the $TM_{CIS}A$ patients using J_H6 segments are accumulating SHM at a higher rate than the $V_H4^+J_H4^+$ plasmablasts from the same patients. This suggests that the peripheral plasmablast B cell pool of $TM_{CIS}A$ patients is both antigen driven and undergoing V_H receptor editing in the periphery of TM patients.

B cells from ectopic germinal centers of RA patients have also demonstrated this phenomenon (366). Interestingly, we also see evidence of V_H receptor editing in V_H4^+ and V_H1^+ B cell pools from the periphery of established MS patients. Peripheral B cells from MS patients had a skewed ratio of J_H4:J_H6 in both the V_H4^+ and V_H1^+ B cell pools due to a significant increase of the J_H6 segment usage and accumulation of SHM, but lack the intensity of SHM selection and receptor editing demonstrated only in the $V_H4^+J_H6^+$ plasmablasts from $TM_{CIS}A$ patients.

We were interested in whether we could find genomic evidence of these $V_H4^+J_H6^+$ plasmablasts with high SHM in the CSF of these $TM_{CIS}A$ patients. Our data suggest that they are not accumulating since V_H4^+ B cells from the CSF of the $TM_{CIS}A$ patients that utilize J_H6 segments do not accumulate SHM to a greater extent than J_H4 segment-using V_H4^+ B cells from the same patients. Instead, there was no selection between $V_H4^+J_H4^+$ and $V_H4^+J_H6^+$ B cells in the CSF of the $TM_{CIS}A$ patients. However, it is possible that they reside within the brain tissue and are not found circulating in the CSF as readily as their memory B cell counterparts. In either case, receptor editing is not prominent in the CSF B cell compartment of these groups.

In conclusion, we have found a unique phenotype of expanded plasmablasts that is unique to a subset of TM_{CIS} patients, which is not observed in ON_{CIS} patients. These cells exhibit evidence of heavy chain receptor editing through positive selective pressure of $V_H4^+J_H6^+$ B cells. Additionally, this plasmablast expansion amplifies in the periphery proportionally with time to clinical visit, suggesting that chronic untreated neuroinflammation can expand the V_H4^+ plasmablasts in these patients. Receptor editing may be a driving force contributing to J_H6 selection in the periphery, but is a mechanism absent in the CSF compartment where disease pathology is localized and autoreactive B

cells continue to expand. Perhaps this expansion of abnormally selected plasmablasts at the early stage of TM_{CIS} affects the course of neuroinflammation in these patients.

Acknowledgements

The authors thank the patients who consented to sampling for this study. Bonnie Darnell, Angie Mobley, Julia McClouth, Ann-Marie Schaefer, and Elizabeth Curry are thanked for their technical expertise in cell sorting. This study was supported by grants from the National Multiple Sclerosis Society (NMSS) to NLM (RG3267 and RG4653). AJL, WHR, EMC, CTH were supported by NIH NRSA5 T32 AI 005284-28 from NIAID. LGC's contributions were funded by 1R01AI097403-01.

FIGURE LEGENDS FOR CHAPTER FOUR: RESULTS

Figure 4-1. ***Percentage of CD27^{high} B cells in CSF (A) and PB (B) of patients initially presenting with ON$_{CIS}$ or TM$_{CIS}$.*** The TM$_{CIS}$ patients were segregated into two groups: TM$_{CIS}$A (Above) and TM$_{CIS}$B (Below) using the mean of the ON$_{CIS}$ group plus 2 s.e.m. as the cutoff criterion. This was done separately for both the CSF (C) and the PB (D) compartments. Bars shown in the plots are the means with s.e.m. The mean, s.e.m., and *N* are shown below each respective group. Additionally, the average cells/mL in each group for (C) and (D) are also shown below. Representative flow plots for the gating of CD19^{+}CD27^{-} naïve B cells, CD19^{+}CD27^{+} memory B cells, and CD19^{+}CD27^{high} plasmablasts are shown in a TM$_{CIS}$ and ON$_{CIS}$ patient CSF (E).

Figure 4-2. ***Gene and mutation characteristics of V_H4^+ B cells in the CSF.*** All data in (A-F) are shown for each of the five patient groups, indicated above (A) and (B). The panels are: percent V_H4 family gene usage out of entire V_H repertoire with the dotted line representing V_H4% in the HCPB repertoire (A), mutation frequencies (MF) of V_H4^+ B cells compared to V_H3^+ B cells within the same group (B), ratio of J_H4:J_H6 gene segment usage with the dotted line representing J_H4:J_H6 in the HCPB repertoire (C), MF of $V_H4^+J_H4^+$ B cells compared to $V_H4^+J_H6^+$ B cells within the same group (D), mean CDR3 charge (E), and mean CDR3 amino acid length (F). P-values were calculated using a Chi-square analysis for (A–D). P-values for (E) and (F) were calculated using a Student's t-test. *p<0.05, **p<0.001, #p<0.0001. The means and ratios are shown below each respective group as applicable. The number of patients per group is 11 MS, 17 CIS, 6 ON$_{CIS}$, 6 TM$_{CIS}$A, and 5 TM$_{CIS}$B.

Figure 4-3. ***Gene and mutation characteristics of V_H1^+ B cells in the CSF.*** All data in (A-F) are shown for each of the five patient groups, indicated above (A) and (B). The panels are: percent V_H1 family gene usage out of entire V_H repertoire with the dotted line representing V_H1% in the HCPB repertoire (A), mutation frequencies (MF) of V_H1^+ B cells compared to V_H3^+ B cells within the same group (B), ratio of J_H4:J_H6 gene segment usage with the dotted line representing J_H4:J_H6 in the HCPB repertoire (C), MF of $V_H1^+J_H4^+$ B cells compared to $V_H1^+J_H6^+$ B cells within the same group (D), mean CDR3 charge (E), and mean CDR3 amino acid length (F). P-values were calculated using a Chi-square analysis for (A–D). P-values for (E) and (F) were calculated using a Student's t-test. *p<0.05, **p<0.001, #p<0.0001. The means and ratios are shown below each respective group as applicable. The number of patients per group is 11 MS, 17 CIS, 6 ON_{CIS}, 6 TM_{CIS}A, and 5 TM_{CIS}B.

Figure 4-4. ***Gene and mutation characteristics of V_H4^+ B cells in the PB.*** All data in (A-F) are shown for each of the four patient groups, indicated above (A) and (B). The panels are: percent V_H4 family gene usage out of entire V_H repertoire (A), mutation frequencies (MF) of V_H4^+ B cells compared to V_H3^+ B cells within the same group (B), ratio of J_H4:J_H6 gene segment (C), MF of $V_H4^+J_H4^+$ B cells compared to $V_H4^+J_H6^+$ B cells within the same group (D), mean CDR3 charge (E), and mean CDR3 amino acid length (F). P-values were calculated using a Chi-square analysis for (A–D). P-values for (E) and (F) were calculated using a Student's t-test. *p<0.05, **p<0.001, #p<0.0001. The means and ratios are shown below each respective group as applicable. The number of patients per group is 6 HC, 4 MS, 4 TM_{CIS}A-CD27^{high}, and 4 TM_{CIS}A-CD27$^+$.

Figure 4-5. ***Gene and mutation characteristics of V_H1^+ B cells in the PB.*** All data in (A-F) are shown for each of the four patient groups, indicated above (A) and (B). The panels are: percent V_H1 family gene usage out of entire V_H repertoire (A), mutation frequencies (MF) of V_H1^+ B cells compared to V_H3^+ B cells within the same group (B), ratio of J_H4:J_H6 gene segment (C), MF of $V_H1^+J_H4^+$ B cells compared to $V_H1^+J_H6^+$ B cells within the same group (D), mean CDR3 charge (E), and mean CDR3 amino acid length (F). P-values were calculated using a Chi-square analysis for (A–D). P-values for (E) and (F) were calculated using a Student's t-test. *$p<0.05$, **$p<0.001$, #$p<0.0001$. The means and ratios are shown below each respective group as applicable. The number of patients per group is 6 HC, 4 MS, 4 TM_{CIS}A-$CD27^{high}$, and 4 TM_{CIS}A-$CD27^+$.

Figure 4-1

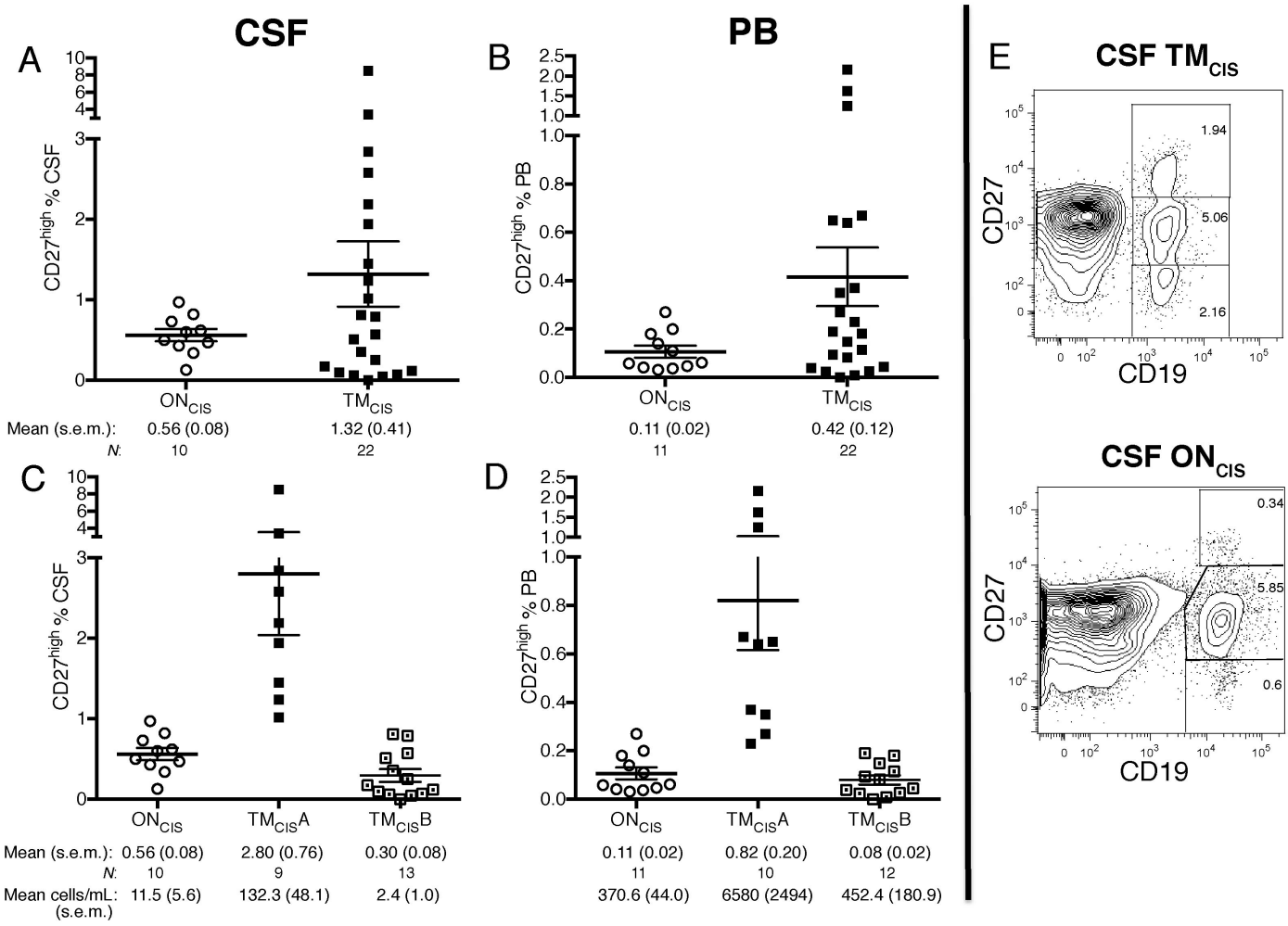
CSF
PB
A
B
C
D
E
CD27high % CSF
CD27high % PB
ONCIS
TMCIS
TMCISA
TMCISB
Mean (s.e.m.): 0.56 (0.08) 1.32 (0.41)
N: 10 22
0.11 (0.02) 0.42 (0.12)
11 22
Mean (s.e.m.): 0.56 (0.08) 2.80 (0.76) 0.30 (0.08)
N: 10 9 13
0.11 (0.02) 0.82 (0.20) 0.08 (0.02)
11 10 12
Mean cells/mL (s.e.m.): 11.5 (5.6) 132.3 (48.1) 2.4 (1.0)
370.6 (44.0) 6580 (2494) 452.4 (180.9)
CSF TMCIS
CSF ONCIS
CD27
CD19
1.94
5.06
2.16
0.34
5.85
0.6

Figure 4-2

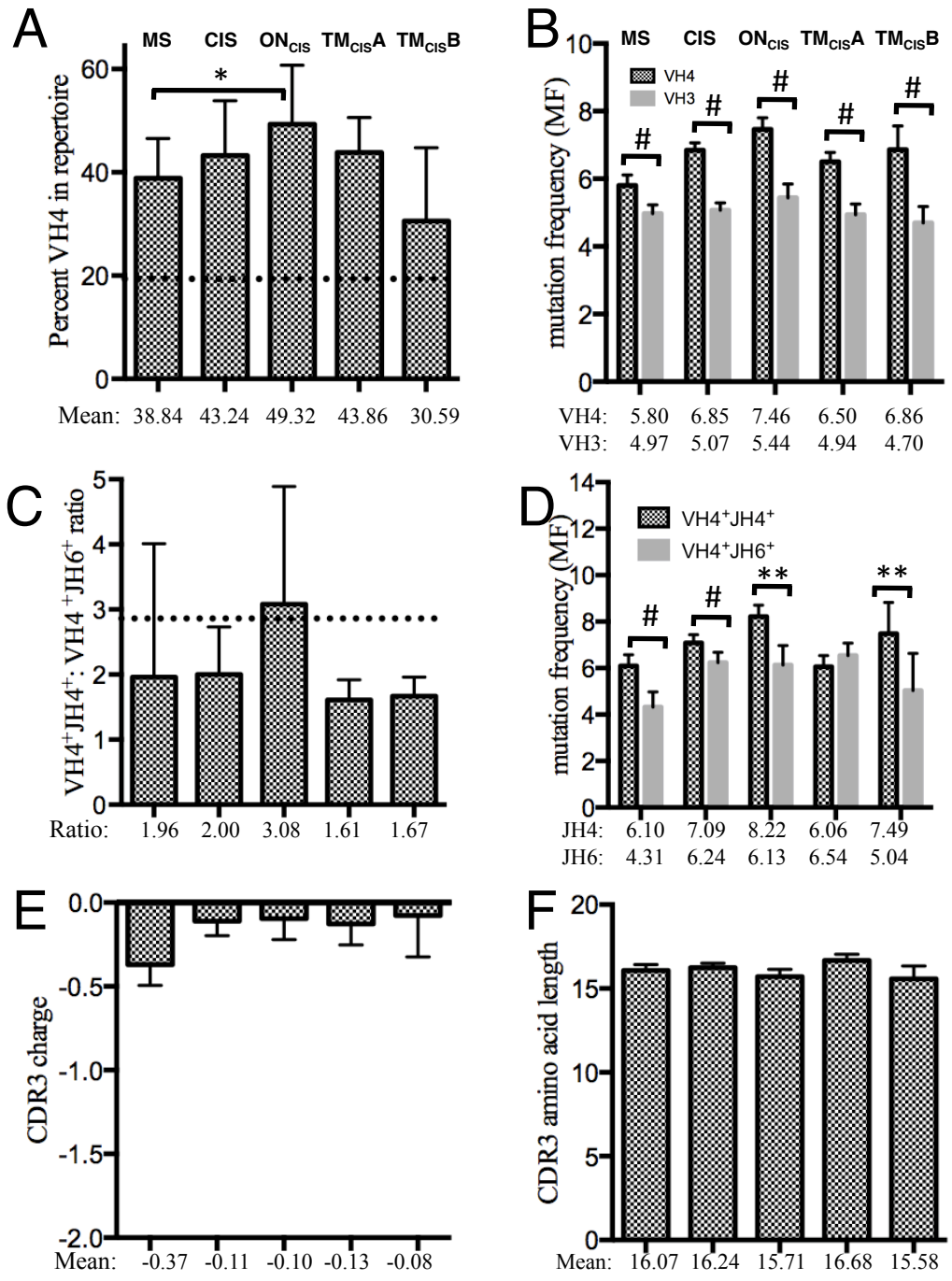
A
MS
CIS
ON_CIS
TM_CIS A
TM_CIS B
Percent VH4 in repertoire
60
40
20
0
*
Mean: 38.84 43.24 49.32 43.86 30.59
B
MS
CIS
ON_CIS
TM_CIS A
TM_CIS B
VH4
VH3
mutation frequency (MF)
10
8
6
4
2
0
#
VH4: 5.80 6.85 7.46 6.50 6.86
VH3: 4.97 5.07 5.44 4.94 4.70
C
VH4+JH4+: VH4+JH6+ ratio
5
4
3
2
1
0
Ratio: 1.96 2.00 3.08 1.61 1.67
D
VH4+JH4+
VH4+JH6+
mutation frequency (MF)
14
12
10
8
6
4
2
0
#
**
JH4: 6.10 7.09 8.22 6.06 7.49
JH6: 4.31 6.24 6.13 6.54 5.04
E
CDR3 charge
0.0
-0.5
-1.0
-1.5
-2.0
Mean: -0.37 -0.11 -0.10 -0.13 -0.08
F
CDR3 amino acid length
20
15
10
5
0
Mean: 16.07 16.24 15.71 16.68 15.58

Figure 4-3

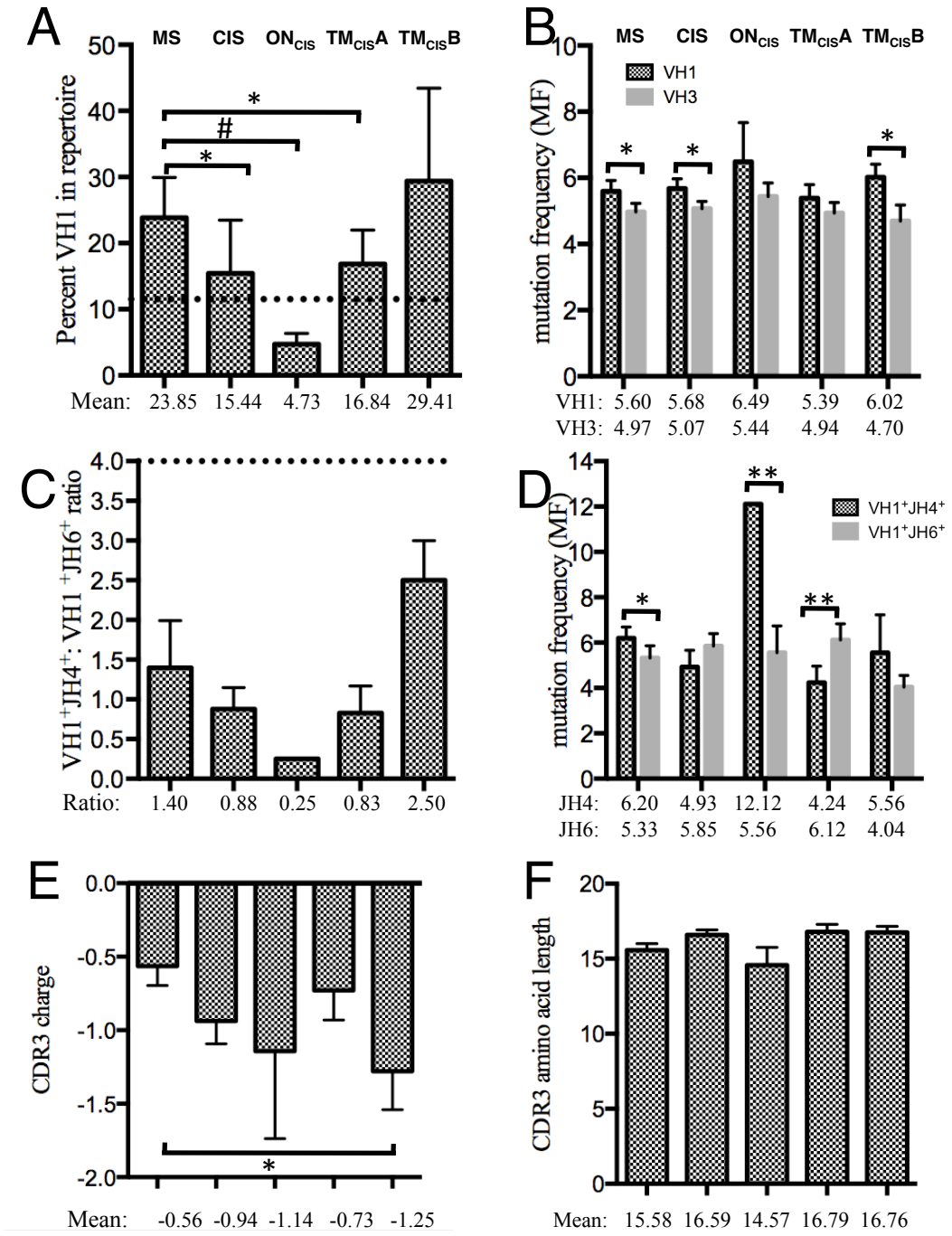
A
MS
CIS
ON$_{CIS}$
TM$_{CIS}$A
TM$_{CIS}$B
Percent VH1 in repertoire
Mean: 23.85 15.44 4.73 16.84 29.41
B
VH1
VH3
mutation frequency (MF)
VH1: 5.60 5.68 6.49 5.39 6.02
VH3: 4.97 5.07 5.44 4.94 4.70
C
VH1$^+$JH4$^+$: VH1 $^+$JH6$^+$ ratio
Ratio: 1.40 0.88 0.25 0.83 2.50
D
VH1$^+$JH4$^+$
VH1$^+$JH6$^+$
mutation frequency (MF)
JH4: 6.20 4.93 12.12 4.24 5.56
JH6: 5.33 5.85 5.56 6.12 4.04
E
CDR3 charge
Mean: -0.56 -0.94 -1.14 -0.73 -1.25
F
CDR3 amino acid length
Mean: 15.58 16.59 14.57 16.79 16.76

Figure 4-4

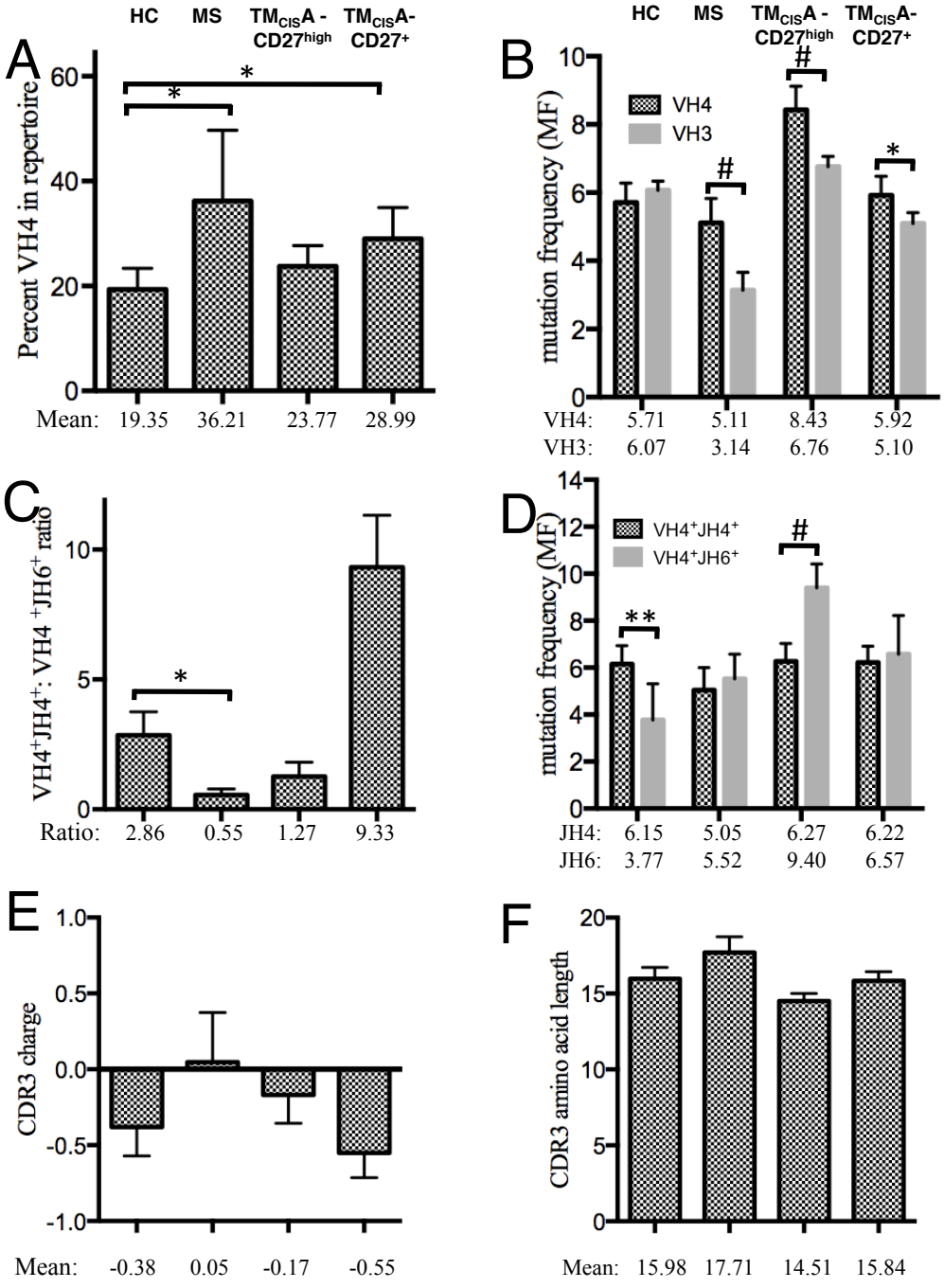
HC
MS
TMCISA - CD27high
TMCISA- CD27+
A
Percent VH4 in repertoire
Mean: 19.35 36.21 23.77 28.99
B
mutation frequency (MF)
VH4
VH3
VH4: 5.71 5.11 8.43 5.92
VH3: 6.07 3.14 6.76 5.10
C
VH4+JH4+: VH4 +JH6+ ratio
Ratio: 2.86 0.55 1.27 9.33
D
mutation frequency (MF)
VH4+JH4+
VH4+JH6+
JH4: 6.15 5.05 6.27 6.22
JH6: 3.77 5.52 9.40 6.57
E
CDR3 charge
Mean: -0.38 0.05 -0.17 -0.55
F
CDR3 amino acid length
Mean: 15.98 17.71 14.51 15.84

Figure 4-5

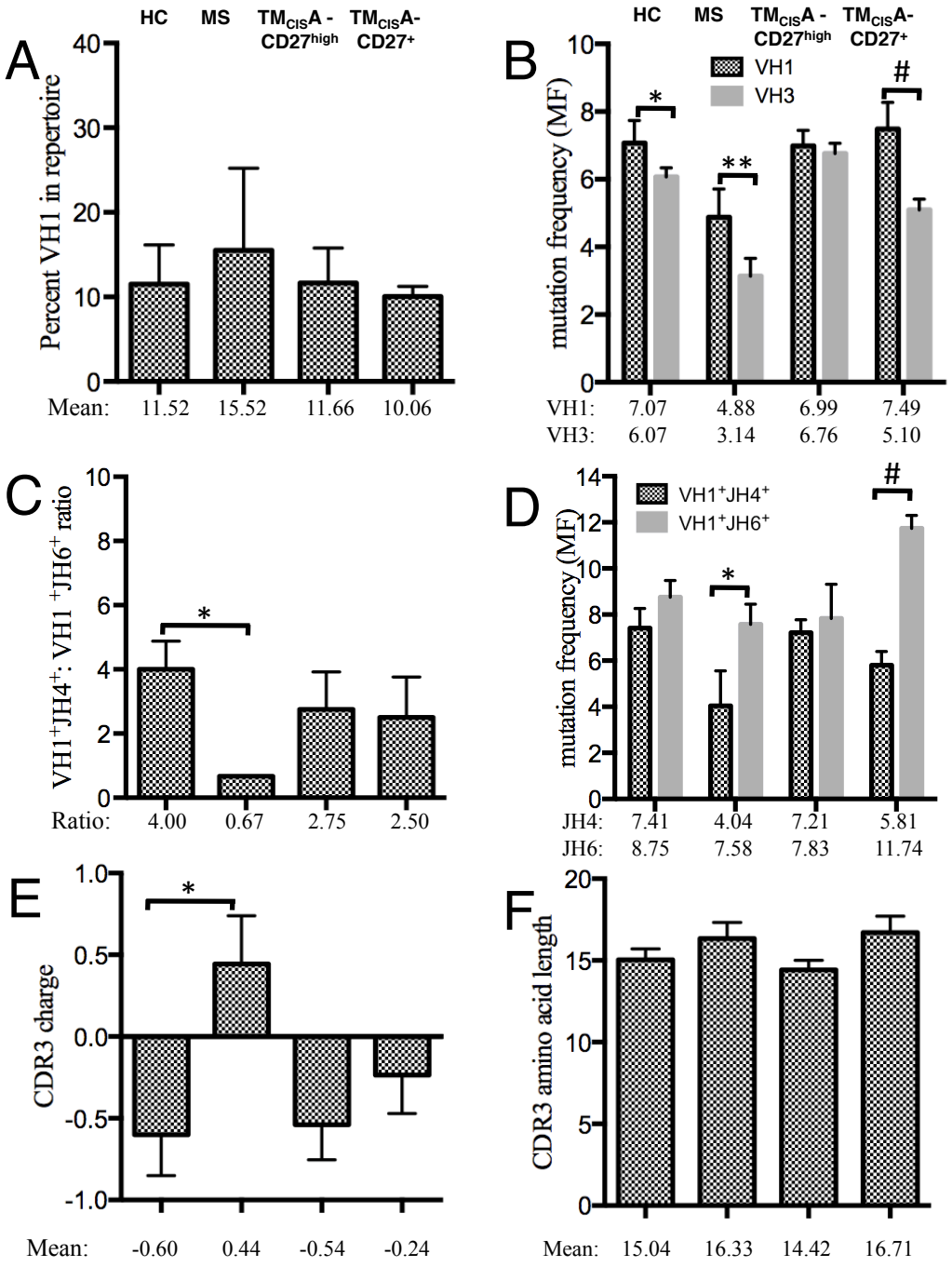
A
HC
MS
TMCISA - CD27high
TMCISA- CD27+
Percent VH1 in repertoire
Mean: 11.52 15.52 11.66 10.06
B
VH1
VH3
mutation frequency (MF)
VH1: 7.07 4.88 6.99 7.49
VH3: 6.07 3.14 6.76 5.10
C
VH1+JH4+: VH1 +JH6+ ratio
Ratio: 4.00 0.67 2.75 2.50
D
VH1+JH4+
VH1+JH6+
mutation frequency (MF)
JH4: 7.41 4.04 7.21 5.81
JH6: 8.75 7.58 7.83 11.74
E
CDR3 charge
Mean: -0.60 0.44 -0.54 -0.24
F
CDR3 amino acid length
Mean: 15.04 16.33 14.42 16.71

TABLES FOR CHAPTER FOUR: RESULTS

Table 4-1. Lymphocyte cell populations in CSF and PB compartments of CIS patients presenting with either ON_{CIS} or TM_{CIS}[1]						
Cerebrospinal Fluid (CSF)						
Cell population	**ON_{CIS} cell%**	**ON_{CIS} cells/mL**	**TM_{CIS} cell%**	**TM_{CIS} cells/mL**	**cell% p-value[2]**	**cells/mL p-value[3]**
$CD45^+$	49.95	2348	37.70	2615	0.38	0.93
$CD4^+$	59.73	1598	53.98	1500	0.35	0.96
$CD8^+$	15.40	339	15.12	450	0.91	0.84
CD4:CD8	4.13		4.39		0.80	
$CD19^+$	4.17	96	4.42	206	0.87	0.61
$CD19^+CD27^-$	0.51	15	0.80	29	0.47	0.57
$CD19^+CD27^+$	3.72	77	3.09	234	0.65	0.61
$CD138^+$	0.52	5	0.78	7	0.38	0.76
N:M B cells	0.16		0.19		0.65	
Peripheral Blood (PB)						
	ON_{CIS} cell%	**ON_{CIS} cells/mL**	**TM_{CIS} cell%**	**TM_{CIS} cells/mL**	**cell% p-value[2]**	**cells/mL p-value[3]**
$CD45^+$	51.88	710500	44.57	778429	0.39	0.76
$CD4^+$	47.44	349750	43.54	330333	0.44	0.85
$CD8^+$	16.95	112888	16.62	116445	0.91	0.92
CD4:CD8	3.09		3.08		0.98	
$CD19^+$	10.55	75689	15.50	126657	0.18	0.40
$CD19^+CD27^-$	9.12	48496	2.46	80719	0.34	0.44
$CD19^+CD27^+$	4.49	31192	6.20	46432	0.34	0.50
$CD138^+$	0.053	301	0.33	1536	0.18	0.11
N:M B cells	1.80		1.86		0.94	

Abbreviations: CSF: cerebrospinal fluid, PB: peripheral blood, MS: Multiple Sclerosis, CIS: Clinically Isolated Syndrome, ON_{CIS}: Optic Neuritis, TM_{CIS}: Transverse Myelitis, N: naïve $CD19^+CD27^-$ B cell, M: memory $CD19^+CD27^+$ B cell

[1] Values shown are the means for each respective group and all cell populations are calculated out of the $CD45^+$ lymphocyte gate

[2] Analyses were done using a two-tailed Student's t-test between ON_{CIS} and TM_{CIS} cell% groups.

[3] Analyses were done using a two-tailed Student's t-test between ON_{CIS} and TM_{CIS} cells/mL groups.

Table 4-2. Classification of TM_{CIS} patients into Above (A) or Below (B) groups within CSF and PB compartments based on $CD27^{high}$ plasmablast population[1]		
Patient	**$CD27^{high}$ % CSF**[2]	**$CD27^{high}$ % PB**[3]
1	**$TM_{CIS}A$**	**$TM_{CIS}A$**
2	**$TM_{CIS}A$**	**$TM_{CIS}A$**
3	**$TM_{CIS}A$**	**$TM_{CIS}A$**
4*	**$TM_{CIS}A$**	**$TM_{CIS}A$**
5	**$TM_{CIS}A$**	*$TM_{CIS}B$*
6	**$TM_{CIS}A$**	**$TM_{CIS}A$**
7*	**$TM_{CIS}A$**	**$TM_{CIS}A$**
8	**$TM_{CIS}A$**	**$TM_{CIS}A$**
9*	*$TM_{CIS}B$*	**$TM_{CIS}A$**
10	*$TM_{CIS}B$*	**$TM_{CIS}A$**
11	*$TM_{CIS}B$*	*$TM_{CIS}B$*
12	*$TM_{CIS}B$*	*$TM_{CIS}B$*
13	*$TM_{CIS}B$*	*$TM_{CIS}B$*
14	*$TM_{CIS}B$*	*$TM_{CIS}B$*
15	*$TM_{CIS}B$*	*$TM_{CIS}B$*
16	*$TM_{CIS}B$*	*$TM_{CIS}B$*
17*	*$TM_{CIS}B$*	**$TM_{CIS}A$**
18	*$TM_{CIS}B$*	*$TM_{CIS}B$*
19	*$TM_{CIS}B$*	*$TM_{CIS}B$*
20	*$TM_{CIS}B$*	*$TM_{CIS}B$*
21	**$TM_{CIS}A$**	*$TM_{CIS}B$*
22	*$TM_{CIS}B$*	*$TM_{CIS}B$*

Abbreviations: CSF: cerebrospinal fluid, PB: peripheral blood, TM_{CIS}: Transverse Myelitis, $TM_{CIS}A$: TM-Above, $TM_{CIS}B$: TM-Below

1 Classification into $TM_{CIS}A$ and $TM_{CIS}B$ was determined by the mean of the Optic Neuritis (ON_{CIS}) group plus 2 s.e.m. and this value as the threshold for splitting the TM_{CIS} group.

2 Threshold for $TM_{CIS}A$= 1.017%

3 Threshold for $TM_{CIS}A$= 0.268%

* $TM_{CIS}A$ patients re-bled for peripheral blood $TM_{CIS}A$-$CD27^{+}$memory and $TM_{CIS}A$-$CD27^{high}$ single cell sorts

Table 4-3. $CD27^{high}$ % in CSF and PB compartments of PND patients		
PND patient	**$CD27^{high}$ % CSF**	**$CD27^{high}$ % PB**
1	0	0.12
2[1]	0.09	2.26*
3	0.09	0.18
4	0.2	0.03
5	0	0.01
6	0.03	0.02
7	0	0.02
8	0	0.01
9	0.05	0.01

Abbreviations: CSF: cerebrospinal fluid, PB: peripheral blood, PND: paraneoplastic neurological disorder
[1] PND patient that was an outlier in the PB compartment possibly due to lymphoma

Table 4-4. Pearson's correlations between CSF Ig synthesis and CSF Ig index with $CD27^{high}$ plasmablast percentage in ON_{CIS}, $TM_{CIS}A$, and $TM_{CIS}B$ patient groups.						
	$CD27^{high}$ % CSF[1]			**$CD27^{high}$ % PB[2]**		
	mean (SD)	*R*	*p-value[3]*	*mean (SD)*	*R*	*p-value[3]*
CSF Ig synthesis rate (mg/24hr)						
ON_{CIS}	9.4 (12.8)	0.71	0.12	11.3 (12.7)	0.66	0.11
$TM_{CIS}A$	12.6 (13.2)	0.47	0.28	10.0 (12.4)	-0.36	0.34
$TM_{CIS}B$	5.1 (7.8)	0.35	0.26	5.9 (8.6)	-0.46	0.18
CSF Ig Index						
ON_{CIS}	0.8 (0.4)	0.70	0.08	0.9 (0.5)	0.56	0.15
$TM_{CIS}A$	1.2 (0.4)	0.46	0.30	1.2 (0.6)	-0.08	0.83
$TM_{CIS}B$	0.9 (0.7)	0.32	0.32	0.9 (0.6)	-0.18	0.62

Abbreviations: CSF: cerebrospinal fluid, PB: peripheral blood, R: Pearson's R, ON_{CIS}: Optic Neuritis, $TM_{CIS}A$: Transverse Myelitis-Above, $TM_{CIS}B$: Transverse Myelitis-Below, SD: standard deviation

[1] The number of patients per $CD27^{high}$ % CSF group is 7 ON_{CIS}, 7 $TM_{CIS}A$, 12 $TM_{CIS}B$

[2] The number of patients per $CD27^{high}$ % Blood group is 8 ON_{CIS}, 9 $TM_{CIS}A$, 10 $TM_{CIS}B$

[3] p-values were calculated using a Pearson's correlation of the $CD27^{high}$ parameter and the clinical measure.

* statistically significant p-values

Table 4-5. Pearson's correlations between age and time of spinal tap from initial attack with $CD27^{high}$ plasmablast percentage in ON_{CIS}, $TM_{CIS}A$, and $TM_{CIS}B$ patient groups.						
	$CD27^{high}$ % CSF[1]			**$CD27^{high}$ % PB[2]**		
	mean (SD)	*R*	*p-value*[3]	*mean (SD)*	*R*	*p-value*[3]
Age (years)						
ON_{CIS}	38.4 (13.4)	-0.20	0.63	38.5 (12.6)	-0.44	0.24
$TM_{CIS}A$	38.0 (14.2)	-0.27	0.52	44.1 (17.0)	-0.07	0.86
$TM_{CIS}B$	48.6 (13.6)	0.06	0.86	44.7 (12.5)	-0.27	0.45
Disease duration at time of sampling (months)[3]						
ON_{CIS}	11.4 (16.7)	-0.07	0.87	10.1 (15.8)	0.18	0.67
$TM_{CIS}A$	6.9 (11.4)	-0.21	0.61	16.9 (33.6)	**0.67**	**0.034***
$TM_{CIS}B$	18.1 (32.4)	0.50	0.10	10.3 (17.2)	-0.22	0.53

Abbreviations: CSF: cerebrospinal fluid, PB: peripheral blood, R: Pearson's R, ON_{CIS}: Optic Neuritis, $TM_{CIS}A$: Transverse Myelitis-Above, $TM_{CIS}B$: Transverse Myelitis-Below, SD: standard deviation

[1] The number of patients per $CD27^{high}$ % CSF group is 8 ON_{CIS}, 8 $TM_{CIS}A$, 12 $TM_{CIS}B$

[2] The number of patients per $CD27^{high}$ % Blood group is 9 ON_{CIS}, 10 $TM_{CIS}A$, 10 $TM_{CIS}B$

[3] p-values were calculated using a Pearson's correlation of the $CD27^{high}$ parameter and the clinical measure.

* statistically significant p-values

CHAPTER FIVE

RESULTS

AIM III: AGS-ENRICHED B CELLS MEDIATE MS PATHOLOGY BY PRODUCING ANTIBODIES THAT TARGET THE BRAIN

Overview and rationale

The presence of B cells sharing a pattern of SHM both in the CSF and CNS of patients at high risk for MS suggests that they are responding to the same set of auto-antigens. However, utilization of the AGS as a molecular diagnostic tool to identify patients that will subsequently develop CDMS does not address the impact of AGS-enriched B cells on disease pathogenesis. Determining the target specificity of AGS-enriched antibodies from CSF B cells of MS patients (early CIS and established CDMS) is the first step towards dissecting the potential role of AGS-enriched antibodies in the pathogenesis of MS. Using AGS enrichment as a genomic marker of antigen driven selection represented in MS disease, we cloned 32 rhAbs from singly sorted CSF B cells to recapitulate the antibody that was present on the surface of the cell at the time of sample collection. In addition to AGS enrichment, 61% of the rhAbs were clonally expanded, another marker of an antigen driven humoral response. These rhAbs are now primary tools to address putative targets and disease involvement of these shared signature B cells.

We hypothesized that regardless of disease presentation or duration, as long as the B cell was AGS-enriched, similar targeting patterns would be expected. In testing the targeting ability of the rhAb panel on both mouse and human tissue, we discovered

targeting to GM rather than WM across all rhAbs tested. The rhAbs also recognized cellular targets in two models of mouse CNS inflammation, stroke and EAE, suggesting that the GM antigens were available in various states of neuroinflammation.

Additionally, further IFC experiments revealed that these rhAbs recognized neuronal nuclei and/or astrocytes in both human and mouse brain tissue. This species-preserved homology of important CNS elements provides promise in addressing the pathogenic potential of these rhAbs, particularly in the context of GM pathology. GM damage is gaining appreciation for its pathological significance in addition to the traditional WM focus. Since this AGS-enrichment within the B cell pool and shared targeting to both neurons and astrocytes are present at both presentations of initial disease, ON_{CIS} and TM_{CIS}, this highlights the importance of elucidating the targets that drive the mutational signature as it is an early biomarker of MS disease and conversion.

AGS-ENRICHED ANTIBODIES TARGET GM NEURONS AND ASTROCYTES

The following study has been submitted.

Ligocki A.J, Rounds W.H., Li M., Henson P.M., Rivas J.R., Guzman A.A., Graves D.G., Greenberg B.M., Frohman E.M., Ward E.S., Stowe A.M., Monson N.L., *Gray matter neuron and astrocyte targeting of multiple sclerosis antibodies*, 2013

Introduction

B cells have been implicated in multiple sclerosis (MS) and have been recognized to play a role in MS pathology in addition to the well-accepted pathological role of T cells. B cells and antibodies are present in both the cerebrospinal fluid (CSF) and the central nervous system (CNS) of patients with MS and clinically isolated syndrome (CIS) patients who are at high risk of developing MS. The most common form of MS lesion is characterized by deposition of antibodies and complement (6), and plasmapheresis treatment of patients harboring these lesions leads to symptom improvement (98). In fact, elevated B cells in the CSF correlates with lesion activity on magnetic resonance imaging (MRI) (117) and both increased intrathecal immunoglobulin synthesis (111) and complement activation (113) are also associated with a more aggressive disease course. Collectively these findings implicate a pathological role for antibodies in the pathoetiology of MS.

Our laboratory discovered a biomarker for conversion from CIS to clinically definite MS (CDMS) in the antibody genomics of V_H4-utilizing B cells in the CSF, termed the antibody gene signature (AGS) (228). This shared pattern of somatic hypermutation at 6 codons along the V_H4 gene implicates that the B cell pools are

recognizing a shared set of antigens in the MS disease state that are not recognized by B cells in healthy individuals. Thus, we hypothesized that AGS-enriched antibodies may bind to targets within the CNS. To address this hypothesis, we generated a panel of 32 full-length recombinant human antibodies (rhAbs) from single CSF B cells whose antibody genes contained AGS-targeted mutations. Surveying B cells and antibodies within the CSF is relevant to CNS disease because there are shared B cell clones between the same MS patient's CSF and CNS (232), as well as between the meninges and CNS (234). Additionally, we also found that B cells isolated from CNS lesions harbor the AGS (340). This panel of 32 rhAbs came from a diverse set of patients including CDMS and two initial CIS presentations: optic neuritis (ON_{CIS}) and transverse myelitis (TM_{CIS}). ON_{CIS} patients present with optic symptoms and lesions along the optic nerve, and TM_{CIS} patients exhibit sensory symptoms with lesions along short segments of the spinal cord. Regardless of either presentation of CIS, both patient types have CSF B cells pools enriched for AGS and are at high risk of converting to CDMS.

CNS targeting of the rhAb panel was determined using immunohistochemistry (IHC) on both mouse and human brain tissue. Surprisingly, the AGS-enriched B cells targeted gray matter (GM) rather than the anticipated myelin-rich white matter (WM), which has been extensively studied in the MS field (9). GM involvement in MS disease symptoms and advancement has been understudied even though the presence of cortical lesions correlates strongly with MS disease severity and progression as opposed to the more easily detected WM lesions (32, 36, 367). In fact, cortical GM demyelination is more extensive than WM (26.5% vs 6.5%) with the percentage of demyelination in the cortex increasing with disability and disease length (31). Immunofluorescence confirmed GM targeting of the rhAbs to astrocyte bodies and processes, and neuronal nuclei in both

human and mouse brain tissue. We also found this targeting pattern in AGS-enriched rhAbs generated from both CIS presentations, ON_{CIS} and TM_{CIS}, as well as established CDMS. This is the first known description of MS derived antibodies sharing a mutational pattern that target GM and this previously unrecognized target of humoral immunity may elucidate the pathology and symptoms stemming from cortical damage in disease.

Results

rhAb selection

We have previously shown that CIS patients at risk to convert and those with CDMS harbor B cells in the CSF with a unique mutational pattern in their V_H4 repertoires termed the Antibody Gene Signature (AGS) (228, 340). A shared pattern of increased replacement mutations at 6 specific codons within V_H4 genes suggests selection and recognition of a shared set of antigens. Therefore, we sought to determine the biological significance of this mutational pattern by testing the binding ability of AGS-enriched antibodies to brain tissue. Using single cell sorting of CSF derived B cells from CDMS, ON_{CIS}, and TM_{CIS} patients, we were able to determine the exact antibody-binding variable regions from PCR amplified V_HJ_H and VκJκ sequences. Using a full-length recombinant human IgG_1 antibody expression vector system, variable regions were cloned and expressed for further study. Only those B cells expressing a V_H4 family gene with mutations in 2 or more of the 6 AGS codons were considered for this analysis.

A total of 32 rhAbs were chosen for expression. The details of 10 rhAbs are shown in Table 5-1 and the remaining 22 in Table 5-2. Briefly, all rhAbs contained mutations at 2 or more of the 6 AGS codons, and the majority (66%) contained 3 or more AGS mutations. Additionally, 60% were also clonally expanded, suggesting an antigen

driven process. These rhAbs were cloned from 10 CSF patient repertoires: 9 rhAbs from 4 CDMS patients, 14 rhAbs from 3 ON_{CIS} patients, and 9 rhAbs from 3 TM_{CIS} patients. Two control rhAbs cloned from SLE patient B cells were provided by Dr. Betty Diamond (The Feinstein Institute for Medical Research) as controls for the human IgG construct. The expected binding of this control set has been extensively published using mouse tissue. B1, the negative control, does not react to brain, whereas G11, the positive control, reacts to NMDARs in the brain as well as dsDNA (337).

AGS-enriched rhAbs bind to mouse brain tissue

The panel of 32 experimental AGS-enriched and clonally expanded rhAbs as well as the 2 control rhAbs was first tested for targeting to mouse brain tissue using DAB. This methodology offers sensitive detection of primary rhAb binding to the tissue. Due to previous work from other laboratories demonstrating a lack of binding of antibodies cloned from CDMS CSF B cells to normal brain tissue or WM (267, 268), we chose to utilize brain tissue from a mouse model of transient stroke as a source of inflammation (339). This provided generalized non-antigen directed inflammation to minimize bias of any specific CNS antigen. The secondary antibody used for detection, goat anti-human IgG, did not react to mouse brain alone (Figure 5-1A). As expected, the negative construct control rhAb B1 also did not react to mouse brain, while the positive control rhAb G11 showed recognition to brain and thus validated the assay (Figure 5-1A).

The full panel of 32 rhAbs was tested on mouse brain by DAB. There was a wide range of staining intensity. However all but two of the 32 rhAbs, WR01 and WR11, displayed binding to brain tissue (Figure 5-1 and Figure 5-2). There was no difference of rhAb staining patterns amongst the three patient groups used to derive the rhAbs. A

common feature was that the binding appears cellular in the cortex and midbrain and was either absent or sparse along the heavily myelinated corpus callosum.

AGS-enriched rhAbs bind to human brain tissue

Four sources of human brain were used for the DAB staining experiments: MS normal appearing gray matter (MS-GM) (Figure 5-3), MS normal appearing white matter (MS-WM) (Figure 5-4), MS white matter plaque (MS-P) (Figure 5-5), and healthy control normal appearing WM (HC-WM) (Figure 5-6). Due to the rhAb staining pattern found in the mouse brain, the tissue source of most interest was the MS-GM. The two negative controls, ABC reagent alone and rhAb B1, did not bind to MS-GM whereas the positive control rhAb G11 bound MS-GM (Figure 5-3A). The 10 AGS-enriched rhAbs from 3 different disease types representing 6 different patients all showed binding to human MS-GM (Figure 5-3B-D). As with the mouse brain DAB (Figure 5-1), the staining appeared to be cellular and exhibited similar staining patterns in the human brain DAB (Figure 5-3).

In contrast, the rhAbs demonstrated poor recognition to MS-WM (Figure 5-4). Plaque tissue from the MS patient showed evidence of damage, and the binding was diminished or absent in MS-P tissue (Figure 5-5). The rhAbs also had weak or no binding to HC-WM (Figure 5-6). A common feature shared by the rhAbs was that testing on all sources of WM tissue resulted in weaker staining patterns than was seen in GM tissue.

AGS-enriched rhAbs target neurons and astrocytes in both mouse and human brain tissue

Due to the location and appearance of the DAB staining, we hypothesized that the rhAbs were binding to either of the two major cell types in the brain, neurons and/or

astrocytes. Therefore, IFC colocalization experiments were performed on 10 of the rhAbs from the initial cohort of 32. These 10 were chosen to sample all three disease subtypes and the same source of mouse brain tissue was utilized in these experiments. B1 and G11 were again used as negative and positive controls for the assay respectively. B1 did not recognize brain tissue (Figure 5-7A and Figure 5-8A), but G11 did recognize mouse brain tissue (Figure 5-7B and Figure 5-8B) as evidenced in both the NeuN and the GFAP colocalization experiments. Similar staining pattern of both B1 and G11 was confirmed in human MS-GM (Figure 5-9).

Three rhAbs, one from each patient type, colocalized with neuronal nuclei identified by NeuN in both mouse and human brain. AJL03 from patient CDMS1 showed similar staining of neuronal nuclei in both species tissue (Figure 5-7C, D). AJL10, from patient $ON_{CIS}2$, showed colocalization with neuronal nuclei with the human targeting being very concentrated in the nucleus compared to a more diffuse staining pattern in mouse (Figure 5-7E, F). Additionally, there were areas of AJL10 binding that were independent of NeuN but were still associated with nuclei as marked by DAPI (Figure 5-7E). AJL15 from patient $TM_{CIS}5$ also colocalized with neuronal nuclei in both mouse and human tissue (Figure 5-7G, H). AGS-enriched B cells that recognize neuronal nuclei in the GM are found in all disease presentations and have conserved recognition between mouse and human species.

In order to see if targeting to astrocytes was present, the other major cell type in the GM in addition to neurons, IFC with GFAP was tested. WR12 and WR13 from the same patient, $ON_{CIS}2$, colocalized with astrocytes and their processes in mouse tissue (Figure 5-8C, E). In human tissue, both rhAbs recognized GFAP-positive astrocyte bodies with additional vessel staining seen with WR12 (Figure 5-8D, F). AJL01 from

patient $TM_{CIS}4$ predominately colocalized with astrocytes with additional staining along the periventricular lining in mouse (Figure 5-8G). AJL01 colocalized to astrocyte endfeet within a vessel in addition to the astrocyte bodies in MS-GM shown (Figure 5-8H). In addition to AGS-enriched B cells that recognize neurons, this mutational pattern also imparts recognition to astrocytes.

Four AGS-enriched rhAbs from all 3 patient types displayed dual-cell targeting. AJL02 from patient CDMS1 predominantly colocalized with NeuN in a ring-like fashion within the nuclei (Figure 5-10A) with minor colocalization with GFAP astrocyte processes (Figure 5-10B). This ring-like staining pattern around neuronal nuclei was also seen in human GM tissue (Figure 5-10C). AJL07 from patient $ON_{CIS}3$, displayed dual-cell targeting to both neurons and astrocytes in mouse brain (Figure 5-10D, E). In MS-GM AJL07 principally stained neuronal nuclei and also a vessel (Figure 5-10F), keeping with the dual-cell targeting observed in mouse. From patient $TM_{CIS}4$, WR10 displayed dual-cell targeting with colocalization to both the edges of neuronal nuclei and astrocyte processes in mouse brain (Figure 5-10G, H). WR10 stained astrocyte bodies, endfeet around a vessel, as well as a neuron seen at the top of the panel in MS-GM (Figure 5-10I). AJL19 from patient $TM_{CIS}6$ reacted similarly to WR10 with dual-cell targeting as it colocalized with both neuronal nuclei and astrocytes (Figure 5-10J, K). Colocalization of AJL19 with neuronal nuclei was also seen in MS-GM (Figure 5-10L).

Discussion

Utilization of the AGS as a molecular diagnostic tool to identify patients that will subsequently develop CDMS does not address the impact of AGS-enriched B cells on disease pathogenesis. Determining the target specificity of AGS-enriched antibodies from

CSF B cells of MS patients (early CIS and established CDMS) is the first step towards dissecting the potential role of AGS-enriched antibodies in the pathogenesis of MS. Using AGS enrichment as a genomic marker of antigen driven selection represented in MS disease, we cloned 32 rhAbs from singly sorted CSF B cells to recapitulate the antibody that was present on the surface of the cell at the time of sample collection. Regardless of initial presentation of disease (ON_{CIS} vs TM_{CIS}), early or established disease (CIS vs CDMS), these rhAbs are recognizing neuronal nuclei and/or astrocytes in both mouse and human GM brain tissue. This AGS is present at all initial disease presentations and durations indicating that the stage of disease does not significantly alter the cellular targeting of the AGS-enriched B cell repertoire. Significant immune system activation precedes the initial clinical presentation of disease and complements the finding that rhAbs cloned from ON_{CIS} and TM_{CIS} patients already display recognition to brain targets. CDMS derived rhAbs also maintain recognition of brain tissue, which corroborates recent findings by others that intrathecal IgG from MS patients recognize similar peptides over time (93).

DAB staining on entire coronal sections from mice allowed for both sensitive detection and a large sampling of multiple brain regions for the initial rhAb testing. Surprisingly the rhAbs showed targeting to cellular targets in the cortex and midbrain with only mild/rare staining along the corpus callosum in mouse tissue. If these rhAbs were strongly targeting WM, there would be accumulation of staining in the corpus callosum that is composed of highly myelinated axonal tracts. Instead, we saw staining in the GM, which has gained appreciation for involvement in CDMS symptoms and disease progression (31, 32, 36, 367). WM lesions are readily detected with gadolinium enhancement on MRI and luxol fast blue staining of postmortem tissue, whereas GM

lesions are more difficult to detect via traditional MRI and IHC, explaining why GM pathology was historically under-recognized (368). Progressive GM loss over time occurs at both CIS and MS stages (35, 38), which suggests that the underlying pathology responsible for the loss is not restricted to later disease stages.

Due to the cortical and cellular appearance of the DAB staining, colocalization with NeuN for neuronal nuclei and GFAP for astrocytes was tested using IFC. We found that cloned rhAbs from AGS-enriched B cells isolated from CDMS, ON_{CIS}, and TM_{CIS} exhibit targeting to neuronal nuclei and astrocytes, with four rhAbs displaying dual-cell recognition. Three of the rhAbs representing all three patient subtypes displayed colocalization with only neuronal nuclei. Targeting of neurons fits well with findings of neuronal loss and degeneration present in MS. Proton magnetic resonance spectroscopy (MRS) measurement of N-acetyl aspartate (NAA), a neuronal marker, is significantly reduced in MS CNS (369), especially as patients progress through disease stages (370), supporting that a loss of neurons is associated with progressive neurodegeneration. Furthermore, extensive subpial demyelination with a gradient of neuronal loss outwards from the meninges is associated with ectopic B cell aggregates (131), which are found in patients with a more severe disease course and are adjacent to cortical lesions (130). Since the rhAbs described in the present study were cloned from B cells in the CSF, which is in close contact with the meninges, these AGS-enriched B cells may be strategically located to contribute to GM neuronal damage. Neurofilaments comprise the axonal/neuronal cytoskeleton and have also been identified as autoantigen targets from MS CSF (288), and titers are correlated with atrophy, axonal damage, as well as clinical disability (290). Immunizing mice with neurofilament induces GM damage as well as deposition of IgG within neuronal cell bodies and axons (293), highlighting the ability of

an intracellular neuronal target to elicit disease. Additionally, the myelin sheaths contained degenerating or dead axons (4) supporting the notion that the classical demyelination seen in MS can also occur secondary to axonal and neuronal damage, as axonal transection is a common feature in MS lesions (3).

The integrity of the blood brain barrier (BBB) is maintained by astrocytes and could be disrupted by rhAbs targeting them for damage or altering their functionality. It is well accepted that the BBB is compromised in CIS and MS patients (18), and any damage that perpetuates this could allow for further influx of inflammatory cells and mediators into the already inflamed CNS. Brain targeting antibodies can be detected in healthy human sera (371) and could gain access to the CNS once the BBB is compromised. The binding of three rhAbs in human and mouse GM clearly shows that these rhAbs can bind to astrocytes by colocalizing with GFAP. Additionally, four rhAbs displayed both astrocyte and neuronal nuclei targeting. IFC on MS-GM showed rhAbs targeting architecture surrounding vessels, which includes astrocyte endfeet as well as endothelial cells, and could contribute to MS pathology by disturbing the BBB. Serum IgG from active MS demonstrates recognition of brain microvascular endothelial cells, which also correlated with BBB disruption (315). The difference in appearance of GFAP positive astrocyte immunostaining between mouse and human brain in this study could be due to the planer orientation of the sectioning with the mouse coronal sections having abundant processes and rare astrocytes cell bodies and the human GM having more immunostained cell bodies and rarer processes (372). There is a gaining appreciation of the extensive functions of astrocytes in health and disease beyond maintaining the BBB (302), and thus pathology could arise if the bound antibody alters the astrocytes' functions.

Another critical role for astrocytes is to support remyelination of lesions by providing support and signals to oligodendrocyte precursor cells (303), which could potentially be hindered by antibody targeting. In fact, failure to remyelinate lesions is a feature of progression in CDMS (373). In the well-studied neurological autoimmune disease neuromyelitis optica (NMO), pathology is attributed to antibodies targeting aquaporin-4 on astrocytes, which leads to both cell death and altered functionality (374) resulting in BBB disruption, cellular dysfunction, and loss of support to neurons. Anti-astrocyte potassium channel antibodies have been found in approximately half of tested MS patient sera (314), which could lead to a decreased ability of astrocytes to maintain proper extracelluar ion levels, thereby promoting cellular damage. More recently, the intracellular astrocyte protein contactin-2/TAG-1 was identified as an autoantigen recognized by MS CSF antibodies and the induced disease in mice exhibited inflammation in both WM and GM regions (299). These findings highlight the importance of an immune reaction directed at intracellular and extracellular astrocyte GM antigens in the pathogenesis and symptoms of MS that predominantly contributes to the AGS enriched B cell pool of these patients.

It is unclear from the current study if these antibodies are pathogenic since several of the rhAbs recognize antigen(s) in the nuclei of neurons rather than an easily accessible cell surface antigen. Furthermore, we do not know if the astrocyte binding rhAbs recognize an extracellular or intracellular target. Intracellular targets are associated with many autoimmune diseases, especially systemic lupus erythematosus (SLE) and Sjogren's. Antibodies to intracellular and intranuclear antigens of neurons can be endocytosed and gain access to their cognate antigens within the cell or nucleus (375) and may contribute to disease pathology (376). Antibodies targeting aquaporin-4 on

astrocytes contribute to NMO pathology and bind to extracelluar targets (308), though more recently a group found that a majority of serum tested from NMO patients recognize intracellular portions of the molecule (377) which overlap with the dominant T cell epitope (378). The B cells that recognize the intracellular portions can acquire and present this epitope to T cells and receive cognate help and cytokines to drive a concerted cellular and humoral immune response to this antigen. Recognition and immune responses towards both intracellular and extracellular antigens are present in various autoimmune diseases and is a shared feature with MS.

In testing our panel of AGS-enriched rhAbs, we discovered that the rhAbs had similar staining patterns in both human and mouse brain tissue. This species-preserved homology of important CNS elements provides promise in addressing the pathogenic potential of these rhAbs, particularly in the context of GM pathology, which is gaining appreciation for its pathological significance in addition to the traditional WM focus. It is unknown whether these rhAbs harbor the ability to initiate pathology or if they perpetuate damage due to exposed antigens. Regardless, either mechanism could contribute significantly to both neuron and astrocyte viability and functionality. Since this AGS-enrichment within the B cell pool and shared targeting to both neurons and astrocytes are present at both presentations of initial disease, ON_{CIS} and TM_{CIS}, this highlights the importance of elucidating the targets that drive the mutational signature as it is an early biomarker of MS disease and conversion.

Acknowledgements

We thank the patients who consented to sampling for this study, including families for post-mortem tissues. We appreciate the generosity of Dr. Betty Diamond for providing

B1 and G11 expression vectors and Dr. Michel Nussenzweig for providing the backbone expression vector constructs for the rhAb cloning. Brain tissue was kindly provided by the Human Brain and Spinal Fluid Resource Center (West Los Angeles Healthcare Center, Los Angeles, CA). The UTSWMC Live Cell Imaging Facility is thanked for confocal microscope training and usage. This study was supported by Grants from the National Multiple Sclerosis Society (NMSS) to NLM (RG3267 and RG4653) and DioGenix, Inc. to NLM. AJL and WHR were supported by Grant no. NIH NRSA5 T32 A1 005284-28 from NIAID.

FIGURE LEGENDS FOR CHAPTER FIVE: RESULTS

Figure 5-1. ***AGS-enriched rhAbs bind to mouse brain.*** DAB images are shown at 20x magnification of the cortex and corpus callosum. The rhAbs in each row are grouped as follows: controls (A), CDMS (B), ON_{CIS} (C), and TM_{CIS} (D). The rhAb designation, patient type, and patient number are shown in the upper right corner of each image. Data are representative of three coronal sections per rhAb. Scale bar represents 100 μm.

Figure 5-2. ***AGS-enriched rhAbs bind to mouse brain.*** The remaining 22 rhAbs not in Figure 3-10 are shown here. DAB images are shown at 20x magnification of the cortex and corpus callosum. The rhAbs in each section are grouped as follows: CDMS (A), ON_{CIS} (B), and TM_{CIS} (C). The rhAb designation, patient type, and patient number are shown in the upper right corner of each image. Data are representative of three coronal sections per rhAb. Scale bar represents 100 μm.

Figure 5-3. ***AGS-enriched rhAbs bind to human MS-GM brain.*** DAB images are shown at 20x magnification of MS-GM. The rhAbs in each row are grouped as follows: controls (A), CDMS (B), ON_{CIS} (C), and TM_{CIS} (D). The rhAb designation, patient type, and patient number are shown in the upper right corner of each panel. Data are representative of three MS-GM sections per rhAb. Scale bar represents 100 μm.

Figure 5-4. ***AGS-enriched rhAb DAB staining on human MS-WM brain.*** DAB images are shown at 20x magnification of MS-WM. The rhAbs in each row are grouped as follows: controls (A), CDMS (B), ON_{CIS} (C), and TM_{CIS} (D). The rhAb designation,

patient type, and patient number are shown in the upper right corner of each panel. Data are representative of three MS-WM sections per rhAb. Scale bar represents 100 μm.

Figure 5-5. ***AGS-enriched rhAb DAB staining on human MS-P plaque.*** DAB images are shown at 20x magnification of MS-P. The rhAbs in each row are grouped as follows: controls (A), CDMS (B), ON_{CIS} (C), and TM_{CIS} (D). The rhAb designation, patient type, and patient number are shown in the upper right corner of each panel. Data are representative of three MS-P sections per rhAb. Scale bar represents 100 μm.

Figure 5-6. ***AGS-enriched rhAb DAB staining on healthy human HC-WM brain.*** DAB images are shown at 20x magnification of HC-WM. The rhAbs in each row are grouped as follows: controls (A), CDMS (B), ON_{CIS} (C), and TM_{CIS} (D). The rhAb designation, patient type, and patient number are shown in the upper right corner of each panel. Data are representative of three HC-WM sections per rhAb. Scale bar represents 100 μm.

Figure 5-7. ***IFC of AGS-enriched rhAbs targeting neuronal nuclei in both mouse and human MS-GM brain: AJL03, AJL10, and AJL15.*** Confocal images are shown at 63x magnification and 126x magnification for human tissue with the colocalization marker for NeuN (for neuronal nuclei) shown as red (Alexa Fluor 594). The primary rhAb is shown as green (Alexa Fluor 488) and nuclei are counterstained blue (DAPI). The images are shown as independent red and green channels above the overlay including DAPI. B1 (SLE-neg) and G11 (SLE-pos) negative and positive controls respectively on mouse brain tissue are shown in panels A and B. Mouse and human (MS-GM) brain tissue IFC are shown for each rhAb labeled above the column: AJL03 (CDMS1) (C, D), AJL10

($ON_{CIS}2$) (E, F), and AJL15 ($TM_{CIS}5$) (G, H). Data are representative of six coronal sections per rhAb on mouse tissue and three sections per rhAb on MS-GM tissue. Scale bar represents 10μm.

Figure 5-8. ***IFC of AGS-enriched rhAbs targeting astrocytes in both mouse and human MS-GM brain: WR12, WR13, and AJL01.*** Confocal images are shown at 63x magnification and 126x magnification for human tissue with the colocalization marker for GFAP (for astrocytes) shown as red (Alexa Fluor 594). The primary rhAb is shown as green (Alexa Fluor 488) and nuclei are counterstained blue (DAPI). The images are shown as independent red and green channels above the overlay including DAPI. B1 (SLE-neg) and G11 (SLE-pos) negative and positive controls respectively on mouse brain tissue are shown in panels A and B. Mouse and human (MS-GM) brain tissue IFC are shown for each rhAb labeled above the column: WR12 ($ON_{CIS}2$) (C, D), WR13 ($ON_{CIS}2$) (E, F), and AJL01 ($TM_{CIS}4$) (G, H). Data are representative of six coronal sections per rhAb on mouse tissue and three sections per rhAb on MS-GM tissue. Scale bar represents 10μm.

Figure 5-9. ***IFC of control rhAbs on human MS-GM brain: B1 and G11.*** Confocal images are shown at 63x magnification with the colocalization marker for NeuN (for neuronal nuclei) shown as red (Alexa Fluor 594), the primary rhAb as green (Alexa Fluor 488), and nuclei counterstained blue (DAPI). The images are shown as independent red and green channels above the overlay including DAPI with the rhAb label above each panel. Data are representative of three MS-GM sections per rhAb. Scale bar represents 10μm.

Figure 5-10. ***IFC of AGS-enriched rhAbs targeting both neuronal nuclei and astrocytes in both mouse and human MS-GM brain: AJL02, AJL07, WR10 and AJL19.*** Confocal images are shown at 63x magnification for mouse tissue and 126x magnification for human tissue with the colocalization marker for NeuN (for neuronal nuclei) across the first row and GFAP (for astrocytes) across the second row shown as red (Alexa Fluor 594). The primary rhAb is shown as green (Alexa Fluor 488) and nuclei are counterstained blue (DAPI). The images are shown as independent red and green channels above the overlay including DAPI. The top two rows are NeuN and GFAP staining on mouse brain tissue with the bottom row showing human brain tissue (MS-GM) with labels of the colocalization marker above the red panel. Each rhAb is labeled above the column: AJL02 (CDMS1) (A-C), AJL07 ($ON_{CIS}3$) (D-F), WR10 ($TM_{CIS}4$) (G-I), and AJL19 ($TM_{CIS}6$) (J-L). Data are representative of six coronal sections per rhAb on mouse tissue and three sections per rhAb on MS-GM tissue. Scale bar represents 10μm.

Figure 5-1

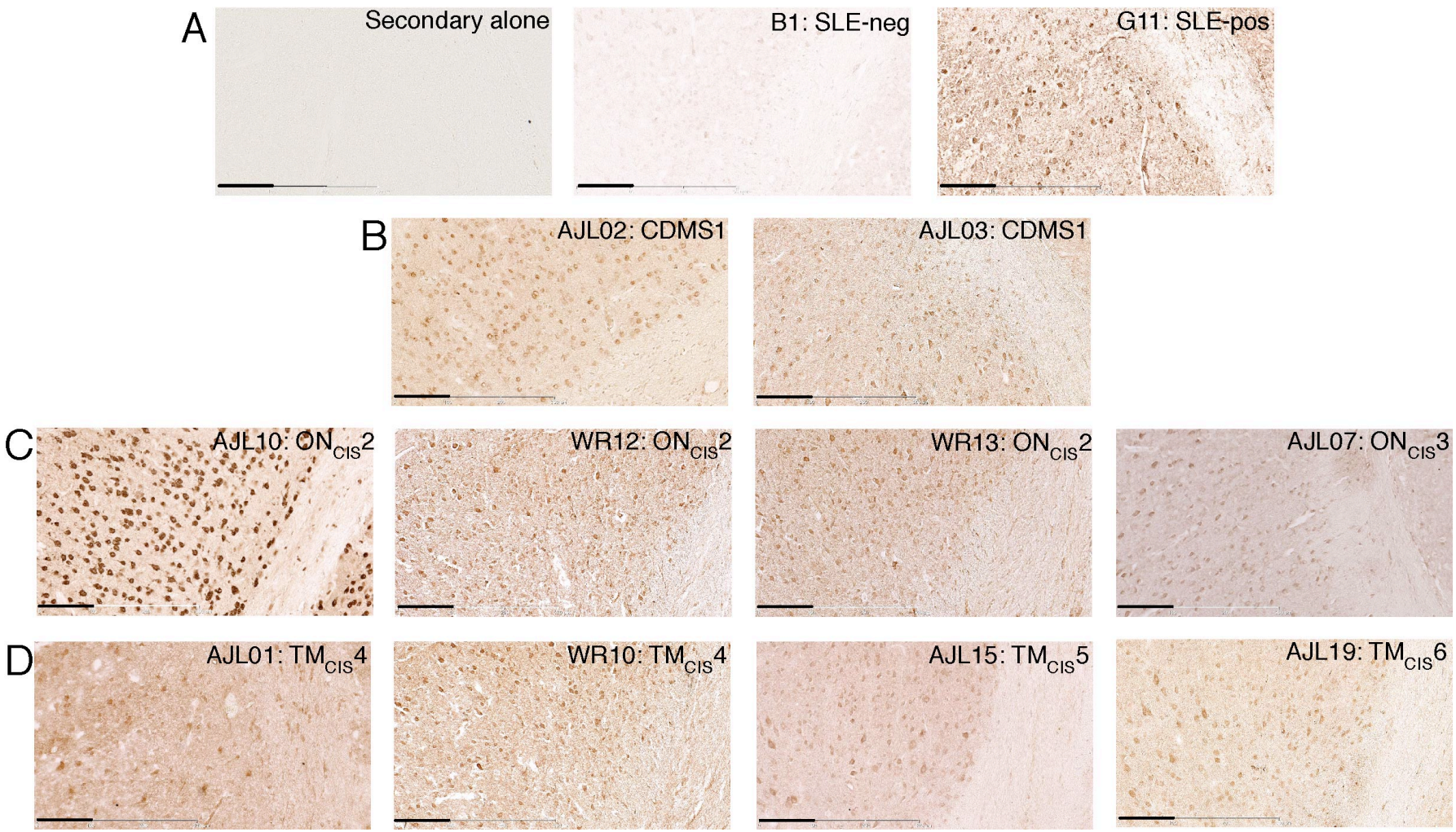
A
Secondary alone
B1: SLE-neg
G11: SLE-pos
B
AJL02: CDMS1
AJL03: CDMS1
C
AJL10: ON$_{CIS}$2
WR12: ON$_{CIS}$2
WR13: ON$_{CIS}$2
AJL07: ON$_{CIS}$3
D
AJL01: TM$_{CIS}$4
WR10: TM$_{CIS}$4
AJL15: TM$_{CIS}$5
AJL19: TM$_{CIS}$6

Figure 5-2

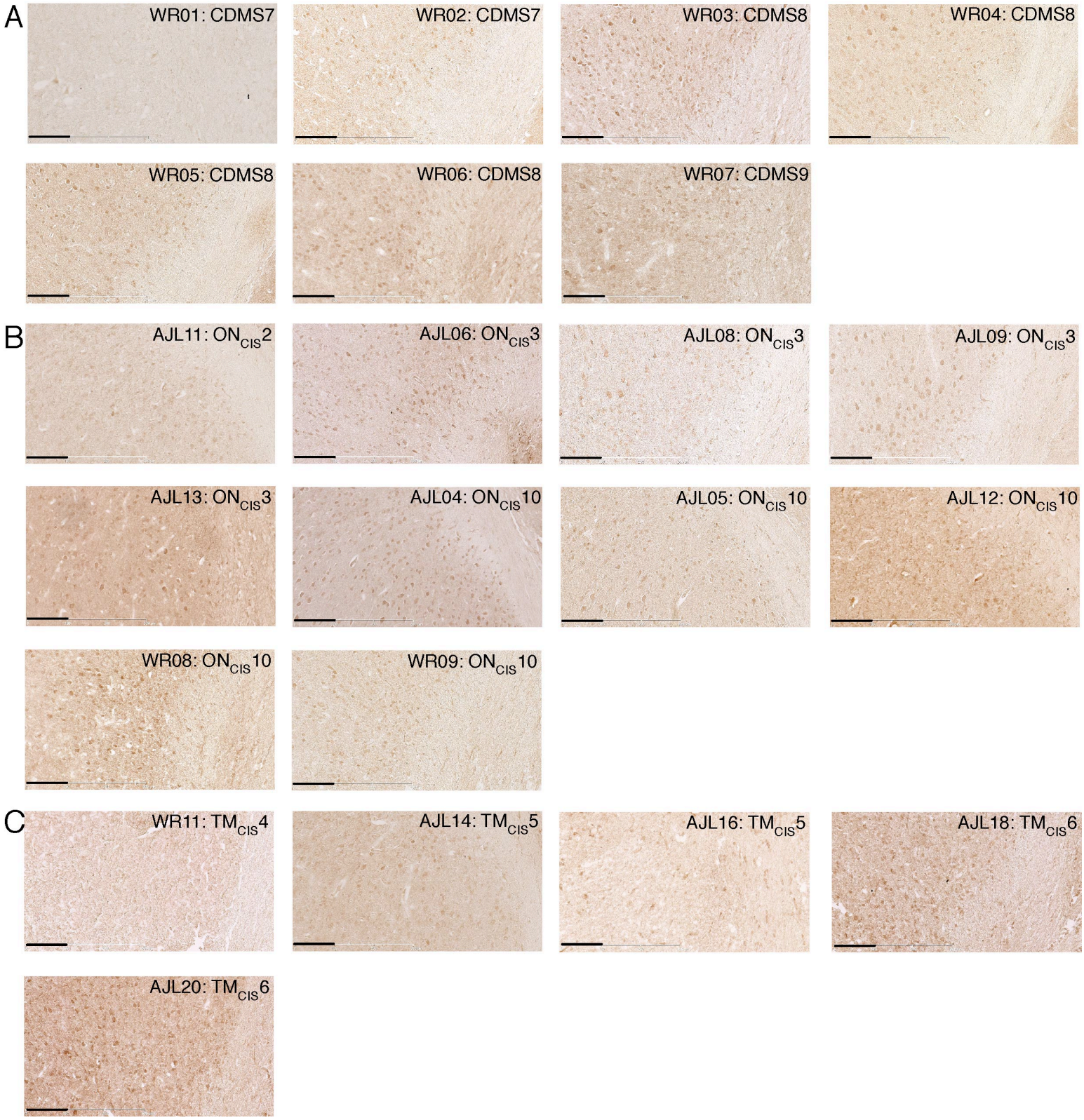
A
WR01: CDMS7
WR02: CDMS7
WR03: CDMS8
WR04: CDMS8
WR05: CDMS8
WR06: CDMS8
WR07: CDMS9
B
AJL11: ON$_{CIS}$2
AJL06: ON$_{CIS}$3
AJL08: ON$_{CIS}$3
AJL09: ON$_{CIS}$3
AJL13: ON$_{CIS}$3
AJL04: ON$_{CIS}$10
AJL05: ON$_{CIS}$10
AJL12: ON$_{CIS}$10
WR08: ON$_{CIS}$10
WR09: ON$_{CIS}$10
C
WR11: TM$_{CIS}$4
AJL14: TM$_{CIS}$5
AJL16: TM$_{CIS}$5
AJL18: TM$_{CIS}$6
AJL20: TM$_{CIS}$6

Figure 5-3

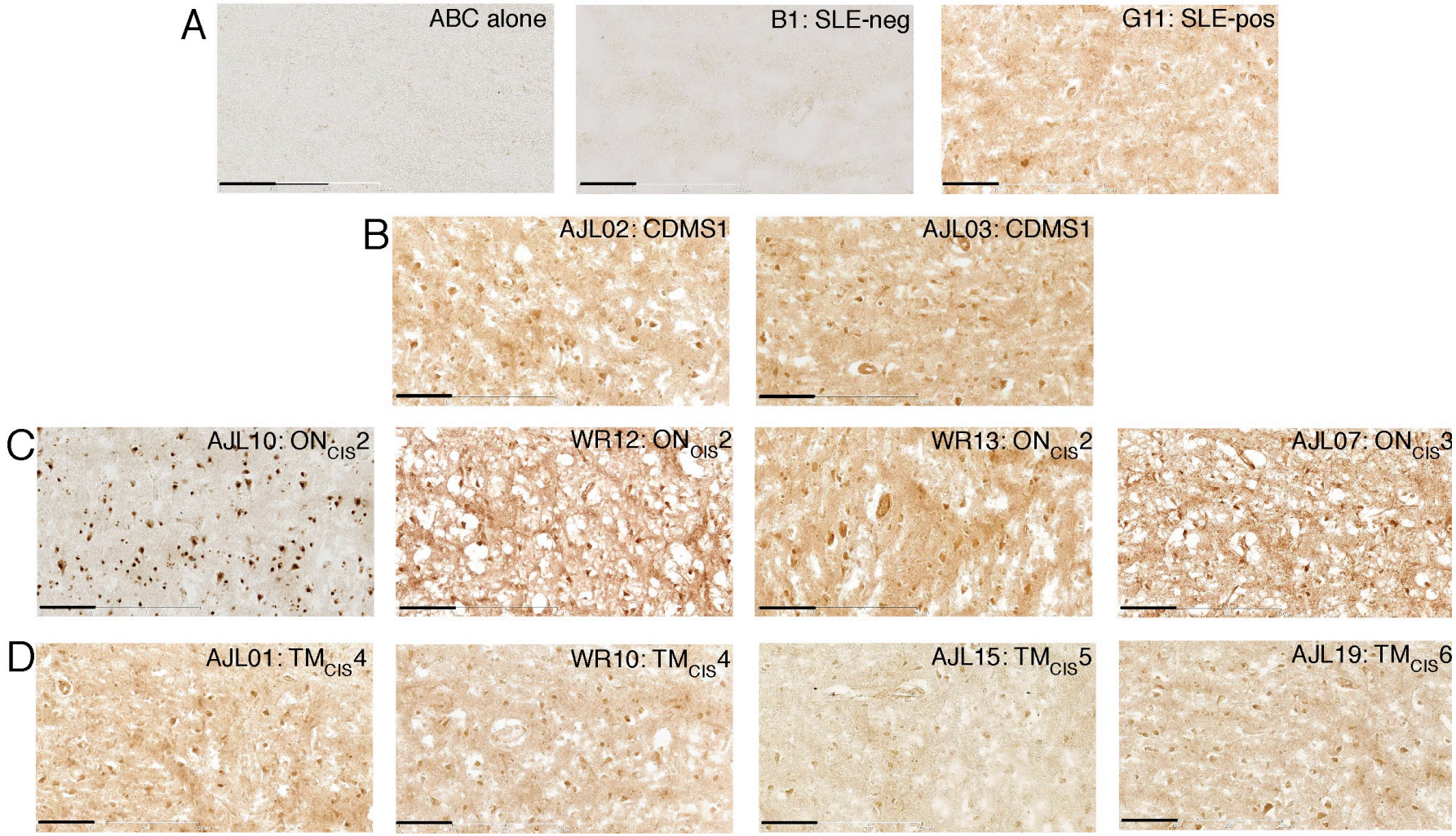
A
ABC alone
B1: SLE-neg
G11: SLE-pos
B
AJL02: CDMS1
AJL03: CDMS1
C
AJL10: ON$_{CIS}$2
WR12: ON$_{CIS}$2
WR13: ON$_{CIS}$2
AJL07: ON$_{CIS}$3
D
AJL01: TM$_{CIS}$4
WR10: TM$_{CIS}$4
AJL15: TM$_{CIS}$5
AJL19: TM$_{CIS}$6

Figure 5-4

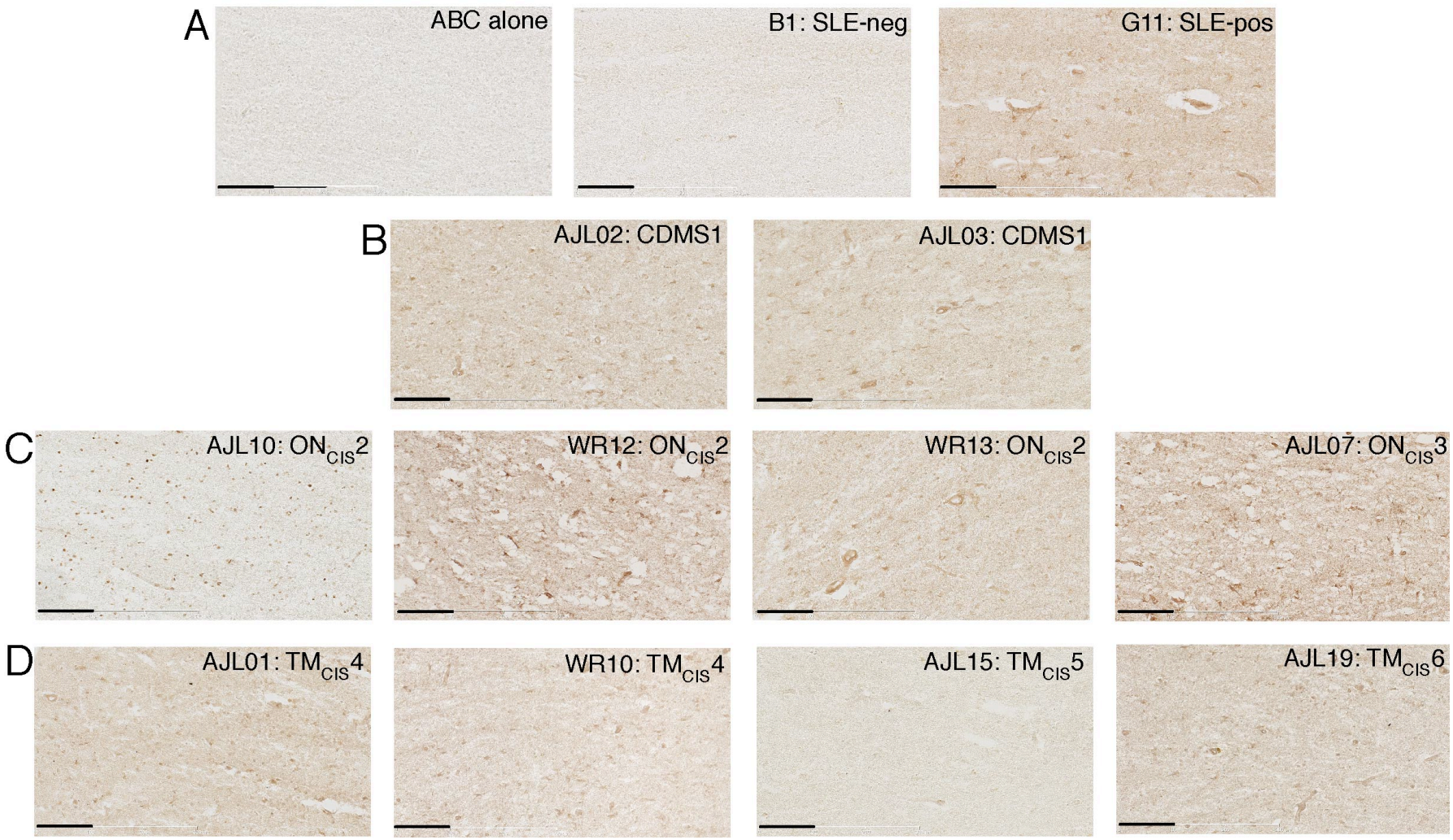
A
ABC alone
B1: SLE-neg
G11: SLE-pos
B
AJL02: CDMS1
AJL03: CDMS1
C
AJL10: ON$_{CIS}$2
WR12: ON$_{CIS}$2
WR13: ON$_{CIS}$2
AJL07: ON$_{CIS}$3
D
AJL01: TM$_{CIS}$4
WR10: TM$_{CIS}$4
AJL15: TM$_{CIS}$5
AJL19: TM$_{CIS}$6

Figure 5-5

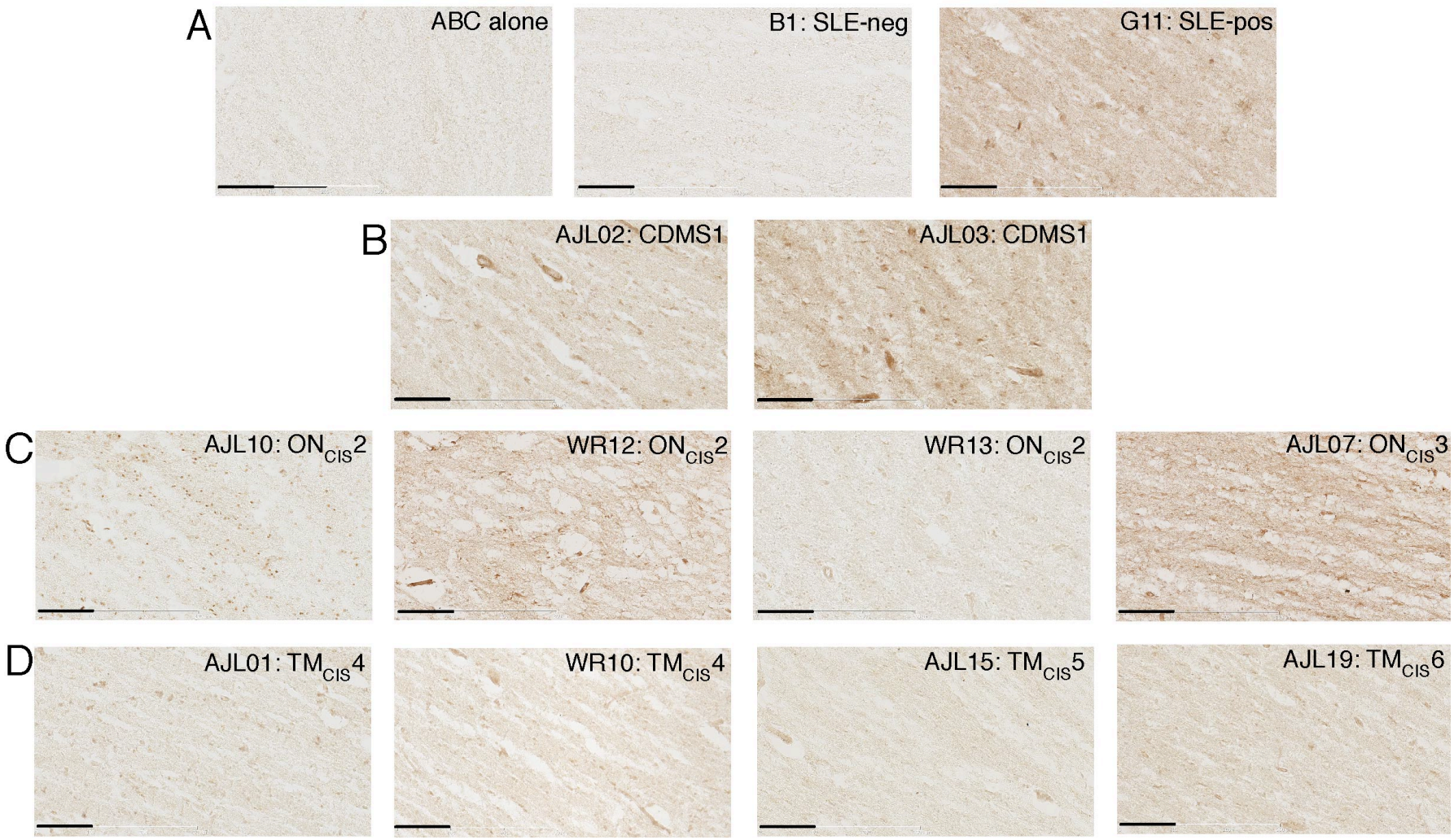
A
ABC alone
B1: SLE-neg
G11: SLE-pos
B
AJL02: CDMS1
AJL03: CDMS1
C
AJL10: ON$_{CIS}$2
WR12: ON$_{CIS}$2
WR13: ON$_{CIS}$2
AJL07: ON$_{CIS}$3
D
AJL01: TM$_{CIS}$4
WR10: TM$_{CIS}$4
AJL15: TM$_{CIS}$5
AJL19: TM$_{CIS}$6

Figure 5-6

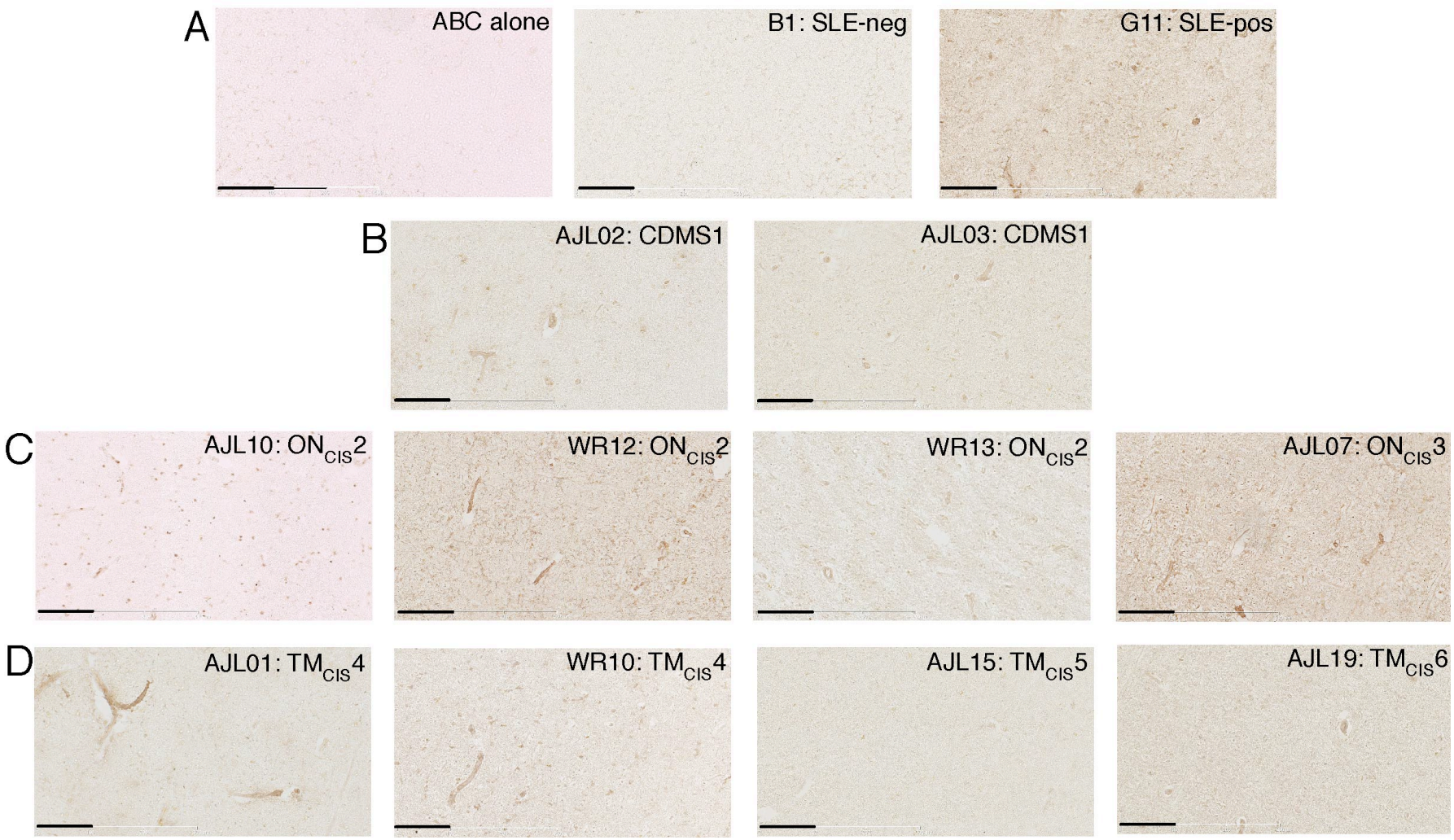
A
ABC alone
B1: SLE-neg
G11: SLE-pos
B
AJL02: CDMS1
AJL03: CDMS1
C
AJL10: ON$_{CIS}$2
WR12: ON$_{CIS}$2
WR13: ON$_{CIS}$2
AJL07: ON$_{CIS}$3
D
AJL01: TM$_{CIS}$4
WR10: TM$_{CIS}$4
AJL15: TM$_{CIS}$5
AJL19: TM$_{CIS}$6

Figure 5-7

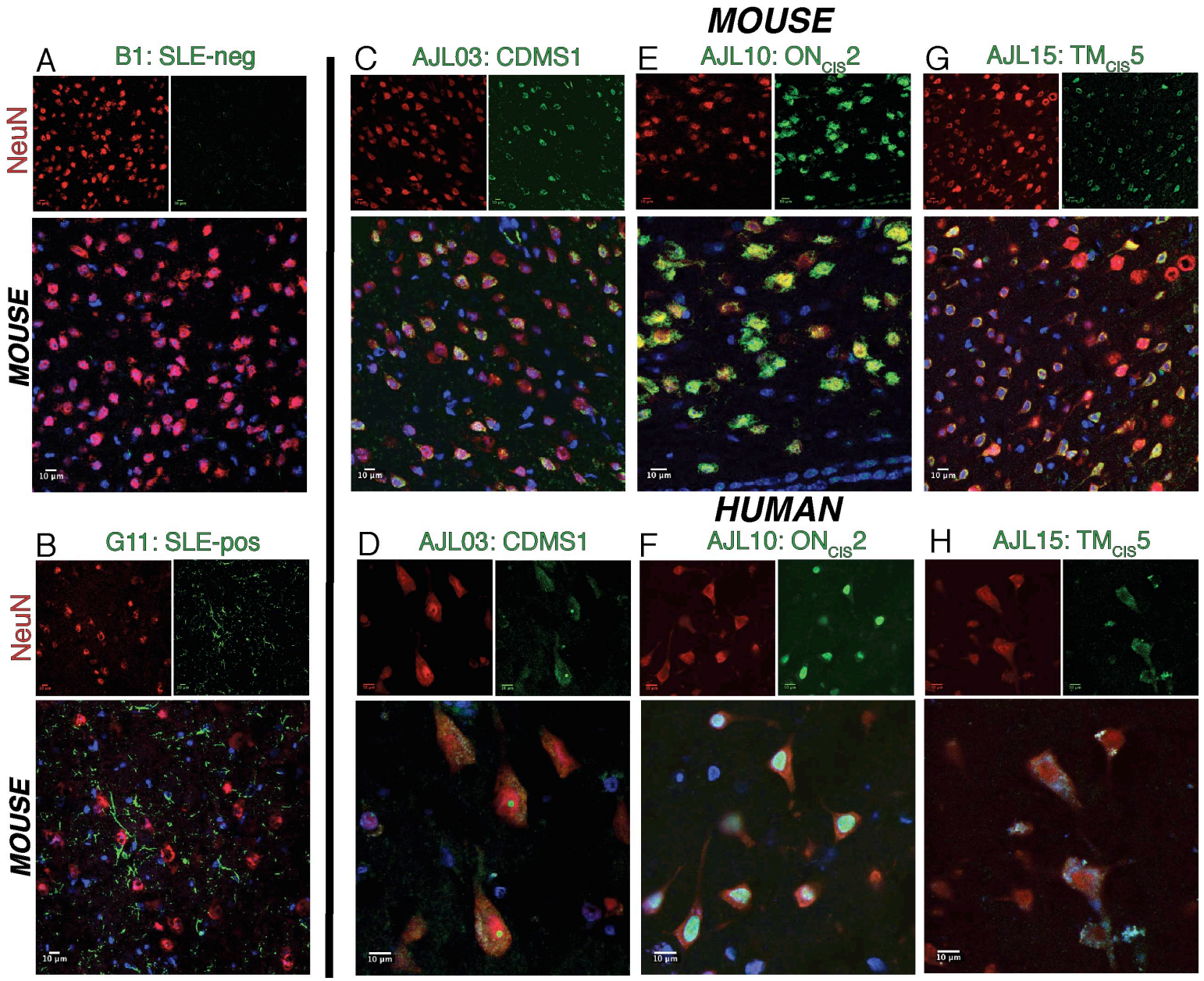
MOUSE
A
B1: SLE-neg
C
AJL03: CDMS1
E
AJL10: ON$_{CIS}$2
G
AJL15: TM$_{CIS}$5
NeuN
MOUSE
10 µm
HUMAN
B
G11: SLE-pos
D
AJL03: CDMS1
F
AJL10: ON$_{CIS}$2
H
AJL15: TM$_{CIS}$5
NeuN
MOUSE
10 µm

Figure 5-8

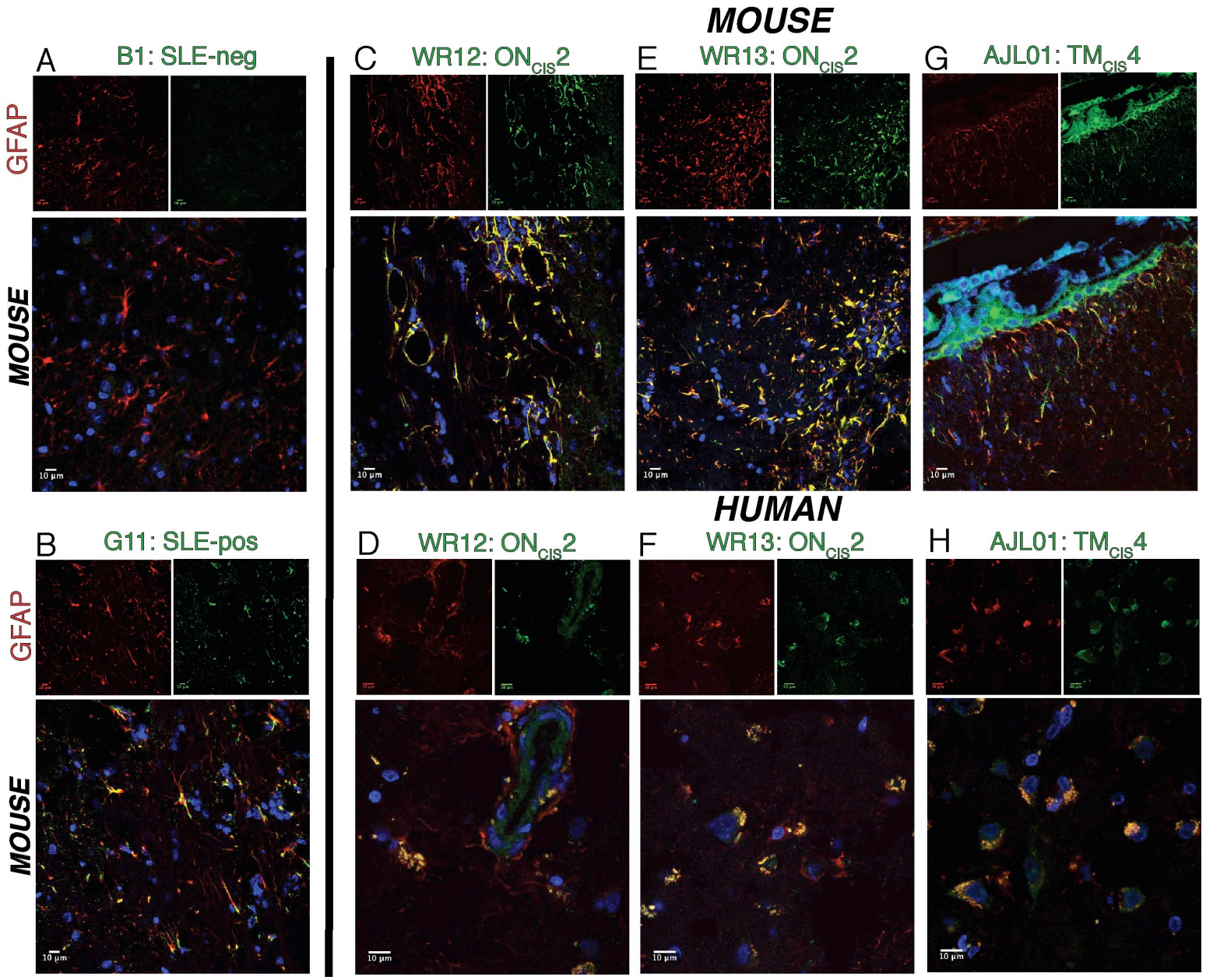
MOUSE
A B1: SLE-neg
C WR12: ON$_{CIS}$2
E WR13: ON$_{CIS}$2
G AJL01: TM$_{CIS}$4
GFAP
MOUSE
10 µm
HUMAN
B G11: SLE-pos
D WR12: ON$_{CIS}$2
F WR13: ON$_{CIS}$2
H AJL01: TM$_{CIS}$4
GFAP
MOUSE
10 µm

Figure 5-9

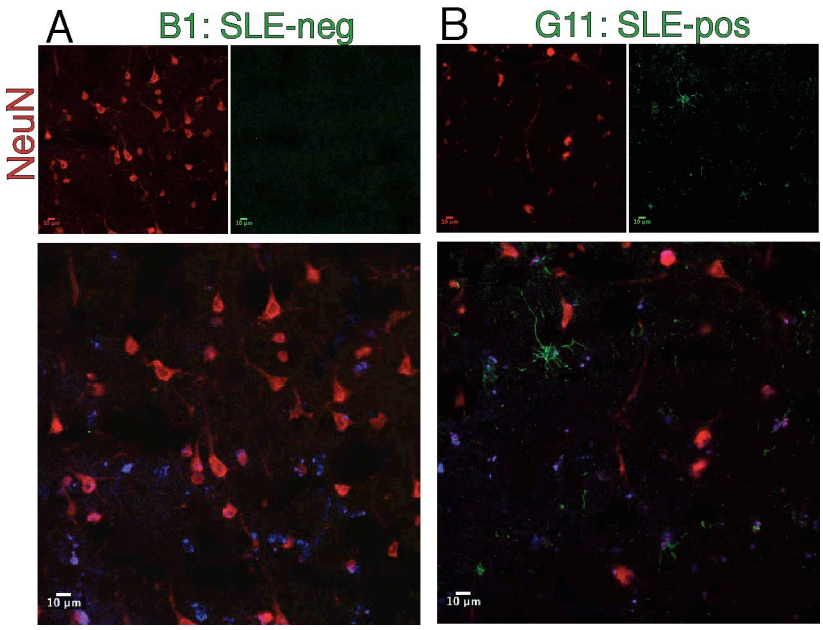

Figure 5-10

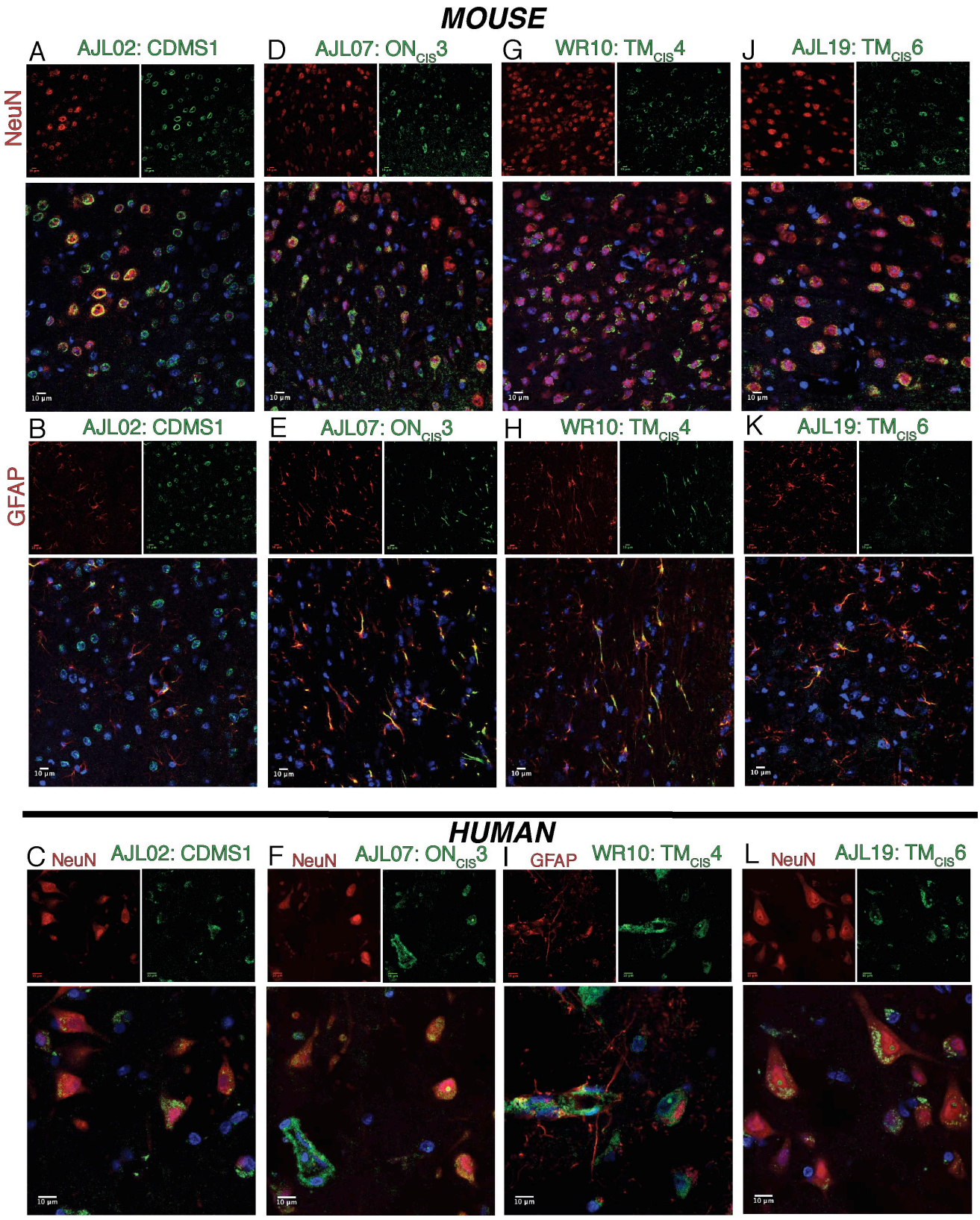
MOUSE
A AJL02: CDMS1
D AJL07: ON$_{CIS}$3
G WR10: TM$_{CIS}$4
J AJL19: TM$_{CIS}$6
NeuN
B AJL02: CDMS1
E AJL07: ON$_{CIS}$3
H WR10: TM$_{CIS}$4
K AJL19: TM$_{CIS}$6
GFAP
HUMAN
C NeuN AJL02: CDMS1
F NeuN AJL07: ON$_{CIS}$3
I GFAP WR10: TM$_{CIS}$4
L NeuN AJL19: TM$_{CIS}$6
10 µm

TABLES FOR CHAPTER FIVE: RESULTS

Table 5-1. Patient, gene, and staining overview of the 10 rhAbs used for DAB and IFC

Patient #	Diagnosis	rhAb	Clone	# AGS[1]	NeuN[2]	GFAP[3]
1	CDMS	AJL02	no	2	+	+
		AJL03	no	2	+	-
2	ON_{CIS}	AJL10	no	4	+	-
		WR12	yes	2	-	+
		WR13	yes	2	-	+
3	ON_{CIS}	AJL07	yes	3	+	+
4	TM_{CIS}	AJL01	yes	3	-	+
		WR10	yes	2	+	+
5	TM_{CIS}	AJL15	yes	4	+	-
6	TM_{CIS}	AJL19	yes	3	+	+

Abbreviations: CDMS: clinically definite multiple sclerosis, ON_{CIS}: clinically isolated syndrome- optic neuritis, TM_{CIS}: clinically isolated syndrome- transverse myelitis, rhAb: recombinant human antibody, AGS: antibody gene signature, NeuN: neuronal nuclei, GFAP: glial fibrillary acid protein

[1] Number of mutated AGS codons (6 total possible) in the V_H4 gene of the rhAb.

[2,3] Positive (+) or negative (-) colocalization as determined by the mouse brain tissue IFC experiments. See Figures 5-7, 5-8, and 5-10 for images.

Table 5-2. Patient, gene, and staining overview of the 22 rhAbs used only for mouse brain tissue DAB.[1]				
Patient #	Diagnosis	rhAb	Clone	# AGS[2]
2	ON_{CIS}	AJL11	no	3
3	ON_{CIS}	AJL06	no	3
		AJL08	yes	3
		AJL09	yes	2
		AJL13	yes	3
4	TM_{CIS}	WR11	yes	2
5	TM_{CIS}	AJL14	no	3
		AJL16	yes	3
6	TM_{CIS}	AJL18	yes	5
		AJL20	no	3
7	CDMS	WR01	yes	2
		WR02	yes	2
8	CDMS	WR03	no	3
		WR04	no	3
		WR05	no	4
		WR06	no	3
9	CDMS	WR07	no	4
10	ON_{CIS}	AJL04	yes	3
		AJL05	yes	4
		AJL12	no	3
		WR08	yes	2
		WR09	yes	2

Abbreviations: CDMS: clinically definite multiple sclerosis, ON_{CIS}: clinically isolated syndrome- optic neuritis, TM_{CIS}: clinically isolated syndrome- transverse myelitis, rhAb: recombinant human antibody, AGS: antibody gene signature

[1] See DAB images of the rhAbs listed here in Figure 5-2.

[2] Number of mutated AGS codons (6 total possible) in the V_H4 gene of the rhAb.

CHAPTER SIX

UNPUBLISHED RESULTS

AIM I: AGS POSITIVE B CELLS ARE ENRICHED IN MS DISEASE

AGS-enriched B cells are present in MS CNS tissue from different laboratory sources

In collaboration with Drs. Hafler and O'Connor (Yale University), we received V_H repertoires from 4 postmortem MS CNS specimens using laser capture microdissection (LCM) to isolate B cells and PCR their V_H regions. The average AGS score of the 4 LCM-CNS repertoires did not differ from CDMS CSF (Figure 6-1, Table 6-1). Interestingly, one of the repertoires was isolated from NAWM (MS-4) and still displayed AGS enrichment.

Post publication, in collaboration with Drs. Fire and Boyd (Stanford University) we received V_H repertoires from 4 postmortem MS CNS specimens using NGS to obtain the antibody sequences. In this data set using a different PCR platform, we were still able to detect an enrichment of AGS in all 4 NGS-CNS repertoires. The average AGS score of the NGS-CNS repertoires was 18.07 and did not differ from CDMS CSF ($p=0.29$) or LCM-CNS ($p=0.34$) (Figure 6-1, Table 6-1). Two of the samples were from lesions, MS-5 from an acute lesion and MS-6 from a chronic active lesion. Both had similar enrichment of the AGS. Two of the samples (MS-7 and MS-8) were obtained from NAWM and also displayed similar AGS enrichment. These data demonstrate that the AGS is not unique to the CSF but is also present in MS CNS tissue antibody repertoires. This genomic marker was also confirmed using three different PCR techniques among three different laboratories.

AGS-enriched B cells are present in the CSF of TM_{CIS} patients

The average AGS score for the initial cohort of 12 ON_{CIS} patients from Drs. Owens and Bennett was 14.47 after their sequences were re-anchored to match the current methodology (Figure 6-2). A small test group of 4 ON_{CIS} patients were recruited at UTSWMC to verify similar AGS enrichment. In fact, the average AGS score for these 4 patients was 10.35, which did not differ from the original cohort ($p=0.09$) (Figure 6-2, Table 6-2). 10 TM_{CIS} patients had an average AGS score of 15.20 that did not differ from the 4 ON_{CIS} patients ($p=0.22$) (Figure 6-2, Table 6-2). Regardless of initial presentation, CIS patients at high risk to convert to CDMS harbor an enrichment of AGS B cells within their CSF repertoire.

AIM II: MUTATION CHARACTERISTICS AND B CELL SUBPOPULATIONS DIFFER BETWEEN CIS PATIENTS PRESENTING WITH ON_{CIS} vs TM_{CIS}

Positive selection of $V_H1^+J_H6^+$ usage in $TM_{CIS}A$ PB memory B cells

The V_H1^+ B cells from MS patients utilized J_H6 segments more often than J_H4 segments in comparison to HCPB (Figure 4-5C). Additionally, MSPB $V_H1^+J_H6^+$ B cells accumulated higher levels of SHM and thus were selected over $V_H1^+J_H4^+$ B cell (Figure 4-5D). Despite V_H1^+ B cells from $TM_{CIS}A$ memory B cells having similar usage of J_H4 and J_H6 segments, J_H6 was positively selected with higher levels of SHM compared to J_H4 (Figure 4-D). This is similar to what was seen in the PB of established MS patients (Figure 4-5D) and CSF of $TM_{CIS}A$ patients (Figure 4-3D). No selection was observed for $V_H1^+J_H6^+$ peripheral $CD27^{high}$ plasmablasts from the $TM_{CIS}A$ patients with regards to usage or mutation accumulation (Figure 4-5C,D).

V_H1^+ CDR3 charge is increased only in the PB of MS patients

The PB V_H1^+ B cell pool of HC, $TM_{CIS}A$-$CD27^{high}$, and $TM_{CIS}A$-$CD27^+$ groups had similar CDR3 charges and lengths (Figure 4-5E). In contrast, the PB V_H1^+ B cells from MS patients had a significant increase in positive charge (Figure 4-5E). This difference in charge was only observed as a slight trend in the V_H4^+ B cell pool from the same MS patients (Figure 4-5E). The CDR3 length of these V_H1^+ B cells did not differ from the other PB repertoire groups (Figure 4-5F).

TM_{CIS}A and TM_{CIS}B patients are equally enriched for AGS

The AGS has been detected in CSF B cells from MS and ON_{CIS} patients (228), and also in B cells isolated at the site of disease in MS brain tissue (340). The AGS is also enriched in CSF B cells from TM_{CIS} patients. However, it remained unknown whether it would differ in TM_{CIS}A patients with an expansion of $CD27^{high}$ plasmablasts in their CSF. The average AGS score calculated for the MS group was 14.87 (Figure 6-3). The ON_{CIS}, TM_{CIS}A and TM_{CIS}B subgroups had average AGS scores that were statistically similar to the MS group and amongst the subgroups (ON_{CIS}, 12.06; TM_{CIS}A, 14.30; TM_{CIS}B, 16.56) (Figure 6-3). Thus, despite an enrichment of CSF plasmablasts in the TM_{CIS}A group, all patients at high risk to develop MS displayed similar AGS scores.

AIM III: AGS-ENRICHED B CELLS MEDIATE MS PATHOLOGY BY PRODUCING ANTIBODIES THAT TARGET THE BRAIN

Validation of tissue preservation

The preservation of CNS tissues were confirmed using cresyl violet staining to visualize the nissl bodies present in neurons and other basophilic molecules in glia as purple. This was especially necessary for the human brain samples, due to the time gap between death and processing in addition to the absence of perfusion to clear fluids and preserve the brain tissue. Three sources of human brain were processed. Normal appearing MS-white matter (WM) and MS-gray matter (GM) were present in a single sample. From this same MS patient, a WM- plaque (P) was also sampled. Lastly, healthy control (HC)-WM was sampled as a non-diseased control.

A mouse brain was extracted and snap-frozen to loosely simulate the initial state of the human brain samples. The cresyl violet stain shown in Figure 6-4A demonstrates that the tissue was preserved using this methodology. The MS-WM, MS-GM, MS-P, and HC-WM also stained positive using cresyl violet (Figure 6-4B-E). The staining was sparser in WM samples than GM samples, which is to be expected given the lower density of neurons and glia present in WM (Figure 6-4C,E). The MS-GM showed large neuronal nuclei indicating that they were preserved (Figure 6-4B). All of these data suggest that the tissues were preserved for IHC and IFC binding experiments of cellular components.

Additional IHC and IFC controls

IgG deposits can be found in healthy brain (Figure 6-5A) and as an artifact of post-mortem tissue preparation (106). Therefore, a set of 10 rhAbs and the 2 control rhAbs were biotinylated to eliminate the need for a species specific secondary antibody.

In addition to the secondary alone or ABC alone, and B1 results, a third negative control was run. Effective blocking of the tissue was tested using a commercial Fc blocking agent (Innovex) to verify if the same staining patterns were seen as with the previous blocking methodology (normal goat serum). There were no differences in the staining patterns as previously shown of either G11 or AJL10 when using the commercial Fc blocking agent on mouse, MS-GM, or MS-WM tissue sources (Figure 6-6). Blocking with normal goat serum is effective in abrogating non-specific binding through endogenous tissue Fc receptors.

Due to the rhAbs being visualized by a secondary Alexa-Fluor 488, possible autofluorescense in this channel could occur when working with brain tissue. The tissue was incubated alone with Alexa-Fluor 488 secondary antibody alone to determine the background autofluorescense. This did not produce a signal in either mouse or human brain tissue (Figure 6-7). This in conjunction with no signal when incubated with the rhAb B1 indicated that staining in the 488-channel was positive in subsequent IFC experiments.

AGS-enriched rhAbs targeting a single cell type

Three rhAbs, one from each patient type, colocalized with neuronal nuclei identified by NeuN in both mouse and human brain: AJL03, AJL10, and AJL15 (Figure

5-7). These three AGS-enriched rhAbs targeted neuronal nuclei and did not colocalize with astrocytes (Figure 6-8).

Three rhAbs, from ON_{CIS} and TM_{CIS} patients, colocalized with astrocytes identified by GFAP in both mouse and human brain: WR12, WR13, and AJL01 (Figure 5-8). These three AGS-enriched rhAbs targeted astrocytes and did not colocalize with neuronal nuclei (Figure 6-9).

Receptor edited AGS-enriched rhAbs

The rhAb cohort also included 5 sets of receptor edited pairs. One pair had an edited heavy chain, WR01 and WR02. The remaining had edited light chains, WR12 and WR13, AJL13 and AJL07, WR11 and WR10, WR08 and WR09. Three out of the five pairs of receptor-edited clones have similar staining patterns (Figure 5-1 and Figure 5-2) suggesting a failure in receptor editing in reducing auto-reactivity in these pairs. The pair with an edited heavy chain, WR01 and the edited WR02, displayed a slight difference in DAB intensity with WR02 appearing darker than WR01 (Figure 5-2A). This is an example of a potential reduction in affinity for the target or maybe a change in antigenic recognition. One of the light chain receptor edited pairs, WR10 and WR11 with a light chain allele replacement, displayed a strikingly different pattern with WR10 showing clear binding to brain tissue (Figure 5-1D) and WR11 not staining to brain (Figure 5-2C). This is an example of successful receptor editing in utilizing a second light chain allele and eliminating auto-reactivity to brain tissue.

From patient $ON_{CIS}2$, a pair of light chain receptor edited clones were tested utilizing IFC: WR13 and its edited clone WR12. Both colocalized with astrocytes and their processes in mouse tissue (Figure 5-8C,E) as well as human tissue (Figure 5-8D,F).

Receptor editing failed to eliminate auto-reactivity since intense colocalization with astrocytes and their endfeet along the corpus callosum remained intact in both the original clone (WR13) and its receptor-edited progeny (WR12).

Titration of dual-targeting AGS-enriched rhAbs

Four AGS-enriched rhAbs (AJL02, AJL07, AJL19, and WR10) colocalized with both neuronal nuclei and astrocytes. However, it is possible that one of the cell types is a preferential target for the rhAb. The amount of rhAb incubated overnight on the brain slice was titrated down (original:1 μg, 3 titrations: 800 ng, 600 ng, and 400 ng) and colocalization with GFAP was evaluated. Two of the rhAbs, AJL02 and WR10, no longer stained astrocytes below 1 μg of rhAb (Figure 6-10 and Figure 6-11). AJL02 still retained a prominent nuclear ringing staining pattern even at the lowest amount of rhAb used (400 ng) (Figure 6-10D). On the other hand, there was no staining visible above background for WR10 at any amount lower than 1 μg of rhAb (Figure 6-11B-D). AJL07 showed minor GFAP colocalization with 800 ng of rhAb, and no staining was visible above background at either 600 ng or 400 ng of rhAb (Figure 6-13B-D). AJL19 retained colocalization with astrocytes at all concentrations of rhAb used (Figure 6-13A-D). There was also minor staining still visible in some neuronal nuclei (Figure 6-13E-G). A summary of the staining seen at different rhAb concentrations is shown in Table 6-3.

Varied nuclear patterns of neuronal nuclei targeting AGS-enriched rhAbs

7 rhAbs (AJL02, AJL03, AJL07, AJL10, AJL15, AJL19, and WR10) that colocalized with neuronal nuclei were further evaluated to identify where in or around the nucleus they were targeting. Lamin A was used as a colocalization marker for the nuclear

membrane. IFC was done on mouse brains obtained from EAE immunized with full-length recombinant human MOG. All previous mouse IFC was conducted on brains from mice with transient stroke as a model of neuroinflammation (339). The 7 rhAbs bound to the EAE mouse brain with the same patterns as the previously demonstrated utilizing stroke mouse brain as a tissue source (Figure 6-14).

Two rhAbs from patient CDMS1, AJL02 and AJL03, both stained nuclei in a different pattern. AJL02 retained the characteristic ring-like stain within the nuclei, seen as the independent green stain within the red lamin A membrane (Figure 6-14A). AJL03 colocalized with lamin A targeting the nuclear membrane itself (Figure 6-14B). AJL10 from $ON_{CIS}2$ targeted the center of the nucleus more intensely than the edges of the lamin A membrane. There was also an area of staining closely ringing the exterior of lamin A (Figure 6-14C), which corroborates the colocalization pattern seen with NeuN (Figure 5-7E). AJL07 from patient $ON_{CIS}3$ colocalized with lamin A (Figure 6-14D), resembling AJL03. WR10, from $TM_{CIS}4$, displayed another pattern of binding with colocalization only on the edges of lamin A (Figure 6-14E), much like the edged pattern seen in the stroke mouse brain (Figure 5-10G). The staining of AJL15, from $TM_{CIS}5$, shared the same colocalization pattern seen with AJL10 (Figure 6-14F). Lastly, AJL19 from $TM_{CIS}6$ colocalized with lamin A across the entire nuclear membrane similarly to AJL03 and AJL07 (Figure 6-14G). All of these AGS-enriched rhAbs bind to neuronal nuclei but display a varied pattern in nuclear targeting.

FIGURE LEGENDS FOR CHAPTER SIX: UNPUBLISHED RESULTS

Figure 6-1. ***AGS scores are enriched in MS CNS B cell repertoires.*** CDMS from CSF (N=6), laser capture microdissection (LCM)-CNS (N=4), and next generation sequencing (NGS)-CNS (N=4) AGS scores are shown. The mean and s.e.m. are plotted on the graph and are shown below each respective group. No significant differences were found among the groups using the student's t-test.

Figure 6-2. ***AGS scores are present in both ON_{CIS} and TM_{CIS} system CSF $CD19^+$ B cell repertoires.*** ON_{CIS} (N=12), new ON_{CIS} (N=4), and new TM_{CIS} (N= 10) AGS scores are show. The mean and s.e.m. are plotted on the graph and are shown below each respective group. No significant differences were found among the groups using the student's t-test.

Figure 6-3. ***AGS scores of CSF $CD19^+$ B cell repertoires are similar among CIS subtypes.*** MS (N=6), ON_{CIS} (N=4), TM_{CIS}A (N=6), and TM_{CIS}B (N=4) AGS scores are shown. The mean and s.e.m. are plotted on the graph and are shown below each respective group. No significant differences were found among the groups using the student's t-test.

Figure 6-4. ***Cresyl violet staining of preserved and processed mouse and human brain.*** Cresyl violet images are shown at 20x magnification. The tissues are: mouse (A), MS-GM (B), MS-WM (C), MS-P (D), and HC-WM (E). The tissue type is shown in the upper right corner of each image. Data are representative of three sections. Scale bar represents 100 μm.

Figure 6-5. ***Normal human brain contains endogenous deposits of IgG.*** HC-WM was tested using the same secondary detection antibody used for mouse brain binding in Figures 3-10 and 3-11. Naturally deposited IgG is present in HC-WM (A) that is not seen with incubation with the ABC reagent alone (B). The treatment of the tissue is shown in the upper right corner of each image. Data are representative of three sections. Scale bar represents 100 μm.

Figure 6-6. ***Similar DAB staining of G11 and AJL10 with commercial FcBlock agent.*** DAB images using FcBlock in place of normal goat serum as a blocking agent are shown at 20x magnification. AJL10 and G11 staining is shown in mouse (A), MS-GM (B), and MS-WM (C) tissue soursces. The rhAb designation, patient type, and patient number are shown in the upper right corner of each image. Data are representative of three sections per rhAb. Scale bar represents 100 μm.

Figure 6-7. ***IFC of secondary alone Alexa Fluor 488 controls on mouse and human MS-GM brain.*** Confocal images are shown at 63x magnification with the Alexa Fluor 594 channel empty, Alexa Fluor 488 as the secondary alone, and nuclei counterstained blue (DAPI). Goat x human Fc Alexa Fluor 488 on mouse tissue is shown in panel A and streptavidin Alexa Fluor 488 is shown in panel B. The images are shown as independent red and green channels above the overlay including DAPI with the 488 detection antibody label above each panel. Data are representative of three sections per rhAb. Scale bar represents 10μm.

Figure 6-8. ***IFC of AGS-enriched rhAbs that do not target astrocytes: AJL03, AJL10, and AJL15.*** Confocal images are shown at 63x magnification with the colocalization marker for GFAP (for astrocytes) shown as red (Alexa Fluor 594). The primary rhAb is shown as green (Alexa Fluor 488) and nuclei are counterstained blue (DAPI). The images are shown as independent red and green channels above the overlay including DAPI. Mouse brain tissue IFC are shown for each rhAb that colocalized with neuronal nuclei in Figure 3-18: AJL03 (CDMS1) (A), AJL10 ($ON_{CIS}2$) (B), and AJL15 ($TM_{CIS}5$) (C). Data are representative of three coronal sections per rhAb. Scale bar represents 10μm.

Figure 6-9. ***IFC of AGS-enriched rhAbs that do not target neuronal nuclei: WR12, WR13, and AJL01.*** Confocal images are shown at 63x magnification with the colocalization marker for NeuN (for neuronal nuclei) shown as red (Alexa Fluor 594). The primary rhAb is shown as green (Alexa Fluor 488) and nuclei are counterstained blue (DAPI). The images are shown as independent red and green channels above the overlay including DAPI. Mouse brain tissue IFC are shown for each rhAb that colocalized with astrocytes in Figure 3-19: WR12 ($ON_{CIS}2$) (A), WR13 ($ON_{CIS}2$) (B), and AJL01 ($TM_{CIS}4$) (C). Data are representative of three coronal sections per rhAb. Scale bar represents 10μm.

Figure 6-10. ***IFC of dual-cell targeting AJL02 (CDMS1) rhAb titrations on mouse brain.*** Confocal images are shown at 63x magnification with the colocalization marker for GFAP (for astrocytes) shown as red (Alexa Fluor 594). The primary rhAb is shown as green (Alexa Fluor 488) and nuclei are counterstained blue (DAPI). The images are shown as independent red and green channels above the overlay including DAPI. Mouse

brain tissue IFC are shown for each rhAb titration: 1 μg (A), 800 ng (B), 600 ng (C), and 400 ng (D). Green ovals are drawn to highlight areas of faint rhAb staining independent of GFAP. Data are representative of three coronal sections per rhAb. Scale bar represents 10μm.

Figure 6-11. ***IFC of dual-cell targeting WR10 ($TM_{CIS}4$) rhAb titrations on mouse brain.*** Confocal images are shown at 63x magnification with the colocalization marker for GFAP (for astrocytes) shown as red (Alexa Fluor 594). The primary rhAb is shown as green (Alexa Fluor 488) and nuclei are counterstained blue (DAPI). The images are shown as independent red and green channels above the overlay including DAPI. Mouse brain tissue IFC are shown for each rhAb titration: 1 μg (A), 800 ng (B), 600 ng (C), and 400 ng (D). Data are representative of three coronal sections per rhAb. Scale bar represents 10μm.

Figure 6-12. ***IFC of dual-cell targeting AJL07 ($ON_{CIS}3$) rhAb titrations on mouse brain.*** Confocal images are shown at 63x magnification with the colocalization marker for GFAP (for astrocytes) shown as red (Alexa Fluor 594). The primary rhAb is shown as green (Alexa Fluor 488) and nuclei are counterstained blue (DAPI). The images are shown as independent red and green channels above the overlay including DAPI. Mouse brain tissue IFC are shown for each rhAb titration: 1 μg (A), 800 ng (B), 600 ng (C), and 400 ng (D). Yellow ovals are drawn to highlight areas of faint rhAb colocalization with GFAP. Data are representative of three coronal sections per rhAb. Scale bar represents 10μm.

Figure 6-13. ***IFC of dual-cell targeting AJL19 ($TM_{CIS}6$) rhAb titrations on mouse brain.*** Confocal images are shown at 63x magnification with the colocalization marker for GFAP (for astrocytes) shown as red (Alexa Fluor 594). The primary rhAb is shown as green (Alexa Fluor 488) and nuclei are counterstained blue (DAPI). The images are shown as independent red and green channels above the overlay including DAPI. Mouse brain tissue IFC are shown for each rhAb titration: 1 μg (A), 800 ng (B,E), 600 ng (C,F), and 400 ng (D,G). Yellow ovals are drawn to highlight areas of faint rhAb colocalization with GFAP. Green ovals are drawn to highlight areas of faint rhAb staining independent of GFAP. Data are representative of three coronal sections per rhAb. Scale bar represents 10μm.

Figure 6-14. ***IFC of 7 neuronal nuclei targeting AGS-enriched rhAbs targeting colocalization with lamin A on EAE mouse brain.*** Confocal images are shown at 126x magnification with the colocalization marker for lamin-A (for nuclear membrane) shown as red (Alexa Fluor 594). The primary rhAb is shown as green (Alexa Fluor 488) and nuclei are counterstained blue (DAPI). The images are shown as independent red and green channels above the overlay including DAPI. EAE mouse brain tissue IFC are shown for each rhAb labeled above the column: AJL02 (CDMS1) (A), AJL03 (CDMS1) (B), AJL10 ($ON_{CIS}2$) (C), AJL07 ($ON_{CIS}3$) (D), WR10 ($TM_{CIS}4$) (E), AJL15 ($TM_{CIS}5$) (F), and AJL19 ($TM_{CIS}6$) (G). Data are representative of three coronal sections per rhAb. Scale bar represents 10μm.

Figure 6-1

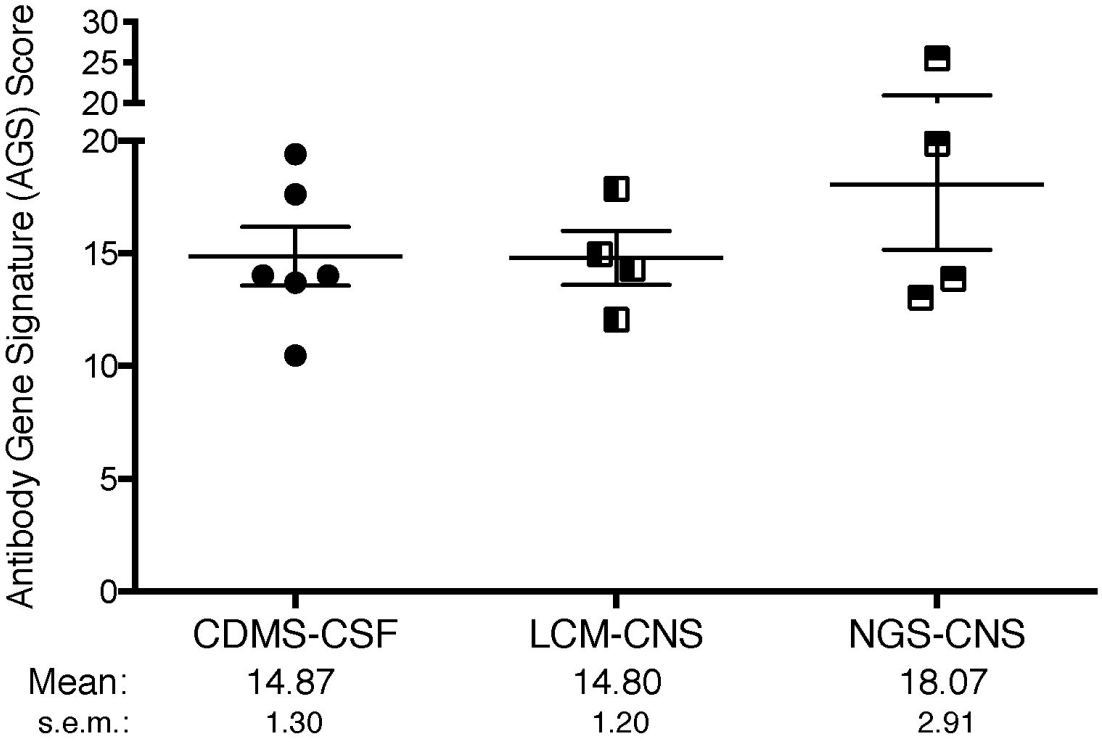
Antibody Gene Signature (AGS) Score
30
25
20
20
15
10
5
0
CDMS-CSF
LCM-CNS
NGS-CNS
Mean:
14.87
14.80
18.07
s.e.m.:
1.30
1.20
2.91

Figure 6-2

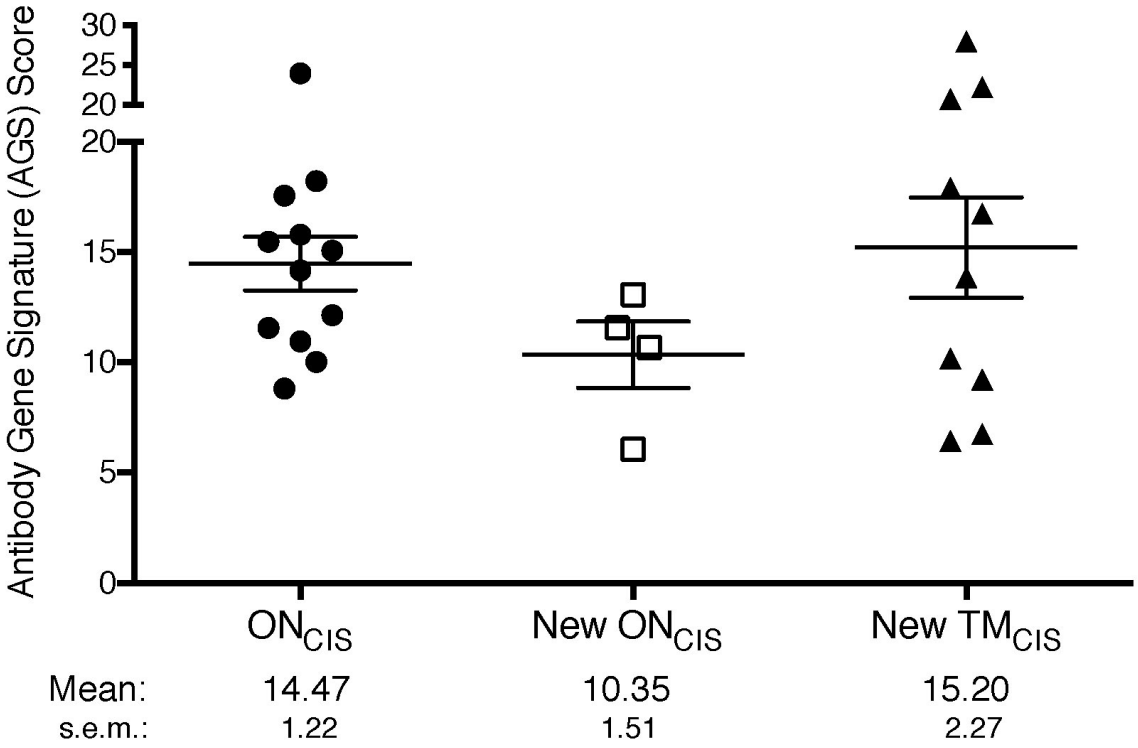
Antibody Gene Signature (AGS) Score
30
25
20
20
15
10
5
0
ON CIS
New ON CIS
New TM CIS
Mean:
14.47
10.35
15.20
s.e.m.:
1.22
1.51
2.27

Figure 6-3

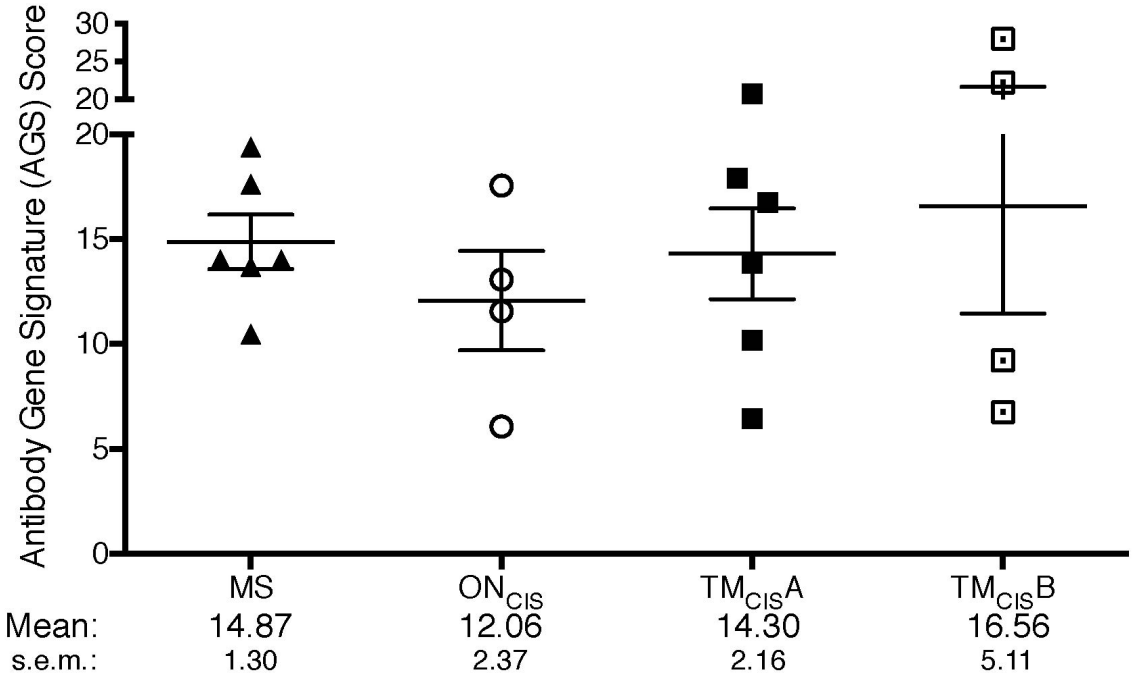
Antibody Gene Signature (AGS) Score
30
25
20
20
15
10
5
0
MS
ON CIS
TM CIS A
TM CIS B
Mean:
14.87
12.06
14.30
16.56
s.e.m.:
1.30
2.37
2.16
5.11

Figure 6-4

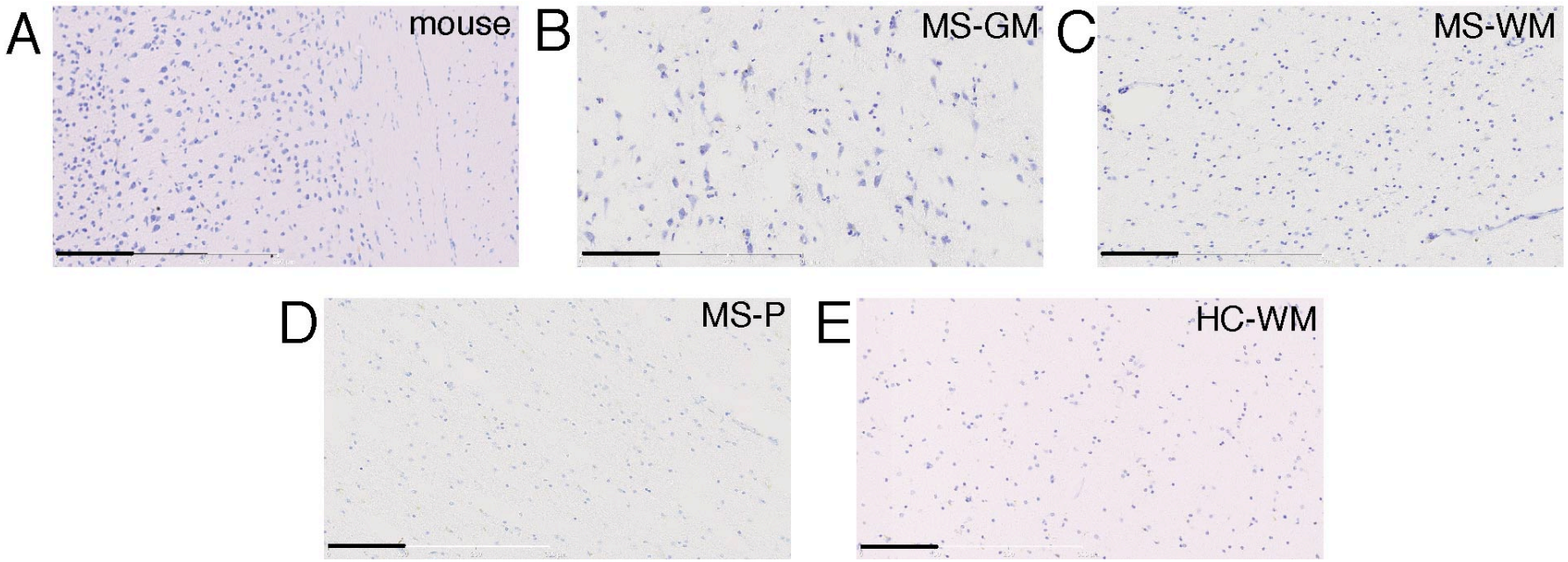

Figure 6-5

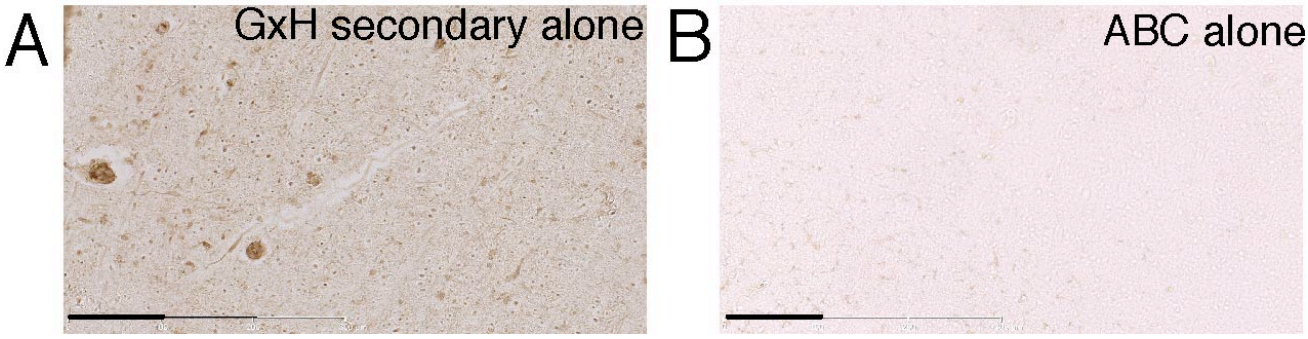

Figure 6-6

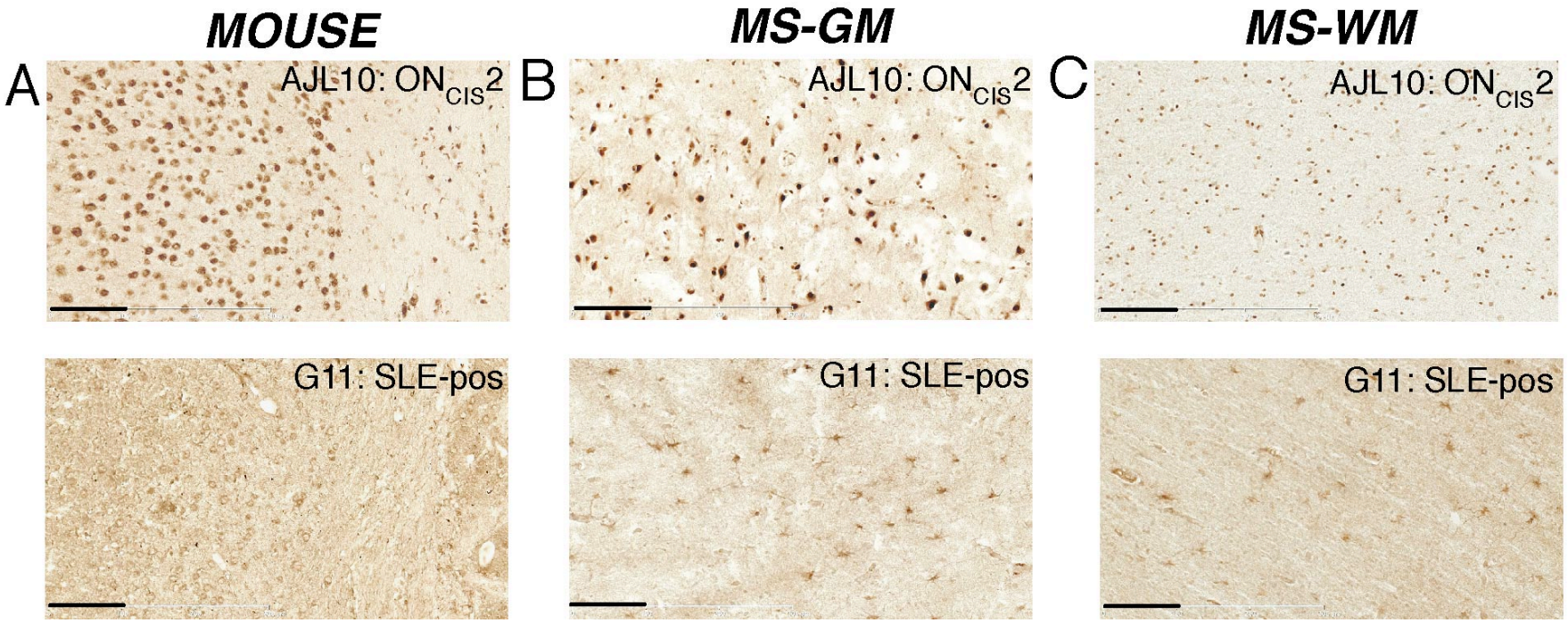
MOUSE
MS-GM
MS-WM
A
B
C
AJL10: ON$_{CIS}$2
AJL10: ON$_{CIS}$2
AJL10: ON$_{CIS}$2
G11: SLE-pos
G11: SLE-pos
G11: SLE-pos

Figure 6-7

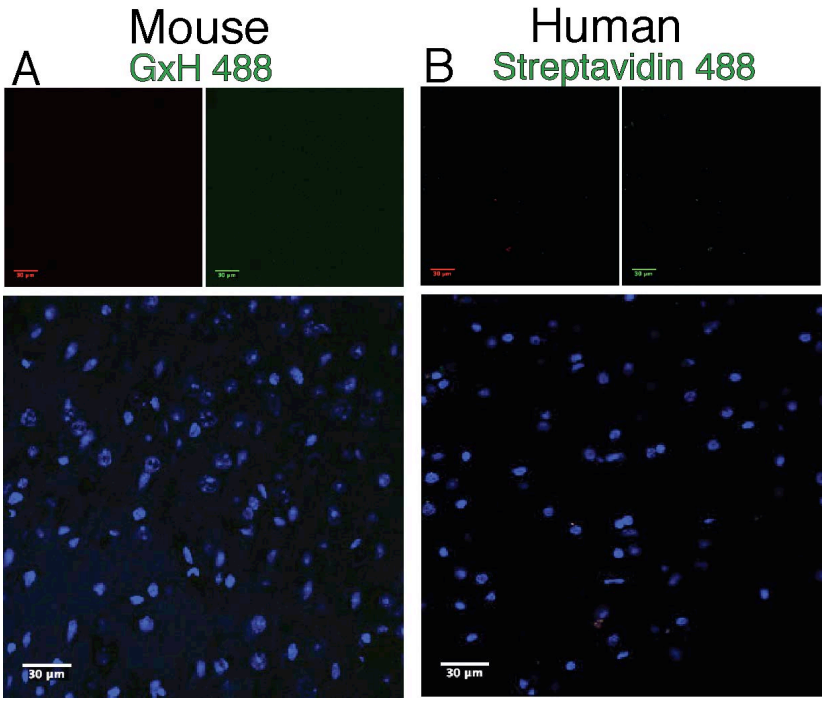

Figure 6-8

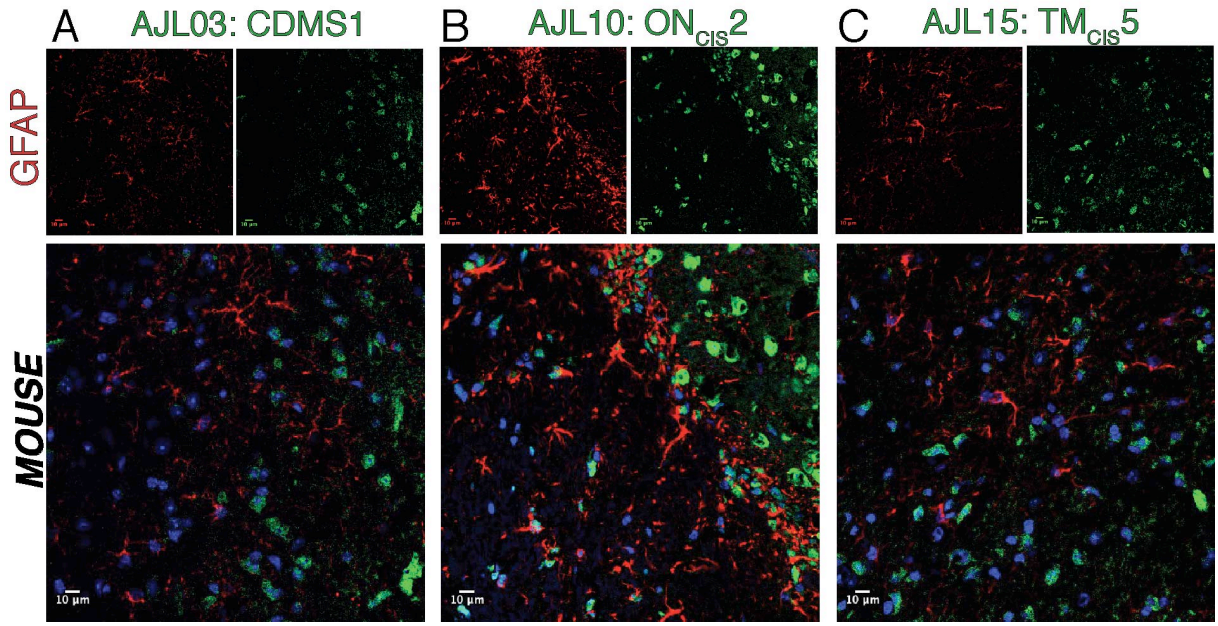
A
AJL03: CDMS1
B
AJL10: ON$_{CIS}$2
C
AJL15: TM$_{CIS}$5
GFAP
MOUSE
10 µm
10 µm
10 µm

Figure 6-9

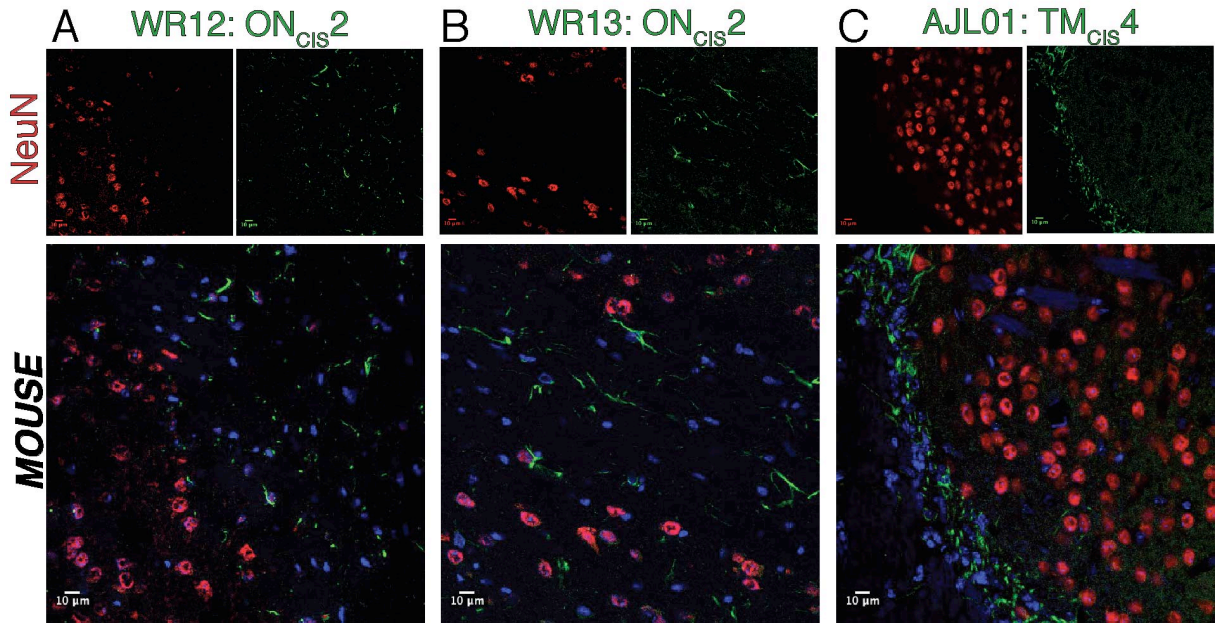
A
WR12: ON$_{CIS}$2
B
WR13: ON$_{CIS}$2
C
AJL01: TM$_{CIS}$4
NeuN
MOUSE
10 µm
10 µm
10 µm

Figure 6-10

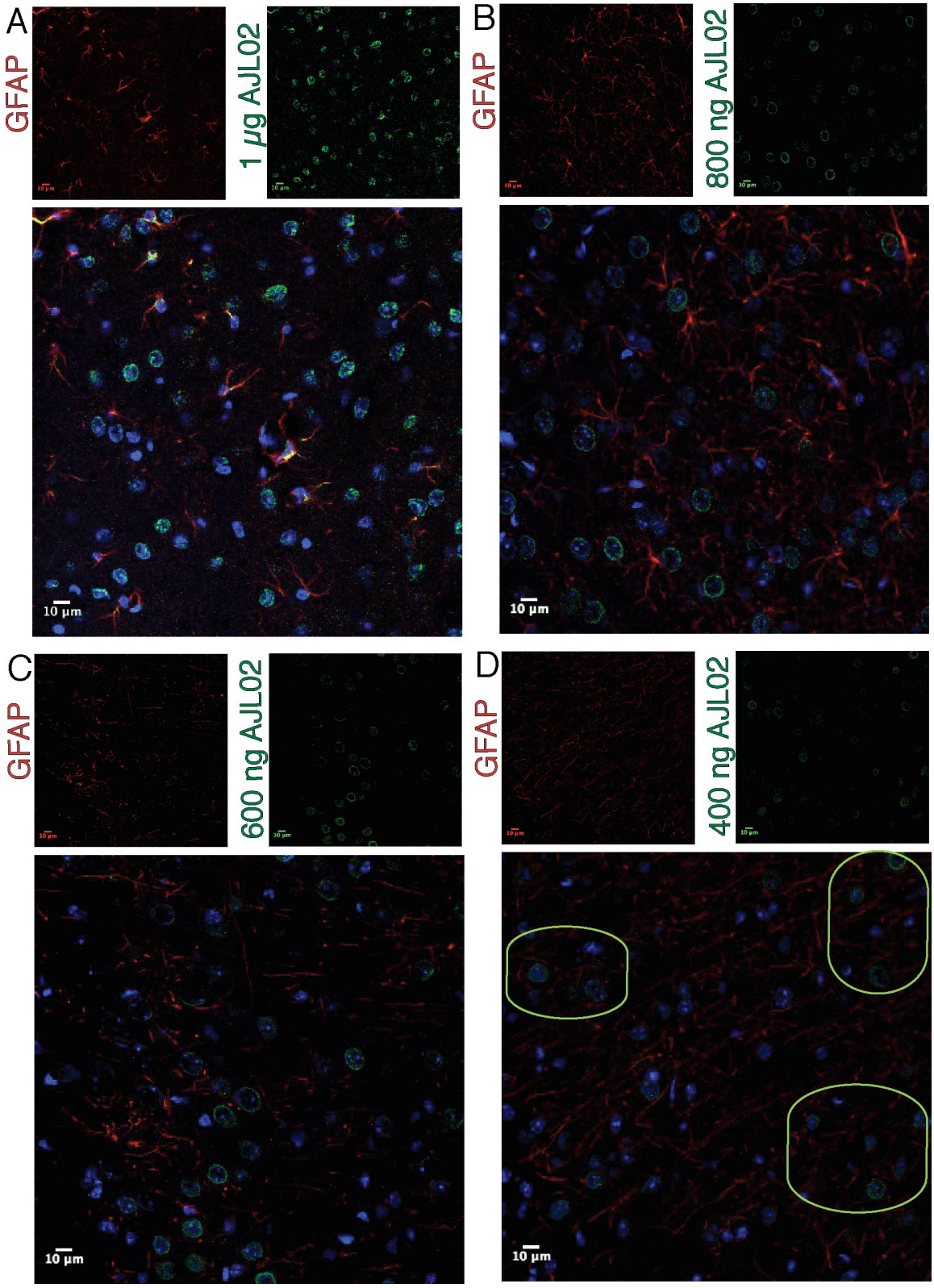
A
GFAP
1 μg AJL02
B
GFAP
800 ng AJL02
10 μm
10 μm
C
GFAP
600 ng AJL02
D
GFAP
400 ng AJL02
10 μm
10 μm

Figure 6-11

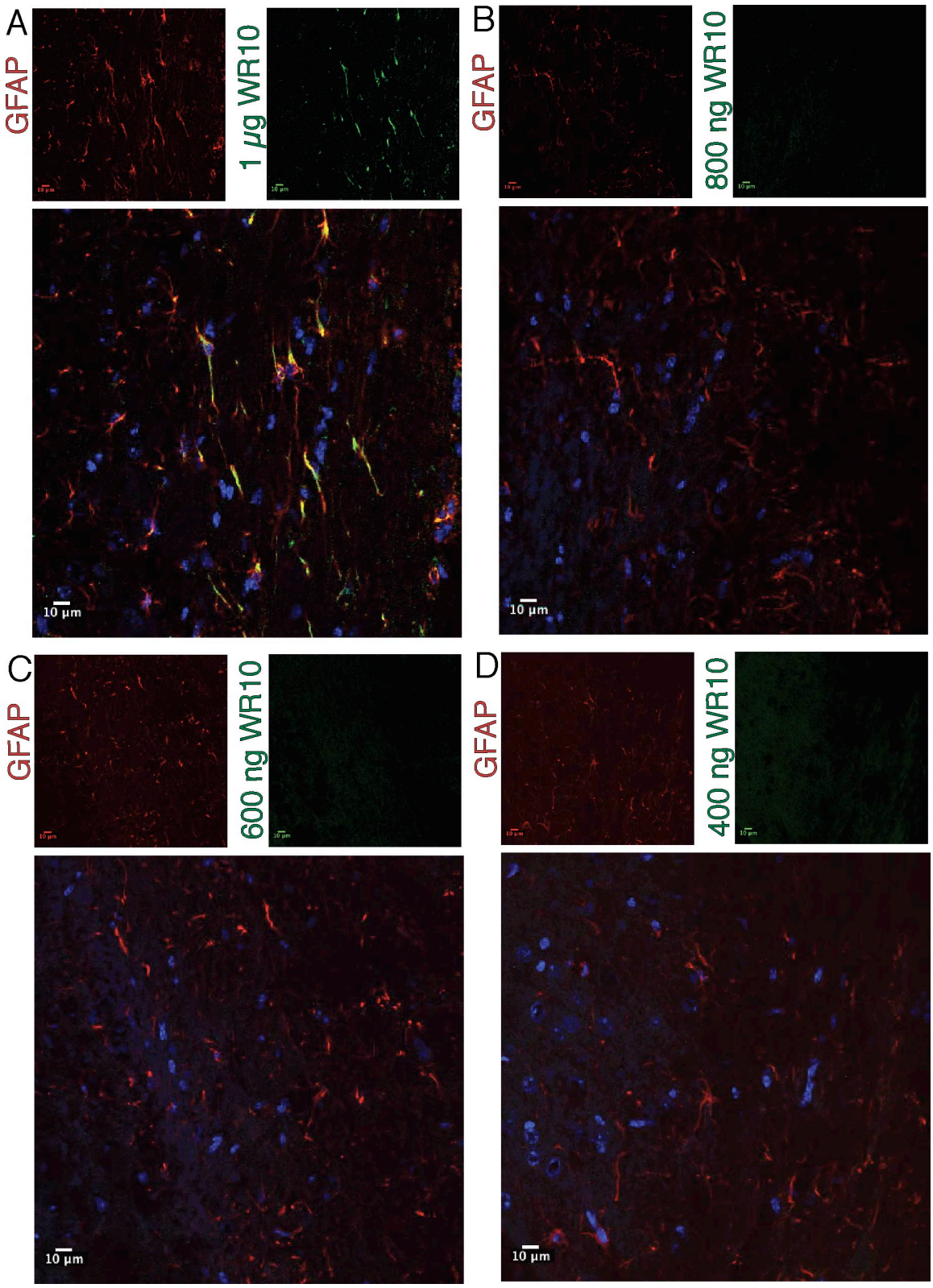
A
GFAP
1 μg WR10
10 μm
B
GFAP
800 ng WR10
10 μm
C
GFAP
600 ng WR10
10 μm
D
GFAP
400 ng WR10
10 μm

Figure 6-12

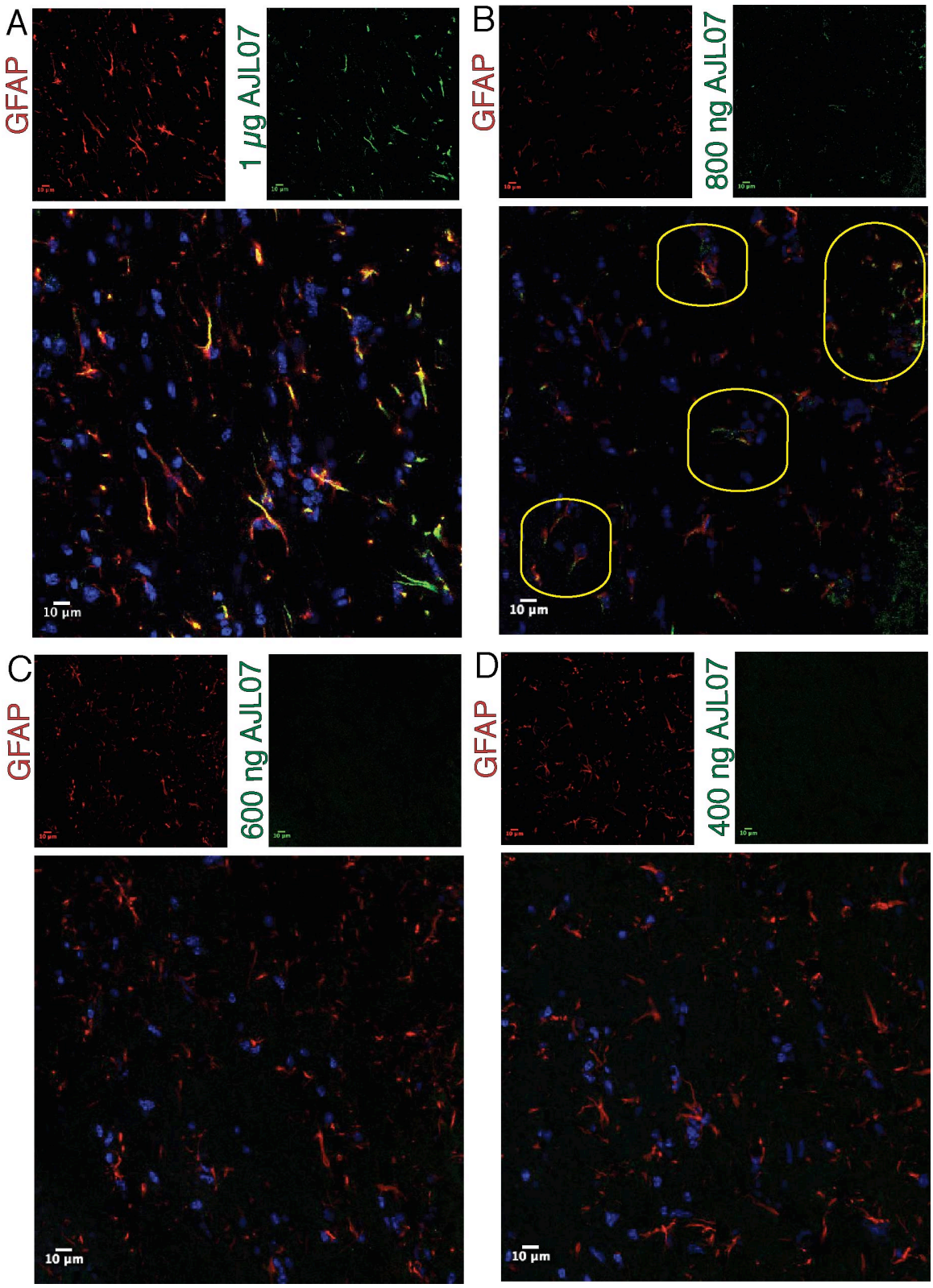
A
GFAP
1 μg AJL07
10 μm
B
GFAP
800 ng AJL07
10 μm
C
GFAP
600 ng AJL07
10 μm
D
GFAP
400 ng AJL07
10 μm

Figure 6-13

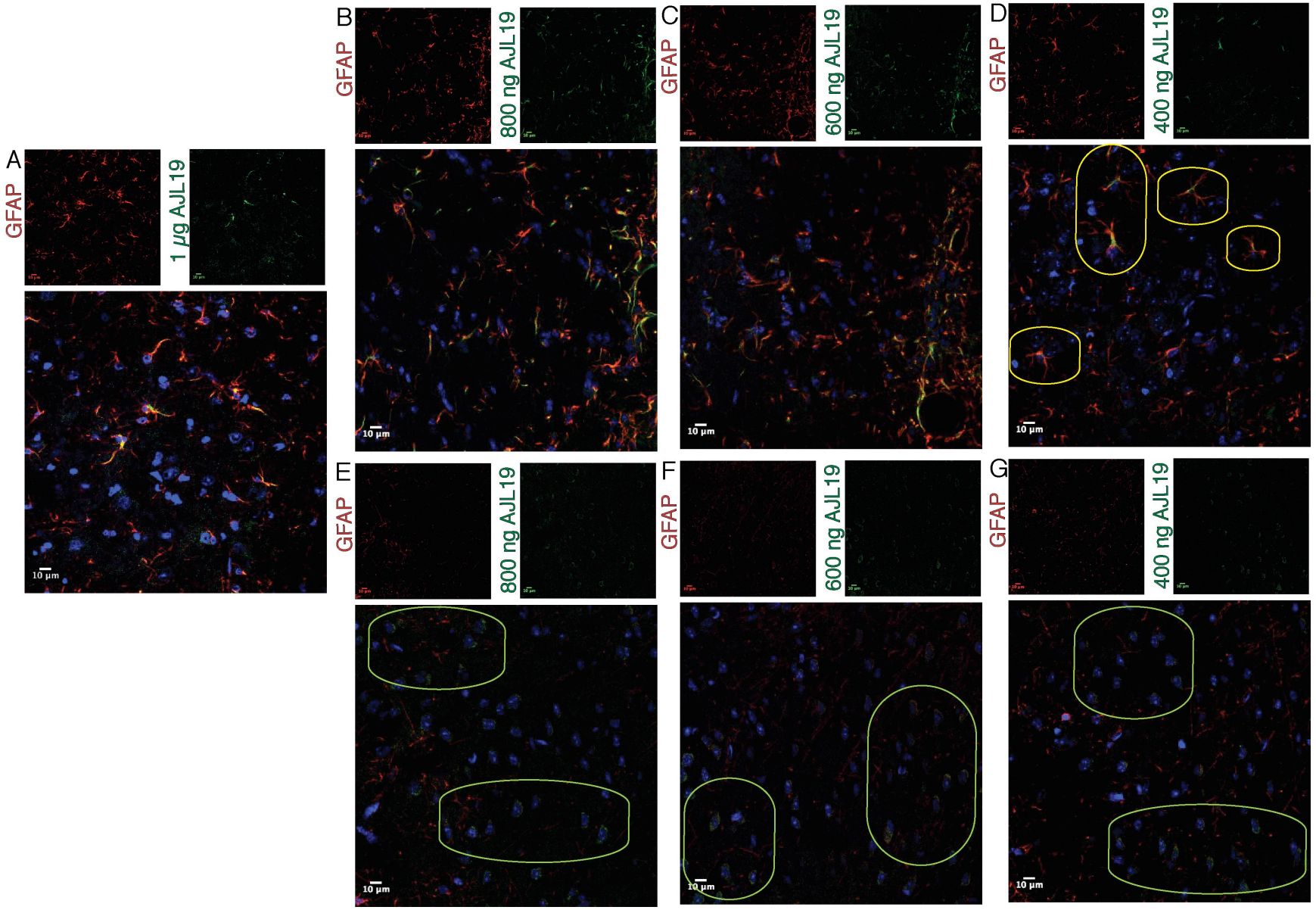
A
GFAP
1 μg AJL19
10 μm
B
GFAP
800 ng AJL19
10 μm
C
GFAP
600 ng AJL19
10 μm
D
GFAP
400 ng AJL19
10 μm
E
GFAP
800 ng AJL19
10 μm
F
GFAP
600 ng AJL19
10 μm
G
GFAP
400 ng AJL19
10 μm

Figure 6-14

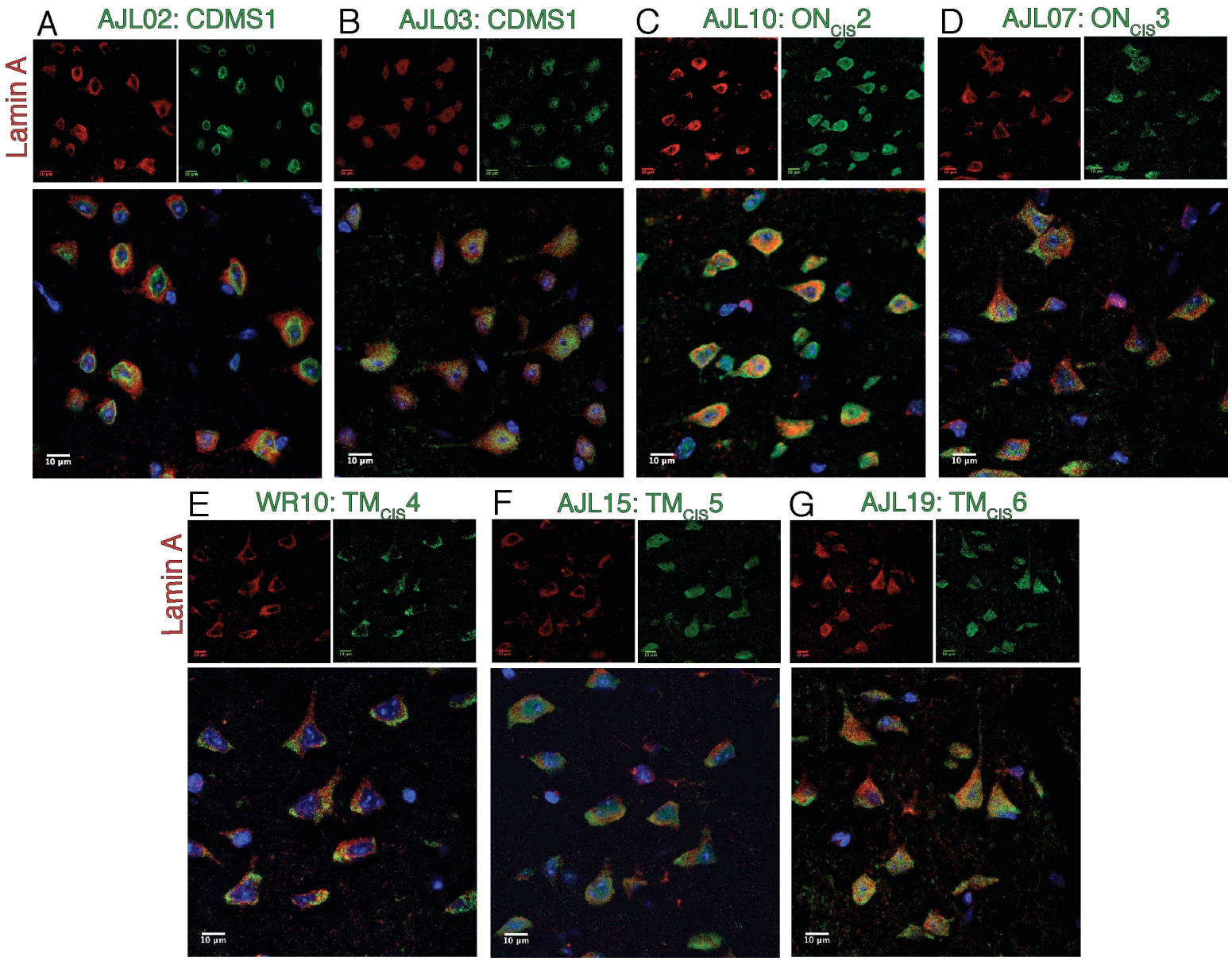
A
AJL02: CDMS1
B
AJL03: CDMS1
C
AJL10: ONCIS2
D
AJL07: ONCIS3
Lamin A
10 µm
E
WR10: TMCIS4
F
AJL15: TMCIS5
G
AJL19: TMCIS6
Lamin A
10 µm

TABLES FOR CHAPTER SIX: UNPUBLISHED RESULTS

Table 6-1. CNS specimen details and AGS scores for NGS-CNS[1] samples

Subject	MS course	Anatomical location	AGS score	#V_H4 sequences with RM
MS-5	acute MS	Plaque	13.03	32
MS-6	RRMS	Plaque	13.87	163
MS-7	RRMS	NAWM	19.86	27
MS-8	acute MS	NAWM	25.51	14

Abbreviations: NGS-CNS: next generation sequencing CNS, RM: replacement mutation, n.a.: not available, RRMS: relapsing remitting MS, NAWM: normal appearing white matter

[1]NGS-CNS V_H sequences provided by Drs. Fire and Boyd

Table 6-2. New ON_{CIS} and TM_{CIS} patient details and AGS scores			
ON_{CIS}			
Patient	Age/gender	AGS score	#V_H4 sequences with RM
CIS348	34/F	13.07	41
CIS831	39/F	10.68	58
CIS426	30/M	11.56	5
CIS563	40/F	6.07	20
TM_{CIS}			
Patient	Age/gender	AGS score	#V_H4 sequences with RM
CIS431	27/F	17.90	14
CIS683	39/F	6.76	4
CIS287	45/F	6.43	5
CIS873	19/F	16.73	21
CIS335	34/F	10.17	57
CIS787	33/M	22.26	14
CIS834	57/F	13.84	22
CIS353	58/F	20.73	7
CIS527	43/F	27.98	5
CIS371	56/F	9.22	19
Abbreviations: $ON_{CIS:}$ clinically isolated syndrome optic neuritis, $TM_{CIS:}$ clinically isolated syndrome transverse myelitis, AGS: antibody gene signature			

Table 6-3. Summary of cellular targeting of the 4 dual-cell reactive rhAbs[1] incubated at titrations of lowering concentrations.			
rhAb	Amount on each brain	Astroctye targeting[2]	Neuronal nuclei targeting[3]
AJL02[4]	1 μg	+	+
	800 ng	-	+
	600 ng	-	+
	400 ng	-	+
AJL07[5]	1 μg	+	+
	800 ng	+	-
	600 ng	-	-
	400 ng	-	-
AJL19[6]	1 μg	+	+
	800 ng	+	+
	600 ng	+	+
	400 ng	+	+
WR10[7]	1 μg	+	+
	800 ng	-	-
	600 ng	-	-
	400 ng	-	-

[1] Dual-reactive rhAbs were those with staining that colocalized with NeuN and GFAP.
[2] Positive colocalization with GFAP shown as a "+"
[3] Positive staining around DAPI similar to previous NeuN colocalization experiments shown as a "+"
[4] Staining panels are shown for AJL02 in Figure 6-10
[5] Staining panels are shown for AJL07 in Figure 6-11
[6] Staining panels are shown for AJL19 in Figure 6-13
[7] Staining panels are shown for WR10 in Figure 6-12

CHAPTER SEVEN

DISCUSSION

The historical and more recent studies of Ig and altered B cell activity implicate involvement in MS pathology. Additionally, dysregulation is already evident in CIS patients suggesting that B cells and their antibodies may play a role in the initiating phases of the disease. All levels of B cell development and function involve binding of cognate antigen to the BCR. Thus, studies of the BCR can offer clues regarding the auto-antigen(s) associated with CNS damage or symptoms. Therefore, scientists have been pursuing research of the altered antibody genomics found in MS and CIS patients. Several groups, including our own, have demonstrated that CSF and CNS B cells are clonally expanded, mutated, and favor V_H4 gene usage. Our laboratory's discovery of a shared mutational pattern, the AGS, in the CSF of both MS and CIS patients suggests that disease-relevant antigen(s) in the CNS is driving them (Figure 7-1). Surveying B cells and antibodies within the CSF is relevant to CNS disease because there are shared B cell clones between the same MS patient's CSF and CNS (232), as well as between the meninges and CNS (234). Additionally, the most common form of MS lesion is characterized by deposition of antibodies and complement (6). Plasmapheresis treatment of patients harboring these lesions leads to improvement of symptoms (98, 99) suggesting that the antibodies in the CSF can deposit within the CNS tissue.

The work presented in this thesis demonstrates that the AGS is found in CSF derived B cells from both presentations of CIS: ON_{CIS} and $TM_{CIS.}$ Not only is this AGS found in the CSF, it is also found at the site of MS disease pathology within the CNS tissue. Furthermore, the first assessments of the biological relevance of the AGS shows

that this shared mutation signature imparts binding to GM neuronal nuclei and astrocytes. Collectively, these data could lead to identifying a greater portion of patients at high risk for developing MS and those that may benefit from treatments to preserve GM integrity.

We found similar AGS enrichment from different tissue sources (CSF and CNS), different laboratories, and different PCR methodologies (single cell Sanger sequencing, LCM, and NGS). This lends confidence to the presence of this MS disease signature discovered in our laboratory, and lends support to its utilization as a potential diagnostic in a third party clinical laboratory setting.

A surprising finding from this current CNS study is that B cells present in NAWM are also enriched for the AGS. It is accepted that there are global CNS inflammation and cellular stress present in MS patients that is not readily detected via traditional MRI or IHC methodologies (9, 370, 379, 380). While antibody is present at a higher level in lesions, adaptive cellular immune responses can be equally detected in both lesions and NAWM (379, 381). This, in conjunction with our finding of AGS enrichment in both lesions and NAWM, implies that B cells may play an early or initiating role in CNS damage apart from perpetuating already present tissue damage. The presence of a strong AGS score in MS CNS tissue antibody repertoires corroborates the hypothesis that B cells in the CSF are also present at the site of the MS disease process. This also supports the clinical relevance of testing and evaluating B cell genomics and phenotypes from the CSF, as it is reflective of what is present in the CNS pool. AGS enrichment both in the CSF and CNS B cells supports the notion that a restricted population of B cells is involved in the biological etiology of the MS disease process.

The initial study of the predictive ability of the AGS on conversion from CIS to MS was done on a cohort of ON_{CIS} patients from a collaborator to blind the laboratory to

the conversion data. Initially, we validated the presence of the AGS in ON_{CIS} patients recruited at UTSWMC and found there to be no difference between these and the original cohort from our collaborator. This reproducibility lends further confidence to the presence of AGS enrichment in the CSF of ON_{CIS} patients. Despite having different lesion locations and prognoses, the TM_{CIS} patients also displayed a similar enrichment of AGS in the CSF. Regardless of initial CIS presentation, patients at a high risk to convert to CDMS harbor an enrichment of AGS B cells within their CSF repertoire. This broadens the utility of the AGS as a diagnostic since it could potentially be applied to both ON_{CIS} and TM_{CIS} patients. These data also suggest that there are shared B cell selective pressures present in both ON_{CIS} and TM_{CIS} patients. It remains unknown why the initial anatomical locations vary but they share generalized CNS targeting of damage. Both patient groups are at higher risk to convert if they have additional abnormal MRI scans of the brain (63). Since all these patients are at high risk for MS, this shared B cell dysregulation implicates a shared underlying pathoetiology among the patients.

We found that a subset of TM_{CIS} patients, stratified as the TM_{CIS}A patient subgroup, had a unique expansion of $CD27^{high}$ plasmablasts in the CSF. The majority of these TM_{CIS}A patients also demonstrated an expansion of plasmablasts in the periphery, which was not seen in either compartment in the ON_{CIS} cohort. The frequency of $CD27^{high}$ plasmablasts is also elevated in several autoimmune diseases and occurs in the diseased tissues where the putative auto-antigens are present (142, 198, 203, 204). Clinical evidence of plasmablast activity has been found in patients with NMO (186), RA (198, 361), and SLE (192, 353, 354, 362) who receive the B cell depleting agent rituximab and are more likely to relapse early if their memory B cells, and more importantly their $CD27^{high}$ plasmablasts return earlier implicating the role of these cells in

the re-emergence of symptoms in autoimmune diseases. Since TM_{CIS} patients typically have a worse prognosis than ON_{CIS} patients (58, 60), this expansion of plasmablasts may contribute to this enhanced disease activity.

Treatment with natalizumab, which blocks the entry of cells into the CNS, was effective in MS patients if they had lower levels of CSF plasmablasts before treatment and maintained low levels post-treatment (177). Other studies have found that during a MS relapse, memory B cells are readily recruited to the CSF with the decrease of these cells in the periphery (119, 120), possibly due the increase in CXCL13, the B cell attractant chemokine, observed in active MS and CIS patients (136, 382) Another factor involved may be due to migration through a very late antigen 4 (VLA-4) dependent mechanism, since memory B cells (116) and plasmablasts (116, 174) express high levels of VLA-4. Trafficking of B cells may be an early disease step, as CIS patients have higher levels of VLA-4 on their transitional B cells than is observed in MS patients (363). Such an initial step would enable B cells to enter the CNS, encounter their auto-antigen and undergo germinal center-like reactions as evidenced by SHM accumulation and altered selection of V_H genes. This matches the current conceptualization of MS pathogenesis with the migration of brain-reactive B cells from the periphery into the brain tissue via the surrounding CSF (9, 10, 125, 129, 346-348). While we do not yet know the prevalence of the AGS in the periphery, work is currently being done using NGS technology in order to sample a large amount of the repertoire in contrast to the single-cell methodology. However, we have shown early B cell disturbances in the periphery of a subset of TM_{CIS} patients that harbor heavily mutated $V_H4^+J_H6^+$ plasmablasts. A proposed model of the cellular movements is shown in Figure 7-2.

Even though increases in plasmablasts have been correlated with clinical markers of disease in other autoimmune diseases, we found no significant correlation in either the CSF or PB compartments with CSF immunoglobulin synthesis or CSF Ig index. However, we found that the percentage of $CD27^{high}$ plasmablasts in the periphery of the $TM_{CIS}A$ group increased the longer the patient had been untreated. This may reflect an accumulation of chronically activated B cells, which develop into plasmablasts in a state of extended neuroinflammation. Presumably, lack of treatment can prolong the immune response time to the triggering antigen(s), and the resulting potent inflammatory milieu may promote aberrant cell activation. This correlation was not seen in the CSF compartment, possibly due to plasmablasts entering niches in the inflamed tissue (364) or exiting back into the periphery over time after expanding in the CSF. Plasmablasts are quite motile (364), but their travel direction in the TM_{CIS} patients is unknown from this current study. The ability to find this signature of expanded $CD27^{high}$ B cells may help diagnostically to indentify TM_{CIS} with a worse prognostic risk, or potentially be used as a biomarker for response to B cell depleting agents or to block cellular entry into the CNS using natalizumab. At this current point, we do not know the impact of presenting with the $TM_{CIS}A$ phenotype on the EDSS once a patient converts to CDMS.

Aberrant selection of V_H4^+ B cells in the CSF measured by elevated levels of mutation accumulation was also observed at the early stages of disease represented by the ON_{CIS}, $TM_{CIS}A$ and $TM_{CIS}B$ patient subgroups. SHM accumulation in peripheral V_H4^+ plasmablasts was extensive in comparison to V_H3^+ plasmablasts in the $TM_{CIS}A$ patients. Furthermore, the V_H4^+ plasmablasts using J_H6 segments accounted for this depth of SHM accumulation. V_H1^+ plasmablasts from the same $TM_{CIS}A$ patients did not demonstrate this level of selection. Taken together, these data suggest that within the peripheral

$CD27^{high}$ plasmablast pool of $TM_{CIS}A$ patients, there is a subgroup of V_H4^+ plasmablasts enriched for J_H6 segment use that are undergoing affinity maturation at a faster rate than their V_H4^+ counterparts that utilize J_H4 segments. Interestingly, the memory B cells from the same $TM_{CIS}A$ patients did not display evidence of receptor editing in the V_H4^+ B cells, but rather in the $V_H1^+J_H6^+$ B cells. This suggests that the $V_H4^+J_H6^+$ B cells could be chronically stimulated and develop into plasmablasts compared to their V_H1^+ counterparts. Therefore it would be informative to the disease pathoetiology to identify the driving auto-antigens of these peripheral $TM_{CIS}A$ plasmablasts.

The estimated percentage of edited V_H rearrangements increases in patients with autoimmune diseases, such as RA (30%), Sjogren's syndrome (22%), and anti-dsDNA encoding antibodies from SLE (21%) (383). We were particularly interested in whether V_H4^+ B cells from the diseased PB and CSF repertoires demonstrated characteristics of receptor editing since V_H4 genes more likely to receptor edit than V_H3^+ B cells (384). This in combination with evidence that V_H replacements can occur during GC reactions in association with active SHM (366, 385, 386) suggests that antigen driven (mutated) V_H4 genes in MS could show signs of V_H replacements. Interestingly, in addition to the $V_H4^+J_H6^+$ peripheral plasmablasts, there is also evidence of V_H receptor editing in V_H4^+ and V_H1^+ B cell pools from the periphery of established MS patients. Peripheral B cells from MS patients had a skewed ratio of J_H4:J_H6 in both the V_H4^+ and V_H1^+ B cell pools and accumulation of SHM in $V_H1^+J_H6^+$ B cells. The $V_H4^+J_H6^+$ B cells from MSPB lack the intensity of SHM selection and receptor editing demonstrated only in the plasmablasts from $TM_{CIS}A$ patients. Collectively, only the PB B cells display significant evidence of V_H receptor editing compared to CSF B cells. This suggests that the signals for editing are still present in the periphery of these patients, but this mechanism is lost in the

diseased CSF compartment. In fact, earlier evidence from our laboratory suggests that despite SHM and intraclonal diversity, some of the CSF B cells are not undergoing typical GC selection as excepted from a B cell emerging from a GC in the periphery (214, 220). In MS and CIS CSF, the accumulation of negative residues in the CDR3s may reflect selection in targeting to positively charged antigens. In fact, one of the putative auto-antigens classically associated with MS is MBP, which is positively charged. The available driving antigens in the GC may be different in the MS periphery versus the CSF, which is localized around the site of pathology. This could explain why the B cells in the PB do not strongly select against positive charges after GC reactions and editing whereas the B cells in the CSF maintain a negative charge.

Determining the target specificity of AGS-enriched antibodies from CSF B cells of MS patients (early CIS and established CDMS) is the first step towards dissecting the potential role of AGS-enriched antibodies in the pathogenesis of MS. Regardless of initial presentation of disease (ON_{CIS} vs TM_{CIS}), early or established disease (CIS vs CDMS), these rhAbs are recognizing neuronal nuclei and/or astrocytes in both mouse and human GM brain tissue. The rhAbs also recognized cellular targets in two models of mouse CNS inflammation, stroke and EAE, suggesting that the GM antigens were available in various states of neuroinflammation. This AGS is present at all initial disease presentations and durations indicating that the stage of disease does not significantly alter the cellular targeting of the AGS-enriched B cell repertoire. Significant immune system activation antecedes the initial clinical presentation of disease and complements the finding that rhAbs cloned from ON_{CIS} and TM_{CIS} patients already display recognition to brain targets. Further analyses of these rhAbs could offer the field what the early auto-

antigens are in the CIS stages and if these expand or are maintained throughout the disease course.

Surprisingly the rhAbs showed targeting to cells in the cortex and midbrain with only mild/rare staining along the corpus callosum in mouse tissue. This targeting to GM, which has gained appreciation for involvement in CDMS symptoms and disease progression (31, 32, 36, 367), may contribute to MS damage. WM lesions are readily detected with gadolinium enhancement on MRI and luxol fast blue staining of postmortem tissue, whereas GM lesions are more difficult to detect via traditional MRI and IHC, explaining why GM pathology was historically under-recognized (368). Cortical lesions are correlated with MS disease severity and progression as opposed to the more easily detected white matter lesions (32, 36, 367). Progressive GM loss over time occurs at both CIS and MS stages (35, 37, 38, 387), which suggest that the underlying pathology responsible for the loss is not restricted to later disease stages.

In addition to the genomic evaluation of receptor editing, we also determined the efficacy of the editing on the targeting of 5 pairs of edited AGS-enriched rhAbs. Receptor editing in human B cell repertoires has been studied at the antibody sequence level from naturally auto-reactive emerging B cells (72). What is demonstrated in this present study is an example of a partial reduction in targeting between WR01 and WR02 and a complete abrogation of brain tissue staining between WR10 and WR11. WR01 displayed a stronger DAB intensity than its edited heavy chain member WR02, which corroborates previous findings in the laboratory using the same variable regions in a Fab construct for IPs with MBP followed by western blotting (255). WR10 and its light chain allele replacement counterpart WR11 displayed strikingly different staining patterns. WR10 displayed clear binding to tissue via DAB and also with colocalization to both astrocytes

and neurons visualized via IFC. WR11 did not stain brain via DAB suggesting that the usage of the second light chain allele eliminated auto-reactivity to brain tissue of this B cell clone. This successful editing was not a common feature in the AGS-enriched rhAb panel. WR12 and WR13 displayed the same reactivity to brain tissue in IHC and IFC experiments. This could be that the light chain editing was not as drastic as the light chain replacement between WR10 and WR11. Rather than using another available light chain allele to completely replace the light chain like in WR10/WR11, WR12 is closely related to WR13 with only an edit to a downstream Jκ gene in WR12. Therefore, there was not enough change to modify the targeting of this pair. AJ07/AJL13 and WR08/WR09 are also light chain receptor edited pairs with out any obvious changes in their antibody targeting.

Seven of the AGS-enriched rhAbs displayed targeting of neuronal nuclei. Targeting of neurons fits well with findings of neuronal loss and degeneration present in MS. Proton magnetic resonance spectroscopy (MRS) measurement of N-acetyl aspartate (NAA), a neuronal marker, is significantly reduced in MS CNS (369), especially as patients progress through disease stages and those with an EDSS over 3 (370, 388, 389), supporting that a loss of neurons is associated with progressive neurodegeneration. Additionally an in vitro experiment found that the level of apoptosis in a neuronal culture incubated with MS CSF was correlated with lesion load (280). Neurofilaments comprise the axonal/neuronal cytoskeleton and have also been identified as auto-antigen targets from MS CSF (288, 291), and titers are correlated with atrophy, axonal damage, as well as clinical disability (289, 290). Immunizing mice with neurofilament induces GM damage as well as deposition of IgG within neuronal cell bodies and axons (293), highlighting the ability of an intracellular neuronal target to elicit disease. Additionally,

the myelin sheaths contained degenerating or dead axons (4) supporting the notion that the classical demyelination seen in MS can also occur secondary to axonal and neuronal damage. Collectively these findings in conjunction with the rhAb targeting suggest that neuronal preservation should be a clinical focus starting at the CIS stage to help patients preserve cognitive functions and keep the EDSS low.

Further characterization of the 7 rhAbs that displayed neuronal nuclei targeting was conducted using lamin A as a marker for the nuclear membrane. Several patterns of nuclear staining were observed as opposed to a singular uniform pattern. The patterns ranged from edging the exterior, overlapping the entire membrane, or ringing the interior. These varied patterns suggest that even though all these AGS-enriched rhAbs bind to neuronal nuclei, they may recognize different targets. From these IFC experiments, it is not known whether the rhAbs are polyreactive to multiple cell types in the brain or whether they are recognizing the same antigen(s) present in both neurons and astrocytes. Therefore, titration experiments on the 4 dual-cell targeting rhAbs were performed to identify if there was a preferential cellular target for the rhAbs. These titrations demonstrated that some rhAbs while being dual-cell targeting at higher concentrations lost some binding at lower concentrations. While the AGS-enriched rhAbs shared a targeting for the two major CNS cellular types, this suggests that their recognition is more complex than a single targeted antigen.

The integrity of the BBB is maintained by astrocytes and could be disrupted by rhAbs targeting them for damage or altering their functionality. It is well accepted that the BBB is compromised in CIS and MS patients (18), and any damage that perpetuates this could allow for further influx of inflammatory cells and mediators into the already inflamed CNS. Brain targeting antibodies can be detected in sera from healthy humans

(371) and could gain access to the CNS once the BBB is compromised. Seven of the AGS-enriched rhAbs displayed targeting to astrocytes. The binding of three rhAbs (those that only bound to astrocytes) in human and mouse GM clearly shows that these rhAbs can bind to astrocytes by colocalizing with GFAP. IFC on MS-GM showed rhAbs targeting architecture surrounding vessels, which includes astrocyte endfeet as well as endothelial cells, and could contribute to MS pathology by disturbing the BBB. Serum IgG from active MS demonstrates recognition of brain microvascular endothelial cells, which also correlated with BBB disruption (315, 317). The intracellular astrocyte protein contactin-2/TAG-1 was identified as an auto-antigen recognized by MS CSF antibodies and the induced disease in mice exhibited inflammation in both WM and GM regions (299, 390). The difference in appearance of GFAP positive astrocyte immunostaining between mouse and human brain in this study could be due to the planer orientation of the sectioning with the mouse coronal sections having abundant processes and rare astrocytes cell bodies and the human GM having more immunostained cell bodies and rarer processes (372). Another critical role for astrocytes is to support remyelination of lesions by providing support and signals to oligodendrocyte precursor cells (303-305), which could potentially be hindered by antibody targeting. In fact, failure to remyelinate lesions is a feature of progression in CDMS (373).

It is unclear from the current study if these antibodies are pathogenic since several of the rhAbs recognize antigen(s) in the nuclei of neurons rather than an easily accessible cell surface antigen. Furthermore, we do not know if the astrocyte binding rhAbs recognize an extracellular or intracellular target. A proposed model of the effects of rhAb binding to either cell type is shown in Figure 7-3. Intracellular targets are associated with many autoimmune diseases, especially SLE and Sjogren's syndrome (391). Antibodies

targeting AQP4 on astrocytes contribute to NMO pathology and bind to extracellular targets (308), though more recently a group found that a majority of sera (377, 392) tested from NMO patients recognize intracellular portions of the molecule which overlap with the dominant TCR epitope (378). The B cells that recognize the intracellular portions could acquire and present this epitope to T cells and receive cognate help and cytokines to drive a concerted cellular and humoral immune response against this antigen. Recognition and immune responses towards both intracellular and extracellular antigens are present in various autoimmune diseases and is a shared feature with MS.

Identifying that a genomic marker shared by MS patients, the AGS, is present in a pool of antibodies with the ability to bind to brain targets could provide direction for novel therapeutic approaches. Additionally, it provides a tool for identifying relevant auto-antigens that has been and continues to be a difficult goal in the field. In evaluating the pool of antibodies with a shared MS genomic pattern, the driving auto-antigens could potentially offer novel future hypotheses for the pathology of disease and CNS damage. Since this GM targeting occurs at the first stage of disease and continues onto CDMS, potential novel treatment targets could be assessed with regards to neurological preservation. This corroborates findings that earlier damage contributes heavily to future prognosis and disability (28, 57, 64-67) and thus highlights the need for early and effective treatments to preserve CNS function. Loss of neurons and axons is associated with irreparable damage and once a threshold of damage is reached, these patients' disease progresses. Treatments that preserve astrocyte functions to promote remyelination and reestablish a tight BBB could counteract antibody assaults to astrocytes and their endfeet. Maintaining neuronal and axonal integrity would be critical in preventing neurodegeneration. Now that we have identified that the diagnostic AGS could not only

identify CIS patients most likely to convert to CDMS but also that this pool of B cells may be contributing to GM damage, there is now a more focused therapeutic target(s) to study that may help patients early in the disease.

FIGURE LEGENDS FOR CHAPTER SEVEN: DISCUSSION

Figure 7-1. ***B cell responses against CNS antigens in MS patients and not healthy donors could lead to AGS enrichment.*** The AGS is a genomic marker of an antigen driven response and it is present in CNS and CSF B cells from MS patients and not the blood of healthy donors. This could be due to the aberrant B cell responses and activation to CNS-antigens in MS patients and the AGS may be a measure of this.

Figure 7-2. ***Proposed direction of B cell movement in CIS patients.*** Peripheral B cells responding to CNS antigens in the context of a GC undergo SHM and clonal expansion. Both memory B cells and plasmablasts are produced. Memory B cells can re-enter the GC and undergo further SHM, produce plasmablasts or migrate to the CNS. Plasmablasts could produce antibodies peripherally or migrate to the CNS and then produce antibodies. Migration to the CNS of both cell types is facilitated by VLA-4, CXCR5, and a permissive BBB. Once these cells are in the CSF, they could migrate to the meninges to initiate ectopic germinal centers, enter the parenchyma, or produce antibodies locally that then could enter the parenchyma. Alternatively they could also exit back into the periphery.

Figure 7-3. ***Potential pathological results from AGS-enriched antibodies targeting neuronal nuclei, astrocytes, or the BBB.*** Neuronal nuclei targeting could lead to a decrease in neuronal functionality potentially followed by cell death. Demyelination could occur by "inside-out" axonal degeneration leaving the myelin sheath empty to degrade. This could increase GM lesions that lead to cognitive symptoms and irreversible

neurodegeneration. Astrocyte targeting could lead to a decrease in astrocyte functionality potentially followed by cell death. This loss of astrocytes, or their functions, decreases the support for remyelination and increases the permeability of the BBB. This in turn could promote the migration of additional immune cells into the CNS that would further increase inflammation and damage.

Figure 7-1

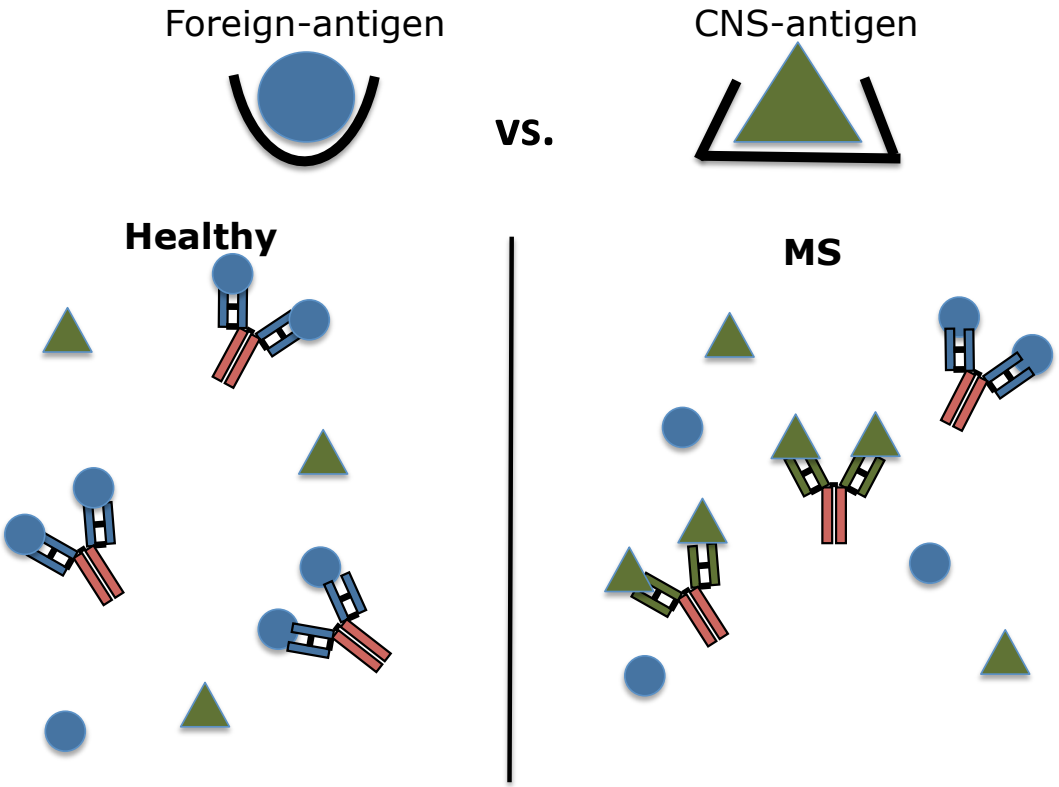

AGS-enriched B cells in MS:

-Responses to CNS antigens not present in HC
-Responses to CNS antigens in MS patients leads to accumulation of shared mutation hotspots
-If these antibodies or the B cells reach the CNS, they could initiate or perpetuate MS damage

Figure 7-2

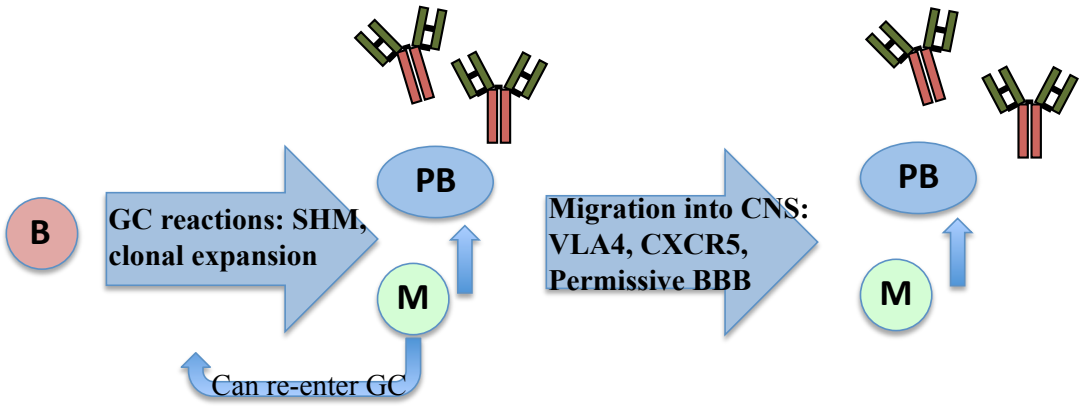

Periphery:

-Responses to CNS antigens driving SHM and clonal expansion
-Production of antigen-driven memory (M) and plasmablasts (B)
-Chronic activation and inflammation leads to more plasmablasts
-Production of antibodies
-Migration to CNS

CNS:

-Production of ectopic germinal centers
-Production of antigen-driven memory (M) and plasmablasts (B)
-Chronic activation and inflammation leads to more plasmablasts
-Production of antibodies
-Memory B cells and plasmablasts now centrally located an could induce damage

Figure 7-3

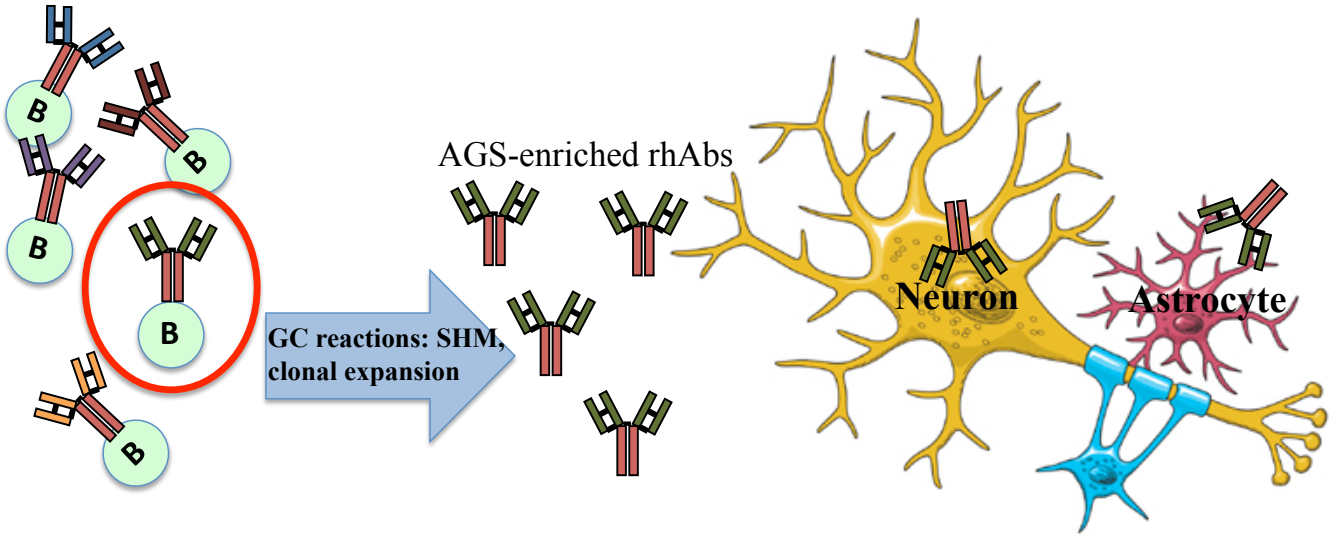

Neuronal nuclei targeting:

1)↓ Neuronal functionality
2)↑Neuronal death
3)↑"inside-out" axonal degeneration
4)↑GM lesions
5)↑Cognitive symptoms and irreversible neurodegeneration

Astrocyte & BBB targeting:

1)↓ Astrocyte functionality
2)↑Astrocyte death
3)↓ Astrocyte support for remyelination
4)↑BBB permeability
5)↑Migration of immune cells into CNS
6)↑Inflammation and damage

CNS cell image modified from http://blog.targethealth.com/?m=201001

CHAPTER EIGHT

FUTURE DIRECTIONS AND CAVEATS

Aim I: AGS positive B cells are enriched in MS disease

AGS-enriched B cells are present in MS CNS tissue

While the number of CNS samples was relatively low, it is difficult to obtain large numbers of post-mortem tissue. All the samples were isolated from CDMS patients. Therefore, it is unknown from this study if these AGS-enriched B cells are present in the CNS only at later stages of the disease or if they could also be found at the first clinical event. Both relapsing and chronic phases displayed enrichment of the AGS in the NAWM and plaques. Finding the signature within the NAWM lends support to the hypothesis that these B cells could contribute to early events in localized tissue damage. If possible, early presence of AGS-enriched B cells in the parenchyma could be addressed by testing CNS tissue from CIS samples, but these would be more difficult to acquire.

It would also be of interest to isolate B cells present in lesions from other neuroimmunological autoimmune diseases, such as NMO, and identify whether the AGS is present at levels similar to MS or if a different antibody signature can be detected. Preliminary work in the laboratory using NMO CSF B cells suggests that a novel AGS can be measured in NMO patients. Work is also currently underway to analyze the repertoires of OND patients utilizing a NGS platform.

AGS-enriched B cells are present in the CSF of TM_{CIS} patients

The presence of AGS enriched B cells in the CSF of TM_{CIS} patients in addition to the previously determined ON_{CIS} patients suggests that this signature is associated with both presentations that are at high risk to convert to CDMS. Some of the patients had low V_H4 sequence numbers, but the average of all the TM_{CIS} patients was similar to the ON_{CIS} patients. Therefore, while it is possible that some of the individual TM_{CIS} patients with lower sequence numbers may not have an accurate AGS, the cohort as a whole provides support that the signature is indeed enriched in this patient group. Furthermore, there is no correlation with the number of sequences and the AGS score.

The ultimate goal for the AGS is to diagnose patients at the time of the initial event to help both the doctors and the patients develop the most optimal treatment plan. Early and accurate diagnosis is important in light of data suggesting that earlier treatment delays the progression of disease leading to increases in disability (28, 57, 64-67). The aim is to prevent as many relapses as possible during the first two years to preventing future disability (28, 60, 68). In fact, DioGenix Inc is currently testing the AGS as a diagnostic tool using the NGS platform. While we see an enrichment of the AGS in this cohort of TM_{CIS} patients, it is unknown what the predicative accuracy of conversion will be. Therefore it is important for the laboratory to continue following this cohort while continuing to sample more patients.

In addition, the EDSS, relapse rate, and conversion time of all CIS patients could be examined to ascertain if there is a correlation with the AGS score and these downstream clinical measures. From another clinical standpoint, assessing whether the AGS scores change after patients progress to CDMS and receive various immunomodulatory therapies could offer information on the clinical significance of the

AGS. Calculating the AGS score after B cell reconstitution following rituximab therapy could offer insights into a mechanism of action. If the AGS-enriched B cells are contributing to damage, it may be possible that the score would fall or that the levels of AGS positive B cells diminish. In RA, it has been found the repopulating B cells exhibit genomic differences in the antibodies with a "resetting" of the B cell repertoire (393-395). Due to the inherent difficulties of following a patient cohort for longitudinal studies, it would be beneficial to include more patients in the group.

It would also be advantageous to assess if the AGS could be detected in the PB compartment utilizing NGS methodology to capture a larger sampling of the B cell repertoire. This is also a far less invasive procedure for sampling cells and would be favored by both the patients and clinicians. With single cell PCR, the sequence signal for the AGS enriched B cells among the entire PB repertoire is too low and the signature is not enriched due to a small sampling size. Currently, work in the laboratory is being done in collaboration with Drs. Fire and Boyd to address this question with matched PB B cell repertoires acquired utilizing the same NGS method as the MS CNS repertoires. These PB B cells were isolated at the same sampling time that the CSF single cell sorts were conducted. Therefore, we have both compartments sampled and sequenced for 10 patients with CSF repertoires presented in this current thesis. Work is underway to optimize filtering and analysis of the NGS data in order to compare it to the paired CSF repertoires. Then the prevalence of the AGS in the PB can be determined and compared to that of the CSF. Currently, CSF samples are only obtained during or shortly after a clinical event and the patient is not sampled again. If the signature could be detected using the blood, patients could be more easily tested before and after therapy to see how various therapeutics affect the AGS score and if it is linked to clinical response.

Aim II: Mutation characteristics and B cell subpopulations differ between CIS patients presenting with ON_{CIS} vs TM_{CIS}

Elevated levels of plasmablasts in a subset of TM_{CIS} patients

It is interesting to posit a unique state of immunopathology supporting this expansion of plasmablasts in patients with TM_{CIS} and not ON_{CIS}. This may be due to a finding that IL-6 is significantly increased in the CSF of TM_{CIS} patients (396). IL-6 is a cytokine that is critical in the development of plasmablasts and plasma cells (123). Additionally, $CD27^{high}$ cells produce high levels of IL-6 post TLR9 stimulation which may perpetuate the cycle of increased plasmablast numbers (397). IL-6 promotes anti-AQP4 autoantibody production in NMO patient plasmablasts (202), so it would be interesting to assess what auto-antigens the antibodies from $CD27^{high}$ plasmablasts recognize. Work is currently underway in the laboratory to address the potential CNS targets of the antibodies from these peripheral plasmablasts utilizing the same cloning techniques described in Aim III. The sera from SLE patients also have increased IL-6 levels (398), which could support expansions of plasmablasts in this disease as well. However, our lab has found that in some cases, naïve B cells from established MS patients have the potential to produce more IL-6 than memory B cells from the same patient (161). Preliminary data have also shown no difference in IL-6 levels from the CSF of ON_{CIS} and TM_{CIS} patients. This suggests that the expansion of plasmablasts in the TM_{CIS} patients may occur through a different yet unknown mechanism than NMO and SLE. ELISA or flow cytometry methodologies on the archived serum and CSF

supernatants could aid in identification of possible cytokines that differ between $TM_{CIS}A$ and $TM_{CIS}B/ON_{CIS}$ patients.

Detection of plasmablasts in the periphery at this early stage of disease may be due to the activation of B cells in the periphery prior to migration into the CNS or visa versa. Unlike plasma cells, plasmablasts are quite motile (364), but their travel direction in the TM_{CIS} patients is unknown from this current study. It would be interesting to track the progression of some of the currently described TM_{CIS} patients and re-sample both their CSF and PB to determine if those with elevated peripheral plasmablasts retain these cells in the blood or if they migrate to the CSF as the disease progresses. All four TM_{CIS} patients re-sampled for this current study had lower levels of plasmablasts in their PB at the re-sample point. There are several factors that could explain this finding. The plasmablasts may have migrated to the inflamed CSF due to VLA-4 being highly expressed on plasmablasts (116, 174). Or they may have migrated to the CNS due the increase in CXCL13, the B cell attractant chemokine, observed in active MS and CIS patients (136, 382). While it is possible that the plasmablasts may dissipate following an attack, the finding that the levels increase in correlation with increased time from initial event to sampling does not support this. Another possibility is that the four patients may have responded favorably to treatment since the first sampling date.

The ability of these $CD27^{high}$ plasmablasts to expand may help to indentify TM_{CIS} with a worse prognostic risk, or be used as a biomarker for response to B cell depleting agents. Also, the TM_{CIS} patients with elevated levels of plasmablasts in the periphery could be candidates for natalizumab therapy to prevent the entry of these cells into the CNS. At this current point, we do not know the impact of presenting with the $TM_{CIS}A$ phenotype on the EDSS once a patient converts to CDMS. This would be an interesting

aspect to follow with this cohort to determine whether the percentage of $CD27^{high}$ cells can be used as a prognostic for future disease.

Altered B cell repertoires in diseased compartments

In addition to the expansion of V_H4 genes in the CSF of MS and CIS patients, there was evidence of positive selection *via* accumulation of SHM in these V_H4^+ B cells. In contrast, V_H4^+ gene usage was not increased in peripheral $CD27^{high}$ plasmablasts from the $TM_{CIS}A$ patients. The normal distribution of V_H gene usage in the $TM_{CIS}A$-$CD27^{high}$ plasmablasts may reflect proper responses to other antigens that the immune system encounters in the periphery. SHM accumulation in peripheral V_H4^+ plasmablasts was extensive in comparison to V_H3^+ plasmablasts in the $TM_{CIS}A$ patients. The antigenic response could be addressed in future experiments by creating monoclonal antibodies and testing their targeting to CNS from the $VH4^+$ pool, using the $VH3^+$/$VH1^+$ pool as a control.

This selection of V_H4^+ B cells in the peripheral plasmablast pool mirrors the selection of $VH4^+$ B cells in the CSF compartments characteristic of antigen driven selection. It is unknown if these plasmablasts then seed the CSF and are early contributors to the V_H4^+ skewing in CIS as disease progresses to MS. Patient CSF and PB could be re-sampled to generate a second time point. Identifying the antibody sequences of these plasmablasts could offer a clue as to the direction of the travel. This approach has been done using NGS and identified ~2% of shared clonal members between the PB and CSF of MS patients tested at a single time point (121). In analyzing the plasmablast antibody repertoire from a second sampling point, intraclonal diversification could be addressed in this cohort. Evidence of this occurring in CDMS has been previously established (218, 219).

Impact of receptor editing on antibody targeting

The $V_H4^+J_H6^+$ plasmablast B cell pool of $TM_{CIS}A$ patients display evidence of being antigen driven and undergoing V_H receptor editing in the periphery of TM_{CIS} patients. This receptor editing could be a mechanism for these plasmablasts to attempt to reduce their auto-reactivity. Interestingly, the memory B cells from the same $TM_{CIS}A$ patients did not display evidence of receptor editing in the V_H4^+ B cells, but rather in the $V_H1^+J_H6^+$ B cells. This suggests that as compared to the V_H1^+ using B cells, the $V_H4^+J_H6^+$ B cells could be chronically stimulated and develop into plasmablasts compared. Comparison of targeting by $V_H4^+J_H6^+$, $V_H4^+J_H4^+$, and their V_H1^+ counterparts could address whether the $V_H4^+J_H6^+$ utilizing B cells are unique in their antigenic recognition explaining the receptor editing and high levels of SHM.

An increase in positive residues in the CDR3 is also associated with heavy chain editing (74, 399). This is attributed to the increase in K and R residues that are normally not encoded in the D_H segments but are inserted upon the imprecise joining of V_H, D_H, and J_H segments in secondary rearrangements. In SLE, the accumulation of positive charges is characteristic of polyreactive antibodies that recognize several self-antigens. When comparing V_H4^+ CDR3 net charges, all groups including HCPB did not show an accumulation of positive charges. This discrepancy may be due to the difference in target auto-antigens in SLE and MS. In SLE, autoantibodies are selected for positive residue enrichment in their CDR3s since they are reactive to negatively charged nucleic acids. In MS and CIS CSF, the accumulation of negative residues in the CDR3s may reflect selection in targeting to positively charged antigens. In fact, one of the putative auto-antigens classically associated with MS is MBP, which is positively charged. Therefore it would be informative to the disease pathoetiology to identify the driving auto-antigens of

these peripheral $TM_{CIS}A$ plasmablasts. As proposed previously, cloning the antibodies from these plasmablasts and addressing their targeting to CNS antigens could be done to address this question. Additionally, since these are peripheral plasmablasts, it would be interesting to see if plasmablasts isolated from the CSF of $TM_{CIS}A$ patients recognize the same antigens or if the targeting profiles differ depending on the compartment.

Aim III: AGS-enriched B cells mediate MS pathology by producing antibodies that target the brain

The impact of AGS mutations on rhAb targeting

The current study demonstrates that both types of initial presentation, TM_{CIS} and ON_{CIS}, as well as established CDMS patients harbor AGS-enriched B cells that target GM neurons and astrocytes. It is likely that the AGS pattern, as a genomic marker of shared antigenic pressures, contributes to the targeting. To test this, all RMs at AGS codons would be reverted to germline while preserving all other mutations along the V_H gene . Comparing the targeting ability and staining patterns of these AGS-revertants using the same IHC and IFC methodologies would offer insight into the impact of these specific AGS mutations. Additionally, this could also provide clues to the relative importance of a single codon in recognizing a target. Analysis of crystallography work on 140 antibodies against proteins, peptides, and haptens, confirmed that SHMs are less abundant at a position beyond the regions of antigen contact (205). Furthermore, in looking at AGS codons presented in that study, 31b has low interactions with peptides and both 56 and 57 have high interactions with peptide (205) suggesting that different AGS codons could contribute to binding of the various complex antigen types in the CNS. With regards to binding, 31b, 56, and 57 are associated with both affinity and specificity whereas 40, 81, and 89 are associated with affinity only (205). This also suggests that FR codons (40, 81, and 89) contribute to affinity by possibly altering the conformation of the antibody and the antigen binding regions. Therefore, some revertants may have the same targets with a lower staining intensity depending on the AGS codons utilized.

Entire revertants to germline (total-revertants) should also be tested to determine if the V_H4 genes used in these B cells could react to either self-antigen or viral/bacterial antigens. It is possible that these AGS-enriched B cells were initially selected for expansion due to the recognition of the germline gene to a CNS cross-reactive viral/bacterial antigen. In fact, in NMO patients, the pathogenic anti-AQP4 antibodies can be cross-reactive to bacterial AQPZ (400). The potential of pathogen reactivity could be addressed using a protein array of common infectious agents for assessing whether AGS-enriched, AGS-revertant, or total-revertants differ in their binding to pathogens.

Evaluation of binding patterns and their implications on rhAb targeting

Three out of the five receptor edited pairs did not appear to have an impact on the GM targeting of the rhAbs. It is possible that using more refined molecular techniques, such as competitive ELISAs, would reveal variations in targeting between the edited pair members. Previous findings in the laboratory using the same variable regions in a Fab construct (WR01, WR02) for IPs with MBP followed by western blotting identified WM antigen targets (255). While this current study does not find staining of the heavily myelinated WM regions in the brain, it is possible that the correct conformation or post-translational modifications were not available. IHC is subjected to multiple vigorous washes and if these rhAbs have a weaker interaction with WM targets than GM then it would not be readily visualized via DAB.

Interestingly, it may be possible for a GM targeting antibody to have cross-reactivity with a WM target. Hybridomas from a PLP immunized mouse were characterized to define the specific regions of binding to PLP and the ability to bind to oligodendrocytes in brain sections (322). Antibody against the PLP 178-191 peptide

bound to various neuronal subtypes across a wide array of species including fish, rodent, and mammal brains (322). This peptide is relatively hydrophobic and buried in the cell membrane, and despite this causes a more severe EAE induction in SJL mice (401). A fusion of PLP 178-191 with MOG 35-55 (MP4) induces a heavily B cell and antibody dependent EAE course (257). This cross-reactivity of a myelin component with neurons arises from conserved pgf sequences, which could increase the potential number of antibody targets and promote cross-reactivity (402). In the current cohort of rhAbs, WR01 tested in Fab form recognized MBP via western blot (255) and AJL10 bound to nuclei that appeared to be oligodendrocytes including the neuronal nuclei shown. It is possible through further investigation for additional cross-reactive rhAbs with WM and neurons in the GM to be discovered in the cohort. Preliminary myelin-peptide array done in collaboration with Dr. Robinson's laboratory at Stanford revealed some rhAb binding to WM antigen peptides, included PLP. Peptide arrays can be difficult to interpret in the context of antibody binding in a biological setting due to the entire protein not being present and the loss of conformational epitopes. Protein based microarrays, such as the commercially available Protoarray (Invitrogen, Life Technologies) could be employed in the future to screen a large number of potential targets without the potential problems common in a peptide array.

Varied patterns of lamin A colocalization suggest that even though these AGS-enriched rhAbs bind to neuronal nuclei, they may recognize different targets. Future experiments on neuronal nuclear extractions may make it possible to elucidate putative targets. Titrations of dual-targeting rhAbs demonstrated that some rhAbs while being dual-cell targeting at higher concentrations lost some binding at lower concentrations. Additionally, it can be hypothesized that the relative binding strength of the rhAbs for

their cellular targets is different among the panel of AGS-enriched rhAbs. Future experiments could indentify the relative affinity of these rhAbs for cellular targets using competitive binding assays. While transcriptomes from brain samples reveal highly unique cellular expressions of proteins between astrocytes and neurons (403), it is still possible that there are some shared proteins in astrocytes and the nuclei of neurons. Moreover, there could be sequence or conformational-derived epitope similarities that allow for the targeting of both cell types.

Pathogenic implications of shared targeting of AGS-enriched rhAbs

The shared targeting across disease presentations and length suggests that these antibodies are potentially binding to disease relevant antigen(s). The pathogenic potential of antibodies has been assayed by their capability to bind to cell lines. Preliminary data with the rhAbs AJL02 and AJL10 show binding to human fetal neuronal progenitor cells. This suggests that the rhAbs may inhibit neuronal repair *in vivo* if they have the ability to target progenitor cells. Flow cytometry of MS serum binding to cultured human cell lines revealed a portion of patients' sera had reactivity against oligodendrocyte precursor cells and not their differentiated counterparts, as well as immature and mature neuronal cells (285). Furthermore, patients with a benign disease course did not display binding above background to the cell lines (285). However, another flow cytometry study did not find binding of MS CSF to a human neuronal cell line (404). A recent study employing an extensive array of *in vitro* techniques to address the antibody binding potential from monoclonal antibodies derived from human-MOG induced EAE. They determined that the most accurate predictor of the disease-exacerbating potential of the mAb injected into mice was the ability to bind to CNS by IFC, and that binding to a cell line did not fully

recapitulate the ability to exacerbate EAE (319). This was also reported using neurofascin isoforms, Nfasc155 and Nfasc186, where antibodies to both isoforms bound to a cell line expressing the protein but only immunization with Nfasc186 would exacerbate EAE and was physiologically relevant (297). A cell-based assay was unable to identify MOG, PLP, or MAG reactivity of an MS patient's sera that partialy colocalized with oligodendrocytes in mice and exacerbated EAE demyelination (100). The CNS is a complex environment with tight cell-cell interactions that may reveal novel epitopes absent on a monotypic-cell line or even the lack of an essential post-translational modification could lead to target unavailability.

AGS-enriched B cells isolated from patient CSF produce antibodies that are able to bind to both mouse and, more importantly, human brain tissue. This species-preserved homology of important CNS elements provides promise for mouse-based experiments addressing the pathogenic potential of these rhAbs. In fact, 7 rhAbs were also tested on EAE brain from mice induced with full-length recombinant human MOG suggesting that these rhAbs could recognize their targets in the context of this mouse model of acute neuroinflammation. A caveat with the current panel of rhAbs is that it is unclear whether they can initiate damage, perpetuate damage, or are unable to find their targets *in vivo*. Mouse models could be utilized to address this question. A mild EAE could be induced by immunizing mice with hMOG 35-55 peptide, and rhAbs can be injected into the mice at the peak of disease to assess the ability of the rhAb to exacerbate disease (319). Using this methodology, Bansal and colleagues discovered that monoclonal antibodies binding to brain tissue *in vitro* possessed the ability to exacerbate disease. Another approach for testing the pathogenic potential of the rhAbs is to perform cranial injections in mice to directly deliver the antibody, which has been used to discover the neurotoxic potential of

SLE derived rhAbs (337). Either of these *in vivo* techniques could elucidate the disease-initiating potential of these rhAbs.

Another question is whether these AGS-enriched rhAbs could mediate damage through either Fc-mediated complement or antibody-mediated cellular cytotoxicity (ADCC) mechanisms. It is possible that the binding of the rhAbs alone, independent of the Fc, could mediate pathology through steric hindrance or antagonistic activities. In fact, antibodies to elements within the nodes of ranvier could lead to steric hindrance of myelination (390). Antibody cross-linking of MOG leads to altered protein and cell morphology with a disruption in MOG partitioning that can contribute to demyelination (405). Astrocyte activation and damage, in the absence of complement activation, has been reported in the spinal cord of mice injected with anti-AQP4 antibody (374). Also, G11 as studied by Dr. Diamond's laboratory has differing effects on neurons depending on the relative concentrations of the antibody: ranging from causing the NMDAR to remain open longer and increasing postsynaptic potentials to neuronal death at higher levels (406). In order to test if Fc independent mechanisms may contribute to AGS-enriched rhAb pathogenic potential, the rhAbs can be digested using pepsin to create a bivalent Fab fragment and independent Fc regions. These bivalent Fab fragments can be injected into mice to determine whether binding to the epitope alone can elicit pathology as compared to full-length rhAb injections.

Clinical implications of AGS-enriched rhAb targeting

The recognition of brain tissue is not restricted to a particular presentation of disease or even the length of disease and it is unknown whether the AGS correlates with disease severity or progression. Since the AGS-enriched rhAbs have a predilection for

GM targets, correlating GM damage may be of clinical interest. Detection of GM lesions *in vivo* can be complicated so alternatively, correlations with GM damage-induced symptoms, such as cognitive declines, could be associated with the AGS.

Identifying a genomic marker shared by MS patients, the AGS, in a pool of antibodies with the ability to bind to brain targets, could provide direction for novel therapeutic approaches. Since this GM targeting occurs at the first stage of disease and continues onto CDMS, potential novel treatment targets could be assessed with regard to neurological preservation. Loss of neurons and axons is associated with irreparable damage and once a threshold of damage is reached, these patients' disease progresses. Treatments that preserve astrocyte functions to promote remyelination and re-establish a tight BBB could counteract antibody assaults to astrocytes and their endfeet. Maintaining neuronal and axonal integrity would be critical in preventing neurodegeneration.

These rhAbs themselves could also become future novel therapeutics. Modifying monoclonal anti-AQP4 antibodies to inhibit Fc effector function has shown promise in mouse models in inhibiting NMO pathology (407, 408) and modifying a polyclonal IgG pool ameliorates EAE severity (409). Similar approaches have been done in mouse models of fetal-alloimmune thrombocytopenia (410), collagen induced arthritis (411), and bullous pemphigoid (412). These findings in different autoimmune diseases highlights the potential in developing mAb therapeutics aimed to block the binding of these AGS-enriched rhAbs to their cellular targets for the purpose of preventing antibody mediated damage to the GM.

There are many future approaches to better define the potential biological implications of the AGS found in a population of CSF B cells from MS and CIS patients. The AGS is already useful as a biomarker of disease conversion in ON_{CIS} patients and is

being tested further to broaden its utility by DioGenix Inc. In addition to a conversion diagnostic, this AGS enrichment could identity patients that would benefit from therapies aimed to preserve GM integrity. As future experiments identify the specific targets recognized on either neuronal nuclei or astrocytes, directed therapies could be employed that are more effective because they are based on the underlying biology of these AGS-enriched B cells.

REFERENCES

1. Geurts JJ, Bo L, Pouwels PJ, Castelijns JA, Polman CH, Barkhof F. Cortical lesions in multiple sclerosis: combined postmortem MR imaging and histopathology. Ajnr. 2005;26(3):572-7.
2. Frohman EM, Racke MK, Raine CS. Multiple sclerosis--the plaque and its pathogenesis. N Engl J Med. 2006;354(9):942-55.
3. Trapp BD, Peterson J, Ransohoff RM, Rudick R, Mork S, Bo L. Axonal transection in the lesions of multiple sclerosis. N Engl J Med. 1998;338(5):278-85.
4. Bitsch A, Schuchardt J, Bunkowski S, Kuhlmann T, Bruck W. Acute axonal injury in multiple sclerosis. Correlation with demyelination and inflammation. Brain. 2000;123 (Pt 6):1174-83.
5. Cepok S, Jacobsen M, Schock S, Omer B, Jaekel S, Boddeker I, et al. Patterns of cerebrospinal fluid pathology correlate with disease progression in multiple sclerosis. Brain. 2001;124(Pt 11):2169-76.
6. Lucchinetti C, Bruck W, Parisi J, Scheithauer B, Rodriguez M, Lassmann H. Heterogeneity of multiple sclerosis lesions: implications for the pathogenesis of demyelination. Ann Neurol. 2000;47(6):707-17.
7. Noseworthy JH, Lucchinetti C, Rodriguez M, Weinshenker BG. Multiple sclerosis. N Engl J Med. 2000;343(13):938-52.
8. Courtney AM, Treadaway K, Remington G, Frohman E. Multiple sclerosis. Med Clin North Am. 2009;93(2):451-76, ix-x.
9. Lassmann H, Bruck W, Lucchinetti CF. The immunopathology of multiple sclerosis: an overview. Brain Pathol. 2007;17(2):210-8.
10. Lassmann H, Bruck W, Lucchinetti C. Heterogeneity of multiple sclerosis pathogenesis: implications for diagnosis and therapy. Trends Mol Med. 2001;7(3):115-21.
11. Frischer JM, Bramow S, Dal-Bianco A, Lucchinetti CF, Rauschka H, Schmidbauer M, et al. The relation between inflammation and neurodegeneration in multiple sclerosis brains. Brain. 2009;132(Pt 5):1175-89. PMCID: 2677799.
12. Sawcer S. The complex genetics of multiple sclerosis: pitfalls and prospects. Brain. 2008;131(Pt 12):3118-31. PMCID: 2639203.
13. Bjartmar C, Kinkel RP, Kidd G, Rudick RA, Trapp BD. Axonal loss in normal-appearing white matter in a patient with acute MS. Neurology. 2001;57(7):1248-52.
14. Bjartmar C, Kidd G, Mork S, Rudick R, Trapp BD. Neurological disability correlates with spinal cord axonal loss and reduced N-acetyl aspartate in chronic multiple sclerosis patients. Ann Neurol. 2000;48(6):893-901.
15. Miller DH, Barkhof F, Frank JA, Parker GJ, Thompson AJ. Measurement of atrophy in multiple sclerosis: pathological basis, methodological aspects and clinical relevance. Brain. 2002;125(Pt 8):1676-95.
16. Leech S, Kirk J, Plumb J, McQuaid S. Persistent endothelial abnormalities and blood-brain barrier leak in primary and secondary progressive multiple sclerosis. Neuropathol Appl Neurobiol. 2007;33(1):86-98.
17. Kirk J, Plumb J, Mirakhur M, McQuaid S. Tight junctional abnormality in multiple sclerosis white matter affects all calibres of vessel and is associated with

blood-brain barrier leakage and active demyelination. J Pathol. 2003;201(2):319-27.
18. de Vries HE, Kooij G, Frenkel D, Georgopoulos S, Monsonego A, Janigro D. Inflammatory events at blood-brain barrier in neuroinflammatory and neurodegenerative disorders: implications for clinical disease. Epilepsia. 2012;53 Suppl 6:45-52.
19. Miller DH, Rudge P, Johnson G, Kendall BE, Macmanus DG, Moseley IF, et al. Serial gadolinium enhanced magnetic resonance imaging in multiple sclerosis. Brain. 1988;111 (Pt 4):927-39.
20. Molyneux PD, Filippi M, Barkhof F, Gasperini C, Yousry TA, Truyen L, et al. Correlations between monthly enhanced MRI lesion rate and changes in T2 lesion volume in multiple sclerosis. Ann Neurol. 1998;43(3):332-9.
21. Wang HY, Matsui M, Saida T. Immunological disturbances in the central nervous system linked to MRI findings in multiple sclerosis. J Neuroimmunol. 2002;125(1-2):149-54.
22. Laman JD, Weller RO. Drainage of Cells and Soluble Antigen from the CNS to Regional Lymph Nodes. J Neuroimmune Pharmacol. 2013.
23. van Zwam M, Huizinga R, Melief MJ, Wierenga-Wolf AF, van Meurs M, Voerman JS, et al. Brain antigens in functionally distinct antigen-presenting cell populations in cervical lymph nodes in MS and EAE. J Mol Med (Berl). 2009;87(3):273-86.
24. de Vos AF, van Meurs M, Brok HP, Boven LA, Hintzen RQ, van der Valk P, et al. Transfer of central nervous system autoantigens and presentation in secondary lymphoid organs. J Immunol. 2002;169(10):5415-23.
25. Fabriek BO, Zwemmer JN, Teunissen CE, Dijkstra CD, Polman CH, Laman JD, et al. In vivo detection of myelin proteins in cervical lymph nodes of MS patients using ultrasound-guided fine-needle aspiration cytology. J Neuroimmunol. 2005;161(1-2):190-4.
26. Hawkins SA, McDonnell GV. Benign multiple sclerosis? Clinical course, long term follow up, and assessment of prognostic factors. J Neurol Neurosurg Psychiatry. 1999;67(2):148-52. PMCID: 1736487.
27. Calabrese M, Filippi M, Rovaris M, Bernardi V, Atzori M, Mattisi I, et al. Evidence for relative cortical sparing in benign multiple sclerosis: a longitudinal magnetic resonance imaging study. Mult Scler. 2009;15(1):36-41.
28. Scalfari A, Neuhaus A, Degenhardt A, Rice GP, Muraro PA, Daumer M, et al. The natural history of multiple sclerosis: a geographically based study 10: relapses and long-term disability. Brain. 2010;133(Pt 7):1914-29. PMCID: 2892939.
29. Miller DH, Leary SM. Primary-progressive multiple sclerosis. Lancet Neurol. 2007;6(10):903-12.
30. Kidd D, Barkhof F, McConnell R, Algra PR, Allen IV, Revesz T. Cortical lesions in multiple sclerosis. Brain. 1999;122 (Pt 1):17-26.
31. Bo L, Vedeler CA, Nyland HI, Trapp BD, Mork SJ. Subpial demyelination in the cerebral cortex of multiple sclerosis patients. J Neuropathol Exp Neurol. 2003;62(7):723-32.
32. Bo L, Geurts JJ, van der Valk P, Polman C, Barkhof F. Lack of correlation between cortical demyelination and white matter pathologic changes in multiple sclerosis. Arch Neurol. 2007;64(1):76-80.

33. Moriarty DM, Blackshaw AJ, Talbot PR, Griffiths HL, Snowden JS, Hillier VF, et al. Memory dysfunction in multiple sclerosis corresponds to juxtacortical lesion load on fast fluid-attenuated inversion-recovery MR images. Ajnr. 1999;20(10):1956-62.
34. Sormani MP, Arnold DL, De Stefano N. Treatment effect on brain atrophy correlates with treatment effect on disability in multiple sclerosis. Ann Neurol. 2013.
35. Chard DT, Griffin CM, Rashid W, Davies GR, Altmann DR, Kapoor R, et al. Progressive grey matter atrophy in clinically early relapsing-remitting multiple sclerosis. Mult Scler. 2004;10(4):387-91.
36. Fisniku LK, Chard DT, Jackson JS, Anderson VM, Altmann DR, Miszkiel KA, et al. Gray matter atrophy is related to long-term disability in multiple sclerosis. Ann Neurol. 2008;64(3):247-54.
37. Fisher E, Rudick RA, Simon JH, Cutter G, Baier M, Lee JC, et al. Eight-year follow-up study of brain atrophy in patients with MS. Neurology. 2002;59(9):1412-20.
38. Valsasina P, Benedetti B, Rovaris M, Sormani MP, Comi G, Filippi M. Evidence for progressive gray matter loss in patients with relapsing-remitting MS. Neurology. 2005;65(7):1126-8.
39. Dalton CM, Chard DT, Davies GR, Miszkiel KA, Altmann DR, Fernando K, et al. Early development of multiple sclerosis is associated with progressive grey matter atrophy in patients presenting with clinically isolated syndromes. Brain. 2004;127(Pt 5):1101-7.
40. Calabrese M, Rinaldi F, Mattisi I, Bernardi V, Favaretto A, Perini P, et al. The predictive value of gray matter atrophy in clinically isolated syndromes. Neurology. 2011;77(3):257-63.
41. De Stefano N, Matthews PM, Filippi M, Agosta F, De Luca M, Bartolozzi ML, et al. Evidence of early cortical atrophy in MS: relevance to white matter changes and disability. Neurology. 2003;60(7):1157-62.
42. Neema M, Arora A, Healy BC, Guss ZD, Brass SD, Duan Y, et al. Deep gray matter involvement on brain MRI scans is associated with clinical progression in multiple sclerosis. J Neuroimaging. 2009;19(1):3-8. PMCID: 2762230.
43. Lucchinetti CF, Popescu BF, Bunyan RF, Moll NM, Roemer SF, Lassmann H, et al. Inflammatory cortical demyelination in early multiple sclerosis. N Engl J Med. 2011;365(23):2188-97. PMCID: 3282172.
44. Schutzer SE, Angel TE, Liu T, Schepmoes AA, Xie F, Bergquist J, et al. Gray matter is targeted in first-attack multiple sclerosis. PLoS One. 2013;8(9):e66117. PMCID: 3769274.
45. Bo L, Vedeler CA, Nyland H, Trapp BD, Mork SJ. Intracortical multiple sclerosis lesions are not associated with increased lymphocyte infiltration. Mult Scler. 2003;9(4):323-31.
46. Miller D, Barkhof F, Montalban X, Thompson A, Filippi M. Clinically isolated syndromes suggestive of multiple sclerosis, part I: natural history, pathogenesis, diagnosis, and prognosis. Lancet Neurol. 2005;4(5):281-8.
47. Atkins EJ, Biousse V, Newman NJ. Optic neuritis. Semin Neurol. 2007;27(3):211-20.
48. Plant GT. Optic neuritis and multiple sclerosis. Curr Opin Neurol. 2008;21(1):16-21.

49. Pau D, Al Zubidi N, Yalamanchili S, Plant GT, Lee AG. Optic neuritis. Eye (Lond). 2011;25(7):833-42. PMCID: 3178158.
50. Kerr DA, Ayetey H. Immunopathogenesis of acute transverse myelitis. Curr Opin Neurol. 2002;15(3):339-47.
51. Harzheim M, Schlegel U, Urbach H, Klockgether T, Schmidt S. Discriminatory features of acute transverse myelitis: a retrospective analysis of 45 patients. J Neurol Sci. 2004;217(2):217-23.
52. Sellner J, Luthi N, Buhler R, Gebhardt A, Findling O, Greeve I, et al. Acute partial transverse myelitis: risk factors for conversion to multiple sclerosis. Eur J Neurol. 2008;15(4):398-405.
53. Scott TF. Nosology of idiopathic transverse myelitis syndromes. Acta Neurol Scand. 2007;115(6):371-6.
54. Bourre B, Zephir H, Ongagna JC, Cordonnier C, Collongues N, Debette S, et al. Long-term follow-up of acute partial transverse myelitis. Arch Neurol. 2012;69(3):357-62.
55. Sa MJ. Acute transverse myelitis: a practical reappraisal. Autoimmun Rev. 2009;9(2):128-31.
56. Pandit L. Transverse myelitis spectrum disorders. Neurol India. 2009;57(2):126-33.
57. Fisniku LK, Brex PA, Altmann DR, Miszkiel KA, Benton CE, Lanyon R, et al. Disability and T2 MRI lesions: a 20-year follow-up of patients with relapse onset of multiple sclerosis. Brain. 2008;131(Pt 3):808-17.
58. Patrucco L, Rojas JI, Cristiano E. Assessing the value of spinal cord lesions in predicting development of multiple sclerosis in patients with clinically isolated syndromes. J Neurol. 2011.
59. Tintore M, Rovira A, Rio J, Nos C, Grive E, Tellez N, et al. Is optic neuritis more benign than other first attacks in multiple sclerosis? Ann Neurol. 2005;57(2):210-5.
60. Confavreux C, Vukusic S, Adeleine P. Early clinical predictors and progression of irreversible disability in multiple sclerosis: an amnesic process. Brain. 2003;126(Pt 4):770-82.
61. Irani DN, Kerr DA. 14-3-3 protein in the cerebrospinal fluid of patients with acute transverse myelitis. Lancet. 2000;355(9207):901.
62. Martinez-Yelamos A, Rovira A, Sanchez-Valle R, Martinez-Yelamos S, Tintore M, Blanco Y, et al. CSF 14-3-3 protein assay and MRI as prognostic markers in patients with a clinically isolated syndrome suggestive of MS. J Neurol. 2004;251(10):1278-9.
63. Brex PA, Ciccarelli O, O'Riordan JI, Sailer M, Thompson AJ, Miller DH. A longitudinal study of abnormalities on MRI and disability from multiple sclerosis. N Engl J Med. 2002;346(3):158-64.
64. Frohman EM, Havrdova E, Lublin F, Barkhof F, Achiron A, Sharief MK, et al. Most patients with multiple sclerosis or a clinically isolated demyelinating syndrome should be treated at the time of diagnosis. Arch Neurol. 2006;63(4):614-9.
65. Rocca MA, Agosta F, Sormani MP, Fernando K, Tintore M, Korteweg T, et al. A three-year, multi-parametric MRI study in patients at presentation with CIS. J Neurol. 2008;255(5):683-91.

66. Greenberg BM. Treatment of acute transverse myelitis and its early complications. Continuum (Minneap Minn). 2011;17(4):733-43.
67. D'Alessandro R, Vignatelli L, Lugaresi A, Baldin E, Granella F, Tola MR, et al. Risk of multiple sclerosis following clinically isolated syndrome: a 4-year prospective study. J Neurol. 2013;260(6):1583-93.
68. Gajofatto A, Bongianni M, Zanusso G, Bianchi MR, Turatti M, Benedetti MD, et al. Clinical and biomarker assessment of demyelinating events suggesting multiple sclerosis. Acta Neurol Scand. 2013.
69. Thrower BW. Clinically isolated syndromes: predicting and delaying multiple sclerosis. Neurology. 2007;68(24 Suppl 4):S12-5.
70. Tsubata T, Wu J, Honjo T. B-cell apoptosis induced by antigen receptor crosslinking is blocked by a T-cell signal through CD40. Nature. 1993;364(6438):645-8.
71. Tsao BP, Hahn BH. Autoimmunity and tolerance in Ig-transgenic mice: murine SLE as a model to study B cell tolerance. Int Rev Immunol. 1994;11(4):305-20.
72. Wardemann H, Yurasov S, Schaefer A, Young JW, Meffre E, Nussenzweig MC. Predominant autoantibody production by early human B cell precursors. Science. 2003;301(5638):1374-7.
73. Casellas R, Shih TA, Kleinewietfeld M, Rakonjac J, Nemazee D, Rajewsky K, et al. Contribution of receptor editing to the antibody repertoire. Science. 2001;291(5508):1541-4.
74. Nemazee D. Receptor editing in lymphocyte development and central tolerance. Nat Rev Immunol. 2006;6(10):728-40.
75. Zhang Z, Burrows PD, Cooper MD. The molecular basis and biological significance of VH replacement. Immunol Rev. 2004;197:231-42.
76. Gay D, Saunders T, Camper S, Weigert M. Receptor editing: an approach by autoreactive B cells to escape tolerance. J Exp Med. 1993;177(4):999-1008. PMCID: 2190958.
77. Retter MW, Nemazee D. Receptor editing occurs frequently during normal B cell development. J Exp Med. 1998;188(7):1231-8. PMCID: 2212498.
78. Tiegs SL, Russell DM, Nemazee D. Receptor editing in self-reactive bone marrow B cells. J Exp Med. 1993;177(4):1009-20. PMCID: 2190975.
79. Zhang Z, Wang YH, Zemlin M, Findley HW, Bridges SL, Burrows PD, et al. Molecular mechanism of serial VH gene replacement. Ann N Y Acad Sci. 2003;987:270-3.
80. Chen C, Nagy Z, Prak EL, Weigert M. Immunoglobulin heavy chain gene replacement: a mechanism of receptor editing. Immunity. 1995;3(6):747-55.
81. Zhang Z, Zemlin M, Wang YH, Munfus D, Huye LE, Findley HW, et al. Contribution of Vh gene replacement to the primary B cell repertoire. Immunity. 2003;19(1):21-31.
82. Meffre E, Davis E, Schiff C, Cunningham-Rundles C, Ivashkiv LB, Staudt LM, et al. Circulating human B cells that express surrogate light chains and edited receptors. Nat Immunol. 2000;1(3):207-13.
83. Kabat EA, Moore DH, Landow H. An Electrophoretic Study of the Protein Components in Cerebrospinal Fluid and Their Relationship to the Serum Proteins. J Clin Invest. 1942;21(5):571-7.

84. Kabat EA, Glusman M, Knaub V. Quantitative Estimation of the Albumin and Gamma Globulin in Normal and Pathologic Cerebrospinal Fluid by Immunochemical Methods. Am J Med. 1948;4:653-62.
85. Kabat EA, Freedman DA, et al. A study of the crystalline albumin, gamma globulin and total protein in the cerebrospinal fluid of 100 cases of multiple sclerosis and in other diseases. Am J Med Sci. 1950;219(1):55-64.
86. Johnson KP, Nelson BJ. Multiple sclerosis: diagnostic usefulness of cerebrospinal fluid. Ann Neurol. 1977;2(5):425-31.
87. Luxton RW, McLean BN, Thompson EJ. Isoelectric focusing versus quantitative measurements in the detection of intrathecal local synthesis of IgG. Clin Chim Acta. 1990;187(3):297-308.
88. Link H, Muller R. Immunoglobulins in multiple sclerosis and infections of the nervous system. Arch Neurol. 1971;25(4):326-44.
89. Jacobs LD, Kaba SE, Miller CM, Priore RL, Brownscheidle CM. Correlation of clinical, magnetic resonance imaging, and cerebrospinal fluid findings in optic neuritis. Ann Neurol. 1997;41(3):392-8.
90. Freedman MS, Thompson EJ, Deisenhammer F, Giovannoni G, Grimsley G, Keir G, et al. Recommended standard of cerebrospinal fluid analysis in the diagnosis of multiple sclerosis: a consensus statement. Arch Neurol. 2005;62(6):865-70.
91. Dobson R, Ramagopalan S, Davis A, Giovannoni G. Cerebrospinal fluid oligoclonal bands in multiple sclerosis and clinically isolated syndromes: a meta-analysis of prevalence, prognosis and effect of latitude. J Neurol Neurosurg Psychiatry. 2013.
92. Reske D, Petereit HF, Heiss WD. Difficulties in the differentiation of chronic inflammatory diseases of the central nervous system--value of cerebrospinal fluid analysis and immunological abnormalities in the diagnosis. Acta Neurol Scand. 2005;112(4):207-13.
93. Yu X, Burgoon M, Green M, Barmina O, Dennison K, Pointon T, et al. Intrathecally synthesized IgG in multiple sclerosis cerebrospinal fluid recognizes identical epitopes over time. J Neuroimmunol. 2011;240-241:129-36. PMCID: 3278397.
94. Bosca I, Magraner MJ, Coret F, Alvarez-Cermeno JC, Simo-Castello M, Villar LM, et al. The risk of relapse after a clinically isolated syndrome is related to the pattern of oligoclonal bands. J Neuroimmunol. 2010;226(1-2):143-6.
95. Ferraro D, Simone AM, Bedin R, Galli V, Vitetta F, Federzoni L, et al. Cerebrospinal fluid oligoclonal IgM bands predict early conversion to clinically definite multiple sclerosis in patients with Clinically Isolated Syndrome. J Neuroimmunol. 2013;257(1-2):76-81.
96. Calabrese M, Federle L, Bernardi V, Rinaldi F, Favaretto A, Varagnolo MC, et al. The association of intrathecal immunoglobulin synthesis and cortical lesions predicts disease activity in clinically isolated syndrome and early relapsing-remitting multiple sclerosis. Mult Scler. 2012;18(2):174-80.
97. Paolino E, Fainardi E, Ruppi P, Tola MR, Govoni V, Casetta I, et al. A prospective study on the predictive value of CSF oligoclonal bands and MRI in acute isolated neurological syndromes for subsequent progression to multiple sclerosis. J Neurol Neurosurg Psychiatry. 1996;60(5):572-5. PMCID: 486374.

98. Keegan M, Konig F, McClelland R, Bruck W, Morales Y, Bitsch A, et al. Relation between humoral pathological changes in multiple sclerosis and response to therapeutic plasma exchange. Lancet. 2005;366(9485):579-82.
99. Magana SM, Keegan BM, Weinshenker BG, Erickson BJ, Pittock SJ, Lennon VA, et al. Beneficial plasma exchange response in central nervous system inflammatory demyelination. Arch Neurol. 2011;68(7):870-8. PMCID: 3134547.
100. Pedotti R, Musio S, Scabeni S, Farina C, Poliani PL, Colombo E, et al. Exacerbation of experimental autoimmune encephalomyelitis by passive transfer of IgG antibodies from a multiple sclerosis patient responsive to immunoadsorption. J Neuroimmunol. 2013.
101. Raine CS, Cannella B, Hauser SL, Genain CP. Demyelination in primate autoimmune encephalomyelitis and acute multiple sclerosis lesions: a case for antigen-specific antibody mediation. Ann Neurol. 1999;46(2):144-60.
102. Storch MK, Piddlesden S, Haltia M, Iivanainen M, Morgan P, Lassmann H. Multiple sclerosis: in situ evidence for antibody- and complement-mediated demyelination. Ann Neurol. 1998;43(4):465-71.
103. Prineas JW, Graham JS. Multiple sclerosis: capping of surface immunoglobulin G on macrophages engaged in myelin breakdown. Ann Neurol. 1981;10(2):149-58.
104. Woyciechowska JL, Brzosko WJ. Immunofluorescence study of brain plaques from two patients with multiple sclerosis. Neurology. 1977;27(7):620-2.
105. Genain CP, Cannella B, Hauser SL, Raine CS. Identification of autoantibodies associated with myelin damage in multiple sclerosis. Nat Med. 1999;5(2):170-5.
106. Barnett MH, Parratt JD, Cho ES, Prineas JW. Immunoglobulins and complement in postmortem multiple sclerosis tissue. Ann Neurol. 2009;65(1):32-46.
107. Mehta PD, Frisch S, Thormar H, Tourtellotte WW, Wisniewski HM. Bound antibody in multiple sclerosis brains. J Neurol Sci. 1981;49(1):91-8.
108. Sadaba MC, Tzartos J, Paino C, Garcia-Villanueva M, Alvarez-Cermeno JC, Villar LM, et al. Axonal and oligodendrocyte-localized IgM and IgG deposits in MS lesions. J Neuroimmunol. 2012;247(1-2):86-94.
109. Stoop MP, Dekker LJ, Titulaer MK, Burgers PC, Sillevis Smitt PA, Luider TM, et al. Multiple sclerosis-related proteins identified in cerebrospinal fluid by advanced mass spectrometry. Proteomics. 2008;8(8):1576-85.
110. Padilla-Docal B, Dorta-Contreras AJ, Fundora-Hernandez H, Noris-Garcia E, Bu-Coifiu-Fanego R, Gonzalez-Hernandez M, et al. C3c intrathecal synthesis evaluation in patients with multiple sclerosis. Arq Neuropsiquiatr. 2007;65(3B):800-2.
111. Sellebjerg F, Jensen CV, Christiansen M. Intrathecal IgG synthesis and autoantibody-secreting cells in multiple sclerosis. J Neuroimmunol. 2000;108(1-2):207-15.
112. Izquierdo G, Angulo S, Garcia-Moreno JM, Gamero MA, Navarro G, Gata JM, et al. Intrathecal IgG synthesis: marker of progression in multiple sclerosis patients. Acta Neurol Scand. 2002;105(3):158-63.
113. Sellebjerg F, Jaliashvili I, Christiansen M, Garred P. Intrathecal activation of the complement system and disability in multiple sclerosis. J Neurol Sci. 1998;157(2):168-74.
114. de Graaf MT, Smitt PA, Luitwieler RL, van Velzen C, van den Broek PD, Kraan J, et al. Central memory CD4+ T cells dominate the normal cerebrospinal fluid. Cytometry B Clin Cytom. 2011;80(1):43-50.

115. Svenningsson A, Andersen O, Edsbagge M, Stemme S. Lymphocyte phenotype and subset distribution in normal cerebrospinal fluid. J Neuroimmunol. 1995;63(1):39-46.
116. Kleine TO, Benes L. Immune surveillance of the human central nervous system (CNS): different migration pathways of immune cells through the blood-brain barrier and blood-cerebrospinal fluid barrier in healthy persons. Cytometry A. 2006;69(3):147-51.
117. Cepok S, Rosche B, Grummel V, Vogel F, Zhou D, Sayn J, et al. Short-lived plasma blasts are the main B cell effector subset during the course of multiple sclerosis. Brain. 2005;128(Pt 7):1667-76.
118. Cepok S, von Geldern G, Grummel V, Hochgesand S, Celik H, Hartung H, et al. Accumulation of class switched IgD-IgM- memory B cells in the cerebrospinal fluid during neuroinflammation. J Neuroimmunol. 2006;180(1-2):33-9.
119. Haas J, Bekeredjian-Ding I, Milkova M, Balint B, Schwarz A, Korporal M, et al. B cells undergo unique compartmentalized redistribution in multiple sclerosis. J Autoimmun. 2011;37(4):289-99.
120. Niino M, Hirotani M, Miyazaki Y, Sasaki H. Memory and naive B-cell subsets in patients with multiple sclerosis. Neurosci Lett. 2009;464(1):74-8.
121. von Budingen HC, Kuo TC, Sirota M, van Belle CJ, Apeltsin L, Glanville J, et al. B cell exchange across the blood-brain barrier in multiple sclerosis. J Clin Invest. 2012;122(12):4533-43.
122. Kuenz B, Lutterotti A, Ehling R, Gneiss C, Haemmerle M, Rainer C, et al. Cerebrospinal fluid B cells correlate with early brain inflammation in multiple sclerosis. PLoS One. 2008;3(7):e2559. PMCID: 2438478.
123. Perez L, Alvarez-Cermeno JC, Rodriguez C, Roldan E, Brieva JA. B cells capable of spontaneous IgG secretion in cerebrospinal fluid from patients with multiple sclerosis: dependency on local IL-6 production. Clin Exp Immunol. 1995;101(3):449-52. PMCID: 1553234.
124. Henderson AP, Barnett MH, Parratt JD, Prineas JW. Multiple sclerosis: distribution of inflammatory cells in newly forming lesions. Ann Neurol. 2009;66(6):739-53.
125. Meinl E, Krumbholz M, Hohlfeld R. B lineage cells in the inflammatory central nervous system environment: migratoin, maintenance, local antibody production, and therapeutic modulation. Annals of Neurology. 2006;59(6):880-92.
126. Esiri MM. Immunoglobulin-containing cells in multiple-sclerosis plaques. Lancet. 1977;2(8036):478.
127. Prineas JW, Wright RG. Macrophages, lymphocytes, and plasma cells in the perivascular compartment in chronic multiple sclerosis. Lab Invest. 1978;38(4):409-21.
128. Magliozzi R, Howell O, Vora A, Serafini B, Nicholas R, Puopolo M, et al. Meningeal B-cell follicles in secondary progressive multiple sclerosis associate with early onset of disease and severe cortical pathology. Brain. 2007;130(Pt 4):1089-104.
129. Serafini B, Rosicarelli B, Magliozzi R, Stigliano E, Aloisi F. Detection of ectopic B-cell follicles with germinal centers in the meninges of patients with secondary progressive multiple sclerosis. Brain Pathol. 2004;14(2):164-74.

130. Howell OW, Reeves CA, Nicholas R, Carassiti D, Radotra B, Gentleman SM, et al. Meningeal inflammation is widespread and linked to cortical pathology in multiple sclerosis. Brain. 2011;134(Pt 9):2755-71.
131. Magliozzi R, Howell OW, Reeves C, Roncaroli F, Nicholas R, Serafini B, et al. A Gradient of neuronal loss and meningeal inflammation in multiple sclerosis. Ann Neurol. 2010;68(4):477-93.
132. Fu YX, Huang G, Wang Y, Chaplin DD. B lymphocytes induce the formation of follicular dendritic cell clusters in a lymphotoxin alpha-dependent fashion. J Exp Med. 1998;187(7):1009-18. PMCID: 2212211.
133. Corcione A, Casazza S, Ferretti E, Giunti D, Zappia E, Pistorio A, et al. Recapitulation of B cell differentiation in the central nervous system of patients with multiple sclerosis. Proc Natl Acad Sci U S A. 2004;101(30):11064-9. PMCID: 503741.
134. Corcione A, Aloisi F, Serafini B, Capello E, Mancardi GL, Pistoia V, et al. B-cell differentiation in the CNS of patients with multiple sclerosis. Autoimmun Rev. 2005;4(8):549-54.
135. Kowarik MC, Cepok S, Sellner J, Grummel V, Weber MS, Korn T, et al. CXCL13 is the major determinant for B cell recruitment to the CSF during neuroinflammation. J Neuroinflammation. 2012;9:93. PMCID: 3418196.
136. Sellebjerg F, Bornsen L, Khademi M, Krakauer M, Olsson T, Frederiksen JL, et al. Increased cerebrospinal fluid concentrations of the chemokine CXCL13 in active MS. Neurology. 2009;73(23):2003-10.
137. Kuerten S, Schickel A, Kerkloh C, Recks MS, Addicks K, Ruddle NH, et al. Tertiary lymphoid organ development coincides with determinant spreading of the myelin-specific T cell response. Acta Neuropathol. 2012;124(6):861-73.
138. Kivisakk P, Imitola J, Rasmussen S, Elyaman W, Zhu B, Ransohoff RM, et al. Localizing central nervous system immune surveillance: meningeal antigen-presenting cells activate T cells during experimental autoimmune encephalomyelitis. Ann Neurol. 2009;65(4):457-69. PMCID: 3305810.
139. Roxanis I, Micklem K, McConville J, Newsom-Davis J, Willcox N. Thymic myoid cells and germinal center formation in myasthenia gravis; possible roles in pathogenesis. J Neuroimmunol. 2002;125(1-2):185-97.
140. Magalhaes R, Stiehl P, Morawietz L, Berek C, Krenn V. Morphological and molecular pathology of the B cell response in synovitis of rheumatoid arthritis. Virchows Arch. 2002;441(5):415-27.
141. Takemura S, Braun A, Crowson C, Kurtin PJ, Cofield RH, O'Fallon WM, et al. Lymphoid neogenesis in rheumatoid synovitis. J Immunol. 2001;167(2):1072-80.
142. Hansen A, Odendahl M, Reiter K, Jacobi AM, Feist E, Scholze J, et al. Diminished peripheral blood memory B cells and accumulation of memory B cells in the salivary glands of patients with Sjogren's syndrome. Arthritis Rheum. 2002;46(8):2160-71.
143. Salomonsson S, Jonsson MV, Skarstein K, Brokstad KA, Hjelmstrom P, Wahren-Herlenius M, et al. Cellular basis of ectopic germinal center formation and autoantibody production in the target organ of patients with Sjogren's syndrome. Arthritis Rheum. 2003;48(11):3187-201.
144. Armengol MP, Juan M, Lucas-Martin A, Fernandez-Figueras MT, Jaraquemada D, Gallart T, et al. Thyroid autoimmune disease: demonstration of thyroid antigen-specific B cells and recombination-activating gene expression in

chemokine-containing active intrathyroidal germinal centers. Am J Pathol. 2001;159(3):861-73. PMCID: 1850445.
145. Zhang M, Wang Z, Graner MW, Yang L, Liao M, Yang Q, et al. B cell infiltration is associated with the increased IL-17 and IL-22 expression in the lungs of patients with tuberculosis. Cell Immunol. 2011;270(2):217-23.
146. Stuve O, Bennett JL, Hemmer B, Wiendl H, Racke MK, Bar-Or A, et al. Pharmacological treatment of early multiple sclerosis. Drugs. 2008;68(1):73-83.
147. Teleshova N, Bao W, Kivisakk P, Ozenci V, Mustafa M, Link H. Elevated CD40 ligand expressing blood T-cell levels in multiple sclerosis are reversed by interferon-beta treatment. Scand J Immunol. 2000;51(3):312-20.
148. Liu Z, Pelfrey CM, Cotleur A, Lee JC, Rudick RA. Immunomodulatory effects of interferon beta-1a in multiple sclerosis. J Neuroimmunol. 2001;112(1-2):153-62.
149. Byrnes AA, McArthur JC, Karp CL. Interferon-beta therapy for multiple sclerosis induces reciprocal changes in interleukin-12 and interleukin-10 production. Ann Neurol. 2002;51(2):165-74.
150. Krumbholz M, Faber H, Steinmeyer F, Hoffmann LA, Kumpfel T, Pellkofer H, et al. Interferon-beta increases BAFF levels in multiple sclerosis: implications for B cell autoimmunity. Brain. 2008;131(Pt 6):1455-63.
151. Hemmer B, Stuve O, Kieseier B, Schellekens H, Hartung HP. Immune response to immunotherapy: the role of neutralising antibodies to interferon beta in the treatment of multiple sclerosis. Lancet Neurol. 2005;4(7):403-12.
152. Tanaka M, Tanaka K, Komori M. Interferon-beta(1b) treatment in neuromyelitis optica. Eur Neurol. 2009;62(3):167-70.
153. Palace J, Leite MI, Nairne A, Vincent A. Interferon Beta treatment in neuromyelitis optica: increase in relapses and aquaporin 4 antibody titers. Arch Neurol. 2010;67(8):1016-7.
154. Shimizu Y, Yokoyama K, Misu T, Takahashi T, Fujihara K, Kikuchi S, et al. Development of extensive brain lesions following interferon beta therapy in relapsing neuromyelitis optica and longitudinally extensive myelitis. J Neurol. 2008;255(2):305-7.
155. Teitelbaum D, Webb C, Bree M, Meshorer A, Arnon R, Sela M. Suppression of experimental allergic encephalomyelitis in Rhesus monkeys by a synthetic basic copolymer. Clin Immunol Immunopathol. 1974;3(2):256-62.
156. Johnson KP, Brooks BR, Cohen JA, Ford CC, Goldstein J, Lisak RP, et al. Copolymer 1 reduces relapse rate and improves disability in relapsing-remitting multiple sclerosis: results of a phase III multicenter, double-blind placebo-controlled trial. The Copolymer 1 Multiple Sclerosis Study Group. Neurology. 1995;45(7):1268-76.
157. Comi G, Filippi M, Wolinsky JS. European/Canadian multicenter, double-blind, randomized, placebo-controlled study of the effects of glatiramer acetate on magnetic resonance imaging--measured disease activity and burden in patients with relapsing multiple sclerosis. European/Canadian Glatiramer Acetate Study Group. Ann Neurol. 2001;49(3):290-7.
158. Miller A, Shapiro S, Gershtein R, Kinarty A, Rawashdeh H, Honigman S, et al. Treatment of multiple sclerosis with copolymer-1 (Copaxone): implicating mechanisms of Th1 to Th2/Th3 immune-deviation. J Neuroimmunol. 1998;92(1-2):113-21.

159. Weber MS, Prod'homme T, Youssef S, Dunn SE, Rundle CD, Lee L, et al. Type II monocytes modulate T cell-mediated central nervous system autoimmune disease. Nat Med. 2007;13(8):935-43.
160. Harp CT, Lovett-Racke AE, Racke MK, Frohman EM, Monson NL. Impact of myelin-specific antigen presenting B cells on T cell activation in multiple sclerosis. Clinical Immunology. 2008;128:382-91.
161. Ireland SJ, Blazek M, Harp CT, Greenberg B, Frohman EM, Davis LS, et al. Antibody-independent B cell effector functions in relapsing remitting Multiple Sclerosis: Clues to increased inflammatory and reduced regulatory B cell capacity. Autoimmunity. 2012;45(5):400-14.
162. Corboy JR, Goodin DS, Frohman EM. Disease-modifying Therapies for Multiple Sclerosis. Curr Treat Options Neurol. 2003;5(1):35-54.
163. Hartung HP, Gonsette R, Konig N, Kwiecinski H, Guseo A, Morrissey SP, et al. Mitoxantrone in progressive multiple sclerosis: a placebo-controlled, double-blind, randomised, multicentre trial. Lancet. 2002;360(9350):2018-25.
164. Fidler JM, DeJoy SQ, Gibbons JJ, Jr. Selective immunomodulation by the antineoplastic agent mitoxantrone. I. Suppression of B lymphocyte function. J Immunol. 1986;137(2):727-32.
165. Matloubian M, Lo CG, Cinamon G, Lesneski MJ, Xu Y, Brinkmann V, et al. Lymphocyte egress from thymus and peripheral lymphoid organs is dependent on S1P receptor 1. Nature. 2004;427(6972):355-60.
166. Chiba K, Yanagawa Y, Masubuchi Y, Kataoka H, Kawaguchi T, Ohtsuki M, et al. FTY720, a novel immunosuppressant, induces sequestration of circulating mature lymphocytes by acceleration of lymphocyte homing in rats. I. FTY720 selectively decreases the number of circulating mature lymphocytes by acceleration of lymphocyte homing. J Immunol. 1998;160(10):5037-44.
167. Chun J, Hartung HP. Mechanism of action of oral fingolimod (FTY720) in multiple sclerosis. Clin Neuropharmacol. 2010;33(2):91-101. PMCID: 2859693.
168. Kappos L, Radue EW, O'Connor P, Polman C, Hohlfeld R, Calabresi P, et al. A placebo-controlled trial of oral fingolimod in relapsing multiple sclerosis. N Engl J Med. 2010;362(5):387-401.
169. Kowarik MC, Pellkofer HL, Cepok S, Korn T, Kumpfel T, Buck D, et al. Differential effects of fingolimod (FTY720) on immune cells in the CSF and blood of patients with MS. Neurology. 2011;76(14):1214-21.
170. del Pilar Martin M, Cravens PD, Winger R, Frohman EM, Racke MK, Eagar TN, et al. Decrease in the numbers of dendritic cells and CD4+ T cells in cerebral perivascular spaces due to natalizumab. Arch Neurol. 2008;65(12):1596-603.
171. Khademi M, Bornsen L, Rafatnia F, Andersson M, Brundin L, Piehl F, et al. The effects of natalizumab on inflammatory mediators in multiple sclerosis: prospects for treatment-sensitive biomarkers. Eur J Neurol. 2009;16(4):528-36.
172. Stuve O. The effects of natalizumab on the innate and adaptive immune system in the central nervous system. J Neurol Sci. 2008;274(1-2):39-41.
173. Stuve O, Marra CM, Jerome KR, Cook L, Cravens PD, Cepok S, et al. Immune surveillance in multiple sclerosis patients treated with natalizumab. Ann Neurol. 2006;59(5):743-7.
174. Planas R, Jelcic I, Schippling S, Martin R, Sospedra M. Natalizumab Treatment Perturbs Memory- and Marginal Zone-like B-cell Homing in Secondary Lymphoid Organs in Multiple Sclerosis. Eur J Immunol. 2011.

175. Polman CH, O'Connor PW, Havrdova E, Hutchinson M, Kappos L, Miller DH, et al. A randomized, placebo-controlled trial of natalizumab for relapsing multiple sclerosis. N Engl J Med. 2006;354(9):899-910.
176. Krumbholz M, Meinl I, Kumpfel T, Hohlfeld R, Meinl E. Natalizumab disproportionately increases circulating pre-B and B cells in multiple sclerosis. Neurology. 2008;71(17):1350-4.
177. Villar LM, Garcia-Sanchez MI, Costa-Frossard L, Espino M, Roldan E, Paramo D, et al. Immunological markers of optimal response to natalizumab in multiple sclerosis. Arch Neurol. 2012;69(2):191-7.
178. Gunnarsson M, Malmestrom C, Axelsson M, Sundstrom P, Dahle C, Vrethem M, et al. Axonal damage in relapsing multiple sclerosis is markedly reduced by natalizumab. Ann Neurol. 2011;69(1):83-9.
179. Hauser SL, Waubant E, Arnold DL, Vollmer T, Antel J, Fox RJ, et al. B-cell depletion with rituximab in relapsing-remitting multiple sclerosis. N Engl J Med. 2008;358(7):676-88.
180. Cross AH, Stark JL, Lauber J, Ramsbottom MJ, Lyons JA. Rituximab reduces B cells and T cells in cerebrospinal fluid of multiple sclerosis patients. J Neuroimmunol. 2006;180(1-2):63-70. PMCID: 1769354.
181. Martin Mdel P, Cravens PD, Winger R, Kieseier BC, Cepok S, Eagar TN, et al. Depletion of B lymphocytes from cerebral perivascular spaces by rituximab. Arch Neurol. 2009;66(8):1016-20.
182. Rommer PS, Patejdl R, Winkelmann A, Benecke R, Zettl UK. Rituximab for secondary progressive multiple sclerosis: a case series. CNS Drugs. 2011;25(7):607-13.
183. Kappos L, Li D, Calabresi PA, O'Connor P, Bar-Or A, Barkhof F, et al. Ocrelizumab in relapsing-remitting multiple sclerosis: a phase 2, randomised, placebo-controlled, multicentre trial. Lancet. 2011;378(9805):1779-87.
184. Monson NL, Cravens P, Hussain R, Harp CT, Cummings M, de Pilar Martin M, et al. Rituximab therapy reduces organ-specific T cell responses and ameliorates experimental autoimmune encephalomyelitis. PLoS One. 2011;6(2):e17103. PMCID: 3040191.
185. Sze DM, Toellner KM, Garcia de Vinuesa C, Taylor DR, MacLennan IC. Intrinsic constraint on plasmablast growth and extrinsic limits of plasma cell survival. J Exp Med. 2000;192(6):813-21. PMCID: 2193289.
186. Kim SH, Kim W, Li XF, Jung IJ, Kim HJ. Repeated treatment with rituximab based on the assessment of peripheral circulating memory B cells in patients with relapsing neuromyelitis optica over 2 years. Arch Neurol. 2011;68(11):1412-20.
187. Ferraro AJ, Drayson MT, Savage CO, MacLennan IC. Levels of autoantibodies, unlike antibodies to all extrinsic antigen groups, fall following B cell depletion with Rituximab. Eur J Immunol. 2008;38(1):292-8.
188. Cambridge G, Isenberg DA, Edwards JC, Leandro MJ, Migone TS, Teodorescu M, et al. B cell depletion therapy in systemic lupus erythematosus: relationships among serum B lymphocyte stimulator levels, autoantibody profile and clinical response. Ann Rheum Dis. 2008;67(7):1011-6.
189. Ioannou Y, Lambrianides A, Cambridge G, Leandro MJ, Edwards JC, Isenberg DA. B cell depletion therapy for patients with systemic lupus erythematosus results in a significant drop in anticardiolipin antibody titres. Ann Rheum Dis. 2008;67(3):425-6.

190. Scully M, Cohen H, Cavenagh J, Benjamin S, Starke R, Killick S, et al. Remission in acute refractory and relapsing thrombotic thrombocytopenic purpura following rituximab is associated with a reduction in IgG antibodies to ADAMTS-13. Br J Haematol. 2007;136(3):451-61.
191. Vancsa A, Szabo Z, Szamosi S, Bodnar N, Vegh E, Gergely L, et al. Longterm Effects of Rituximab on B Cell Counts and Autoantibody Production in Rheumatoid Arthritis: Use of High-sensitivity Flow Cytometry for More Sensitive Assessment of B Cell Depletion. J Rheumatol. 2013;40(5):565-71.
192. Lazarus MN, Turner-Stokes T, Chavele KM, Isenberg DA, Ehrenstein MR. B-cell numbers and phenotype at clinical relapse following rituximab therapy differ in SLE patients according to anti-dsDNA antibody levels. Rheumatology (Oxford). 2012;51(7):1208-15. PMCID: 3380246.
193. Colliou N, Picard D, Caillot F, Calbo S, Le Corre S, Lim A, et al. Long-term remissions of severe pemphigus after rituximab therapy are associated with prolonged failure of desmoglein B cell response. Sci Transl Med. 2013;5(175):175ra30.
194. Levine TD, Pestronk A. IgM antibody-related polyneuropathies: B-cell depletion chemotherapy using Rituximab. Neurology. 1999;52(8):1701-4.
195. Zaja F, Russo D, Fuga G, Perella G, Baccarani M. Rituximab for myasthenia gravis developing after bone marrow transplant. Neurology. 2000;55(7):1062-3.
196. Schneider S, Bruns A, Moewes B, Holzknecht B, Hausdorf G, Riemekasten G, et al. Simultaneous cytometric analysis of (auto)antigen-reactive T and B cell proliferation. Immunobiology. 2002;206(5):484-95.
197. Winges KM, Gilden DH, Bennett JL, Yu X, Ritchie AM, Owens GP. Analysis of multiple sclerosis cerebrospinal fluid reveals a continuum of clonally related antibody-secreting cells that are predominantly plasma blasts. J Neuroimmunol. 2007;192(1-2):226-34.
198. Sellam J, Rouanet S, Hendel-Chavez H, Abbed K, Sibilia J, Tebib J, et al. Blood memory B cells are disturbed and predict the response to rituximab in patients with rheumatoid arthritis. Arthritis Rheum. 2011;63(12):3692-701.
199. Odendahl M, Jacobi A, Hansen A, Feist E, Hiepe F, Burmester GR, et al. Disturbed peripheral B lymphocyte homeostasis in systemic lupus erythematosus. J Immunol. 2000;165(10):5970-9.
200. Jacobi AM, Odendahl M, Reiter K, Bruns A, Burmester GR, Radbruch A, et al. Correlation between circulating CD27high plasma cells and disease activity in patients with systemic lupus erythematosus. Arthritis Rheum. 2003;48(5):1332-42.
201. Arce E, Jackson DG, Gill MA, Bennett LB, Banchereau J, Pascual V. Increased frequency of pre-germinal center B cells and plasma cell precursors in the blood of children with systemic lupus erythematosus. J Immunol. 2001;167(4):2361-9.
202. Chihara N, Aranami T, Sato W, Miyazaki Y, Miyake S, Okamoto T, et al. Interleukin 6 signaling promotes anti-aquaporin 4 autoantibody production from plasmablasts in neuromyelitis optica. Proc Natl Acad Sci U S A. 2011;108(9):3701-6. PMCID: 3048150.
203. Lin Q, Gu JR, Li TW, Zhang FC, Lin ZM, Liao ZT, et al. Value of the peripheral blood B-cells subsets in patients with ankylosing spondylitis. Chin Med J (Engl). 2009;122(15):1784-9.

204. Tarlton NJ, Green CM, Lazarus NH, Rott L, Wong AP, Abramson ON, et al. Plasmablast frequency and trafficking receptor expression are altered in pediatric ulcerative colitis. Inflamm Bowel Dis. 2012. PMCID: 3404263.
205. Raghunathan G, Smart J, Williams J, Almagro JC. Antigen-binding site anatomy and somatic mutations in antibodies that recognize different types of antigens. J Mol Recognit. 2012;25(3):103-13.
206. Brezinschek HP, Brezinschek RI, Lipsky PE. Analysis of the heavy chain repertoire of human peripheral B cells using single-cell polymerase chain reaction. J Immunol. 1995;155(1):190-202.
207. Brezinschek HP, Foster SJ, Brezinschek RI, Dorner T, Domiati-Saad R, Lipsky PE. Analysis of the human VH gene repertoire. Differential effects of selection and somatic hypermutation on human peripheral CD5(+)/IgM+ and CD5(-)/IgM+ B cells. J Clin Invest. 1997;99(10):2488-501. PMCID: 508090.
208. Briney BS, Willis JR, McKinney BA, Crowe JE, Jr. High-throughput antibody sequencing reveals genetic evidence of global regulation of the naive and memory repertoires that extends across individuals. Genes Immun. 2012.
209. Tian C, Luskin GK, Dischert KM, Higginbotham JN, Shepherd BE, Crowe JE, Jr. Evidence for preferential Ig gene usage and differential TdT and exonuclease activities in human naive and memory B cells. Mol Immunol. 2007;44(9):2173-83. PMCID: 1859862.
210. Jackson KJ, Kidd MJ, Wang Y, Collins AM. The Shape of the Lymphocyte Receptor Repertoire: Lessons from the B Cell Receptor. Front Immunol. 2013;4:263. PMCID: 3759170.
211. Owens GP, Burgoon MP, Anthony J, Kleinschmidt-DeMasters BK, Gilden DH. The immunoglobulin G heavy chain repertoire in multiple sclerosis plaques is distinct from the heavy chain repertoire in peripheral blood lymphocytes. Clin Immunol. 2001;98(2):258-63.
212. Baranzini SE, Jeong MC, Butunoi C, Murray RS, Bernard CC, Oksenberg JR. B cell repertoire diversity and clonal expansion in multiple sclerosis brain lesions. J Immunol. 1999;163(9):5133-44.
213. Smith-Jensen T, Burgoon MP, Anthony J, Kraus H, Gilden DH, Owens GP. Comparison of immunoglobulin G heavy-chain sequences in MS and SSPE brains reveals an antigen-driven response. Neurology. 2000;54(6):1227-32.
214. Monson NL, Hans-Peter Brezinschek, Ruth I. Brezinschek, Angela Mobley, Gwen K. Vaughan, Elliot M. Frohman, et al. Receptor revision and atypical mutational characteristics in clonally expanded B cells from the cerebrospinal fluid of recently diagnosed mutiple sclerosis patients. Journal of Neuroimmunology. 2005;158:170-81.
215. Qin Y, Duquette P, Zhang Y, Talbot P, Poole R, Antel J. Clonal expansion and somatic hypermutation of V(H) genes of B cells from cerebrospinal fluid in multiple sclerosis. J Clin Invest. 1998;102(5):1045-50. PMCID: 508971.
216. Qin Y, Duquette P, Zhang Y, Olek M, Da RR, Richardson J, et al. Intrathecal B-cell clonal expansion, an early sign of humoral immunity, in the cerebrospinal fluid of patients with clinically isolated syndrome suggestive of multiple sclerosis. Lab Invest. 2003;83(7):1081-8.
217. Owens GP, Ritchie AM, Burgoon MP, Williamson RA, Corboy JR, Gilden DH. Single-cell repertoire analysis demonstrates that clonal expansion is a prominent

feature of the B cell response in multiple sclerosis cerebrospinal fluid. J Immunol. 2003;171(5):2725-33.
218. Colombo M, Dono M, Gazzola P, Roncella S, Valetto A, Chiorazzi N, et al. Accumulation of clonally related B lymphocytes in the cerebrospinal fluid of multiple sclerosis patients. J Immunol. 2000;164(5):2782-9.
219. Colombo M, Dono M, Gazzola P, Chiorazzi N, Mancardi G, Ferrarini M. Maintenance of B lymphocyte-related clones in the cerebrospinal fluid of multiple sclerosis patients. Eur J Immunol. 2003;33(12):3433-8.
220. Harp C, Lee J, Lambracht-Washington D, Cameron E, Olsen G, Frohman E, et al. Cerebrospinal fluid B cells from multiple sclerosis patients are subject to normal germinal center selection. J Neuroimmunol. 2007;183(1-2):189-99. PMCID: 2034205.
221. Ritchie AM, Gilden DH, Williamson RA, Burgoon MP, Yu X, Helm K, et al. Comparative analysis of the CD19+ and CD138+ cell antibody repertoires in the cerebrospinal fluid of patients with multiple sclerosis. J Immunol. 2004;173(1):649-56.
222. Bennett JL, Haubold K, Ritchie AM, Edwards SJ, Burgoon M, Shearer AJ, et al. CSF IgG heavy-chain bias in patients at the time of a clinically isolated syndrome. J Neuroimmunol. 2008;199(1-2):126-32. PMCID: 2572301.
223. Haubold K, Owens GP, Kaur P, Ritchie AM, Gilden DH, Bennett JL. B-lymphocyte and plasma cell clonal expansion in monosymptomatic optic neuritis cerebrospinal fluid. Ann Neurol. 2004;56(1):97-107.
224. Hendricks J, Visser A, Dammers PM, Burgerhof JG, Bos NA, Kroese FG. Class-switched marginal zone B cells in spleen have relatively low numbers of somatic mutations. Mol Immunol. 2011;48(6-7):874-82.
225. Galicia G, Boulianne B, Pikor N, Martin A, Gommerman JL. Secondary B Cell Receptor Diversification Is Necessary for T Cell Mediated Neuro-Inflammation during Experimental Autoimmune Encephalomyelitis. PLoS One. 2013;8(4):e61478. PMCID: 3632548.
226. Dorner T, Foster SJ, Farner NL, Lipsky PE. Somatic hypermutation of human immunoglobulin heavy chain genes: targeting of RGYW motifs on both DNA strands. Eur J Immunol. 1998;28(10):3384-96.
227. Dorner T, Brezinschek HP, Foster SJ, Brezinschek RI, Farner NL, Lipsky PE. Delineation of selective influences shaping the mutated expressed human Ig heavy chain repertoire. J Immunol. 1998;160(6):2831-41.
228. Cameron EM, Spencer S, Lazarini J, Harp CT, Ward ES, Burgoon M, et al. Potential of a unique antibody gene signature to predict conversion to clinically definite multiple sclerosis. Journal of Neuroimmunology. 2009;213:123-30.
229. Owens GP, Kraus H, Burgoon MP, Smith-Jensen T, Devlin ME, Gilden DH. Restricted use of VH4 germline segments in an acute multiple sclerosis brain. Ann Neurol. 1998;43(2):236-43.
230. Owens GP, Winges KM, Ritchie AM, Edwards S, Burgoon MP, Lehnhoff L, et al. VH4 gene segments dominate the intrathecal humoral immune response in multiple sclerosis. J Immunol. 2007;179(9):6343-51.
231. Singh V, Stoop MP, Stingl C, Luitwieler RL, Dekker LJ, Vanduijn MM, et al. Cerebrospinal fluid derived immunoglobulin G of different multiple sclerosis patients share mutated sequences in complementarity determining regions. Mol Cell Proteomics. 2013.

232. Obermeier B, Lovato L, Mentele R, Bruck W, Forne I, Imhof A, et al. Related B cell clones that populate the CSF and CNS of patients with multiple sclerosis produce CSF immunoglobulin. J Neuroimmunol. 2011;233(1-2):245-8. PMCID: 3090654.
233. Birgit Obermeier RM, Joachim Malotka, Josef Kellermann, Tania Kumpfel, Hartmut Wekerle, Friedrich Lottspeich, Reinhard Hohlfeld, Klaus Dornmair. Matching of oligoclonal immunoglobulin transcriptomes and proteomes of cerebrospinal fluid in multiple sclerosis. Nature Medicine. 2008;14(6):688-93.
234. Lovato L, Willis SN, Rodig SJ, Caron T, Almendinger SE, Howell OW, et al. Related B cell clones populate the meninges and parenchyma of patients with multiple sclerosis. Brain. 2011.
235. Vyshkina T, Kalman B. Autoantibodies and neurodegeneration in multiple sclerosis. Lab Invest. 2008;88(8):796-807.
236. Beyer NH, Lueking A, Kowald A, Frederiksen JL, Heegaard NH. Investigation of autoantibody profiles for cerebrospinal fluid biomarker discovery in patients with relapsing-remitting multiple sclerosis. J Neuroimmunol. 2012;242(1-2):26-32.
237. Lalive PH. Autoantibodies in inflammatory demyelinating diseases of the central nervous system. Swiss Med Wkly. 2008;138(47-48):692-707.
238. Appel SH, Bornstein MB. The Application of Tissue Culture to the Study of Experimental Allergic Encephalomyelitis. Ii. Serum Factors Responsible for Demyelination. J Exp Med. 1964;119:303-12. PMCID: 2137833.
239. Seil FJ, Falk GA, Kies MW, Alvord EC, Jr. The in vitro demyelinating activity of sera from guinea pigs sensitized with whole CNS and with purified encephalitogen. Exp Neurol. 1968;22(4):545-55.
240. Linington C, Bradl M, Lassmann H, Brunner C, Vass K. Augmentation of demyelination in rat acute allergic encephalomyelitis by circulating mouse monoclonal antibodies directed against a myelin/oligodendrocyte glycoprotein. Am J Pathol. 1988;130(3):443-54. PMCID: 1880661.
241. Schluesener HJ, Sobel RA, Linington C, Weiner HL. A monoclonal antibody against a myelin oligodendrocyte glycoprotein induces relapses and demyelination in central nervous system autoimmune disease. J Immunol. 1987;139(12):4016-21.
242. Diego Franciotta, Marco Salvetti, Francesco Lolli, Barbara Serfini, Aloisi F. B cells and multiple sclerosis. The Lancet Neurology. 2008;7:852-8.
243. Farrell RA, Antony D, Wall GR, Clark DA, Fisniku L, Swanton J, et al. Humoral immune response to EBV in multiple sclerosis is associated with disease activity on MRI. Neurology. 2009;73(1):32-8.
244. Yao SY, Stratton CW, Mitchell WM, Sriram S. CSF oligoclonal bands in MS include antibodies against Chlamydophila antigens. Neurology. 2001;56(9):1168-76.
245. Hughes LE, Smith PA, Bonell S, Natt RS, Wilson C, Rashid T, et al. Cross-reactivity between related sequences found in Acinetobacter sp., Pseudomonas aeruginosa, myelin basic protein and myelin oligodendrocyte glycoprotein in multiple sclerosis. J Neuroimmunol. 2003;144(1-2):105-15.
246. Fraussen J, Vrolix K, Martinez-Martinez P, Losen M, De Baets MH, Stinissen P, et al. B cell characterization and reactivity analysis in multiple sclerosis. Autoimmun Rev. 2009;8(8):654-8.

247. Quarles RH. Comparison of CNS and PNS myelin proteins in the pathology of myelin disorders. J Neurol Sci. 2005;228(2):187-9.
248. Berger T, Rubner P, Schautzer F, Egg R, Ulmer H, Mayringer I, et al. Antimyelin antibodies as a predictor of clinically definite multiple sclerosis after a first demyelinating event. N Engl J Med. 2003;349(2):139-45.
249. Vogt MH, Teunissen CE, Iacobaeus E, Heijnen DA, Breij EC, Olsson T, et al. Cerebrospinal fluid anti-myelin antibodies are related to magnetic resonance measures of disease activity in multiple sclerosis. J Neurol Neurosurg Psychiatry. 2009;80(10):1110-5.
250. Zhou D, Srivastava R, Nessler S, Grummel V, Sommer N, Bruck W, et al. Identification of a pathogenic antibody response to native myelin oligodendrocyte glycoprotein in multiple sclerosis. Proc Natl Acad Sci U S A. 2006;103(50):19057-62. PMCID: 1748176.
251. Breij EC, Heijnen P, van der Goes A, Teunissen CE, Polman CH, Dijkstra CD. Myelin flow cytometry assay detects enhanced levels of antibodies to human whole myelin in a subpopulation of multiple sclerosis patients. J Neuroimmunol. 2006;176(1-2):106-14.
252. O'Connor KC, Appel H, Bregoli L, Call ME, Catz I, Chan JA, et al. Antibodies from inflamed central nervous system tissue recognize myelin oligodendrocyte glycoprotein. J Immunol. 2005;175(3):1974-82.
253. Gaertner S, de Graaf KL, Greve B, Weissert R. Antibodies against glycosylated native MOG are elevated in patients with multiple sclerosis. Neurology. 2004;63(12):2381-3.
254. Tejada-Simon MV, Hong J, Rivera VM, Zhang JZ. Skewed autoantibody reactivity to the extracellular domain of myelin oligodendrocyte glycoprotein in multiple sclerosis. Immunology. 2002;107(4):403-10. PMCID: 1782818.
255. Lambracht-Washington D, O'Connor KC, Cameron EM, Jowdry A, Ward ES, Frohman E, et al. Antigen specificity of clonally expanded and receptor edited cerebrospinal fluid B cells from patients with relapsing remitting MS. J Neuroimmunol. 2007;186(1-2):164-76. PMCID: 2709235.
256. Genain CP, Nguyen MH, Letvin NL, Pearl R, Davis RL, Adelman M, et al. Antibody facilitation of multiple sclerosis-like lesions in a nonhuman primate. J Clin Invest. 1995;96(6):2966-74. PMCID: 186008.
257. Kuerten S, Pauly R, Rottlaender A, Rodi M, Gruppe TL, Addicks K, et al. Myelin-reactive antibodies mediate the pathology of MBP-PLP fusion protein MP4-induced EAE. Clin Immunol. 2011;140(1):54-62.
258. Challa DK, Bussmeyer U, Khan T, Montoyo HP, Bansal P, Ober RJ, et al. Autoantibody depletion ameliorates disease in murine experimental autoimmune encephalomyelitis. MAbs. 2013;5(5).
259. Angelucci F, Mirabella M, Frisullo G, Caggiula M, Tonali PA, Batocchi AP. Serum levels of anti-myelin antibodies in relapsing-remitting multiple sclerosis patients during different phases of disease activity and immunomodulatory therapy. Dis Markers. 2005;21(2):49-55.
260. Klawiter EC, Piccio L, Lyons JA, Mikesell R, O'Connor KC, Cross AH. Elevated intrathecal myelin oligodendrocyte glycoprotein antibodies in multiple sclerosis. Arch Neurol. 2010;67(9):1102-8.
261. Tewarie P, Teunissen CE, Dijkstra CD, Heijnen DA, Vogt M, Balk L, et al. Cerebrospinal fluid anti-whole myelin antibodies are not correlated to magnetic

resonance imaging activity in multiple sclerosis. J Neuroimmunol. 2012;251(1-2):103-6.
262. Kuhle J, Pohl C, Mehling M, Edan G, Freedman MS, Hartung HP, et al. Lack of association between antimyelin antibodies and progression to multiple sclerosis. N Engl J Med. 2007;356(4):371-8.
263. Lampasona V, Franciotta D, Furlan R, Zanaboni S, Fazio R, Bonifacio E, et al. Similar low frequency of anti-MOG IgG and IgM in MS patients and healthy subjects. Neurology. 2004;62(11):2092-4.
264. Karni A, Bakimer-Kleiner R, Abramsky O, Ben-Nun A. Elevated levels of antibody to myelin oligodendrocyte glycoprotein is not specific for patients with multiple sclerosis. Arch Neurol. 1999;56(3):311-5.
265. O'Connor KC, Chitnis T, Griffin DE, Piyasirisilp S, Bar-Or A, Khoury S, et al. Myelin basic protein-reactive autoantibodies in the serum and cerebrospinal fluid of multiple sclerosis patients are characterized by low-affinity interactions. J Neuroimmunol. 2003;136(1-2):140-8.
266. Gori F, Mulinacci B, Massai L, Avolio C, Caragnano M, Peroni E, et al. IgG and IgM antibodies to the refolded MOG(1-125) extracellular domain in humans. J Neuroimmunol. 2011;233(1-2):216-20.
267. Owens GP, Bennett JL, Lassmann H, O'Connor KC, Ritchie AM, Shearer A, et al. Antibodies produced by clonally expanded plasma cells in multiple sclerosis cerebrospinal fluid. Ann Neurol. 2009;65(6):639-49.
268. von Budingen HC, Harrer MD, Kuenzle S, Meier M, Goebels N. Clonally expanded plasma cells in the cerebrospinal fluid of MS patients produce myelin-specific antibodies. Eur J Immunol. 2008;38(7):2014-23.
269. Elliott C, Lindner M, Arthur A, Brennan K, Jarius S, Hussey J, et al. Functional identification of pathogenic autoantibody responses in patients with multiple sclerosis. Brain. 2012;135(Pt 6):1819-33. PMCID: 3359756.
270. Prineas JW, Barnard RO, Kwon EE, Sharer LR, Cho ES. Multiple sclerosis: remyelination of nascent lesions. Ann Neurol. 1993;33(2):137-51.
271. Niehaus A, Shi J, Grzenkowski M, Diers-Fenger M, Archelos J, Hartung HP, et al. Patients with active relapsing-remitting multiple sclerosis synthesize antibodies recognizing oligodendrocyte progenitor cell surface protein: implications for remyelination. Ann Neurol. 2000;48(3):362-71.
272. Reindl M, Khantane S, Ehling R, Schanda K, Lutterotti A, Brinkhoff C, et al. Serum and cerebrospinal fluid antibodies to Nogo-A in patients with multiple sclerosis and acute neurological disorders. J Neuroimmunol. 2003;145(1-2):139-47.
273. Lovato L, Cianti R, Gini B, Marconi S, Bianchi L, Armini A, et al. Transketolase and 2',3'-cyclic-nucleotide 3'-phosphodiesterase type I isoforms are specifically recognized by IgG autoantibodies in multiple sclerosis patients. Mol Cell Proteomics. 2008;7(12):2337-49.
274. Walsh MJ, Murray JM. Dual implication of 2',3'-cyclic nucleotide 3' phosphodiesterase as major autoantigen and C3 complement-binding protein in the pathogenesis of multiple sclerosis. J Clin Invest. 1998;101(9):1923-31. PMCID: 508779.
275. Bronstein JM, Lallone RL, Seitz RS, Ellison GW, Myers LW. A humoral response to oligodendrocyte-specific protein in MS: a potential molecular mimic. Neurology. 1999;53(1):154-61.

276. Aslam M, Kalluri SR, Cepok S, Kraus V, Buck D, Srivastava R, et al. The antibody response to oligodendrocyte specific protein in multiple sclerosis. J Neuroimmunol. 2010;221(1-2):81-6.
277. Colombo E, Banki K, Tatum AH, Daucher J, Ferrante P, Murray RS, et al. Comparative analysis of antibody and cell-mediated autoimmunity to transaldolase and myelin basic protein in patients with multiple sclerosis. J Clin Invest. 1997;99(6):1238-50. PMCID: 507938.
278. Niland B, Perl A. Evaluation of autoimmunity to transaldolase in multiple sclerosis. Methods Mol Med. 2004;102:155-71.
279. Alcazar A, Regidor I, Masjuan J, Salinas M, Alvarez-Cermeno JC. Axonal damage induced by cerebrospinal fluid from patients with relapsing-remitting multiple sclerosis. J Neuroimmunol. 2000;104(1):58-67.
280. Cid C, Alcazar A, Regidor I, Masjuan J, Salinas M, Alvarez-Cermeno JC. Neuronal apoptosis induced by cerebrospinal fluid from multiple sclerosis patients correlates with hypointense lesions on T1 magnetic resonance imaging. J Neurol Sci. 2002;193(2):103-9.
281. Zhang Y, Da RR, Guo W, Ren HM, Hilgenberg LG, Sobel RA, et al. Axon reactive B cells clonally expanded in the cerebrospinal fluid of patients with multiple sclerosis. J Clin Immunol. 2005;25(3):254-64.
282. Zhang Y, Da RR, Hilgenberg LG, Tourtellotte WW, Sobel RA, Smith MA, et al. Clonal expansion of IgA-positive plasma cells and axon-reactive antibodies in MS lesions. J Neuroimmunol. 2005;167(1-2):120-30.
283. Meyer R, Weissert R, Diem R, Storch MK, de Graaf KL, Kramer B, et al. Acute neuronal apoptosis in a rat model of multiple sclerosis. J Neurosci. 2001;21(16):6214-20.
284. Einstein O, Friedman-Levi Y, Grigoriadis N, Ben-Hur T. Transplanted neural precursors enhance host brain-derived myelin regeneration. J Neurosci. 2009;29(50):15694-702.
285. Lily O, Palace J, Vincent A. Serum autoantibodies to cell surface determinants in multiple sclerosis: a flow cytometric study. Brain. 2004;127(Pt 2):269-79.
286. Kuhle J, Leppert D, Petzold A, Regeniter A, Schindler C, Mehling M, et al. Neurofilament heavy chain in CSF correlates with relapses and disability in multiple sclerosis. Neurology. 2011;76(14):1206-13.
287. Teunissen CE, Iacobaeus E, Khademi M, Brundin L, Norgren N, Koel-Simmelink MJ, et al. Combination of CSF N-acetylaspartate and neurofilaments in multiple sclerosis. Neurology. 2009;72(15):1322-9.
288. Fialova L, Bartos A, Svarcova J, Zimova D, Kotoucova J. Serum and cerebrospinal fluid heavy neurofilaments and antibodies against them in early multiple sclerosis. J Neuroimmunol. 2013.
289. Silber E, Semra YK, Gregson NA, Sharief MK. Patients with progressive multiple sclerosis have elevated antibodies to neurofilament subunit. Neurology. 2002;58(9):1372-81.
290. Eikelenboom MJ, Petzold A, Lazeron RH, Silber E, Sharief M, Thompson EJ, et al. Multiple sclerosis: Neurofilament light chain antibodies are correlated to cerebral atrophy. Neurology. 2003;60(2):219-23.
291. Bartos A, Fialova L, Soukupova J, Kukal J, Malbohan I, Pit'ha J. Elevated intrathecal antibodies against the medium neurofilament subunit in multiple sclerosis. J Neurol. 2007;254(1):20-5.

292. Huizinga R, Gerritsen W, Heijmans N, Amor S. Axonal loss and gray matter pathology as a direct result of autoimmunity to neurofilaments. Neurobiol Dis. 2008;32(3):461-70.
293. Huizinga R, Heijmans N, Schubert P, Gschmeissner S, t Hart BA, Herrmann H, et al. Immunization with neurofilament light protein induces spastic paresis and axonal degeneration in Biozzi ABH mice. J Neuropathol Exp Neurol. 2007;66(4):295-304.
294. Svarcova J, Fialova L, Bartos A, Steinbachova M, Malbohan I. Cerebrospinal fluid antibodies to tubulin are elevated in the patients with multiple sclerosis. Eur J Neurol. 2008;15(11):1173-9.
295. Terryberry JW, Thor G, Peter JB. Autoantibodies in neurodegenerative diseases: antigen-specific frequencies and intrathecal analysis. Neurobiol Aging. 1998;19(3):205-16.
296. Mathey EK, Derfuss T, Storch MK, Williams KR, Hales K, Woolley DR, et al. Neurofascin as a novel target for autoantibody-mediated axonal injury. J Exp Med. 2007;204(10):2363-72. PMCID: 2118456.
297. Lindner M, Ng JK, Hochmeister S, Meinl E, Linington C. Neurofascin 186 specific autoantibodies induce axonal injury and exacerbate disease severity in experimental autoimmune encephalomyelitis. Exp Neurol. 2013.
298. Charles P, Tait S, Faivre-Sarrailh C, Barbin G, Gunn-Moore F, Denisenko-Nehrbass N, et al. Neurofascin is a glial receptor for the paranodin/Caspr-contactin axonal complex at the axoglial junction. Curr Biol. 2002;12(3):217-20.
299. Derfuss T, Parikh K, Velhin S, Braun M, Mathey E, Krumbholz M, et al. Contactin-2/TAG-1-directed autoimmunity is identified in multiple sclerosis patients and mediates gray matter pathology in animals. Proc Natl Acad Sci U S A. 2009;106(20):8302-7. PMCID: 2688870.
300. Forooghian F, Cheung RK, Smith WC, O'Connor P, Dosch HM. Enolase and arrestin are novel nonmyelin autoantigens in multiple sclerosis. J Clin Immunol. 2007;27(4):388-96. PMCID: 2705966.
301. Gelderblom M, Daehn T, Schattling B, Ludewig P, Bernreuther C, Arunachalam P, et al. Plasma levels of neuron specific enolase quantify the extent of neuronal injury in murine models of ischemic stroke and multiple sclerosis. Neurobiol Dis. 2013;59:177-82.
302. Brosnan CF, Raine CS. The astrocyte in multiple sclerosis revisited. Glia. 2013;61(4):453-65.
303. Talbott JF, Loy DN, Liu Y, Qiu MS, Bunge MB, Rao MS, et al. Endogenous Nkx2.2+/Olig2+ oligodendrocyte precursor cells fail to remyelinate the demyelinated adult rat spinal cord in the absence of astrocytes. Exp Neurol. 2005;192(1):11-24. PMCID: 2813490.
304. Sorensen A, Moffat K, Thomson C, Barnett SC. Astrocytes, but not olfactory ensheathing cells or Schwann cells, promote myelination of CNS axons in vitro. Glia. 2008;56(7):750-63.
305. Faulkner JR, Herrmann JE, Woo MJ, Tansey KE, Doan NB, Sofroniew MV. Reactive astrocytes protect tissue and preserve function after spinal cord injury. J Neurosci. 2004;24(9):2143-55.
306. Pekovic D, Raine CS, Traugott U. Increase in anti-astrocyte antibodies in the serum of guinea pigs during active stages of experimental autoimmune encephalomyelitis. J Neuroimmunol. 1990;26(3):251-9.

307. Wang D, Ayers MM, Catmull DV, Hazelwood LJ, Bernard CC, Orian JM. Astrocyte-associated axonal damage in pre-onset stages of experimental autoimmune encephalomyelitis. Glia. 2005;51(3):235-40.
308. Bennett JL, Lam C, Kalluri SR, Saikali P, Bautista K, Dupree C, et al. Intrathecal pathogenic anti-aquaporin-4 antibodies in early neuromyelitis optica. Ann Neurol. 2009;66(5):617-29. PMCID: 3180961.
309. Bradl M, Misu T, Takahashi T, Watanabe M, Mader S, Reindl M, et al. Neuromyelitis optica: pathogenicity of patient immunoglobulin in vivo. Ann Neurol. 2009;66(5):630-43.
310. Saikali P, Cayrol R, Vincent T. Anti-aquaporin-4 auto-antibodies orchestrate the pathogenesis in neuromyelitis optica. Autoimmun Rev. 2009;9(2):132-5.
311. Kinoshita M, Nakatsuji Y, Kimura T, Moriya M, Takata K, Okuno T, et al. Anti-aquaporin-4 antibody induces astrocytic cytotoxicity in the absence of CNS antigen-specific T cells. Biochem Biophys Res Commun. 2010;394(1):205-10.
312. Kinoshita M, Nakatsuji Y, Kimura T, Moriya M, Takata K, Okuno T, et al. Neuromyelitis optica: Passive transfer to rats by human immunoglobulin. Biochem Biophys Res Commun. 2009;386(4):623-7.
313. Saadoun S, Waters P, Bell BA, Vincent A, Verkman AS, Papadopoulos MC. Intra-cerebral injection of neuromyelitis optica immunoglobulin G and human complement produces neuromyelitis optica lesions in mice. Brain. 2010;133(Pt 2):349-61. PMCID: 2822632.
314. Srivastava R, Aslam M, Kalluri SR, Schirmer L, Buck D, Tackenberg B, et al. Potassium channel KIR4.1 as an immune target in multiple sclerosis. N Engl J Med. 2012;367(2):115-23.
315. Trojano M, Defazio G, Ricchiuti F, De Salvia R, Livrea P. Serum IgG to brain microvascular endothelial cells in multiple sclerosis. J Neurol Sci. 1996;143(1-2):107-13.
316. Long Y, Gao C, Qiu W, Hu X, Peng F, Lu Z. Antibodies target microvessels in neuromyelitis optica and multiple sclerosis patients. Neurol Res. 2013.
317. Proia P, Schiera G, Salemi G, Ragonese P, Savettieri G, Di Liegro I. Neuronal and BBB damage induced by sera from patients with secondary progressive multiple sclerosis. Int J Mol Med. 2009;24(6):743-7.
318. Schiera G, Sala S, Gallo A, Raffa MP, Pitarresi GL, Savettieri G, et al. Permeability properties of a three-cell type in vitro model of blood-brain barrier. J Cell Mol Med. 2005;9(2):373-9.
319. Bansal P, Khan T, Bussmeyer U, Challa DK, Swiercz R, Velmurugan R, et al. The Encephalitogenic, Human Myelin Oligodendrocyte Glycoprotein-Induced Antibody Repertoire Is Directed toward Multiple Epitopes in C57BL/6-Immunized Mice. J Immunol. 2013;191(3):1091-101.
320. Kuhle J, Lindberg RL, Regeniter A, Mehling M, Hoffmann F, Reindl M, et al. Antimyelin antibodies in clinically isolated syndromes correlate with inflammation in MRI and CSF. J Neurol. 2007;254(2):160-8.
321. Somers V, Govarts C, Somers K, Hupperts R, Medaer R, Stinissen P. Autoantibody profiling in multiple sclerosis reveals novel antigenic candidates. J Immunol. 2008;180(6):3957-63.
322. Greenfield EA, Reddy J, Lees A, Dyer CA, Koul O, Nguyen K, et al. Monoclonal antibodies to distinct regions of human myelin proteolipid protein simultaneously

recognize central nervous system myelin and neurons of many vertebrate species. J Neurosci Res. 2006;83(3):415-31.
323. Quintana FJ, Farez MF, Viglietta V, Iglesias AH, Merbl Y, Izquierdo G, et al. Antigen microarrays identify unique serum autoantibody signatures in clinical and pathologic subtypes of multiple sclerosis. Proc Natl Acad Sci U S A. 2008;105(48):18889-94. PMCID: 2596207.
324. Quintana FJ, Farez MF, Izquierdo G, Lucas M, Cohen IR, Weiner HL. Antigen microarrays identify CNS-produced autoantibodies in RRMS. Neurology. 2012;78(8):532-9. PMCID: 3280015.
325. Kanter JL, Narayana S, Ho PP, Catz I, Warren KG, Sobel RA, et al. Lipid microarrays identify key mediators of autoimmune brain inflammation. Nat Med. 2006;12(1):138-43.
326. Cid C, Alvarez-Cermeno JC, Salinas M, Alcazar A. Anti-heat shock protein 90beta antibodies decrease pre-oligodendrocyte population in perinatal and adult cell cultures. Implications for remyelination in multiple sclerosis. J Neurochem. 2005;95(2):349-60.
327. Beltran E, Hernandez A, Lafuente EM, Coret F, Simo-Castello M, Bosca I, et al. Neuronal antigens recognized by cerebrospinal fluid IgM in multiple sclerosis. J Neuroimmunol. 2012;247(1-2):63-9.
328. Tiller T, Meffre E, Yurasov S, Tsuiji M, Nussenzweig MC, Wardemann H. Efficient generation of monoclonal antibodies from single human B cells by single cell RT-PCR and expression vector cloning. J Immunol Methods. 2008;329(1-2):112-24. PMCID: 2243222.
329. Lefranc MP. IMGT, the international ImMunoGeneTics database. Nucleic Acids Res. 2001;29(1):207-9. PMCID: 29797.
330. Willis SN, Mallozzi SS, Rodig SJ, Cronk KM, McArdel SL, Caron T, et al. The microenvironment of germ cell tumors harbors a prominent antigen-driven humoral response. J Immunol. 2009;182(5):3310-7.
331. Boyd SD, Marshall EL, Merker JD, Maniar JM, Zhang LN, Sahaf B, et al. Measurement and clinical monitoring of human lymphocyte clonality by massively parallel VDJ pyrosequencing. Sci Transl Med. 2009;1(12):12ra23. PMCID: 2819115.
332. van Dongen JJ, Langerak AW, Bruggemann M, Evans PA, Hummel M, Lavender FL, et al. Design and standardization of PCR primers and protocols for detection of clonal immunoglobulin and T-cell receptor gene recombinations in suspect lymphoproliferations: report of the BIOMED-2 Concerted Action BMH4-CT98-3936. Leukemia. 2003;17(12):2257-317.
333. Ligocki AJ, Rounds WH, Cameron EM, Harp CT, Frohman EM, Courtney AM, et al. Expansion of CD27 plasmablasts in transverse myelitis patients that utilize VH4 and JH6 genes and undergo extensive somatic hypermutation. Genes Immun. 2013.
334. Kabat EA, Wu TT, Bilofsky H, Reid-Miller M, Perry H. Sequences of Proteins of Immunological Interest. Washington, D.C.: United States Department of Health and Human Services; 1983.
335. Champe PC, Harvey RA. Lippincott's Illustrated Reviews: Biochemistry. 2nd ed: Lippincott-Raven Publishers; 1994.

336. Yurasov S, Wardemann H, Hammersen J, Tsuiji M, Meffre E, Pascual V, et al. Defective B cell tolerance checkpoints in systemic lupus erythematosus. J Exp Med. 2005;201(5):703-11. PMCID: 2212839.
337. Zhang J, Jacobi AM, Wang T, Berlin R, Volpe BT, Diamond B. Polyreactive autoantibodies in systemic lupus erythematosus have pathogenic potential. J Autoimmun. 2009;33(3-4):270-4. PMCID: 2783480.
338. Inoue H, Nojima H, Okayama H. High efficiency transformation of *Escherichia coli* with plasmids. Gene. 1990;96:23-8.
339. Stowe AM, Altay T, Freie AB, Gidday JM. Repetitive hypoxia extends endogenous neurovascular protection for stroke. Ann Neurol. 2011;69(6):975-85. PMCID: 3117913.
340. Ligocki AJ, Lovato L, Xiang D, Guidry P, Scheuermann RH, Willis SN, et al. A unique antibody gene signature is prevalent in the central nervous system of patients with multiple sclerosis. J Neuroimmunol. 2010;226(1-2):192-3.
341. Antel J, Bar-Or A. Roles of immunoglobulins and B cells in multiple sclerosis: From pathogenesis to treatment. Journal of Neuroimmunology. 2006;180:3-8.
342. Owens GP, Bennett JL, Gilden DH, Burgoon MP. The B cell response in multiple sclerosis. Neurological Research. 2006;28(3):236-44.
343. Duddy M, Bar-Or A. B-cells in Multiple Sclerosis. The International MS Journal. 2006;13:84-90.
344. McFarland HF. The B cell--old player, new position on the team. N Engl J Med. 2008;358(7):664-5.
345. Monson NL, Cravens PD, Frohman EM, Hawker K, Racke MK. Effect of Rituximab on the peripheral blood and cerebrospinal fluid b cells in patients with primary progressive multiple sclerosis. Archives of Neurology. 2005;62:258-64.
346. Uccelli A, Aloisi F, Pistoia V. Unveiling the enigma of the CNS as a B-cell fostering environment. Trends Immunol. 2005;26(5):254-9.
347. Pittock SJ, Lucchinetti CF. The pathology of MS: new insights and potential clinical applications. Neurologist. 2007;13(2):45-56.
348. Ransohoff RM, Kivisakk P, Kidd G. Three or more routes for leukocyte migration into the central nervous system. Nat Rev Immunol. 2003;3(7):569-81.
349. Gajofatto A, Monaco S, Fiorini M, Zanusso G, Vedovello M, Rossi F, et al. Assessment of outcome predictors in first-episode acute myelitis: a retrospective study of 53 cases. Arch Neurol. 2010;67(6):724-30.
350. Rot U, Ledinek AH, Jazbec SS. Clinical, magnetic resonance imaging, cerebrospinal fluid and electrophysiological characteristics of the earliest multiple sclerosis. Clin Neurol Neurosurg. 2008;110(3):233-8.
351. Tintore M, Rovira A, Arrambide G, Mitjana R, Rio J, Auger C, et al. Brainstem lesions in clinically isolated syndromes. Neurology. 2010;75(21):1933-8.
352. Frohman EM, Filippi M, Stuve O, Waxman SG, Corboy J, Phillips JT, et al. Characterizing the mechanisms of progression in multiple sclerosis: evidence and new hypotheses for future directions. Arch Neurol. 2005;62(9):1345-56.
353. Yang DH, Chang DM, Lai JH, Lin FH, Chen CH. Significantly higher percentage of circulating CD27(high) plasma cells in systemic lupus erythematosus patients with infection than with disease flare-up. Yonsei Med J. 2010;51(6):924-31. PMCID: 2995985.
354. Boekel ET, Prins M, Vrielink GJ, de Kieviet W, Siegert CE. Longitudinal studies of the association between peripheral CD27++ plasma cells and systemic lupus

erythematosus disease activity: preliminary results. Ann Rheum Dis. 2011;70(7):1341-2.
355. de Graaf M, de Beukelaar J, Bergsma J, Kraan J, van den Bent M, Klimek M, et al. B and T cell imbalances in CSF of patients with Hu-antibody associated PNS. J Neuroimmunol. 2008;195(1-2):164-70.
356. Pranzatelli MR, Travelstead AL, Tate ED, Allison TJ, Verhulst SJ. CSF B-cell expansion in opsoclonus-myoclonus syndrome: a biomarker of disease activity. Mov Disord. 2004;19(7):770-7.
357. Blaes F, Tschernatsch M. Paraneoplastic neurological disorders. Expert Rev Neurother. 2010;10(10):1559-68.
358. Zuckerman NS, Hazanov H, Barak M, Edelman H, Hess S, Shcolnik H, et al. Somatic hypermutation and antigen-driven selection of B cells are altered in autoimmune diseases. J Autoimmun.
359. Kalinina O, Doyle-Cooper CM, Miksanek J, Meng W, Prak EL, Weigert MG. Alternative mechanisms of receptor editing in autoreactive B cells. Proc Natl Acad Sci U S A. 2011;108(17):7125-30. PMCID: 3084116.
360. Meffre E, Milili M, Blanco-Betancourt C, Antunes H, Nussenzweig MC, Schiff C. Immunoglobulin heavy chain expression shapes the B cell receptor repertoire in human B cell development. J Clin Invest. 2001;108(6):879-86. PMCID: 200933.
361. Owczarczyk K, Lal P, Abbas AR, Wolslegel K, Holweg CT, Dummer W, et al. A plasmablast biomarker for nonresponse to antibody therapy to CD20 in rheumatoid arthritis. Sci Transl Med. 2011;3(101):101ra92.
362. Vital EM, Dass S, Buch MH, Henshaw K, Pease CT, Martin MF, et al. B cell biomarkers of rituximab responses in systemic lupus erythematosus. Arthritis Rheum. 2011;63(10):3038-47.
363. Lee-Chang C, Top I, Zephir H, Dubucquoi S, Trauet J, Dussart P, et al. Primed status of transitional B cells associated with their presence in the cerebrospinal fluid in early phases of multiple sclerosis. Clin Immunol. 2011;139(1):12-20.
364. Odendahl M, Mei H, Hoyer BF, Jacobi AM, Hansen A, Muehlinghaus G, et al. Generation of migratory antigen-specific plasma blasts and mobilization of resident plasma cells in a secondary immune response. Blood. 2005;105(4):1614-21.
365. Barbas SM, Ditzel HJ, Salonen EM, Yang WP, Silverman GJ, Burton DR. Human autoantibody recognition of DNA. Proc Natl Acad Sci U S A. 1995;92(7):2529-33. PMCID: 42251.
366. Itoh K, Meffre E, Albesiano E, Farber A, Dines D, Stein P, et al. Immunoglobulin heavy chain variable region gene replacement As a mechanism for receptor revision in rheumatoid arthritis synovial tissue B lymphocytes. J Exp Med. 2000;192(8):1151-64. PMCID: 2195868.
367. Vercellino M, Plano F, Votta B, Mutani R, Giordana MT, Cavalla P. Grey matter pathology in multiple sclerosis. J Neuropathol Exp Neurol. 2005;64(12):1101-7.
368. Pirko I, Lucchinetti CF, Sriram S, Bakshi R. Gray matter involvement in multiple sclerosis. Neurology. 2007;68(9):634-42.
369. Kapeller P, McLean MA, Griffin CM, Chard D, Parker GJ, Barker GJ, et al. Preliminary evidence for neuronal damage in cortical grey matter and normal appearing white matter in short duration relapsing-remitting multiple sclerosis: a quantitative MR spectroscopic imaging study. J Neurol. 2001;248(2):131-8.

370. Davie CA, Barker GJ, Thompson AJ, Tofts PS, McDonald WI, Miller DH. 1H magnetic resonance spectroscopy of chronic cerebral white matter lesions and normal appearing white matter in multiple sclerosis. J Neurol Neurosurg Psychiatry. 1997;63(6):736-42. PMCID: 2169838.
371. Levin EC, Acharya NK, Han M, Zavareh SB, Sedeyn JC, Venkataraman V, et al. Brain-reactive autoantibodies are nearly ubiquitous in human sera and may be linked to pathology in the context of blood-brain barrier breakdown. Brain Res. 2010;1345:221-32.
372. Pham H, Ramp AA, Klonis N, Ng SW, Klopstein A, Ayers MM, et al. The astrocytic response in early experimental autoimmune encephalomyelitis occurs across both the grey and white matter compartments. J Neuroimmunol. 2009;208(1-2):30-9.
373. Bramow S, Frischer JM, Lassmann H, Koch-Henriksen N, Lucchinetti CF, Sorensen PS, et al. Demyelination versus remyelination in progressive multiple sclerosis. Brain. 2010;133(10):2983-98.
374. Chan KH, Zhang R, Kwan JS, Guo VY, Ho PW, Ho JW, et al. Aquaporin-4 autoantibodies cause asymptomatic aquaporin-4 loss and activate astrocytes in mouse. J Neuroimmunol. 2012;245(1-2):32-8.
375. Reichlin M. Cellular dysfunction induced by penetration of autoantibodies into living cells: cellular damage and dysfunction mediated by antibodies to dsDNA and ribosomal P proteins. J Autoimmun. 1998;11(5):557-61.
376. Vincent A, Lily O, Palace J. Pathogenic autoantibodies to neuronal proteins in neurological disorders. J Neuroimmunol. 1999;100(1-2):169-80.
377. Kampylafka EI, Routsias JG, Alexopoulos H, Dalakas MC, Moutsopoulos HM, Tzioufas AG. Fine specificity of antibodies against AQP4: epitope mapping reveals intracellular epitopes. J Autoimmun. 2011;36(3-4):221-7.
378. Arellano B, Hussain R, Zacharias T, Yoon J, David C, Zein S, et al. Human aquaporin 4281-300 is the immunodominant linear determinant in the context of HLA-DRB1*03:01: relevance for diagnosing and monitoring patients with neuromyelitis optica. Arch Neurol. 2012;69(9):1125-31.
379. Zeis T, Graumann U, Reynolds R, Schaeren-Wiemers N. Normal-appearing white matter in multiple sclerosis is in a subtle balance between inflammation and neuroprotection. Brain. 2008;131(Pt 1):288-303.
380. Allen IV, McQuaid S, Mirakhur M, Nevin G. Pathological abnormalities in the normal-appearing white matter in multiple sclerosis. Neurol Sci. 2001;22(2):141-4.
381. Lindberg RL, De Groot CJ, Certa U, Ravid R, Hoffmann F, Kappos L, et al. Multiple sclerosis as a generalized CNS disease--comparative microarray analysis of normal appearing white matter and lesions in secondary progressive MS. J Neuroimmunol. 2004;152(1-2):154-67.
382. Brettschneider J, Czerwoniak A, Senel M, Fang L, Kassubek J, Pinkhardt E, et al. The chemokine CXCL13 is a prognostic marker in clinically isolated syndrome (CIS). PLoS One. 2010;5(8):e11986. PMCID: 2916843.
383. Liu Y, Fan R, Zhou S, Yu Z, Zhang Z. Potential contribution of VH gene replacement in immunity and disease. Ann N Y Acad Sci. 2005;1062:175-81.
384. Longo NS, Grundy GJ, Lee J, Gellert M, Lipsky PE. An activation-induced cytidine deaminase-independent mechanism of secondary VH gene rearrangement

in preimmune human B cells. J Immunol. 2008;181(11):7825-34. PMCID: 2718577.
385. Lenze D, Greiner A, Knorr C, Anagnostopoulos I, Stein H, Hummel M. Receptor revision of immunoglobulin heavy chain genes in human MALT lymphomas. Mol Pathol. 2003;56(5):249-55. PMCID: 1187334.
386. de Wildt RM, Hoet RM, van Venrooij WJ, Tomlinson IM, Winter G. Analysis of heavy and light chain pairings indicates that receptor editing shapes the human antibody repertoire. J Mol Biol. 1999;285(3):895-901.
387. Bergsland N, Horakova D, Dwyer MG, Dolezal O, Seidl ZK, Vaneckova M, et al. Subcortical and cortical gray matter atrophy in a large sample of patients with clinically isolated syndrome and early relapsing-remitting multiple sclerosis. Ajnr. 2012;33(8):1573-8.
388. Wattjes MP, Harzheim M, Lutterbey GG, Klotz L, Schild HH, Traber F. Axonal damage but no increased glial cell activity in the normal-appearing white matter of patients with clinically isolated syndromes suggestive of multiple sclerosis using high-field magnetic resonance spectroscopy. Ajnr. 2007;28(8):1517-22.
389. Matthews PM, Pioro E, Narayanan S, De Stefano N, Fu L, Francis G, et al. Assessment of lesion pathology in multiple sclerosis using quantitative MRI morphometry and magnetic resonance spectroscopy. Brain. 1996;119 (Pt 3):715-22.
390. Derfuss T, Linington C, Hohlfeld R, Meinl E. Axo-glial antigens as targets in multiple sclerosis: implications for axonal and grey matter injury. J Mol Med. 2010;88(8):753-61.
391. Racanelli V, Prete M, Musaraj G, Dammacco F, Perosa F. Autoantibodies to intracellular antigens: generation and pathogenetic role. Autoimmun Rev. 2011;10(8):503-8.
392. Alexopoulos H, Kampylafka EI, Chatzi I, Travasarou M, Karageorgiou KE, Dalakas MC, et al. Reactivity to AQP4 epitopes in relapsing-remitting multiple sclerosis. J Neuroimmunol. 2013;260(1-2):117-20.
393. Palanichamy A, Muhammad K, Roll P, Kleinert S, Dorner T, Tony HP. Rituximab therapy leads to reduced imprints of receptor revision in immunoglobulin kappa and lambda light chains. J Rheumatol. 2012;39(6):1130-8.
394. Palanichamy A, Roll P, Theiss R, Dorner T, Tony HP. Modulation of molecular imprints in the antigen-experienced B cell repertoire by rituximab. Arthritis Rheum. 2008;58(12):3665-74.
395. Rouziere AS, Kneitz C, Palanichamy A, Dorner T, Tony HP. Regeneration of the immunoglobulin heavy-chain repertoire after transient B-cell depletion with an anti-CD20 antibody. Arthritis Res Ther. 2005;7(4):R714-24. PMCID: 1175025.
396. Kaplin AI, Deshpande DM, Scott E, Krishnan C, Carmen JS, Shats I, et al. IL-6 induces regionally selective spinal cord injury in patients with the neuroinflammatory disorder transverse myelitis. J Clin Invest. 2005;115(10):2731-41. PMCID: 1224298.
397. Cognasse F, Hamzeh-Cognasse H, Lafarge S, Chavarin P, Pozzetto B, Richard Y, et al. Identification of two subpopulations of purified human blood B cells, CD27-CD23+ and CD27high CD80+, that strongly express cell surface Toll-like receptor 9 and secrete high levels of interleukin-6. Immunology. 2008;125(3):430-7. PMCID: 2669146.

398. Nagafuchi H, Suzuki N, Mizushima Y, Sakane T. Constitutive expression of IL-6 receptors and their role in the excessive B cell function in patients with systemic lupus erythematosus. J Immunol. 1993;151(11):6525-34.
399. Sekiguchi DR, Eisenberg RA, Weigert M. Secondary heavy chain rearrangement: a mechanism for generating anti-double-stranded DNA B cells. J Exp Med. 2003;197(1):27-39. PMCID: 2193805.
400. Ren Z, Wang Y, Duan T, Patel J, Liggett T, Loda E, et al. Cross-immunoreactivity between bacterial aquaporin-Z and human aquaporin-4: potential relevance to neuromyelitis optica. J Immunol. 2012;189(9):4602-11. PMCID: 3586280.
401. Greer JM, Kuchroo VK, Sobel RA, Lees MB. Identification and characterization of a second encephalitogenic determinant of myelin proteolipid protein (residues 178-191) for SJL mice. J Immunol. 1992;149(3):783-8.
402. Cohn M. Degeneracy, mimicry and crossreactivity in immune recognition. Mol Immunol. 2005;42(5):651-5.
403. Cahoy JD, Emery B, Kaushal A, Foo LC, Zamanian JL, Christopherson KS, et al. A transcriptome database for astrocytes, neurons, and oligodendrocytes: a new resource for understanding brain development and function. J Neurosci. 2008;28(1):264-78.
404. Kang EH, Shen GQ, Morris R, Metzger A, Lee EY, Lee YJ, et al. Flow cytometric assessment of anti-neuronal antibodies in central nervous system involvement of systemic lupus erythematosus and other autoimmune diseases. Lupus. 2008;17(1):21-5.
405. Marta CB, Taylor CM, Coetzee T, Kim T, Winkler S, Bansal R, et al. Antibody cross-linking of myelin oligodendrocyte glycoprotein leads to its rapid repartitioning into detergent-insoluble fractions, and altered protein phosphorylation and cell morphology. J Neurosci. 2003;23(13):5461-71.
406. Faust TW, Chang EH, Kowal C, Berlin R, Gazaryan IG, Bertini E, et al. Neurotoxic lupus autoantibodies alter brain function through two distinct mechanisms. Proc Natl Acad Sci U S A. 2010;107(43):18569-74. PMCID: 2972998.
407. Tradtrantip L, Ratelade J, Zhang H, Verkman AS. Enzymatic deglycosylation converts pathogenic neuromyelitis optica anti-aquaporin-4 immunoglobulin G into therapeutic antibody. Ann Neurol. 2013;73(1):77-85. PMCID: 3567850.
408. Tradtrantip L, Asavapanumas N, Verkman AS. Therapeutic Cleavage of Anti-Aquaporin-4 Autoantibody in Neuromyelitis Optica by an Igg-Selective Proteinase. Mol Pharmacol. 2013.
409. Benkhoucha M, Molnarfi N, Santiago-Raber ML, Weber MS, Merkler D, Collin M, et al. IgG glycan hydrolysis by EndoS inhibits experimental autoimmune encephalomyelitis. J Neuroinflammation. 2012;9:209. PMCID: 3458989.
410. Bakchoul T, Greinacher A, Sachs UJ, Krautwurst A, Renz H, Harb H, et al. Inhibition of HPA-1a alloantibody-mediated platelet destruction by a deglycosylated anti-HPA-1a monoclonal antibody in mice: toward targeted treatment of fetal-alloimmune thrombocytopenia. Blood. 2013;122(3):321-7. PMCID: 3716199.
411. Nandakumar KS, Collin M, Olsen A, Nimmerjahn F, Blom AM, Ravetch JV, et al. Endoglycosidase treatment abrogates IgG arthritogenicity: importance of IgG glycosylation in arthritis. Eur J Immunol. 2007;37(10):2973-82.

412. Wang G, Ujiie H, Shibaki A, Nishie W, Tateishi Y, Kikuchi K, et al. Blockade of autoantibody-initiated tissue damage by using recombinant fab antibody fragments against pathogenic autoantigen. Am J Pathol. 2010;176(2):914-25. PMCID: 2808096.